CRANFIELD UNIVERSITY

School of Industrial and Manufacturing Science

PhD Thesis

Academic Year 2003-2004

NIKOLAOS ANGELIDIS

DAMAGE SENSING IN CFRP COMPOSITES USING ELECTRICAL POTENTIAL TECHNIQUES

Supervisor: Prof. P E Irving

February 2004

This thesis is submitted in partial fulfilment of the requirements
for the degree of Doctor of Philosophy

ABSTRACT

This Thesis investigates the damage sensing capabilities of the electrical potential measurement technique in carbon fibre reinforced polymer composites.

Impact damage was introduced in multidirectional laminates and its effect on potential distribution studied. It was found that delaminations and fibre breakages within the laminate can be detected and located by measuring potential changes on the external composite surface. The extent and size of potential changes were significantly affected by the position of the current electrodes in relation to the potential measurement probes.

A numerical model was developed investigating the effect of different size delaminations, located in various positions within the lamina, on electrical potential distributions on the external ply, and a quantitative analysis of the numerical results is presented. The numerical simulations demonstrated that the measured potential changes on the external ply were in proportion to the delamination size. The numerical and experimental results were compared and the optimum configuration of current electrodes and potential probes for damage detection selected.

The response of electrical potential to mechanical strain, in unidirectional and multidirectional samples was also investigated. It was found that the conductive medium, used for introducing the current, defines the piezo-resistance performance of the composite. A finite element model was developed able to predict the effect of inhomogeneous current introduction in unidirectional specimens on electrical potential and piezo-resistance. The effects of temperature and water absorption on potential measurements were also presented.

To my Parents,

Charilao & Vasiliki

PUBLICATIONS

1. N Khemiri, N Angelidis, P E Irving, '*Self sensing of delamination damage in composite materials using electrical potential techniques*', presented to 2001 meeting of Smart Structures & Materials, Ed C Chang; Stanford, California, September 2001
2. N Khemiri, N Angelidis, P E Irving, '*Experimental and finite element study of the electrical potential technique for damage detection in CFRP laminates*', presented to conference of Smart Structures & Demonstrators, Herriot Watt University, Edinburgh, December 2001
3. P E Irving, N Angelidis, N Khemiri, '*The Electrical potential techniques for damage detection in carbon fibre composites*', presented at International workshop on advanced NDE techniques, Capetown, SA, April 2002
4. N Angelidis, N Khemiri, P Irving, '*Damage Detection in CFRP Laminates Using Electrical Potential Techniques',* presented at the European Workshop on Smart Structures in Engineering and Technology, France-Giens, May 2002
5. N Angelidis, N Khemiri, P Irving, '*Electrical Behaviour of CFRP under Mechanical Loading'*, presented at the First European Workshop on Structural Health Monitoring, France-Paris, July 2002
6. N Angelidis, P E Irving, 'Self-sensing of impact damage in CFRP by means of electrical potential changes', presented at the 4th International Workshop in Health Monitoring, Stanford, California, September 2003
7. N Angelidis, N Khemiri, P E Irving, '*Experimental and finite element study of the electrical potential technique for damage detection in CFRP laminates*', submitted to Smart Materials and Structures Journal
8. N Angelidis, C Wei, P E Irving, 'The electrical resistance response of continuous carbon fibre composite laminates to mechanical strain', submitted to Composites Structures Journal

ACKNOWLEDGEMENTS

I would like to express my deepest sense of gratitude to Prof. P E Irving for giving me the opportunity to on this project, and for his continuous guidance and mental support all these years. His optimism and continuous encouragement provided me constant inspiration to overcome the challenges.

The financial support of the Engineering and Physical Sciences Research Council (EPSRC) and Defence Science and Technology Laboratory (DSTL), is greatly acknowledged.

I would like to thank the technical staff, Mr Tony Scott, Mr Jim Hurley, and Mr Andrew Dyer, for their valuable help in the specimen preparation, and testing equipment.

Finally I would like to thank my family, who has always been encouraging and supportive in my choice to live abroad the last three years.

CONTENTS

3. CONDUCTION PROCESSES IN CARBON FIBRES AND RESINS

4. CONDUCTION PROCESSES IN CFRP

PART III

RESULTS

7. POTENTIAL FIELDS

8. EFFECT OF EXTERNAL PARAMETERS

9. NUMERICAL ANALYSIS

PART IV

DISCUSSION

10. DISCUSSION

LIST OF FIGURES

LIST OF TABLES

NOMENCLATURE

Symbol	Description	Unit
A	Cross-sectional area	[m^2]
$Å$	Ångstrom	1 x 10^{-10} m
A_c	Cross-sectional area of composite	[m^2]
A_f	Cross-sectional area of fibres	[m^2]
a	Temperature coefficient of resistivity	[Ω.m/°C]
D	Diffusion constant	m^2/sec
ΔR	Change in resistance	[Ω]
ΔV	Potential change	[V]
δ_{ec}	Ineffective length	[m]
E	Voltage difference, Electrical field	[V]
E_c	Activation energy	[eV]
E_f	Fermi level	[eV]
ε	Mechanical strain	Dimensionless
ε_L	Longitudinal Strain	Dimensionless
ε_r	Radial strain	Dimensionless
ε_τ	Transverse Strain	Dimensionless
g	Electrical conductance at elements interface	S/mm^2
I	Current	[A]
J	Current Density	[A/m^2]
k	Boltzmans constant	1.38×10^{-23} J/atom.K
L, l	Length of conductor	[m]
μ	Mobility of charge carriers	[m^2/V.sec]
μ_n	Mobility of negative charge carriers	[m^2/V.sec]

μ_p	Mobility of positive charge carriers	[m^2/V.sec]
μ_e	Mobility of free electrons	[m^2/V.sec]
μ_h	Mobility of electron holes	[m^2/V.sec]
n, N	Number of charge carriers, carbon fibres	Dimensionless
n_n	Number of negative charge carriers	Dimensionless
n_p	Number of positive charge carriers	Dimensionless
v	Poisson's ratio, concentration of conducting elements	Dimensionless
v_c	Percolation threshold	Dimensionless
q	Electrical charge in Coulomb	[C]
q_n	Electrical negative charge	-1.602×10^{-19} C
q_p	Electrical positive charge	1.602×10^{-19} C
R	Resistance	[Ω]
R_c	Composite resistance	[Ω]
R_e	Electrode resistance	[Ω]
R_f	Fibre Resistance	[Ω]
R_0	Electrical resistance at zero strain parallel to the fibres	[Ω]
R_{90}	Electrical resistance at zero strain transverse to the fibres	[Ω]
r	Radius of wire/carbon fibres	[m]
ρ	Electrical Resistivity	[Ω.m]
ρ_c	Resistivity of Composite	[Ω.m]
ρ_f	Resistivity of carbon fibre	[Ω.m]
ρ_m	Resistivity of matrix	[Ω.m]
ρ_{rt}	Room temperature resistivity	[Ω.m]
ρ_t	Resistivity through thickness direction	[Ω.m]
ρ_0	Temperature independent constant, longitudinal electrical resistivity of composite	[Ω.m]
ρ_{90}	Transverse resistivity (90° direction)	[Ω.m]
S	Closed surface	[m^2]
σ	Electrical Conductivity	[$(\Omega.m)^{-1}$]
σ_{eff}	Effective conductivity	[$(\Omega.m)^{-1}$]

T	Absolute temperature in Celcius	[°C]
T_{rt}	Room temperature	[°C]
t	Rate of conductivity change	Dimensionless
V	Voltage	[V]
V_c	Critical concentration of conducting fillers	Dimensionless
V_f	Fibres volume fraction	Dimensionless
V_{min}	Minimum Potential	[V]

SYMBOLS ABBREVIATIONS

BSU	Basic Structural Unit
CAD	Computer Aided Design
CCC	Conductive Carbon Cement
CFRP	Carbon fibre reinforced plastics
CP	Cross ply
DAQ	Data Acquisition
DC	Direct contact
DICY	Dicyandiamide
DMM	Digital Multimeter
EIT	Electrical Impedance Tomography
EMT	Effective Medium Theory
EP	Electrical Potential
FE	Finite Element
FEM	Finite Element Model
GEM	General Effective Media
GF	Gauge Factor
GFRP	Glass fibre reinforced plastics
GLS	Global Load Sharing

HM	High Modulus
HT	High Strength
IM	Intermediate Modulus
ISO	International Organisation for Standardisation
PAN	Polyacrylonitrile
PES	Polyethersulphone
PC	Personal Computer
QI	Quasi-isotropic
RH	Relative humidity
SM	Standard Modulus
TCR	Temperature Coefficient of resistivity
T_{HT}	Heat Treatment Temperature
UD	Unidirectional
UHM	Ultra High Modulus

1 INTRODUCTION

The benefits of composite materials in modern air and spacecraft are well known. Compared to metals, composites can provide reduced weight, superior structural properties, and the capability to be formed into custom shapes to meet unique requirements. In use, these materials are subjected to high alternating stresses or impacts that can cause damage growth and ultimately structural failure.

The main types of damage are delamination, matrix cracks and fibre breaks. Once the damage appears it can grow and reduce the strength of the structure. Maintaining structural integrity is an ever increasing problem since structural failure can lead to loss of life, loss of asset value and environmental pollution, and the risk of these occurring needs to be reduced to an acceptable level. To ensure safety and reliability of composite structures during their lifetime it is imperative to detect, and locate the various types of damage using non-destructive techniques, which can continuously monitor the structure.

Many techniques are in development to detect and quantify impact damage. All of the techniques have advantages and disadvantages in terms of accuracy, expense, robustness and level of instrumentation required. Despite their extensive usage, non-destructive evaluation (NDE) techniques have been problematic to employ for continuous

monitoring. Currently successful laboratory non-destructive testing methods, such as X-radiographic inspection, ultrasonics, acoustic emission, microscopy, are impractical for service inspection of large integrated subsystems. Among them, acoustic emission has been popularly employed to detect defects. This technique can provide qualitative information about the determination and location of defects; however, quantitative characterisation is not straight forward. Microscopy techniques provide valuable information about the accumulation of damage on an exposed surface of a laminate; however, these techniques fail to provide complete information about the global extent and distribution of damage throughout the laminate. Ultrasonic techniques require calibration standards for each material and thickness, while for the detection of fibre cracks special methods have to be employed. X-ray techniques fail to detect internal fibre breaks and the application cost is increased. It is clear that a technique for inspection of composites need to be developed.

Structural health monitoring and smart structures are of current research interest. The aim is to detect and locate damage or degradation in structural components and to provide this information quickly and in a form easily understood by the operators or occupants of the structure. Many of them involve sensing of strains and acoustic waves using embedded or surface mounted optic fibres or piezo-transducers; however, the use of external sensors has its own problems. Fibre optics have exceptional advantages in communication and data transmission technology. Before employing fibre optics to sense damage in carbon fibres reinforced polymers (CFRP) structures, technical problems have to be solved, related to the effect on structural integrity and degradation of mechanical properties.

An alternative technique still relatively unexplored, is the electrical potential technique, which exploits the electrical conductivity of carbon fibre as a direct damage sensing element. Electrical conductivity is one of the fundamental properties of materials and is related to the atomic level; it is influenced by structural and environmental changes in the material. These can be impact damage, mechanical strain, temperature or moisture. Therefore any change in electrical conductivity can be related to a change in the internal state of the structure.

The electrical potential technique detects the presence of internal or external damage, by measuring changes in the potential field on the surface of a current carrying composite laminate, caused by impact or other forms of damage such as fatigue. The presence of cracks and delaminations causes modification of the current path along and between the carbon fibres; this leads to a change in the electrical potential field around the damage zone. The changes in potential field can be measured and characterised in terms of the size of the detectable changes, and the spatial extent of the disturbance from the delamination site.

No implanted sensors are required for this technique, and theoretically the advantages are its accuracy and simplicity. Moreover, it provides in-situ sensing of the entire structure. Key questions to be addressed are the sensitivity and ability of the technique to locate damage sites within a large area of composite structure. There is relatively little research work published on this technique; the majority of the work has been concerned with the resistivity change, due to damage, on unidirectional composite samples highlighting the possibility of real time monitoring of static and fatigue damage in continuous fibre polymer matrix composites, carbon fibre carbon-matrix composite and short carbon fibre polymer-matrix composite.

In this research work the main concern was the application of this technique to monitor delaminations on composite material plates caused by impact damage. The electrical resistance was measured using either the four point and two point measurement technique. The experimental set-up for each method is shown in Figure 1. 1 A constant current source and a voltmeter were used in this investigation for measuring the electrical potential. In the four point method (Figure 1. 1 (a)), a known current is introduced through the outer probes in the sample and the voltage drop across the two inner probes is measured using a voltmeter; the resistance is then calculated using Ohm's law. This method measures the sample resistance and eliminates the contact resistance, since the very high resistance of the voltmeter (>1GΩ) will only allow to a negligible current to flow to the measurements circuit. The electrodes contact resistance is eliminated by averaging the voltage for reversal of direction current.

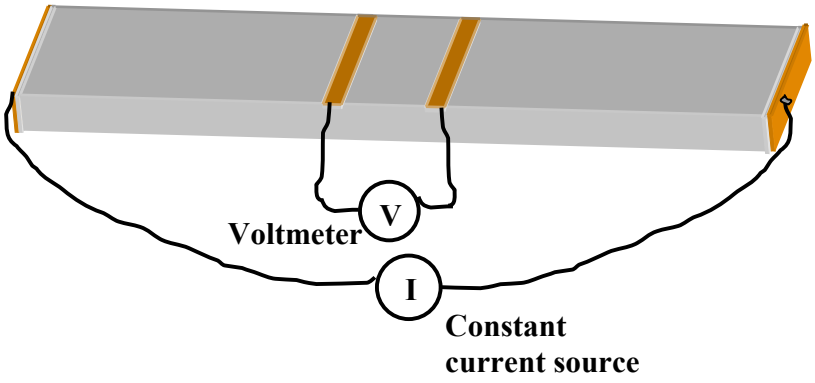

a) Four point method

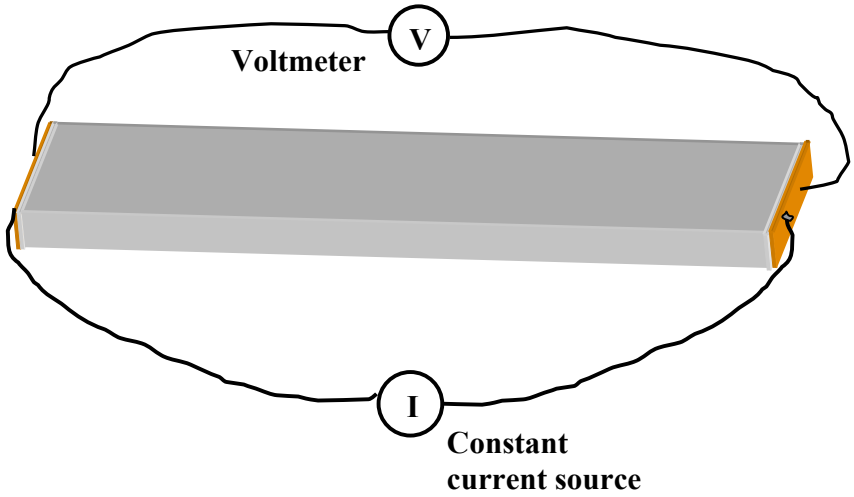

b) Two point method

Figure 1. 1: Four point (a) and two point (b) resistance measurement method.

In the two point potential measurement method (Figure 1. 1 (b)), the same electrodes are used for passing the current and measuring the potential. In this case the contact resistance will form part of the measured resistance. For the purposes conversion of potential measurements to resistance, only the four point method can eliminate the effect of contact resistance.

This Thesis is divided in four parts; the literature overview, the experimental procedures, the results and numerical analysis, and finally the discussion and conclusions. Chapter 2 reviews the physical conduction processes of materials in general. Chapter 3 presents the literature review of the conduction processes of carbon fibres. These processes are related to the structure and physical properties of a single carbon fibre. The effect of different mechanical and environmental condition on electrical resistivity is presented and detailed reviews of electrical properties of carbon fibres and resins are given.

Chapter 4 deals with the electrical properties of CFRP composites. These properties are related to the conduction mechanisms between adjacent tows of carbon fibres rather than individual fibres. Various theoretical models for conduction processes in damaged and undamaged CFRP composites such as two parallel resistance models, rule of mixtures, percolation theory, are also analyzed. The literature overview is concluded in Chapter 5 with the review of the main forms of impact damage, and their effect on electrical conduction processes.

Chapter 6 deals with the materials, manufacture techniques, and test programs used in this research study. All experimental configurations with the different types of specimens are presented together with the electrical and mechanical equipment used for the experimental work. The various computational programs that were used for acquiring and validating all experimental data are also presented.

Chapter 7 presents the results for potential fields in composite laminates. The conducted investigation included the influence of current input location and stacking sequence on potential distribution fields on undamaged plates. Damage in the form of holes and impact damage is introduced in multidirectional laminates and their effect on potential contours is presented. Chapter 8 presents the results from the effect of external parameters such as mechanical loading, temperature and humidity on electrical potential.

Chapter 9 presents the principles and the results from the finite element analysis. The effect of different mesh sizes on potential distribution on unidirectional and

multidirectional samples is reviewed in detail and numerical models are given, simulating potential distribution on undamaged and damaged multidirectional laminates.

Chapter 10 summarizes and discusses all experimental and numerical findings. A numerical model is presented demonstrating the effect of inhomogeneous current distribution in unidirectional samples on electrical potential. The discussion of the results includes the comparison between experimental and numerical findings, and a quantitative evaluation of impact, mechanical and environmental loads is presented. Finally, in Chapter 11 the main conclusions and future work are presented.

2 PHYSICS OF ELECTRICAL CONDUCTION

The study of the electrical conduction of materials, in general, is an essential tool in order to investigate the electrical properties of the fibres and the polymer resins. The literature sources used for the following investigation are books on physics of electrical conduction and material science [1]-[12].

This Chapter is organised as follows. Section 2.1 and Section 2.2 present the Ohm's and Kirchhoff's law respectively, and the fundamental equations that govern electrical conduction processes in materials. Section 2.3 refers to the electrical conductivities of various materials while Section 2.4 presents the general principles that govern the electrical conduction in materials. Finally, the effect of temperature on the electrical conduction processes is given in Section 2.5.

2.1 Ohm's Law

The conduction of electricity in materials is by means of individual atomic scale species called charge carriers. The simplest example of charge carriers is the **electron**, a particle with 1.602×10^{-19} C of negative charge which is the elemental unit of electricity. Another type of charge carrier is the **electron hole**, which is a missing electron in an electron cloud. Finally the last type is **ion,** in ionic materials, that can serve either as negative charge carriers (anions) or as positive (cations).

One of the most important electrical characteristics of a solid material is the ease with which it transmits an electrical current. Ohm's law relates the current I, or time rate of charge passage, to the applied voltage V as follows:

$$V = IR \qquad (2.1)$$

where R is the resistance of the material through which the current is passing as the electrons collide with the atoms in the lattice structure of the conducting material or other imperfections such as impurity atoms, vacancies, dislocations. The units for V, I and R are respectively volt (V), ampere (A), and ohm (Ω).

The value of R is influenced by specimen configuration. The resistivity ρ, is independent of the specimen geometry and related to the resistance through the expression

$$\rho = \frac{RA}{L} \qquad (2.2)$$

where A is the cross-sectional area of the specimen and L is its length.

The most convenient parameter for establishing an electrical classification system for materials is the electrical conductivity which is the reciprocal of resistivity:

$$\sigma = \frac{1}{\rho} \qquad (2.3)$$

When the charge transport takes place through the volume of the material (such as in metals or semiconductors) the corresponding resistivity is named volume or bulk resisitivity. However, in the case of insulators, the charge transport may take place only along a surface or in a thin layer of the charged body; in that case the resistivity is named as surface resistivity.

2.2 Kirchhoff's Law

Two additional laws of electric circuits share a position of importance with Ohm's law. Steady currents have a continuous nature; they have no sources or sinks (Ending places). Therefore as much current must flow into a volume as leaves it. Thus, in general, the integral of the normal component of the current density J over a closed surface S must equal zero [12]. This is Kirchhoff's *current law* for a finite region which is expressed by the following equation:

$$\oint_S J \cdot dS = 0 \qquad (2.4)$$

In an electric circuit with various junction points this law states that the sum of the currents entering or leaving a junction point at any instant is equal to zero. A junction point is that place in a circuit where two or more circuit elements are joined together (independent node). The current law may be expressed mathematically as

$$\sum_{j=1}^{k} I_j = 0 \qquad (2.5)$$

where k denotes the number of independent nodes.

For a small volume element ΔV located inside a conducting medium, the current density is a vector having the direction of the current flow. In general it has three rectangular

components that vary with position and Kirchhoff's law is expressed by the following equation:

$$\nabla \cdot J = 0 \qquad (2.\ 6)$$

This is a differential relation involving J at a point.

Kirchhoff's voltage law states that at any time instant the sum of voltages in a closed circuit is zero. A generalized formulation of Kirchhoff's *voltage law* is written as

$$\sum_{j=1}^{k} V_j = 0 \qquad (2.\ 7)$$

where V_j represents the voltage drop of the j_{th} element in any given closed circuit which is assumed to have k elements.

2.2.1 Current density

For current distributed uniformly throughout the cross-section of a wire, the current density J is given by the equation:

$$J = \frac{I}{A} \qquad (2.\ 8)$$

In addition to equation (2.1), Ohm's law may be expressed as

$$J = \sigma \cdot E \qquad (2.\ 9)$$

where E is the voltage difference between two points divided by the distance separating them, given by:

$$E = \frac{V}{L} \qquad (2.\ 10)$$

2.3 Electrical Conductivity

The range of electrical conductivity observed in materials covers a range of 25 orders of magnitude; this is one of the largest variations in any materials property. The range of conductivity of materials is illustrated in Figure 2. 1.

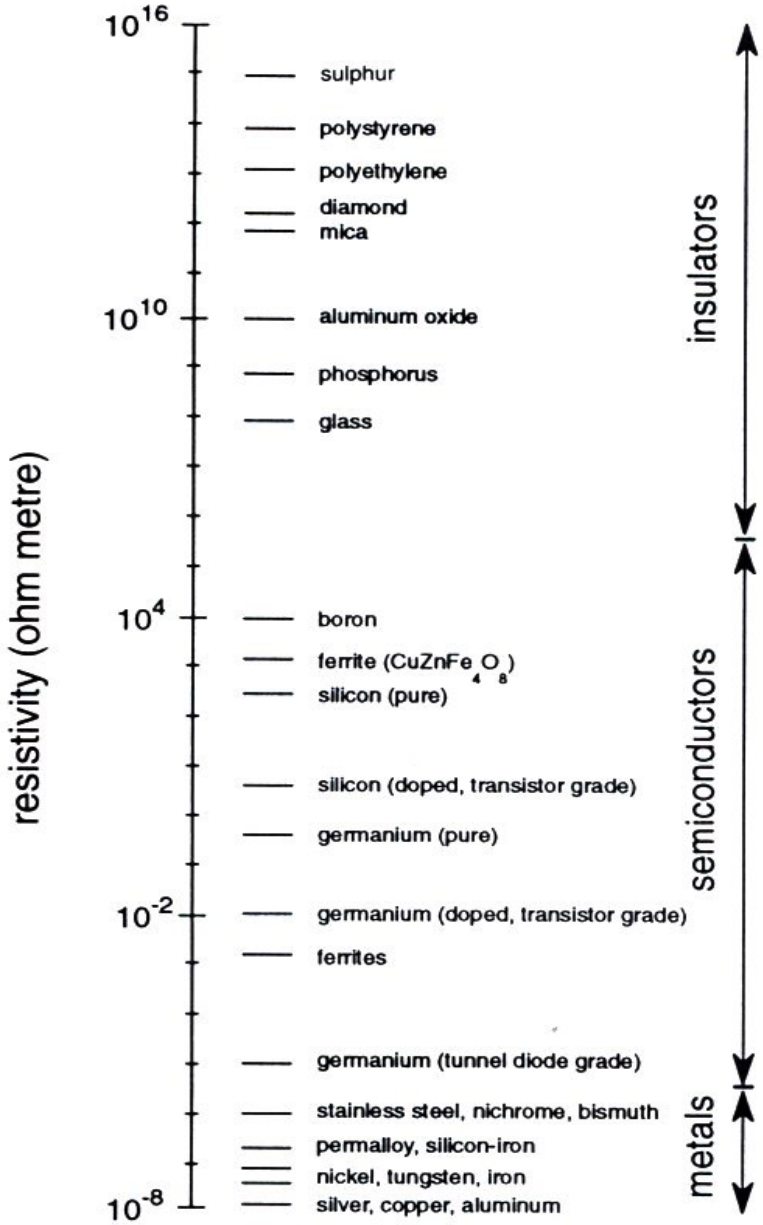

Figure 2. 1 Conductivities of various elements, compounds and polymers [5].

The electrical conductivity is related to two basic parameters; the charge carrier density *n*, and the charge carrier mobility μ, which are affected by the same parameters as the electrical resistance. When the conduction is due to electrons, the conductivity is given from the following equation:

$$\sigma = n \cdot |q| \cdot \mu \qquad (2.\ 11)$$

where *n* is the number of charge carriers per unit volume (e.g. m^{-3}), $|q|$ is the absolute magnitude of the electrical charge in Coulombs, and μ is the mobility of the charge carriers.

When both positive and negative charge carriers are contributing to conduction then equation (2.11) yields,

$$\sigma = n_n|q_n|\mu_n + n_q|q_p|\mu_p \qquad (2.\ 12)$$

where subscripts *n* and *p* denote the negative and positive charge carriers, or electron holes and electrons respectively. In semiconductors there are only two types of charge carrier (free electrons and electron holes) and equation (2.12) can be modified as following:

$$\sigma = n|q|\mu_e + n|q|\mu_h \qquad (2.\ 13)$$

where subscripts *e* and *h* denote electrons and holes respectively.

Finally if the conduction in an insulator is due to ions, it is expressed from the following equation (Einstein relation):

$$\sigma_{ion} = \frac{Dq^2 n}{kT} \qquad (2.\ 14)$$

where D is the diffusion constant, k is Boltzmans constant, and T is the absolute temperature [5]. In insulators the conduction is due to electrons or ions and both equations (2. 2) & (2. 3) can be used.

2.4 Energy Levels and Energy Bands

Conduction mechanisms in materials are generally explained using band theory. In all conductors, semiconductors and insulating materials, the magnitude of the electrical conductivity is strongly dependent on the number of electrons available to participate in the conduction process.

For each individual atom there exist discrete energy levels that may be occupied by electrons. At relative large separation distances, each atom is independent of all the others and will have the atomic energy levels and electron configuration as if isolated. As the atoms come within close proximity of one another, electrons are acted upon or perturbed by electrons of adjacent atoms, producing high and low electron energy bands.

The higher energy band is called the conduction band and is empty of electrons. The lower energy band is called valence band and it is filled with electrons. The energy corresponding to the highest filled state at 0 K is called the Fermi energy, E_f.

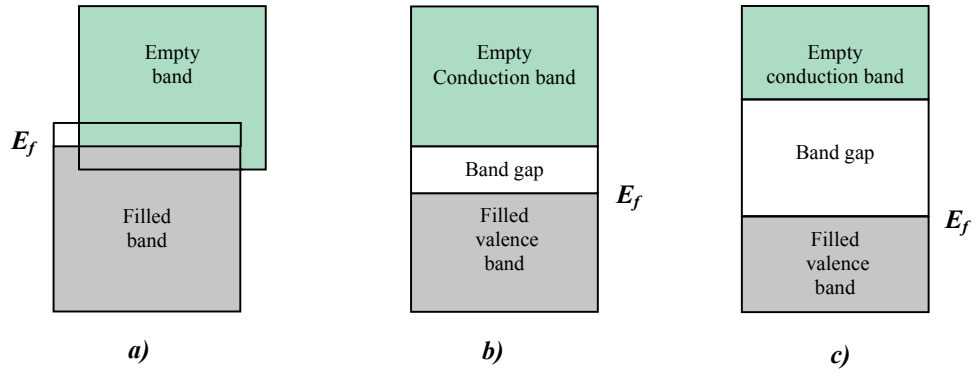

Figure 2. 2: The various possible electron band structures in solids at 0 K [10].

The electrical properties of a solid material are a consequence of its electron band structure; three main types of band structures are described. In the first band structure (Figure 2. 2 (a)), found in metals, the valence band is only partially filled, permitting high mobility of outer orbital electrons throughout the solid, allowing an overlap of filled and empty outer bands. The energy gap is zero, illustrating why metals are such good conductors. The Fermi level at 0 K corresponds to a level in the middle of the band and this makes metals electrical conductors.

The final two band structures are similar. One band (valence band) that is completely filled with electrons is separated from an empty conduction band, and an energy band gap lies between them.

For a semiconductor, (Figure 2. 2 (b)), the energy gap is less than 2 eV. In that case the electrons can be promoted into the conduction band by thermal excitation allowing electrical conduction.

However, for insulators (Figure 2. 2 (c)), the energy gap is greater than 2 eV and the electrons cannot be promoted into the conduction band by thermal excitation. This explains why the electrical conduction in an insulator is extremely low.

2.5 Influence of Temperature

The effect of temperature on conductivity in materials is illustrated in Figure 2. 3. In metals an increase in temperature above 0K, results in a linear drop in conductivity and increase of resistivity [10]. This drop in conductivity is predominantly due to the drop in electron mobility with increasing temperature. By increasing thermal agitation of the crystalline structure, electrons cannot move through crystalline structure as effectively as when the structure is nearly perfect.

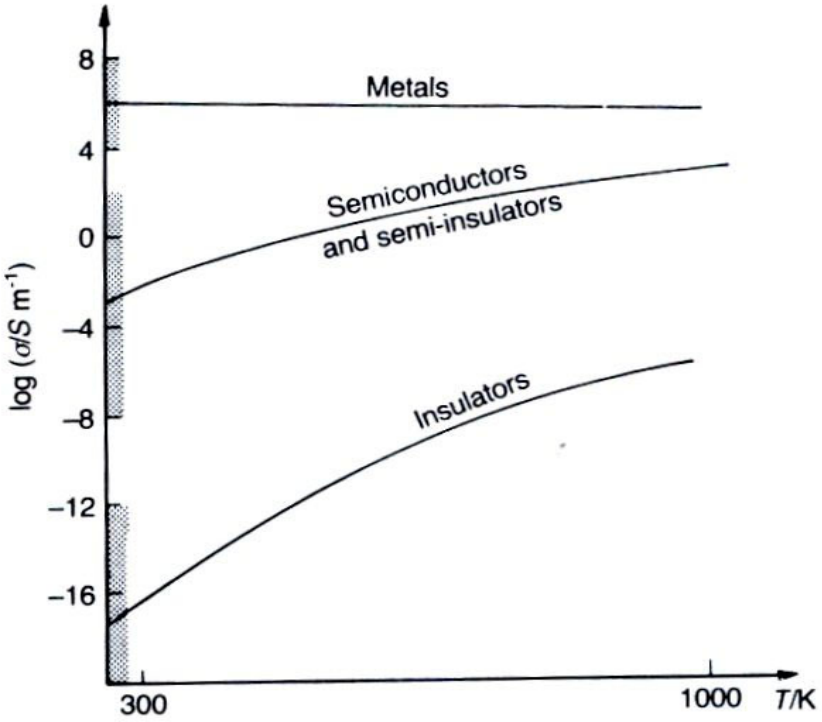

Figure 2. 3: Variation of electrical conductivity of conductors and insulators with temperature [11].

The relationship between electrical resistivity and temperature is given by:

$$\rho = \rho_{rt}[1 + \alpha(T - T_{rt})] \qquad (2.\ 15)$$

where ρ_{rt} is the room temperature value of resistivity, α the temperature coefficient of resistivity, and T_{rt} the room temperature.

In insulators and semiconductors the resistivity decreases monotonically with increasing temperature from above 0K. This is due to the fact that the concentration of electrons and holes increases with temperature, since more thermal energy is available to excite

electrons from the valence to the conduction bands. The temperature dependence of resistivity is given by:

$$\rho = \rho_0 e^{\frac{E_c}{kT}} \qquad (2.16)$$

where ρ_0 is a temperature independent constant, and E_c is the activation energy for the electrical conduction process.

3 CONDUCTION PROCESSES IN CARBON FIBRES AND RESINS

Fibres are used as continuous reinforcements in unidirectional composites by aligning a large number of them in a thin plate or shell, called ply. There are many types of carbon fibres depending on the precursor used. The mechanical properties vary greatly with the precursor used and the processing condition employed, as these determine the perfection and alignment of the crystals. Commercial carbon and graphite fibres are manufactured from organic polymers the most significant of whom are rayon, polyacrylonitrile (PAN), and pitch. Of the three precursors, PAN has proven to be the most suitable for developing the carbon structure needed to produce high strength fibres. However, new fibres are always under test. Two examples of recent introductions are *hollow* fibres and *coiled* fibres [13].

The Chapter is organised as follows: Section 3.1 refers to the structure of graphite and carbon fibres. Section 3.2 analyzes the conduction processes in carbon fibres and graphite. The effects of temperature, humidity and mechanical loading on electrical resistivity of carbon fibres are also presented. Finally the electrical resistivity properties of epoxy resins and the effect of moisture are given in Section 3.3.

3.1 Structure in Carbon Fibres

Elemental carbon occurs in three forms: diamond, graphite and fullerenes. Diamond is isotropic and is an electric insulator because the bonding energy levels are completely filled [14]. In contrast graphite has a layered structure, is anisotropic and electrical conductor especially parallel to the layers [15]. Fullerene is also classified as conductor and if it is doped with additional electrons, it can be classified as superconductor.

The crystallographic structure of graphite is shown in Figure 3. 1. It consists of multiple layers of carbon atoms (graphene layers) which are separated by a distance of 0.335 nm; a-axis is extended parallel to the fibre direction while b-axis represents the transverse direction; c-axis is perpendicular in the basal plane (a-b). In the plane of each layer, the carbon atoms are linked by covalent bonds in a two dimensional hexagonal network formation, 0.142 nm apart [16], [17].

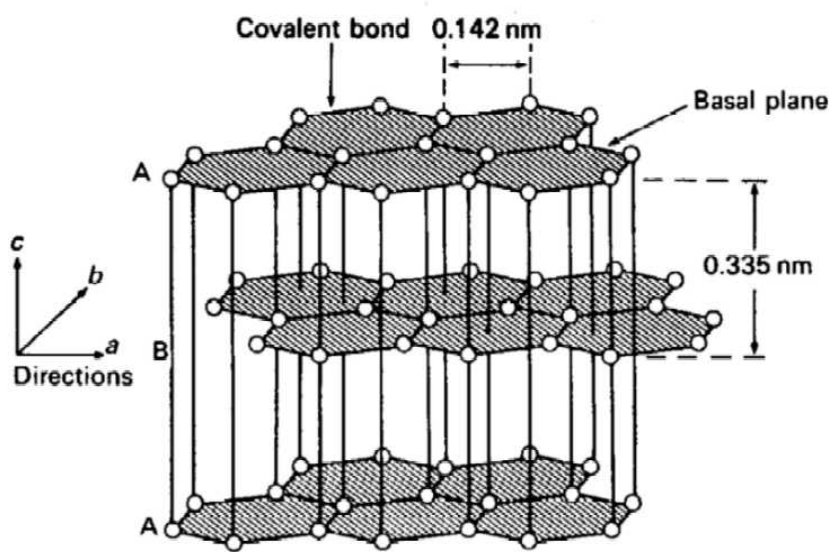

Figure 3. 1 The crystal structure of hexagonal single graphite [17].

Carbon fibres are modified from graphite. The main types of carbon fibres are PAN and pitch derived fibres. Pitch fibres are generally produced from petroleum asphaltene or coal tar. PAN fibres are acrylic-based fibres and they contain at least 85% of acrylonitrile

[18]. Ultimate fibre mechanical properties are not significantly affected by the type of precursor. However, the processing techniques are much different among the various precursors. The main focus in this Chapter has been on the manufacturing processes of PAN-based fibres since this type of fibres was used in this research.

The heat treatment temperature (T_{HT}) of the precursor defines the mechanical properties of the fibres. The major steps in the preparation of PAN carbon fibres are stabilization, carbonization and graphitization. Stabilization generally calls for a heat treatment in the range of 200°C to 300°C in an oxygen-containing atmosphere, with the result that the polymer backbone of the precursor undergoes a series of chemical reactions that ultimately result in the formation of polynaphthyridine, a substance with the preferred structural form for the formation of graphite [18].

The carbonization step involves heating the stabilized precursor fibre to temperatures up to 1000°C in an inert or mildly oxidizing atmosphere. Carbonization can take anywhere from a few minutes to several hours. In one type of process, fibres possessing high modulus and high strength are obtained by first heating PAN fibres in an oxidizing atmosphere until they are permeated with oxygen. The fibres are then heated further, to initiate carbonization, while being held under tension in a non-oxidizing atmosphere. Finally, to increase the ultimate tensile strength, the fibres are heat-treated in an inert atmosphere between 1300°C and 1800°C. After carbonization, well-defined hexagonal networks develop, which are typically aligned with an average angle of 20° to the fibre axis [18].

Graphitization occurs by heating the carbonized fibre to high temperature (up to 3000°C) in an inert atmosphere. The process can last anywhere from 1 to 20 minutes. Tensioning the fibres during graphitization improves ultimate mechanical properties (such as the modulus) by further improving the orientation of the planes with respect to the fibre axis.

Carbon fibres based on PAN precursor generally have a higher tensile strength than a fibre based on any other precursor; this is due to a lack of surface defects, which act as

stress concentrators and, hence, reduce tensile strength. The classification of PAN carbon fibres based on modulus range is as follows [18]:

- Ultra High Modulus (UHM) Grade: > 440 GPa
- High Modulus (HM) Grade: 320-440 GPa
- Intermediate Modulus (IM) Grade: 265-320 GPa
- Standard Modulus (SM) Grade: < 265

The microstructure of graphite carbon fibre influences its properties; the crystalline form of the fibre is the ideal structure. Usually, fibres include impurities in their structure, which contribute to the degradation of their properties. Apart from the impurities, the orientation of the crystals is another crucial factor, determining the final properties of the fibres. X-ray and electron diffraction, and scanning and transmission electron microscopy are, perhaps, the most effective methods for investigating the structure of carbon fibres.

Numerous models have been proposed from different researchers for the microstructure of carbon fibres [19], [20]. Diefendord and Tokarsky [21] proposed that the basic structural unit (BSU) of PAN based carbon fibre consists of undulating ribbon-shaped layers. As the modulus of the fibre increases, these ribbons thicken and the amplitude of the undulation increases. However, to account for the lateral cohesion of carbon fibres, they proposed that the ribbons form a basket weave structure as shown in Figure 3. 2.

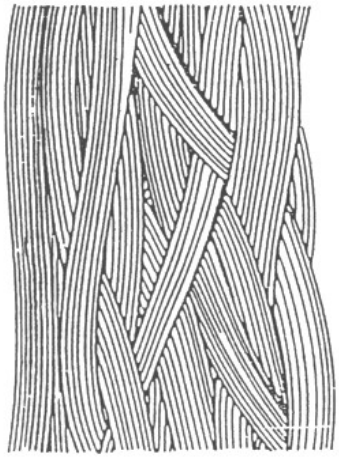

Figure 3. 2 Diefendorf and Tokarsky model for the structure of PAN-based carbon fibres [21].

Oberlin and Guigon [22] proposed that the lamellae consist of folded and crumpled sheets of layer planes which are linked to each other at their boundaries. For temperatures below 800°C the BSU, which consist of short lengths (10 Å) of two or three parallel carbon layers, start to pile up and form a disordered columnar structure as impurities and volatiles are released. Between 800°C and 1500°C, the columnar structure increases in length with a higher degree of orientation of the BSU. Between 1500°C and 1900°C the columnar structure disappears as wavy ribbons or wrinkled layers are formed by the joining of adjacent columns. By about 2100°C most of the waviness has disappeared, and in plane defects have been greatly reduced. Above 2100°C stiff, flat carbon fibres are observed and three-dimensional crystal growth commences [18]. Thus, the graphitization corresponds to the removal of structural defects and increase of the orientation parallel to the fibre axis.

Two different models have been proposed. For the *high-strength fibres (HT)*, (Figure 3. 3 (a), lamellae are formed by sheets of BSU associated edge-to-edge in a zigzag form, with twisting and tilting at the boundaries. When these sheets touch each other, either transversely or longitudinally, they become bonded to each other.

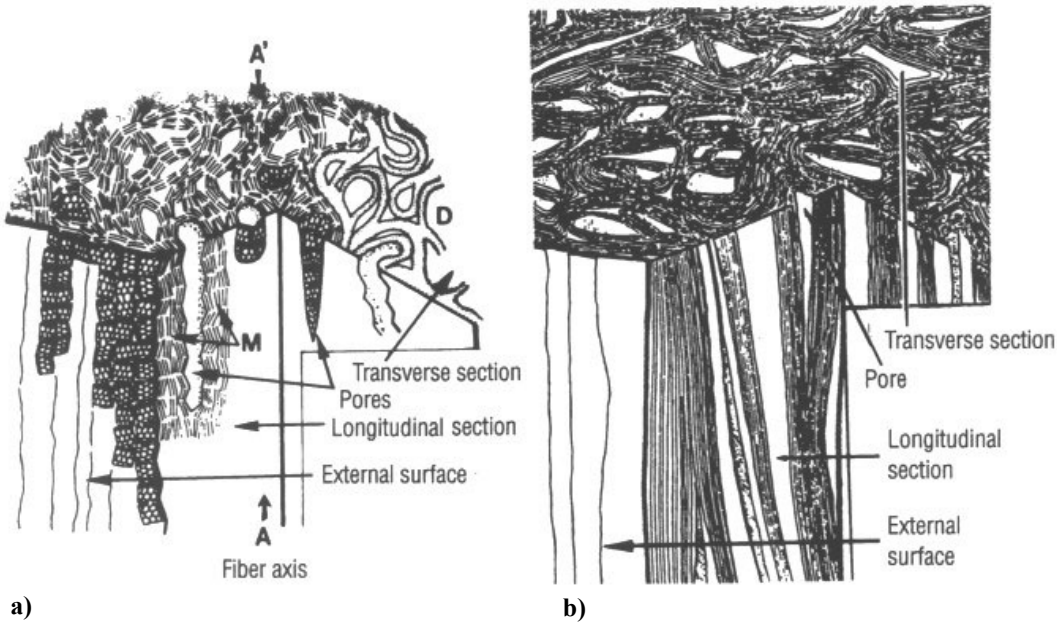

Figure 3. 3 Structural models for PAN-based HT and HM carbon fibres based on transmission electron microscopy studies [22].

For the *high-modulus fibres (HM)* model, (Figure 3. 3 (b)) the bent layers are more perfect and consist of larger BSUs, with elongated and entangled pores. There are also fewer boundaries between the BSUs; thus, the borders approach the classical definition of grain boundaries.

3.2 Conduction in Graphite and Carbon Fibres

After the graphitization procedure, the electric properties of carbon depend on its microstructure and T_{HT}. At the one extreme, including what is known as graphitic, the structure approximates to that of a single crystal. At the other extreme, including what is known as carbon fibres, lattice defects and impurities will modify the electronic structure in several ways [23]. The electric properties of graphite and carbon are anisotropic. Along the layer axis, fibres can be classified as a narrow band semimetal, which is the region from semiconductors to conductors.

According to the band theory the electrons in the graphite atom can be promoted from the valence band to the conduction band, since the energy gap at room temperature is between 0.03 eV and 0.04 eV, well below the limit of 2 eV [17]. As a consequence the graphite behaves as a conductor even at room temperature. The conduction process transverse to the layer axis is more complicated; graphite in that direction can be classified as semiconductor. The conduction is due to hopping of charge carriers between the graphene layers. A disorder between those planes, such as defects or impurities, would lead to rearrangement of the structure and to a correlated change in concentration, mobility and other parameters of the charge carriers [17].

The conduction mechanisms in carbon fibres are also affected by the T_{HT}, which is one of the most important stages during the production of carbon fibres. Mrozowski [24] developed a model to explain the major changes in the electronic structure which occur as T_{HT} is increased. Figure 3. 4 shows that the increase of T_{HT} leads to an increase in electric conductivity by reducing the energy gap between valence and conduction band.

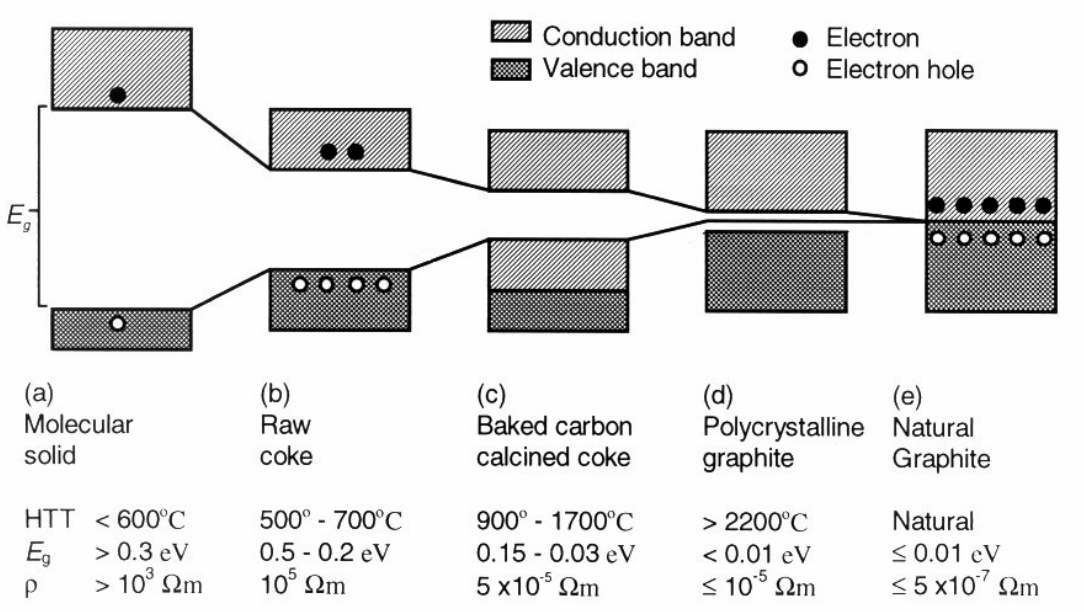

Figure 3. 4 The band structure of carbon fibres after different heat treatments [17].

At $T_{HT} \leq 1300$, the ex-polymer fibres are not really carbon fibres but rather partially pyrolyzed. As the temperature increases, a carbonization occurs leading to the formation of the planes of graphite and improving of crystal orientation; a slow rise in electric conductivity during graphitization points to the fact that the structure gradually becomes more perfect and the number of electrons removed from the conduction band would be gradually eliminated as a result of growth of crystals during graphitization [24]. The regions shown in Figure 3. 4 (d), (e) correspond to the three dimensional graphite. For T_{HT} greater than 3500 °C, the structure of carbon can approach that of single crystal graphite; similar changes in conductivity in PAN-based fibres have been reported by other researchers as well [25], [26], [27]. As it can be seen, the increase of the T_{HT} and the fibre modulus leads to an increase of the electrical conductivity of carbon fibres.

3.2.1 Electrical resistivity of carbon fibres

The electrical resistivity of carbon fibres has been studied extensively because of the usefulness of employing parameters, such as room temperature resistivity, as a diagnostic tool of other fibres properties including the structural perfection.

For the majority of investigations, the longitudinal resistivity of fibres was measured instead of the transverse. The measurements have been taken using the four probe method, in which two current leads are attached to the ends of a single fibre, or bundle of fibres, and two potential probes are introduced at about quarter of the length of the fibre from the end; contacts are usually applied with gold or silver epoxy.

Shindo [28] was the first to report the effects of carbonisation of PAN fibres on electrical resistivity. He reported the resistivity decreased from 5 Ω.m at 750°C to 20 μΩ.m after heating to 1000°C. It was suggested that this change is due to the carbonisation of the PAN precursor which led to the development of length and order in the crystallites. The rate of decrease of resistivity slows down for temperature between 1000°C and 2500°C.

The effects of T_{HT} of carbon fibres on the electrical resistivity have also been reported by other investigators [15], [23], [29], [30].

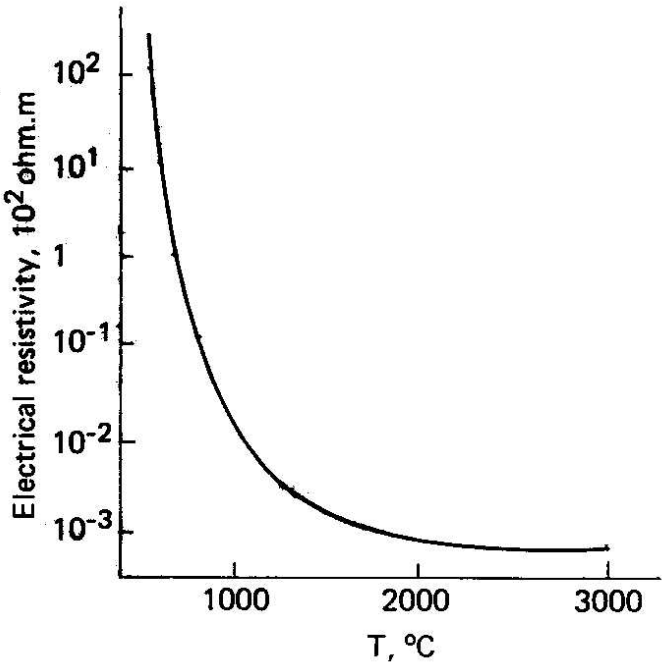

Figure 3. 5 Change of electrical resistivity of carbon fibre with heat treatment temperature (T_{HT}) [25].

Up to T_{HT} 1000-1100°C, the electrical resistivity drops sharply and then, with realization of the structure typical of carbon fibres, changes only slightly (Figure 3. 5).

It has also been suggested that the resistivity value of carbon fibres (at room temperature) is always higher than those of crystal graphite, regardless of the extent of carbonisation. This results from the residual defects, such as impurities or scattering effects of crystalline boundaries, remaining in the fibres [29].

In modern techniques and after investigating the effects of processes, carbon fibres are manufactured with consistent physical properties [31]. Table 3. 1 and Table 3. 2 show the electrical resistivity of crystal graphite and commercial carbon fibres. As it can be seen, an increase in the modulus of carbon fibres leads to lower values of electrical resistivity. As explained in Section 3.2, due to the high T_{HT} required for producing high modulus fibres, the fibres structure becomes more perfect, compared to low modulus fibres, improving simultaneously the orientation of the graphene planes and increasing the conductivity.

Other factors affecting the electrical resistivity, other than the $T_{HT,}$ are the crystallite size, the precursor material and the fibre diameter. For example, the resistivity ranges from 0.25-1.75 μΩ.m for fibres with diameters ranging from 1.6 to 34 μm respectively [32].

Table 3. 1 Electrical properties of single crystal graphite and bulk graphite [33].

Material	***Longitudinal Resistivity (μΩ.m)***	***Transverse Resistivity (μΩ.m)***
Graphite Crystal	0.4 (// to the graphite plane)	40-30000 (⊥ to the graphite plane)

Table 3. 2 Electrical properties of carbon fibres [33].

Trade Name	*Type*	*Longitudinal Resistivity (μΩ.m)*	*Modulus (GPa)*
Torayca T300	PAN	16.0	230
Torayca T300J	PAN	20.0	230
Celion GY-80	PAN	6.0	572
Celion G50-300	PAN	10.0	358
Celion G30-600	PAN	15.0	234
Type I 303/B	PAN	8.5	319
Type II 341/B	PAN	13.9	235
P100	Pitch	2.5	690
Thornel P120S	Pitch	2.2	827
Thornel P100S	Pitch	2.5	724
Thornel P75S	Pitch	7.0	520
Thornel P55S	Pitch	8.5	380
Thornel P-25	Pitch	13.0	160

3.2.2 Effect of temperature and humidity

The effect of increasing temperature on electrical resistivity of carbon fibres has been studied by numerous researchers [15], [17], [34], [35]. The change in resistance of carbon fibres with temperature is highly affected by the structure of the fibre. Graphite and more perfect pyrolytic fibres (with $T_{HT} \geq 2700°C$) have a positive temperature coefficient of resistivity; this arises from the fact that due to their almost perfect crystal structure they behave as metals in which the carrier mobility decreases with rising temperature (Section 2.5). However, all the other types of carbon fibres act as semiconductors, in which the resistivity decreases with increasing temperature. Figure 3. 6, illustrates the effect of

temperature on the electrical resistivity for different types of carbon and for a single graphite crystal.

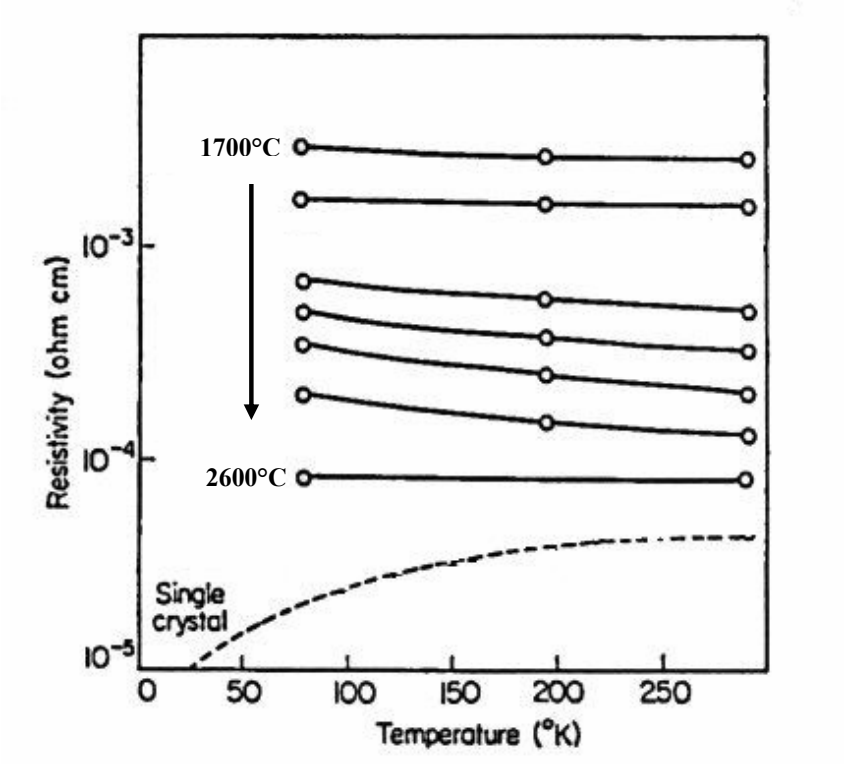

Figure 3. 6 Electrical resistivity as a function of temperature for industrial polycrystalline graphite and single graphite crystal. The dotted curve is the resistivity of a single crystal and the other curves are for a series of pyrolytic graphites deposited at temperatures between 1700°C and 2600°C [17].

No detailed data have been reported, in the literature, on the change in the electrical properties of carbon fibres with humidity variation. Pan [36] reported a decrease in electrical resistance of pitch-based carbon fibres with humidity varying from 27%-90%. The author suggested that this was due to the hopping conduction of protons dissociated from absorbed water molecules. He also reported that the change in electrical resistivity was dependent on the precursor from which the fibres were made; PAN-based carbon fibres, in contrast to pitch fibres, showed hardly any change in electrical resistivity.

Some studies [37] showed that the water absorption of carbon is not as active in the basal direction (0 0 1) as in the (1 1 0) and (1 0 0) directions. PAN fibres have more axial (basal) preferred orientation than pitch based fibres which it can be assumed are

randomly oriented; in other words, more active species would appear on the surface of the pitch-based fibres promoting the absorption of water onto the surface.

3.2.3 Piezo-resistance

Piezo-resistance is the change in resistance which occurs when a fibre is strained. The change in electrical resistivity of carbon fibres must be understood first, because this will significantly affect the electrical response of CFRP to mechanical strain, which is one of the main issues of this study.

Numerous measurements have been made on the piezo-resistance of ex-PAN fibres [15], [23], [38], [39]. As shown in Figure 3. 7, most fibres showed a linear increase in resistance above 0.1% strain.

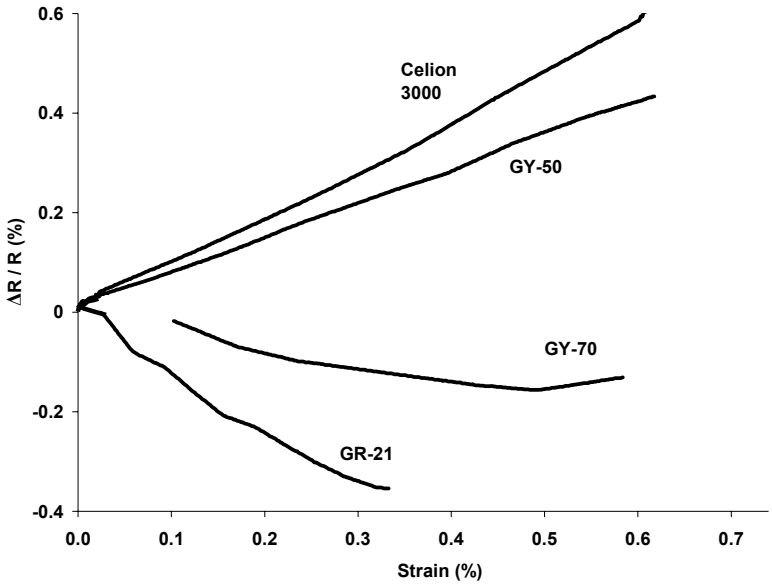

Figure 3. 7 Change of resistance ΔR/R with increasing longitudinal strain for ex-PAN fibres, redrawn from [23].

An obvious source of piezo-resistance is the geometrical effect of mechanical strain on fibres. As discussed in Chapter 2, the resistance of a conductor is a function of three variables:

$$R = \rho \frac{L}{A} \qquad (3.1)$$

When a fibre is put under uniaxial tension, it will increase in length and decrease in diameter. Both of these effects will contribute to the increase of the resistance assuming that the resistivity does not change. It is therefore useful to separate the geometric effects from changes in resistivity, which can produce either a negative or positive contribution to the piezo-resistance.

Equation (3.1) can be differentiated to yield the sources of small changes in resistance:

$$dR = \frac{\rho}{A} dL - \frac{\rho L}{A^2} dA + \frac{L}{A} d\rho \qquad (3.2)$$

or, in terms of relative resistance [40]:

$$\frac{dR}{R} = \left[\frac{dL}{L} - \frac{dA}{A} \right] + \frac{d\rho}{\rho} \qquad (3.3)$$

The first two terms are due to geometrical effects and the third term is due to changes in the resistivity itself. The fibre cross-section is:

$$A = \pi \cdot r^2 \qquad (3.4)$$

where r is the initial radius of the fibre.

Differentiating once again:

$$dA = 2\pi \cdot r dr \qquad (3.5)$$

Substituting this into equation (3.3), and simplifying:

$$\frac{dR}{R} = \left[\frac{dL}{L} - 2\frac{dr}{r}\right] + \frac{d\rho}{\rho} \qquad (3.6)$$

The two terms within the brackets contain the two orthogonal unit strains, ε_L and ε_r, that are produced when the fibre is stretched:

$$\frac{dR}{R} = \left[\varepsilon_L - 2\varepsilon_r\right] + \frac{d\rho}{\rho} \qquad (3.7)$$

Further, the radial strains are the compressive Poisson strains corresponding to the longitudinal tensile strain:

$$\varepsilon_r = \frac{dr}{r} = -\nu\frac{dL}{L} = -\nu\varepsilon_L \qquad (3.8)$$

where ν is Poisson's ratio. Substituting this result into equation (3.7) and simplifying, we obtain that the relative resistance change would appear to be influenced by both the mechanical and electrical properties of the strained conductor:

$$\frac{dR}{R} = [\varepsilon_L(1+2\nu)] + \frac{d\rho}{\rho} \qquad (3.9)$$

The increase in resistance with mechanical strain (often termed piezo-resistivity) is usually characterised by the gauge factor (**GF)**, defined as:

$$GF = \frac{\Delta R}{R_0\varepsilon_L} \qquad (3.10)$$

where ΔR is the increase in resistance caused by application of a strain ε_L and R_0 is the resistance at zero strain.

For piezo-resistance changes caused purely by deformation induced geometrical changes and not by resistivity changes, the gauge factor can be shown to be equal to:

$$GF = (1 + 2\nu) \qquad (3.\ 11)$$

Resistivity also changes with applied strain due to changes in the density of electrons per unit volume of material; it can be shown that for finite deformation intervals [40]:

$$\frac{\Delta R}{R} = 2\varepsilon_L + \varepsilon_L^2 \qquad (3.\ 12)$$

and the gauge factor:

$$GF = 2 + \varepsilon_L \qquad (3.\ 13)$$

Thus, although the GF can be as low as 2 at strains approaching zero, it is strain dependent, and will increase for increasing strain. Real metallic materials exhibit a range of non ideal behaviours when ΔR/R is plotted against applied strain for a range of deformations, and gauge factors from 2 to 4 are frequently reported. Carbon fibres [23], [39], [41], [42] have a resistivity from 1.5-20 μΩ.m, depending on the fibre type. The T300 low modulus fibres used in this work have a resistivity of 17 μΩ.m [19]. No data on the piezo-resistance of T300 fibres themselves could be found, but Dresselhaus [23] reports values of between 2 and 3 for the GF of a range of low modulus fibres at strains up to 0.3-0.5%.

The degree of crystallite orientation would significantly affect the response of electrical resistance of carbon fibres to mechanical strain [25], [38], [39], [40], [41], [42], [43]. As

mentioned previously, (Section 3.2), the graphite crystallite has marked electrical anisotropy. The resistivity parallel to the c-axis, (Figure 3. 1), is of the order of 10^3 times the resistivity perpendicular to the c-axis [38]. Consequently any reorientation during straining will have a marked influence on the electrical resistance of the fibres.

Curtis et al [43] showed that crystallites with the greatest misorientation experience the greatest rotation when fibres are strained. Subsequently, poorly oriented fibres (those in which many of the crystallites have c-axes inclined at large angles to the fibre axis) would show maximum reorientation and the maximum effect on the electrical resistance.

Investigations on the piezo-resistance of ex-PAN and pitch fibres revealed that low modulus fibres have a linear positive piezo-resistance [23]. This linear positive change can be explained by the changes in shape. However, high modulus ex-PAN and pitch fibres were found to have a negative piezo-resistance. It has been suggested [23] that the changes in the piezo-resistance could be understood in terms of electron density changes. The electron density changes occur because straining the fibres pushes the graphite basal planes closer together, so that the carrier density increases. The increase in 3-D ordering of the graphite leads to an increase of modulus, which explains the negative nature of piezo-resistance in high modulus fibres.

The T_{HT} of carbon fibres also affects the piezo-resistance. Investigations on ex-PAN, and pitch fibres have shown positive changes in resistance with increasing strain when the T_{HT} of the fibres is between 1000°C and 2400°C [29], [44] with GF varying between 1.3-1.8 [39]. In addition, negative ratios have been reported at lower strains and positive at higher strains when the fibres are treated at 2700°C.

3.3 Electrical Resistivity of Epoxy Resins

Epoxy based resin systems have been widely used in the aerospace industry due to the high heat resistance, greater than 200°C, good environmental resistance and high

strength. The use of additives such as flexibilisers, fillers, in epoxy systems can modify their properties.

Polymers are insulators of non-crystalline nature. Their poor electrical conductivity is because of the unavailability of large number of free electrons to participate in the conduction process. The values of electrical volume resistivity were first used to ascertain whether phenolic polymers can be employed as insulating materials [45]. After the extensive use of polymers, electrical resistivity measurement techniques were developed in order to measure indirectly the effect of other factors on polymer structures such as state of cure, moisture and effects of additives. The investigations of epoxy resin whose data influence electrical resistivity measurements of CFRPs are described below. The electrical properties of epoxy resins can be changed during curing and post-curing. Table 3. 3 shows some typical values of volume resistivity of different types of epoxy resins [33].

Table 3. 3 Electrical properties of epoxy resin [33].

Type	***Volume Resistivity (Ω.m)***
EH25	7.34×10^{11}
M18	9.0×10^{12}
M36	1.25×10^{13}

3.3.1 Effect of moisture

The effects of relative humidity **(RH)** on the electrical resistance of several plastic laminates were studied at General Electric as reported by Kroschwitz [46]. It has been found that both volume and surface resistivity decrease with exposure time to 90%

humidity environment. The author has also reported that surface resistivity decreases rapidly, often by several orders of magnitude, during the first minutes of exposure to high humidity environment, than the volume resistivity.

The increase in conductivity was attributed to the interaction of water molecules with epoxy resin. Permeability, controlled largely by the vapour pressure of the water, is the important factor at high humidity, where moisture penetrates slowly into the polymer. Similar observations were also reported by other researchers [47], [48] who investigated the effect of humidity not on pure resin, but on epoxy laminates reinforced with glass fibres**.** The authors have reported that apart from decrease of electrical resistivity with time of exposure, the conductance for the same time of exposure increases as the relative humidity (RH) increases; they also reported the reversible nature of the moisture since no chemical change takes place after exposing the samples to moisture.

4 CONDUCTION PROCESSES IN CARBON FIBRE REINFORCED POLYMER COMPOSITES

This Chapter is concerned with the literature survey of electrical resistivity measurements of carbon fibre reinforced polymer composites. The electrical potential technique utilises the electrical conduction of carbon fibres to form a sensing network. The electrical conduction processes are extremely complex in continuous CFRP composites.

There is a low resistivity along the fibres and high resistivity transverse to the fibre direction; therefore, when a current is applied to a composite sample, the electrons flow easily along each individual fibre. Transverse current flow proceeds via many paths of longitudinal fibres and fibre-fibre contacts. The transverse and through thickness resistivity will also be a function of fibre volume fraction as well as the number and area of contact points. The conductivity through thickness in a unidirectional laminate is very similar to the transverse conductivity. In multidirectional laminates, the presence of additional layers of fibres with different orientations will further complicate the conduction process.

This Chapter is organised as follows: In Section 4.1 the basic concept of electrical resistivity measurements in composites and typical electrical resisitivity values of CFRP composites are given. Section 4.2 presents the theoretical models to predict the electrical properties of CFRP. The effects of fibres orientation and volume fraction on electrical resistivity are given in Section 4.3 and Section 4.4. The response of electrical resistance to mechanical strain occupies a significant part in this charter and it is developed in Section 4.5. Finally the effects of temperature and humidity on electrical resistivity are presented in Section 4.6.

4.1 Electrical Resistivity Measurements

Composite materials are formed by the combination of two or more materials in order to achieve properties (physical, chemical, etc.) that are superior to those of its constituents. Carbon fibre reinforced polymers composites are inherently inhomogeneous materials, consisting of reinforcing fibres, which in general are electrically conductive, dispersed in an insulating matrix resin. CFRP composites can be used in unidirectional **(UD)** form, in which there is only one orientation of the fibres.

For most engineering applications, multidirectional rather than unidirectional laminates are used. Figure 4. 1 shows three layers of a composite structure as well as the direction of the fibres.

Normal engineering volume fractions in composites vary between 50-60%. In the direction along fibres, CFRP composites can be considered electrically homogenous and the electrical conductivity along fibres axis can be calculated by the summation of the conductivity of individual fibres. The electrical conductivity in the direction transverse to fibre axes depends on the fibre-fibre contact between reinforcing fibres [51], [52], [53], [54], [55].

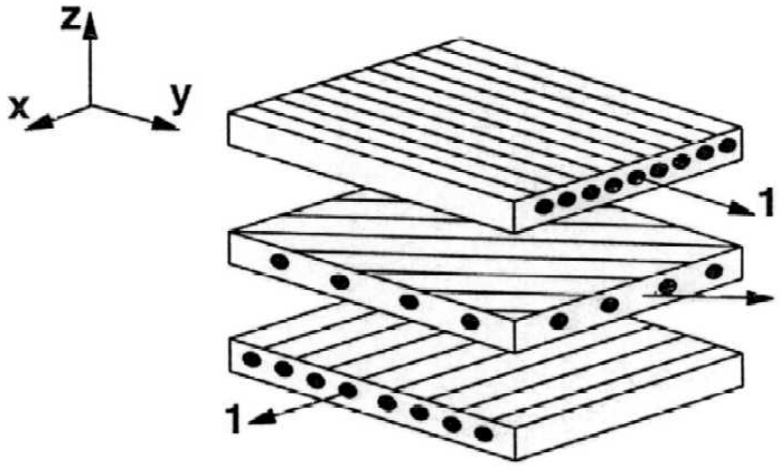

Figure 4. 1 Assembly of three layers of composite into a laminate [50].

The resistivity of unidirectional CFRP composite is highly anisotropic. There is low resistivity along fibres and high resistivity transverse to the fibre direction. This can be seen in Figure 4. 2.

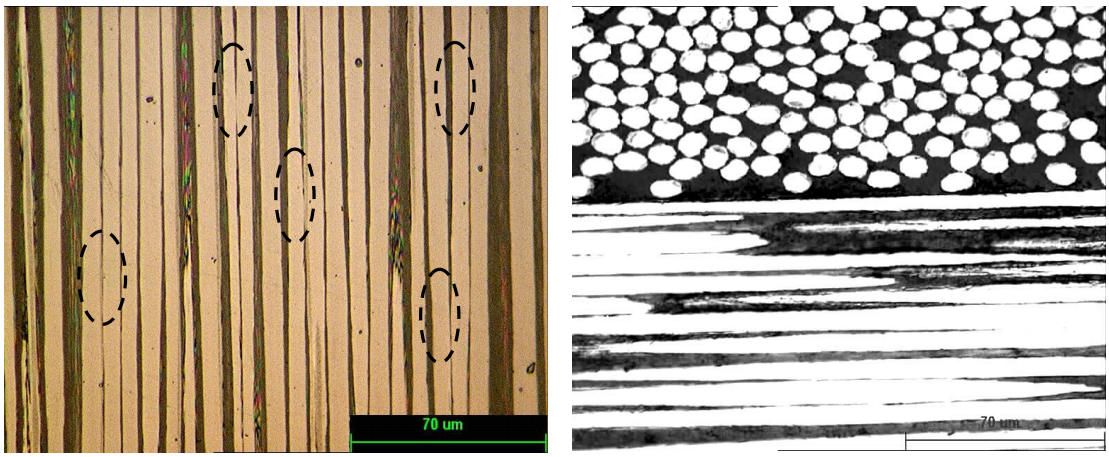

Figure 4. 2 Micro image of carbon fibre alignment in a composite a) parallel to the fibre direction and b) cross-section. Dotted circles indicate possible contact points for transverse electrical conduction in this cross-section [51].

When a current is applied to a composite sample, the electrons flow easily along each individual fibre. Fibres are separated by insulating resin. As a consequence of the very low specific resistivity of the carbon fibres and the insulating character of the epoxy matrix, the electrical resistivity in the longitudinal direction only depends on the properties of the carbon fibres. The resistivity parallel to the fibres of a unidirectional laminate with a 60% volume fraction of T300 fibres has been measured as 0.022 mΩ.m [56].

The resistivity of the composite ρ_c, including the insulating matrices, parallel to the fibres can be calculated using:

$$\rho_c = \rho_f / V_f \qquad (4.\ 1)$$

where ρ_f is the longitudinal resistivity of the carbon fibres, and V_f the volume fraction of fibres.

The current will flow with greater difficulty transverse to the fibre direction. In most cases, carbon fibres are coated with polymer sizing agents for handling protection or interface strength improvement. Electrons have to overcome these barriers to complete conduction. As Figure 4. 2 shows, transverse conductivity can only be achieved via fibre-to-fibre contact. As a consequence, the transverse resistivity is found to be as high as 310 mΩ.m, more than 10^4 times greater than the longitudinal [56], [57]. The fibre volume fraction strongly affects the formation of connecting electrical network within the composite as is discussed in the following section. Table 4. 1 illustrates the longitudinal and the transverse resistivity, for different types and volume fraction of carbon fibres.

Table 4. 1 Electrical resistivity of unidirectional CFRP composites [33].

Material Type Fibre/Resin	***Volume Fraction V_f (%)***	***Longitudinal Resistivity ($\mu\Omega m$)***	***Transverse Resistivity ($\mu\Omega m$)***	***ρ_v/ρ_L***
Type I/Epoxy	40	22	4347	198
Type I/Epoxy	50	19	2703	142
Type I/Epoxy	60	15	1961	131
Type II/Epoxy	40	40	8333	208
Type II/Epoxy	50	29	3226	111
Type II/Epoxy	60	24	1724	72
CF/Epoxy	40	110	15000	136
CF/Epoxy	50	90	5000	56
CF/Epoxy	60	75	2000	27
CF/Epoxy	65	25	10000	23
CF/Epoxy	70	65	1500	400
XAS/Epoxy	65	154	600000	3896

The conductivity through thickness in a unidirectional laminate is very similar to the transverse conductivity [58]. However, other investigators report smaller values of through thickness conductivity which are 2.5 and 10 times less than conductivity transverse to the fibre direction [57], [59]; this is attributed to the existence of resin rich interlaminar regions in the thickness direction, which deteriorates the creation of a conductive path in that direction. The quality of the autoclave manufacturing processes, such as debulking of the laminate prior to curing, may also affect the through thickness conduction processes by decreasing the rich resin regions and so the electrical resistivity.

4.2 Electrical Conduction Models

Electrical conduction models have been developed in order to predict the resistance of composite materials. These models form the basis of predicting the effect of damage on resistivity. The ultimate goal is to predict the electrical response of CFRP structures to mechanical loading and/or damage. Initial simulations were based on very simple models derived from mechanics of materials and electrical circuit analysis methods. However, due to the high anisotropy of electrical properties of CFRP composites and their complicated pattern of damage, later, more complicated models were developed.

4.2.1 Longitudinal resistivity

As mentioned in Section 4.1, the longitudinal conduction in unidirectional CFRP composites is fibre dominated. The carbon fibres are the conductors while the resin act as insulator and its role is not critical in the conductivity procedure. The electrical properties in the longitudinal direction depend on the fibres volume fraction and can be predicted using the parallel resistance model and the rule of mixtures.

4.2.1.1 Parallel resistance model

The resistance of a unidirectional composite in the longitudinal direction can be calculated considering the fibres as resistors connected in parallel in an electric circuit [60]. The connected fibres are connected at the ends with electrodes to measure the

electrical resistance. The resistance of the composite R_c can be calculated by dividing the resistance of fibres by their total number:

$$R_c = \frac{R_f}{N} \qquad (4.\ 2)$$

where R_f is the resistance of a single fibre, and N is the total number of fibres. The form of the parallel resistance model is represented in Figure 4. 3.

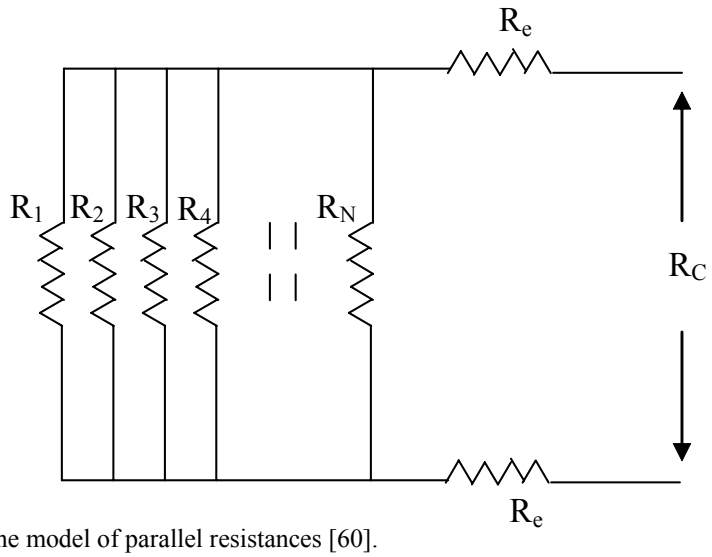

Figure 4. 3: The model of parallel resistances [60].

Re is the electrode resistance.

The resistance of the single fibre is calculated from the fibre resistivity following the relationship:

$$R_f = \frac{\rho_f L}{A_f} \qquad (4.\ 3)$$

where A_f is the cross-sectional area of the fibre.

The number of fibres can be calculated from the volume fraction of the composite, $V_{f,}$ according to the following equation:

$$N = \frac{A_c V_f}{A_f} \qquad (4.\ 4)$$

By substitution of equations (4.3) and (4.4) in equation (4.2) the following is obtained:

$$R_c = \frac{\rho_f L}{A_c V_f} \qquad (4.\ 5)$$

The equation above relates the longitudinal resistance of the composite to the fibre resistivity, volume fraction and specimen length. In equation (4.5), should also be added the contact resistance, which consists of the conductive resistance between the probes and the composite, and the resistance of the copper strips are used for introducing the current. The final equation takes the form of:

$$R_c = \frac{\rho_f L}{A_c V_f} + 2R_e \qquad (4.\ 6)$$

Prabhakaran [61] proposed that the CFRP laminates can be modelled using a parallel resistance approach; he used this model to simulate crack growth behaviour for multidirectional specimens subjected to tensile loading. However, the parallel resistance model is not suitable for multidirectional laminates. In a composite structure, broken fibres are still able to carry electrical current. When their orientation and loading conditions are proper, they create electrically conductive paths in the transverse and in the through thickness direction.

Due to its simplicity, the parallel resistance model cannot explain the fibre contact phenomena of the broken fibres within either unidirectional or multidirectional composites.

Takeda and co-workers [63], [64], [65], [66] developed some new models which predict this convoluted electrical behaviour. Based on experimental results, they developed the theory of the 'electrical ineffective length' over which a broken fibre loses its current carrying capacity. Figure 4. 4 shows this configuration. The electrical ineffective length is a function of fibre volume fraction [67]. Their modified DC circuit model of parallel arrays of resistors consists of parallel cells of fibre composite of length equal to the electrical ineffective length δ_{ec}, which are connected by conductive paths in a way that the resistance change of one cell does not affect the neighbouring cells in series with it.

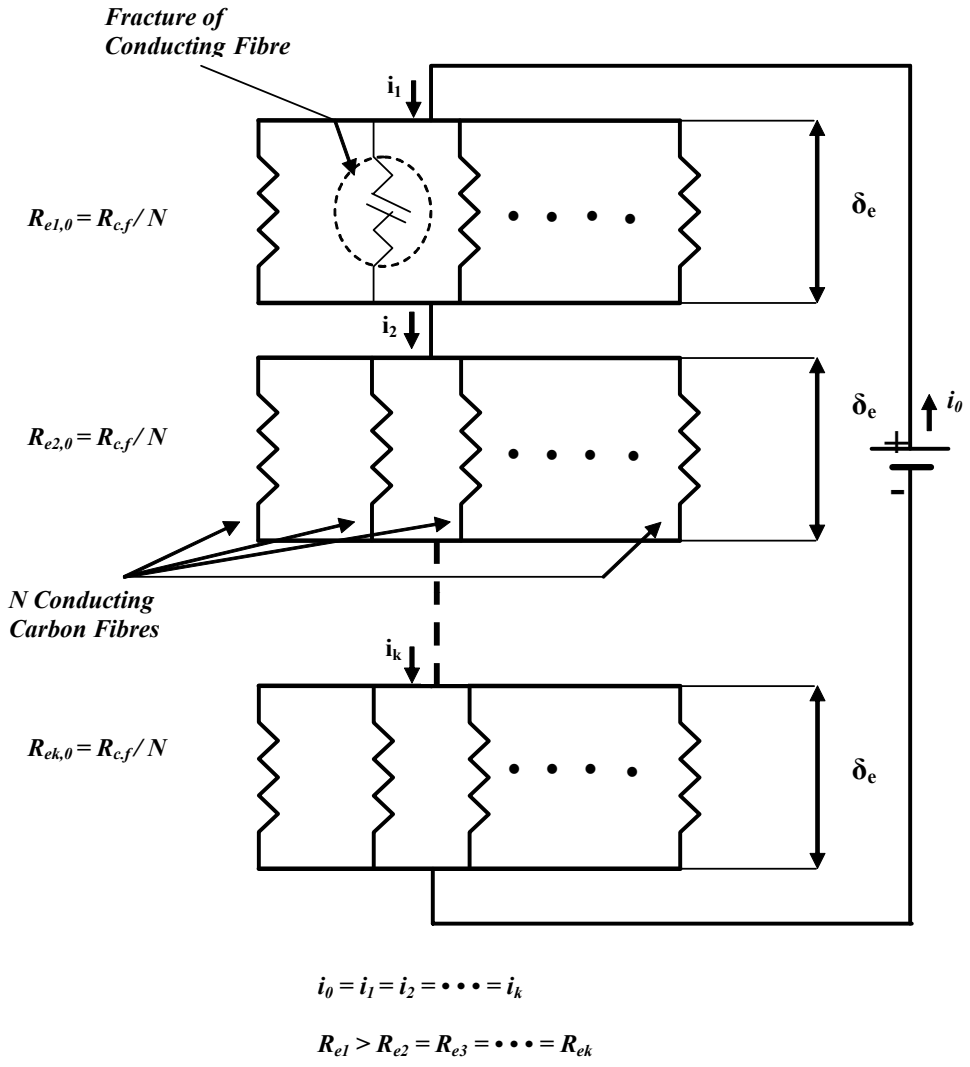

Figure 4. 4: DC series circuit with equally spaced discrete parallel cells (reprinted from [62]).

Using the Global Load Sharing (GLS) equation for mechanical ineffective length [68], and the Weibull distribution function [69], the authors developed a simple mathematical expression which correlates the electrical resistance change to the number of broken fibres within the electrical ineffective length, under tensile loading [62]; the proposed equation can be inverted to estimate the extent of mechanical damage from measurements of the electrical resistance. The GLS model assumes that the load, lost by a fibre at some axial position due to fibre breakage, is transferred equally to all unbroken (elastic) fibres in the cross-sectional plane. The Weibull distribution function describes the statistical spread of strengths, for the cumulative probability of fibre failure.

4.2.1.2 Rule of mixtures

In general, the properties of the composites are an average of the properties of the constituents. The former can be identified using the so called 'rule of mixtures' [70]. The electric conductivity is obtained as follows:

$$\sigma_0 = \sigma_f V_f + \sigma_m (1 - V_f) \qquad (4.\ 7)$$

where σ_m is electrical conductivity of matrix resin.

Since the matrix resin is usually an electric insulator, σ_m vanishes; that implies the following relationship:

$$\sigma_0 = \sigma_f V_f \qquad (4.\ 8)$$

Equation (4.8) represents the linear relationship between electric conductivity along the fibre direction and fibre volume fraction.

Knibbs et al [71] used the rule of mixtures to predict longitudinal electrical properties of unidirectional CFRP specimens. They reported that the rule of mixture predictions is 5% lower than the experimentally measured resistivity, suggesting that this may be due to fibre misorientation. Todoroki also, used the rule of mixtures to calculate the longitudinal and transverse resistivity of unidirectional CFRP composites [57].

4.2.2 Transverse resistivity

The resistivity transverse to the fibre direction is quite complex. It is a 3-D problem, with electrical conduction occurring in other directions apart from the longitudinal. This is because there are contacts between fibres of adjacent tows. In other words, a fraction of fibres of one tow touch a fraction of fibres of an adjacent tow here and there along the length of the fibres. These contacts result from the fact that fibres are not perfectly straight or parallel (even though the lamina is called unidirectional). Effective medium theory and percolation theory have been used in order to study the transverse conductivity.

4.2.2.1 Effective medium theory

The effective medium theory (EMT) can be dated to a 1935 paper by Bruggeman [72] as is reported by Kováčik [73]; he introduced the classical theory of conduction of mixtures to calculate the conductivity of two or more phase composites. The effective medium theory states that the average effects of random resistors may be represented by an effective medium. This defined as the medium in which the effects of external fields applied to a random resistor network are assumed to be equal to internal fields [74].

When the effective conductivities of the two phases are comparable, the effective conductivity σ_{eff} can be determined by the rule of mixtures and it is linearly dependent on the volume fraction. When the difference between electrical conductivities of constituent phase increases, the dependence of the effective conductivity on the volume fraction becomes non-linear and is modelled using the effective medium theory; the mathematical details of effective medium theory can be found elsewhere in the literature [75].

The drawback of EMT is that it fails to predict the conduction processes when the electrical conductivities of the two phases significantly differ between them [76], [77]. This is the case in CFRP where the carbon fibres are highly conductive and the resin is considered as insulator. In this case the transverse conductivity can be predicted using percolation theory.

Hence modified effective medium theories were developed, such as General Effective Media (GEM) equation, in order to predict the electrical properties of CFRP composites by taking into consideration the fibre-to-fibre contacts.

4.2.2.2 Percolation theory

As discussed in Section 4.2.2, in CFRP composites, the transverse and through thickness electrical conduction is due to fibre-fibre conducts which are extended randomly in the composite. The conductivity in these directions will be highly dependent on the number of fibre contacts.

The most general approach to description of charge transport in conducting polymeric composites in relation to the content of conducting particles is provided by percolation theory [78]. The percolation theory is a statistical method and it calculates whether particles are in contact with each other or not, in a certain material environment. Inherent to the theory is the fact that at some critical probability, called the *'percolation threshold'*, a connected network of sites is formed which spans the sample, causing the system to 'percolate'. The fraction of fibres or fillers required to achieve percolation can be modelled by a Monte Carlo method [78]. Predictions have shown good agreement with experimental data, but the results are dependent on many variables, including lattice size, particle-particle penetration, and particle dimensions.

Simple models of the ordering of globular particles in the resistor network in the non-conducting matrix revealed that the conductivity σ of the percolation system depends on the concentration of conducting elements V as a power law:

$$\sigma = \sigma_0 (V - V_c)^t \qquad (4.\ 9)$$

where V_c is the critical volume fraction (percolation threshold). The critical exponent t expresses the rate of conductivity change in the region of V_c, and σ_0 is the conductivity of the conducting phase.

Figure 4. 5 illustrates the percolation phenomenon in composite materials. At low concentration of conducting fillers, below Vc, the composite behaves as an insulator, while above Vc as a conductor.

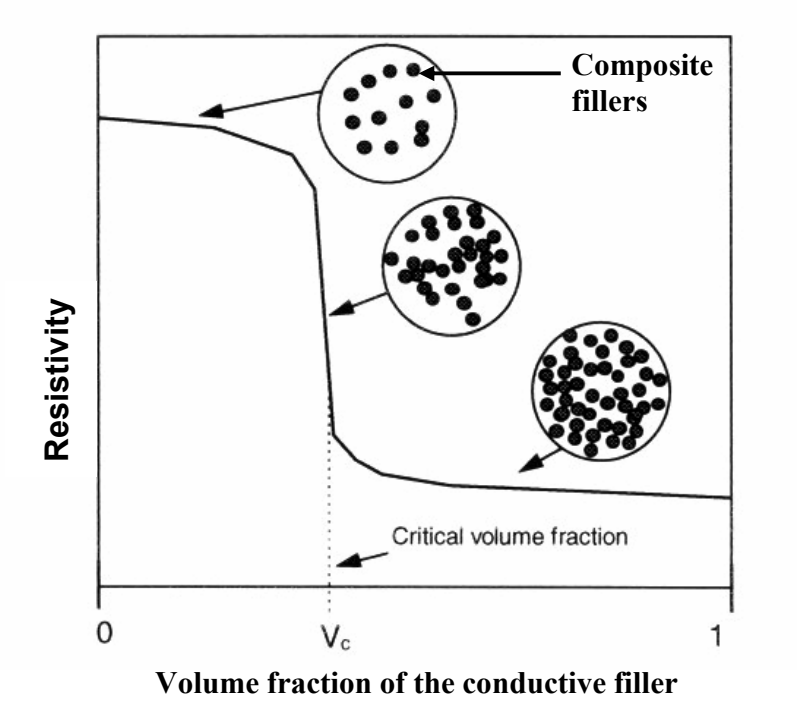

Figure 4. 5: Percolation theory as applied to composites [80].

The effect of fibre volume fraction on electrical conductivity of composites has been studied using *site* and *bond* percolation models [79], [80], [81]. Figure 4. 6, shows the site percolation on a square lattice. Site percolation occurs when the sites of a lattice are occupied randomly until a continuous linkage is formed and adjacent filled sites are assumed to be connected. Bond percolation occurs when all the sites are occupied but the bonds between the sites are randomly occupied. At low values of concentration V, only a small number of occupied sites exist. As Figure 4. 6 shows, when the concentration V is increased, the average size of clusters increases. At the critical concentration V_c, a large cluster appears which connects opposite edges of the lattice. This cluster is called *infinite cluster*. When V is increased further, the density of the infinite cluster increases since more and more sites become part of the infinite cluster, and the average size of the finite clusters, which do not belong to the infinite cluster, decreases.

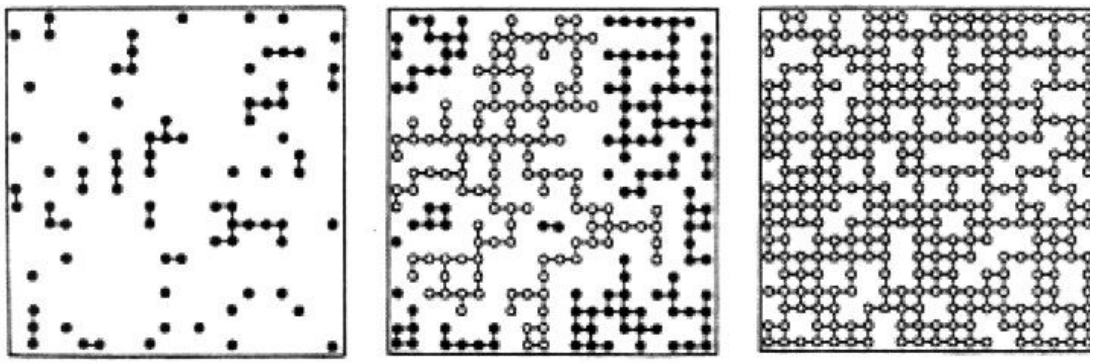

Figure 4. 6: Site percolation on the square lattice: The small circles represent the occupied sites for three different concentrations: V=0.2, 0.59 and 0.80. Nearest-neighbour cluster sites are connected by lines representing the bonds. Filled circles are used for finite clusters, while open circles mark the large *infinite* cluster [81].

As reported in the literature, percolation theory is especially critical for short fibre reinforced and particulate composites because before percolation threshold is reached, the electrically conducting composite materials behave as insulators or semiconductors.

However, after the percolation threshold is exceeded the conductivity increases rapidly to a maximum level which is not significantly affected any more with a further addition of carbon fibres [82], [83], [84].

The percolation theory has widely been used in order to predict the behaviour of mixtures with conducting and insulating components. However, the major drawback is that it is not able to accurately predict the percolation threshold in a conductive composite, and it cannot predict the actual conductivity of such a sample. For that reason other models are proposed as well. Weber and Kamal [85] used the fibre-contact model in order to calculate the volume resistivity of fibre reinforced polymers. Their predictions showed good agrrement with experimental data. Microstructural parameters, such as filler concentration and dimensions, aspect ratio and orientation of fibres were also taken into account. In their model, the conductivity of the matrix was estimated to be so low that it did not have any influence on the conductivity of the composites.

Percolation theory has proved to be extremely helpful in predicting the effect of volume fraction in simple spheres of short carbon fibres polymer composites. Unfortunately the volume fraction of the laminates used in this investigation is 60%, well above the percolation threshold which is approximately 31% for this type of material [81]. This implies that conduction processes will occur. In addition, the composite material consists of long fibres which crimp and touch each other along the length forming a complex conductive network. This implies the use of experimental configurations for the creation of an accurate model, describing the current conduction paths within a composite structure, formed by unidirectional layers.

4.3 Effect of Fibre Orientation

The resistivity of unidirectional CFRP as a function of fibre orientation was also investigated by various researchers. Knibbs and Morris [86] observed that the electrical resistivity increases linearly with the square of the sine of fibre direction angle. Similar observations are also reported elsewhere [87], [88]. Simultaneously, the transverse

resistivity (90° fibre orientation) was ten percent higher than this of other fibre directions. The increase of resistivity with increase of the fibre orientation angle was confirmed later by other researchers. In general, as the authors reported, the resistivity of such high anisotropy samples is very sensitive to quite small changes in fibre misalignment, and hence slight non-uniformities in the composite blocks could account for discrepancy.

Belani et al [89] used a single sample to investigate the effects of fibre orientation on resistivity. The authors measured the resistance between two electrodes at different locations; however, their measurements were not really representative of the effects of fibre orientation. Tse et al [90] studied the effects of sample dimensions on the electrical resistivity of samples with different fibre orientation angles. The authors observed a non-linear increase in resistivity with fibre orientation angle. They also reported that increase in resistivity with increases in sample length and constant width deviated from linear behaviour. Tse et al suggest that wide, short samples should be used for measuring resistivity to confine the applied field to the direction of resistivity measurement.

4.4 Effect of Volume Fraction

The fibre volume fraction of composite appears to be a highly influential factor in the conductivity process in both longitudinal and transverse directions. The ideal conductance in CFRP composites can be calculated by multiplying fibre volume fraction with the electric conductance of graphite fibre. In the transverse direction, conducting properties are related to the density of fibre to fibre contacts and percolation effects can be assumed to be the dominant process.

The increase in volume fraction increases the number of fibres available for electrical conduction and hence decreases the resistivity [57], [63], [91], [92]. In addition, the through thickness resistivity was found to be more sensitive in fibres volume than the transverse (90°) or longitudinal [57], [63].

4.5 Effect of Mechanical Loading

Damage due mechanical loading is one of the most common causes of failure of structures, as most structures encounter static or dynamic loading. Changes in resistance can be caused by a wide range of mechanisms such as fibre breakages, delaminations, and mechanical strain. Only fibre breakages and delaminations are relevant to structural integrity; therefore, it is essential to understand how electrical resistance changes in response to the other factors in order to evaluate structural integrity.

The effect of mechanical loading on individual fibres has been described previously in Chapter 3, (Section 3.2.3). The electric resistance change method has been employed recently by many researchers to identify internal damage such as delaminations and matrix cracks in carbon fibre reinforced plastics laminates. Irving and Thiagarajan [56] have showed that the irreversible changes in resistance during static and fatigue loading may be correlated with carbon fibre fracture. Resistance changes also early in the fatigue life of a sample, may be correlated with the eventual life. They concluded that monitoring current flow parallel to the fibres is successful in detection of fibre breaks [93].

Schulte is considered as one of the establishers of the use of electrical potential as damage sensing tool; he and his colleagues [53], [92], [94], [95], [96], studied the effects of mechanical loading in CFRP laminates using electrical resistivity measurements. The authors reported that the electric resistance in the fibre direction rises with the increase of applied tensile load in the fibre direction. The measurements were taken using a two probe method. These increases in resistance occur only during fatigue fibre breaks. Using the two probe technique, they have also investigated the response of fatigue loading on electrical resistance in a cross ply sample. They observed increases in resistance at initial life and at different stress levels. Variations in electrical resistivity could be related to the reduction of the longitudinal modulus. A reduction in resistance during fatigue life was attributed to the increases in temperature.

Damage detection under loading and increase of electrical resistance with load applied parallel to the fibre direction have also been reported by other researchers [61], [97], [98], [99], [100], [101]. Muto et al [99] pointed out that the loading history of a CFRP structure could be estimated by measuring the residual resistance of the CFRP after unloading. Rask and Robinson [102] studied the electrical resistance of unidirectional carbon composite as an indicator of strain in undamaged composites and as an indicator of fibre breaks in damaged composites. The authors reported the strain response and sensitivity of CFRP separated and insulated at the middle by a strip of Glass Fibres Reinforced Plastic (GFRP), observing that the change in resistance up to a certain level is reversible in a cyclic testing; Rask and Robinson also detected fibre breaks by increasing the strain levels and by observing irreversible changes in the resistance.

Abry and Salvia in agreement with the previous researchers, reported that strong changes in resistance in unidirectional samples were associated with damage propagation such as fibre breakages. An initial linear increase in resistance was attributed to the elongation of the fibres. The authors observed that each drop in modulus corresponded to an increase in resistance; the magnitude of these changes was dependent on the fibre volume fraction [91]. In the case of cross ply specimens, they were also able to detect transverse intralaminar cracks [103]. Abry and Salvia also found positive piezo-resistance changes for both unidirectional and cross ply specimens [91], [103], reporting that an electrically conductive path exists throughout the longitudinal and transverse direction of the composites. Thus, it is possible to monitor the electrical resistance of the entire composite using an electrode set on the surface.

Chung [104] reports early fatigue damage in UD specimens, during the first tenth (or less) of the fatigue life. For continuous CFRP composites the resistance increased during early fatigue due to matrix damage and fibre fractures. The irreversible part of the change in electrical resistance was due to damage; the reversible part was due to dimensional changes. The matrix cracking between the tows of lamina decreases the number of fibre-fibre contacts in the plane of the lamina, thus, decreasing the transverse conductivity. The effect of fibre fracture on the longitudinal conductivity in unidirectional samples is

significant, and Chung reports that the electrical resistance of CFRP increases stepwise when the electrically conductive carbon fibres are broken so that the longitudinal conductivity can indicate damage in the form of fibre fracture [54]. In similar experiments in cross ply specimens Wang et al report the detection of matrix cracks as well initiated in 90° plies which experienced tensile stress in 0° direction [105].

A considerable amount of their work was also focused on the response of the electrical potential to mechanical strain. Wang and Chung [108] report that changes in resistance in unidirectional continuous CFRP composites are not only due to dimensional changes but due to changes in the resistivity as well. In contrast to all the listed above researchers, they report that the longitudinal electrical resistance decreases reversibly with an increase in loading parallel to the fibre direction, and the transverse resistance increases reversibly upon loading tension in the same direction as before. Similar results have also presented by Cho et al. [106]. Wang and Chung attribute those changes to the reversible change in the degree of fibre alignment and the consequent decrease in the chance that adjacent fibre layers touch one other. Gauge factors varying from -35.7 to -37.6 and from 34.2 to 48.7 are also reported for the above configurations [107], [108], [109]. It is not clear to which extent these large values of GF may also be attributed to the processes followed for manufacturing the specimens. The authors also refer that the resistivity baseline gradually decreased as cycling progressed, particularly in the first few cycles because of the damage associated with plastic deformation, which causes an irreversible increase of the chance for fibres of adjacent laminae to touch one another.

For cross ply specimens, Chung reports decrease of electrical resistance upon loading in the direction parallel to the fibre direction (0°) and increase upon unloading in every cycle; this behaviour is explained by the fact that the presence of the 90° layers has a negligible effect on the chance that the adjacent fibre layers touch one another. However, when the potential is measured perpendicular to the fibre direction and for the same direction of loading as previously, the resistance increases upon loading and decreases upon unloading [105], [110].

Song, Park and Takeda [111] developed experimental and numerical methods to correlate the mechanical damage and the change in electrical resistance under repeat loading and unloading. The authors concluded that the change of electrical resistance had a close relation with the damage process. However, when the strain was removed, the electrical resistance decreased but did not return along the initial line and left some permanent change in electrical resistance. The remaining electrical resistance was dependent upon the maximum applied strain, and they concluded that CFRP composites have the ability to memorize the maximum applied strain, in the form of residual electrical resistance. In later investigations, Song and Takeda revealed that in CFRP subjected to constant-stress fatigue loading the resistance change due to cumulative fatigue damage was greater than static testing, by a factor of 10 [112]. They have also correlated change in strain and electrical resistance of CFRP specimens with appearances of delamination evolution.

Todoroki and his team used the four probe electrical resistance method to measure delamination crack length for edge cracks of modes I and II [113]. Experiments in thin composite samples revealed that delamination detection of known position and size is also achievable by placing electrodes onto the specimen surface and introducing current parallel to the fibre direction (0° fibres) [52]. The authors also constructed numerical models simulating the current distribution within the composite samples.

In addition to the detection of damage due to mechanical loading, some researchers attempted to solve the inverse problem, which is the estimation of location and size of damage from measuring electrical resistance changes between adjacent electrodes, using experimental configurations and finite element models. Schulte and his colleagues focused on establishing a relationship between the conductivity and damage related variables throughout the composite structure, using Electrical Impedance Tomography (EIT). By placing various electrodes at the edges of the sample and numerical simulations they constructed a conductivity map of the whole structure capable of detecting damage such as holes at various positions [114]. Todoroki et al, also investigated the inverse problem [115], [116]. The authors concluded that the electric resistance change method with response surfaces is very effective experimentally and analytically. The reliability,

however, of this method still has to be tested since in some cases the location of damage was successfully predicted [117], while in other cases a large error of estimation remains for delamination location [118].

Summarizing the observations reported in this section, in relation to the response of electrical potential to mechanical strain, it can be said that all studies concluded that mechanical strain produces reversible changes in piezo-resistance while damage in the form of fibre breakages or delamination lead to irreversible changes in piezo-resistance. Various opinions exist among researchers, in the matter of the sign of the response of piezo-resistance to mechanical strain in undamaged samples. Salvia and Todoroki report positive piezo-resistance with increasing strain while Chung observed negative changes in resistivity with increasing mechanical strain; this issue was extensively investigated in the present research work.

4.6 Effect of Temperature and Humidity

There is limited literature research available on the effect of environmental conditions such as temperature and humidity on electrical potential in CFRP composites. Belani et al [89] have investigated the effect of moisture absorption on resistivity of CFRP composites. The authors measured the longitudinal and transverse resistivity of specimens exposed to different level of moisture. They observed no increase in longitudinal resistance with increase in moisture content, suggesting that the moisture absorbed by resin or at the interface, did not affect significantly the longitudinal resistance. However, a 50% increase in transverse resistance was measured; they attributed this increase to the increase of fibre to fibre contact pressure in the transverse direction.

Celzard et al [119] studied the thermal variations of electrical resistance for different graphite polymer composites; the authors observed a variety of behaviours depending on the thermal expansion coefficient of the components. After corrections for thermal

expansion effects, one single behaviour was noticed; a decrease in resistivity with increasing temperature.

5 IMPACT DAMAGE IN CARBON FIBRE REINFORCED POLYMER COMPOSITES

This Chapter presents the literature review on the damage mechanisms of carbon fibre reinforced polymer composites subjected to impact. Changes in electrical resistance can be caused by a wide range of mechanisms such as fibre breakage, delamination, which are relevant to structural integrity. It is important to explore the different types of impact damage created in composites and how matrix cracks and fibre breaks form part of this damage.

This Chapter is structured as follows: Section 5.1 gives a general view of impact damage in composites and explains the difference between impact resistance and impact damage tolerance. The basic failure modes under low-velocity impact are described in Section 5.2 and how they affect the electrical resistance. Finally, Section 5.3 presents the electrical analogues of the various forms of impact damage.

5.1 Impact Damage

Carbon fibre reinforced polymer composite laminates are susceptible to service impact damage. An example of in-service impact occurs during aircraft takeoffs and landings, when stones and other small debris from the runway are propelled at high velocities by the tyres. In laminated composite structures, impacts create internal damage that often cannot be detected by visual inspection. Dear and Brown [120], have shown that while the C-scan revealed significant sub-surface damage, there was very little visual damage on the front or rear surfaces; this internal damage can cause severe reductions in residual compressive strength and can grow under load.

Impact damage in composites can be classified into three types: fibre damage, matrix damage and interfacial damage or delaminations. These damage forms will significantly affect the structure integrity. The ability of a structure to sustain a given impact with minimum amount of damage is called *'impact resistance'*, while '*impact damage tolerance*' deals with the ability to sustain a given level of damage with minimum effect on the structural performance. Impact tolerance deals with the overall ability of a structure to sustain a given impact with minimum effect on the structure and thus combines both impact resistance and impact damage tolerance [121].

Generally, impacts are categorized into either low or high velocity, but there is not a clear transition between categories; however, there is a clear difference in the form of damage developed after each event. Sjöblom et al [122] and Shivakumar [123] claim that damage due to high velocity impact is very localized, since the incident energy is dissipated in a very small volume; high velocity impact is characterized by penetration induced fibre breakage [124], [125]. During low-velocity impacts, damage is initiated by matrix cracks which create delaminations at interfaces between plies with different orientations [124], [125]. Cantwell and Morton [126] conveniently classified low velocity as up to 10 $m.s^{-1}$.

5.2 Modes of Failure in Low-Velocity Impact

Most composites are brittle and so the ability to undergo plastic deformation is extremely limited, with the result that energy is frequently absorbed in creating large areas of fracture, with ensuing reductions in both strength and stiffness [127], [128], [129].

Damage in composites often begins on the non-impacted surface or in the form of an internal delamination. Figure 5. 1 shows the form of a damage caused by impact. The heterogeneous and anisotropic nature of CFRP laminates gives rise to four major modes of failure:

1. Matrix damage – cracking occurs parallel to the fibres due to tension, compression or shear.
2. Delamination damage – produced by interlaminar stresses.
3. Fibre damage – in-tension fibre breakage and in-compression fibre buckling.
4. Penetration – the impactor completely perforates the impacted surface.

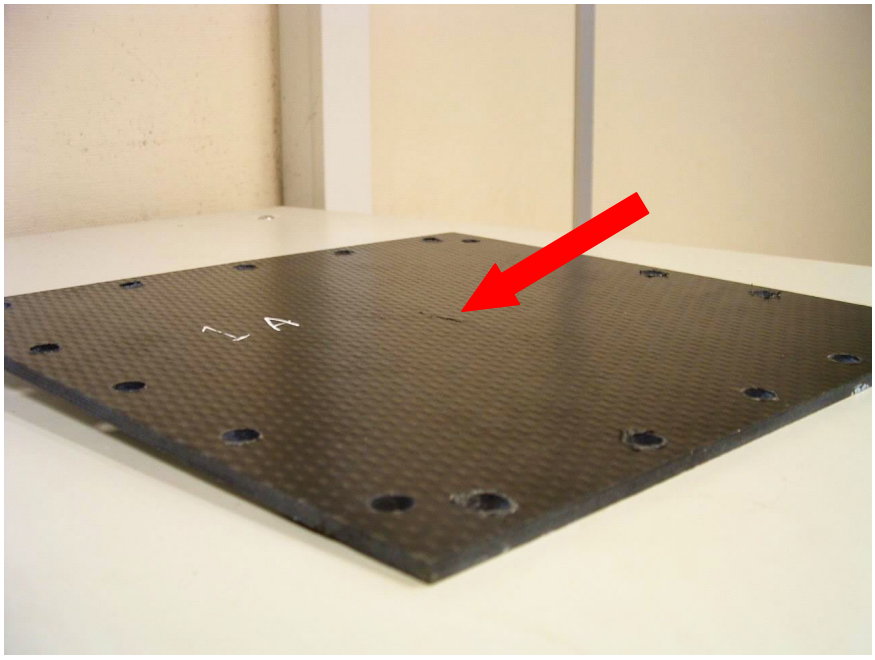

Figure 5. 1: Impact damage as appears on the bottom surface of a quasi-isotropic woven fabric plate.

5.2.1 Matrix damage

Matrix damage is the first type of failure induced by transverse low velocity impact; its role is critical since it can reduce the load-bearing capability of the composite by up to 50%. Two types of matrix cracks are observed; tensile and shear cracks.

Tensile cracks introduced when in-plane normal stresses exceed the transverse tensile strength of the ply. If the target is flexible, tensile cracks may be created due to the tensile flexural stresses in the bottom of the plate; these cracks are perpendicular to the plane of the laminate.

Shear cracks are at an angle from the mid-surface, approximately 45°, and they are formed by the very high transverse shear stress through the material [130] [131] [132]. Matrix cracks (shear cracks) are first induced in the first layer impacted by the projectile because of the high, localized contact stresses, resulting in a pine tree pattern [133] as shown in Figure 5. 2. Cracks on the bottom layer are induced by high tensile bending stresses and are characteristically vertical [129]. Figure 5. 3 and Figure 5. 4 demonstrate the form of an intralaminar shear crack in composites.

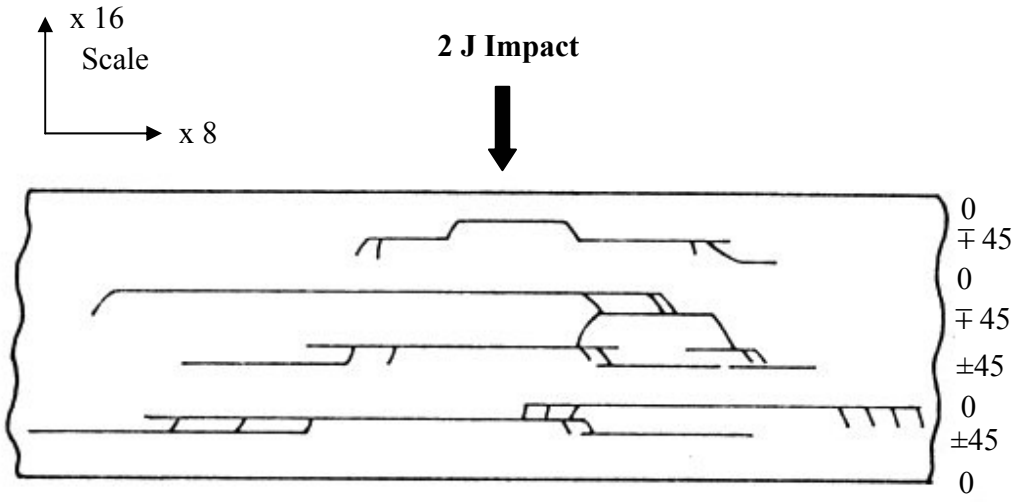

Figure 5. 2: Pine tree damage patterns developed in composite structures [134].

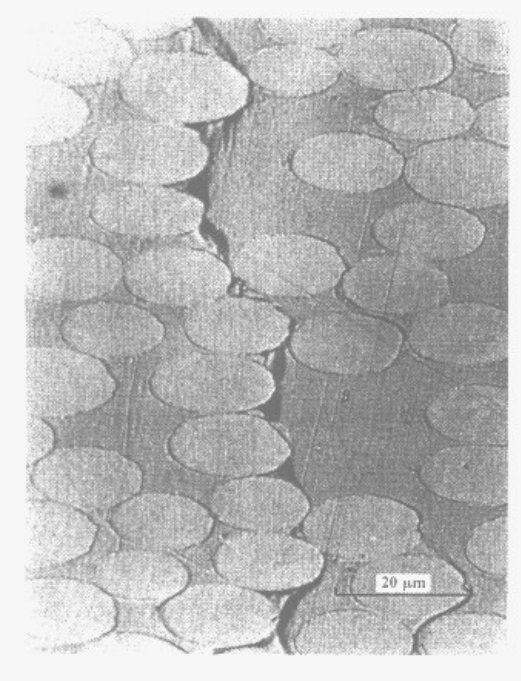

Figure 5. 3 Intralaminar shear crack for fibre-polyester resin lamina [135].

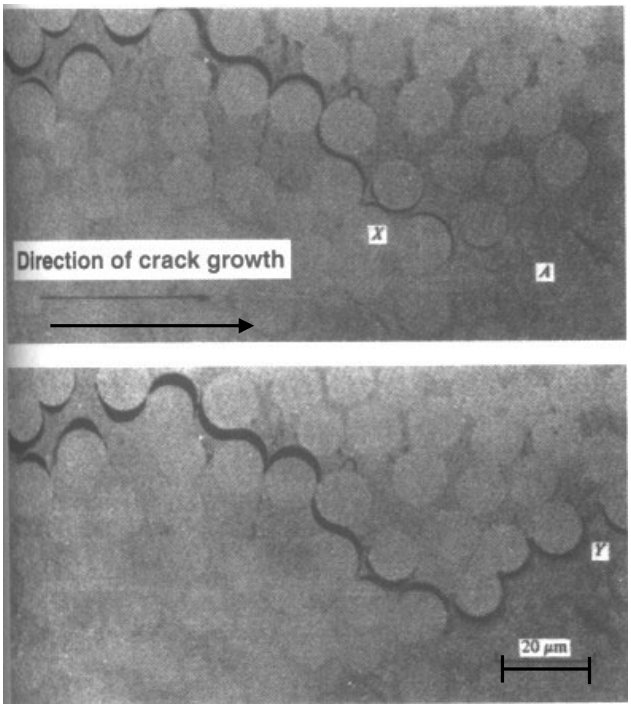

Figure 5. 4: Propagation of a transverse crack for fibre polyester resin [135].

5.2.2 Delamination

Delaminations, that is, the debonding between adjacent laminas, are of most concern since they significantly reduce the strength of the laminate in compression up to 50% [136]. Experimental studies consistently report that delaminations occur at interfaces between plies with different fibre orientation. Studies have also shown that in unidirectional composites, it is also possible for a crack to grow parallel with the fibres separating the layers. For a laminate impacted on its top surface, at interface between plies with different orientation, the delaminated area has an oblong or 'peanut' shape, with its major axis oriented in the direction of the fibres in the lower ply at that interface [130], [137], [138]. The characteristic shape of delaminations is presented in Figure 5. 5. The sizes of delaminations are measured using ultrasonic C-scan, and increases from the interfaces located near the impacted surface to the interfaces near to the opposite surface [130], [139].

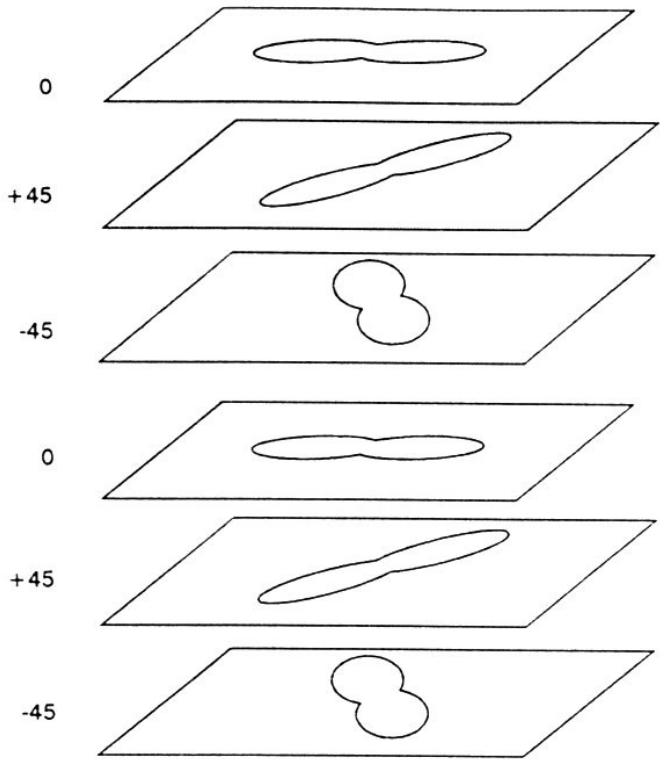

Figure 5. 5 Orientation of delaminations [130].

Delaminations are commonly initiated by opening forces at matrix cracks (mode I) [140] as shown in Figure 5. 6, or transverse cracks in adjacent layers [139], [141]. Experimental and numerical simulations showed that delamination growth is mainly driven by interlaminar shear stresses (mode II), induced by the bending of the laminate during the impact event [138], [140], [141], [142].

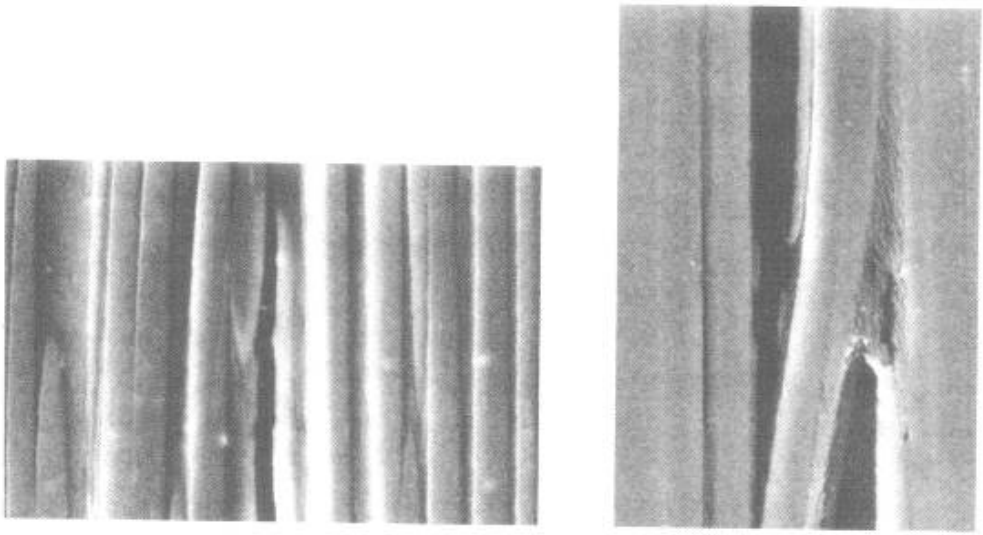

a) b)

Figure 5. 6: Delaminations of composites observed in situ in the Scanning Electron Microscope. a) AS4/3502 shows debonding with very little resin damage b) In T6T145/F155, debonding is visible [135].

5.2.3 Fibre failure

This damage mode generally occurs much later in the fracture process than matrix cracking and delamination. Fibre fracture can be a significant energy absorbing mechanism, particularly at high velocities and is generated by the high through thickness forces during the impact event [143]. Fibres can either fail under the impactor due to locally high stresses and indentation effect (mainly governed by shear forces) or on the non-impacted face can fail due to high bending stresses. Figure 5. 7 shows an example of fibre breakage in composites.

Figure 5. 7 Groups of fibres have failed by shearing forces [135].

5.2.4 Penetration

Penetration is a macroscopic mode of failure and occurs when the fibre failure reaches a critical extent enabling the impactor to completely penetrate through the material [144]. The impact energy penetration threshold rises rapidly with specimen thickness for carbon fibre-reinforced plastic (CFRP) [145].

5.3 Damage Electrical Analogues

As mentioned in Section 5.1, the main types of damage on composites are delamination, matrix cracking and fibre failure. These damages may change the paths in which the current flows through the material, with the consequence the change in the electrical resistance of the composite. The aim of the developed electrical analogues is to produce more sufficient view of the internal mechanisms of damage propagation as well as to predict the extent of the damage.

There is a direct relationship between the electrical conductance and damage processes occurring inside the material; different loading conditions (impact, fatigue) cause different changes in the longitudinal and transverse resistivity. The electrical analogue should be able to give the sensitivity and the accuracy of electrical resistivity measurements for characterising different types of damage mechanisms. In the following paragraphs, the electrical analogy between major damage mechanisms such as fibre breaks, matrix cracks and delamination are described.

5.3.1 Fibre breaks

Figure 5. 8 shows the electrical analogue of a fibre breakage. Current flows along the fibres. The resistance of a composite in the longitudinal direction can be calculated using the model of parallel resistances (Section 4. 2.1.1). This arrangement has carbon fibres as registers connected in parallel; the electrodes should be glued at the ends of the fibres to facilitate the current flow along the fibres. By applying the knowledge of the electrical conductivity mechanisms of CFRP in the fibre direction for damage sensing, fibre cracks can be detected. Fibre fracture causes an increase in the longitudinal resistivity of a lamina. In this case, a fibre break is equivalent to a broken resistor as indicated in Figure 5. 8. The number of fibres may be quantified from the measurement of resistance change.

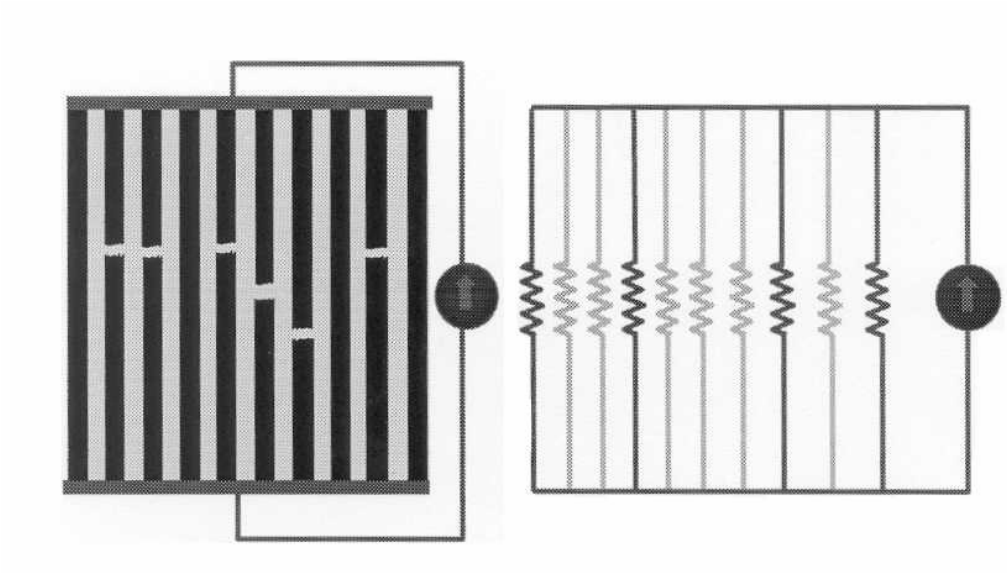

Figure 5. 8: Schematic illustration of damage mechanism of a unidirectional CFRP laminate and its electrical analogue [33].

5.3.2 Matrix cracks

As mentioned in Section 4.2.2, the electrical conductance in the transverse direction in CFRP can occur by fibre-fibre contact. Matrix cracks affect this conduction by separating the adjacent fibres that are responsible for transverse conduction process. This leads to the change of the current transport through the composite and ends up in the increase of the transverse resistivity. This means that the transverse and through thickness resistivities can indicate damage in the form of matrix cracking; eventually, this changes the resistance and hence facilitates quantification of matrix cracks. Figure 5. 9 shows the electrical analogue of a crack matrix.

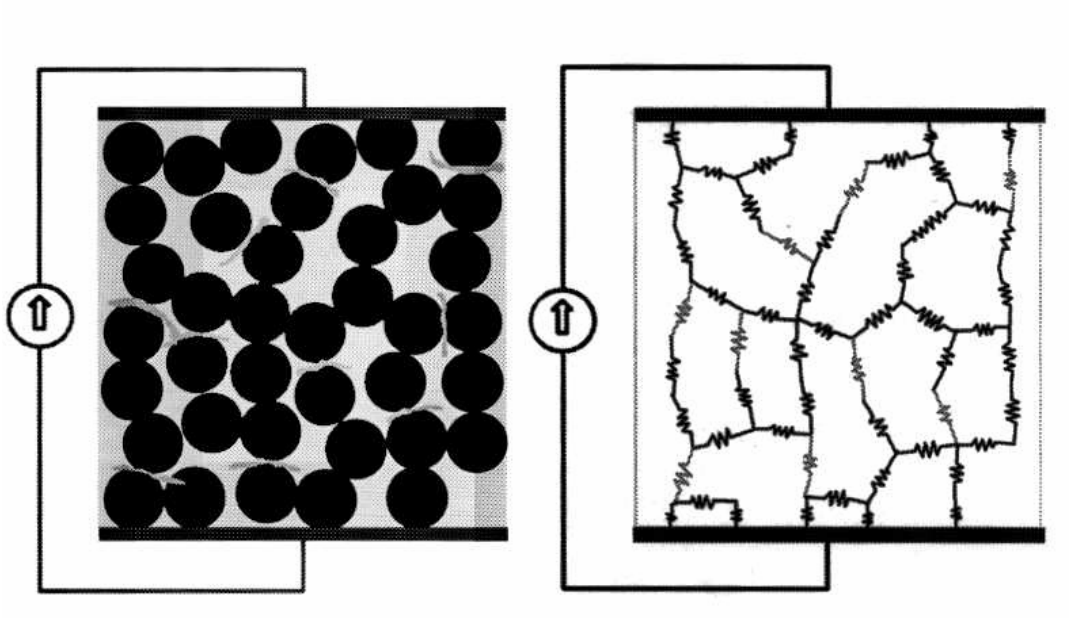

Figure 5. 9: Schematic illustration of damage mechanisms of a unidirectional CFRP laminate and its electrical analogue [33].

5.3.3 Delamination

Delamination cracks in unidirectional CFRP are governed by the transverse conduction process. Delaminations influence the electrical properties of CFRP in a similar way to the fibre breaks; they affect the transverse conductivity, and break the fibre-fibre contact i.e. the resistors in an electrical circuit. The propagation of a delamination decreases the

conduction path because of the broken resistors. Figure 5. 10 shows the electrical analogue for measuring delamination crack growth. The crack growth is continuous.

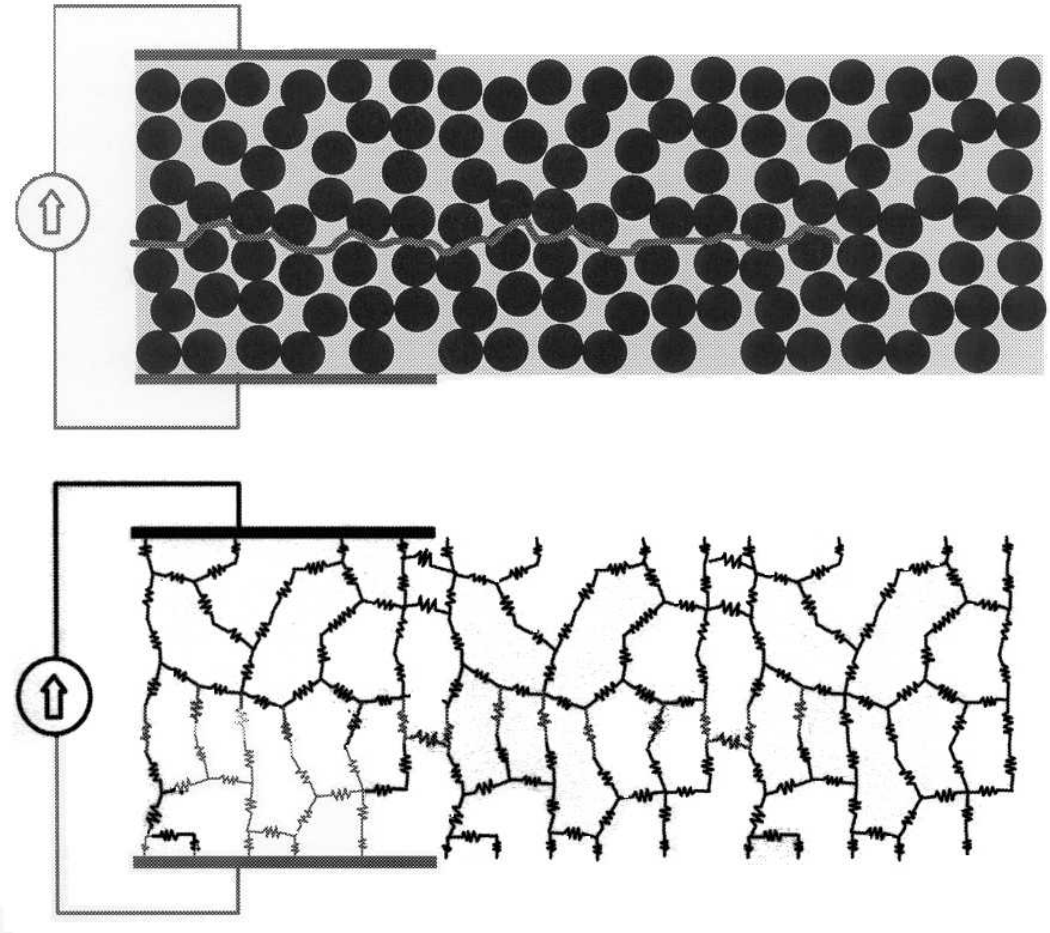

Figure 5. 10: Schematic illustration of damage mechanisms of a unidirectional CFRP laminate and its electrical analogue [33].

6 MATERIALS AND PROCEDURES

This Chapter gives a detailed account of the materials, specimen fabrication, experimental set-up and data acquisition systems used in this investigation. Pre-preg unidirectional and multidirectional specimens in the form of strip were manufactured in order to investigate the effect of mechanical strain, temperature and water absorption, on the electrical potential. The impact damage was also one of the primarily objects of this research and different size energy impacts were applied on various composite plates, and their effect on electrical potential was investigated.

This Chapter is organized as follows: The properties of carbon fibres and epoxy resins are described in Section 6.1. Laminate fabrication methods are presented in Section 6.2. The properties of conductive adhesive are presented in Section 6.3. The details of the design of all specimens used in each experimental configuration, including geometrical parameters and probe instrumentation are described in Section 6.4 while Section 6.5 presents details of the equipment used for all experiments. Finally, the description of the test programs used for the various type experiments, including the data acquisition software, is given in Section 6.6.

6.1 Materials

6.1.1 Carbon fibres

The type of carbon fibre used in this research work was Torayca T300, which is a standard modulus, high strength PAN type of fibre. Table 6. 1 presents the mechanical properties of that type of fibre, in the direction parallel to the fibre.

Table 6. 1: Mechanical properties of Torayca T300 carbon fibre [33].

Properties	*Values*
Tensile Modulus (GPa)	230
Tensile Strength (MPa)	3530
Elongation parallel to the fibre axis (%)	1.5
Longitudinal resistivity (μΩ.m)	17
Thermal Conductivity (W/mK)	6.5
Coefficient of thermal expansion (10^{-6}/ºC)	-0.7
Specific Heat (cal/g ºC)	0.17
Density (g/cm^3)	1.75

6.1.2 Epoxy matrix

The resin used in this investigation was Epoxy-914.

Typical properties of the cured Epoxy-914 are shown in Table 6. 2. Epoxy-914 is a mixed tetra and tri-functional epoxy polymer, dicyanodiamide (DICY) hardener and polyethersulphone (PES) viscosity modifier system.

Table 6. 2: Properties of epoxy resin 914 [33].

Properties	*Value*
Tensile Modulus (GPa)	3.9
Tensile strength (MPa)	48
Failure strain (%)	1.5
Poisson's ratio	0.41
Compression yield strength (MPa)	177
Fracture toughness-K_{Ic} (MPa $m^{1/2}$)	0.7
Fracture toughness-G_{Ic} (J/m^2)	103
Glass transition temperature (ºC)	190
Cured density (g/cm^3)	1.29

6.2 Laminate Fabrication

The laminates were manufactured using pre-impregnated (pre-preg) material named Fibredux 914C-TS(6K)5-34%. Fibredux 914 is the product base, C stands for carbon fibres, T denotes high tensile Torayca carbon, S surface treated, 6K denotes that each tow of fibres used contained six thousands fibres, 5 a cured pre-preg with thickness of 5 thousandth of an inch (0.125 mm) at 60% volume fraction, and finally 34% denotes the resin content of prepreg, nominal % by weight. The fibres were arranged in a unidirectional tape. The pre-preg was cut to the required dimensions and laid-up to the requisite stacking sequences using hand lay-up technique. The final stacked laminate was initially de-balked, in order to remove the trapped air between the various layers, and then vacuum bagged and cured in an autoclave using the optimum cure cycle recommended by the manufacturer.

In the vacuum bag technique, a uniform pressure is applied to the laminate before it is cured, improving consolidation of the fibres and removing the excess resin, air and volatiles from the matrix. The laminate is covered with a flexible bag, under which the

vacuum is applied. The autoclaves are pressure vessels that contain compressed gas during the processing of the composite. The components of the autoclave curing process are shown in Figure 6. 1. After the composite part is laid-up and enclosed in a vacuum bag, full or partial vacuum is drawn within the bag, and gas pressure greater than atmospheric is applied on the exterior of the bag.

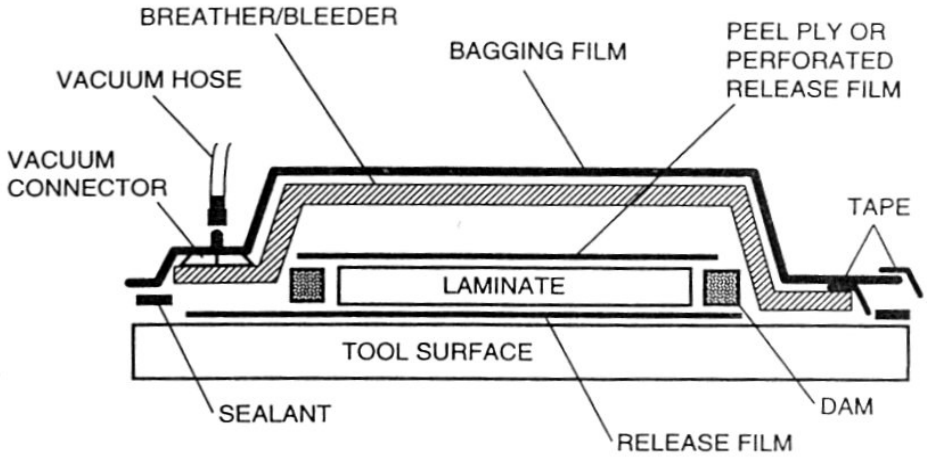

Figure 6. 1: Components of autoclave curing [148].

The part temperature is then raised to initiate cure of the polymer [148]. Higher temperature also reduces the viscosity of the polymer, helping wetting of the reinforcement and consolidation of the composite.

Three types of laminates were used in this investigation. Their stacking sequences are shown in Table 6. 3; unidirectional, cross ply and quasi-isotropic lay-up specimens in a strip form were manufactured in order to study the response of the electrical potential to mechanical strain.

Table 6. 3: Types of laminates fabricated.

Sequence Number (SN)	*Type*	*Materials*	*Stacking Sequence*
1	Unidirectional	T300/Epoxy 914	$[0]_{16}$
3	Cross Ply	T300/Epoxy 914	$[(0/90)_4]_s$
4	Quasi-Isotropic	T300/Epoxy 914	$[0_2/45_2/90_2/-45_2]_s$

The same laminate sequences were used for manufacturing new specimens to investigate the effect of temperature on electrical potential. Cross ply and quasi-isotropic samples in plate forms were manufactured to investigate the response of electrical potential to impact damage. Cross ply tabs were also manufactured for electrically insulating the specimen from the machine grips. More details about the above experimental configuration are given in Section 6. 4.

6.2.1 Composite microstructure

Two samples were manufactured for each lay-up, with dimension 25 x 20 x 2 mm. All samples were encapsulated in Triofix filled acrylic resin. The composite surface was firstly polished using S600 grade of silicon carbide paper, in order to remove any excess resin from the composite surface. An automatic polishing machine manufactured by Buehler was employed. The next stage was to abrade the specimens using a 9 μm diamond powder, in order to obtain a smoother area. The final phase included polishing of the samples using a 0.3 μm oxide powder. Typical pictures of the microstructure of cross ply and quasi-isotropic specimens are shown in Figure 6. 2 and Figure 6. 3 respectively. In the CP plate, the structure formed by the altering of 0/90 it can clearly be seen. The general quality is excellent with no voids or little in the rich resin areas. There is a small tendency for increased concentration of resin at the interface between layers of different orientation and also at the points A, B, C, between layers of the same orientation, reflecting the position of the original boundaries of the pre-preg. This short of feature will contribute to the interface resistance for though thickness current flow.

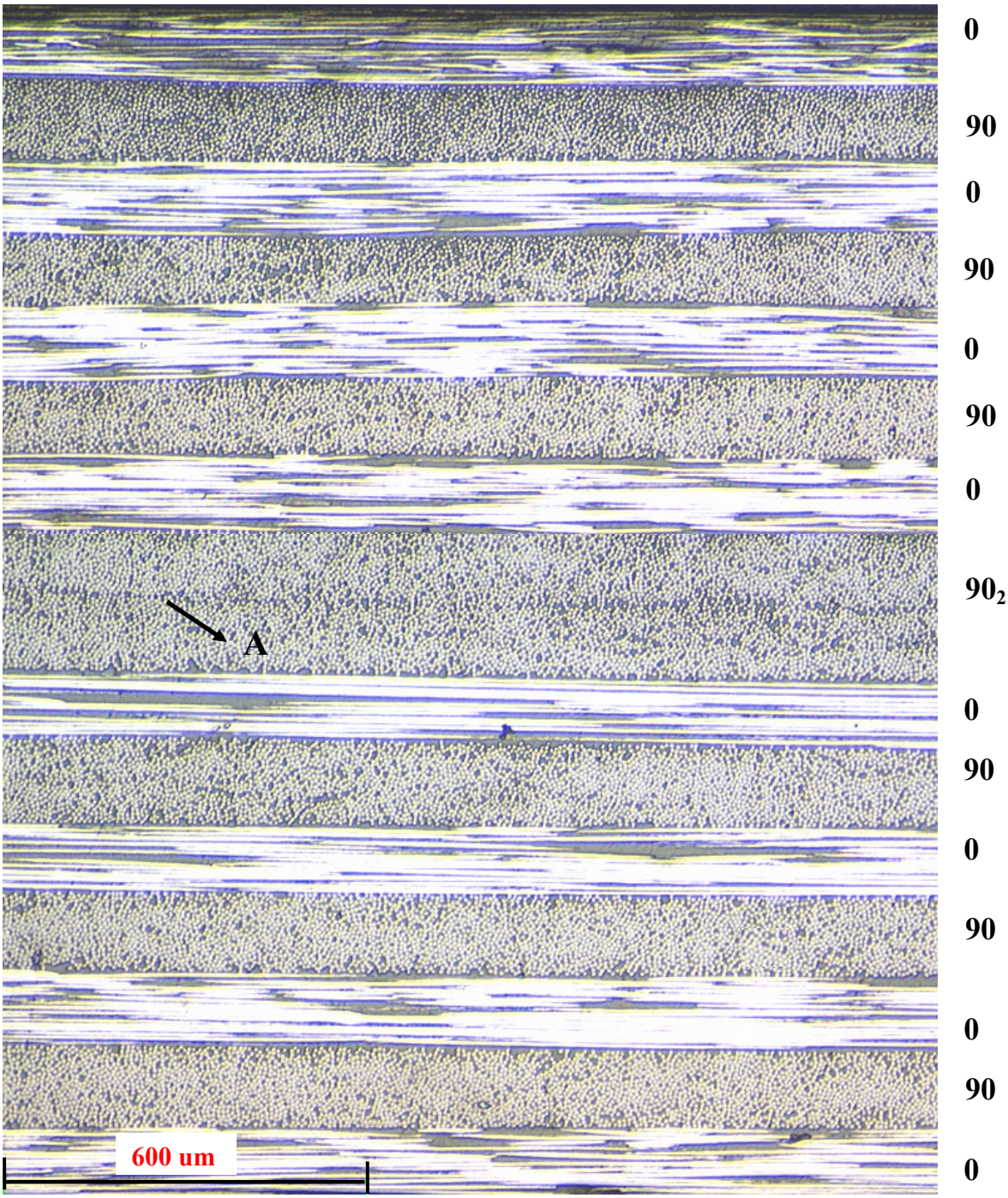

Figure 6. 2: Microstructure of undamaged cross ply plate.

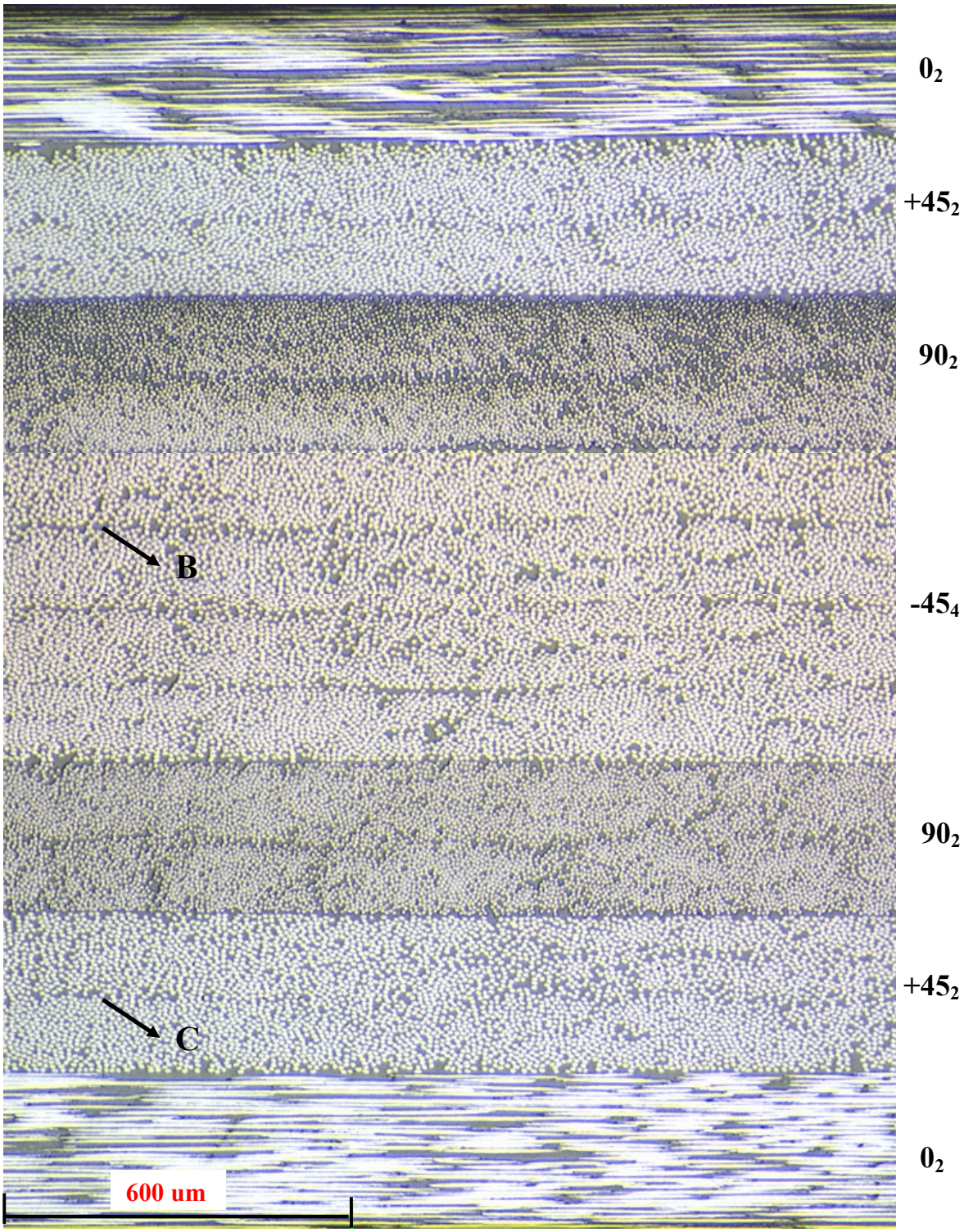

Figure 6. 3: Microstructure of undamaged quasi-isotropic plate.

6.2.2 Carbon fibre volume fraction

Investigations were conducted in order to measure the exact fibre volume fraction in the plates after being cured. Three samples were examined and the volume fraction was calculated in five different locations. A Nikon image analyzer was used, and the fibre volume fraction measured using image analysis measurement methods. In this technique, the carbon fibres are represented by a different colour than the surrounding matrix. By measuring the percentage volume fraction of each colour, accurate values of the fibre volume fraction can be extracted.

Table 6. 4 shows the different fibre volume fractions for different lay-up sequences used in this research study.

Table 6. 4: Measured fibre volume fractions of different lay-up sequences.

Specimens	$[(0/90)_4]_S$	$[0_2/+45_2/90_2/-45_2]_S$
Interface	0/90	0/45 ≡ ± 45/90
%fibre (in ply)	64.8 ±1%	64.6 ±1%
%fibre (interface)	25	33

6.3 Conductive Adhesives

The purpose of the electrically conductive adhesive is to glue an electrical wire or copper contact on the carbon fibres. These contacts are used as current entry, egress points or measurement points; both good conductive and adhesive properties are required. Electrically conductive adhesives are generally made by mixing conductive filler particles in a general adhesive. Three different adhesives were used in this investigation as described below. Their components appeared to significantly influence the response of the electrical potential to mechanical strain as discussed later.

6.3.1 Silver paint

Silver paint known as Electrodag or Silverdag 1415 was used in this investigation. This electrically conductive adhesive contains silver particles and thermoplastic resin binder. The viscosity is very low, allowing an easy application.

Electrodag 1415 also maintains low resistance even after exposure to heat, cold, humidity and salt spray. It is an air drying system that requires no primer or top coat. Due to its low viscosity it has the tendency to flow out of the bonding area; however, it can be a good electrode on an exposed surface, because it sets by solvent evaporation [149].

6.3.2 Carbon cement

Conductive Carbon Cement (CCC) is a paste-like viscous conductive cement used for specimen mounting, featuring good adhesive quality. Due to its good electrical conductivity all conductive specimens are ready for investigating after drying. After air-drying, only carbon (with acrylic binding agents), hydrogen and oxygen are left. It is more viscous than the silver paint and it forms bonding by the process of evaporation of the organic solvent.

6.3.3 Silver epoxy

The conductive silver epoxy adhesive (IONACURE 650) is a two component pure silver filled epoxy adhesive. It combines the adhesive properties of the epoxy with the electrical properties of the silver. Its chemical composition is based on a diepoxide resin of Bisphenol A and a polyamide hardener. The silver loaded epoxy adhesive was primarily used to bond the electrodes of specimen used in mechanical loading.

6.4 Specimen Design

A suitable representative specimen had to be designed to generate sensible mechanical data. The specimens were prepared from the post-cured laminates. An electroplated diamond wheel with a grit size of 44-66 μm was used to cut the specimens for different tests. For a smooth finish, a wheel grit size of 100-120 μm was used. The geometry of the

specimens was varying according to the experiments to perform. The details of specimen design and preparation are described below. To remove the cutting marks and other related defects, the specimens were ground polished on a surface grinder using 240C and 1200C grinding paper.

6.4.1 Specimens subjected to mechanical strain

The specimens used in this investigation were strip formed unidirectional, cross ply and quasi-isotropic. The thickness of each sample was 2 mm (sixteen layers) and the length 280 mm while the width was 25 mm for the majority of them and for some individual cases it was set 30 mm. In all cases, the applied load was parallel to the fibres located on the top layer (0°).

a) Configuration A

This arrangement was used to measure piezo-resistive behaviour with current flow and applied stress parallel with the fibres in unidirectional samples. Eight samples were made and their geometric characteristics are presented in Figure 6. 4. The formation of the current introduction probes is shown in Figure 6. 5.

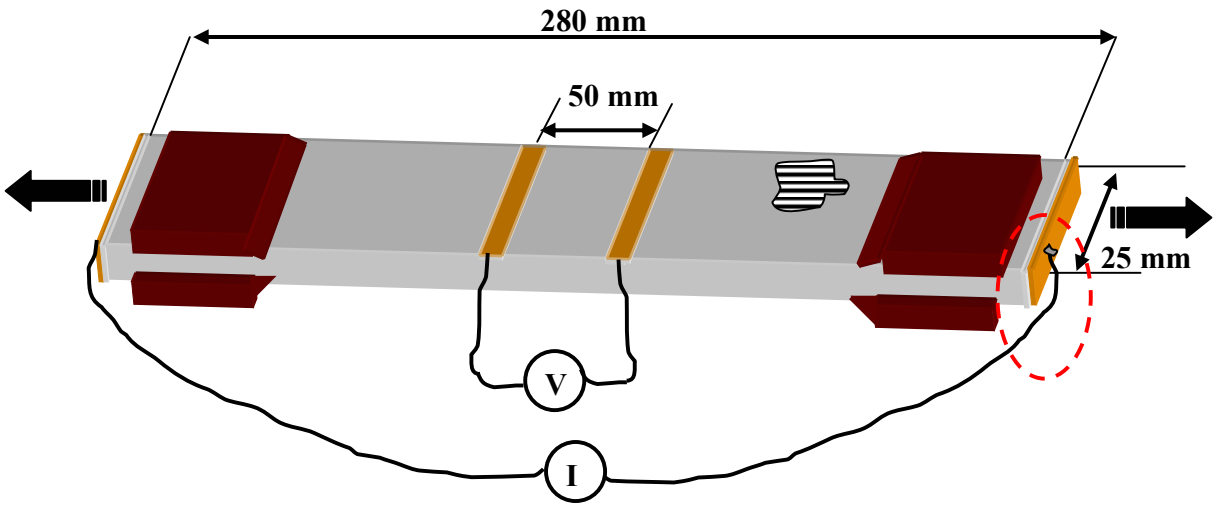

Figure 6. 4: Geometry of specimens subjected to mechanical loading; configuration A.

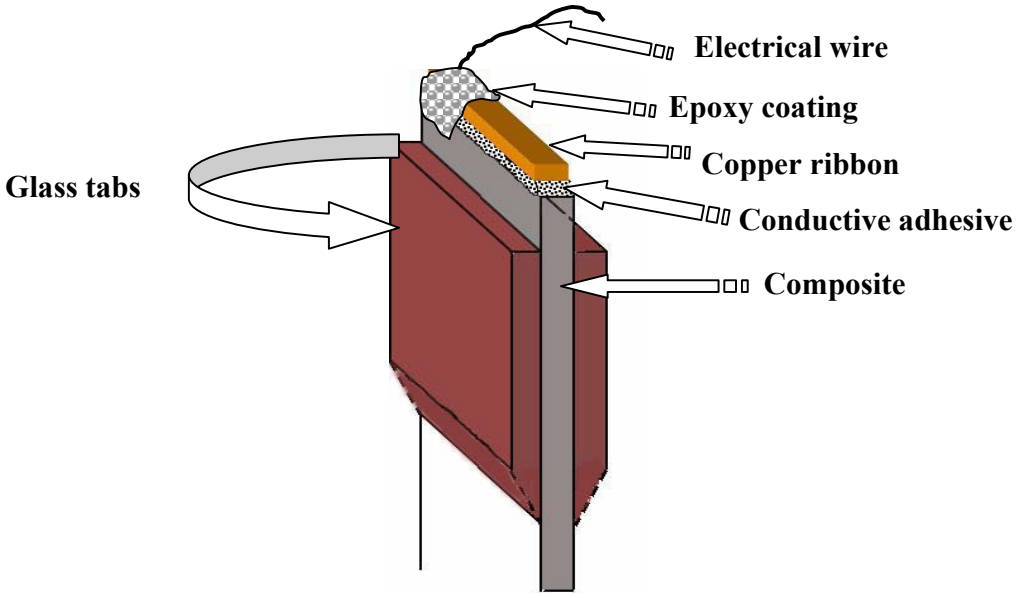

Figure 6. 5: Geometry of the electrode-tab used for mechanical loading; configuration A.

All specimens were encapsulated in Triofix filled acrylic resin. For abrading the samples, the automatic polishing machine was not employed because of the uncommon sample size and configuration; therefore the time and applied pressure were controlled manually. Initially, the composite surface at the ends was polished in order to expose only the carbon fibres. Three stages of abrasion were used. The first two were to remove the cutting marks and any associated damage due to the cutting of the samples from the laminate and to prepare the sample surface for the final polishing. The final stage was the polishing for tests requiring microscopy analysis. The three stages are listed below:

- P500 grade silicon carbide paper for two minutes
- P1200 grade silicon carbide paper for three minutes
- 3 μm aluminium oxide powder for one minute

At the end, all samples were cleaned using acetone.

The current introduction electrodes were formed by bonding a thin copper strip on opposite edges of the sample using silver epoxy, carbon cement or silver paint as shown in Figure 6. 5. A very thin lead was soldered onto the copper, prior to bonding the copper

on the composite. After glueing, the electrode area was coated with commercial grade quick setting epoxy adhesive, to avoid any possible short circuits and damage of the electrode during cycling. Potential measurement electrodes were formed on the surface 50 mm apart using silver paint.

b) Configuration B

In this configuration, the current was introduced via two point contacts on a line parallel with 0° surface fibres and a contact area around 5 mm; eight samples were manufactured in total. On the surface, above and below the symmetric axis, pairs of potential measurement probes have been spaced equally along the fibre direction and they were arranged either along the current flow line or 6 mm away from the current line, while the distance between the parallel arrays of probes was 30 mm; ten samples were made and their geometric characteristics are presented in Figure 6. 6.

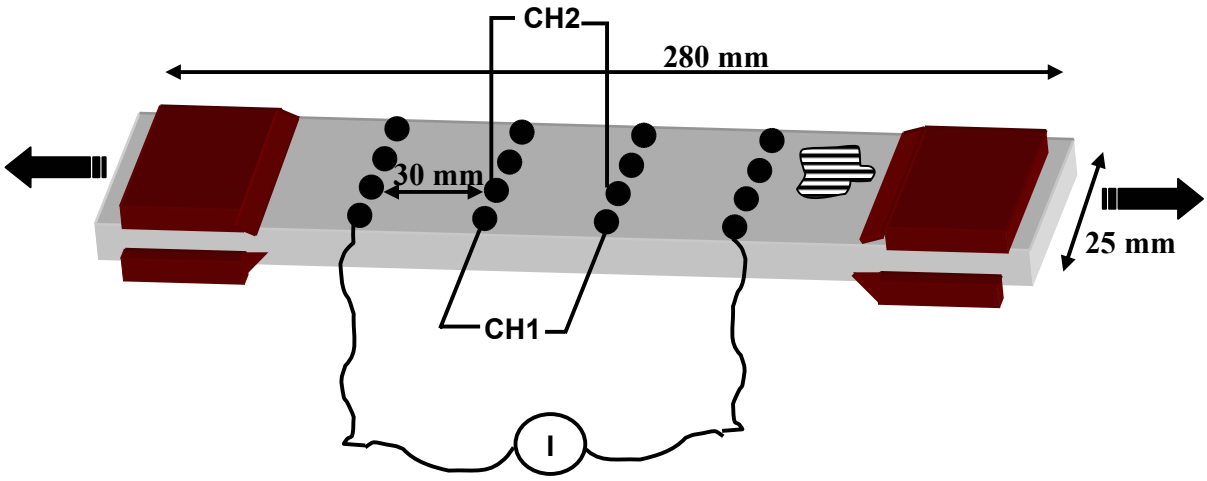

Figure 6. 6: Geometry of specimens subjected to mechanical loading; configuration B.

This configuration was applied to unidirectional, cross ply and quasi-isotropic lay-ups, and it was used to investigate the effects of inhomogeneous current flow on the potential distribution. In the above designation, CH 1 (channel 1), refers to the pair of probes aligned with the current introduction line and CH 2 (channel 2) represents the pair of probes misaligned from the current introduction line. The load was applied parallel to the 0° fibre direction.

c) Configuration C

The same samples as in configuration B were used. The aim of this formation was to examine the electrical resistance, transverse to the fibres. As shown in Figure 6. 7, two current introduction electrodes were aligned transverse to the 0° surface fibres. Two pairs of measurement contacts were arranged between them. As in the previous configuration, to achieve electrical contact on the surface, the fibres needed to be exposed. A circular area with diameter varying between 4 mm and 6 mm was emeried to expose the carbon fibre. To make the contact, the spot was covered with conductive adhesive bonding such as silver paint, and to strengthen the bond, an epoxy coating was added on the contact. A graphical representation of the contact spot is represented in Figure 6. 8.

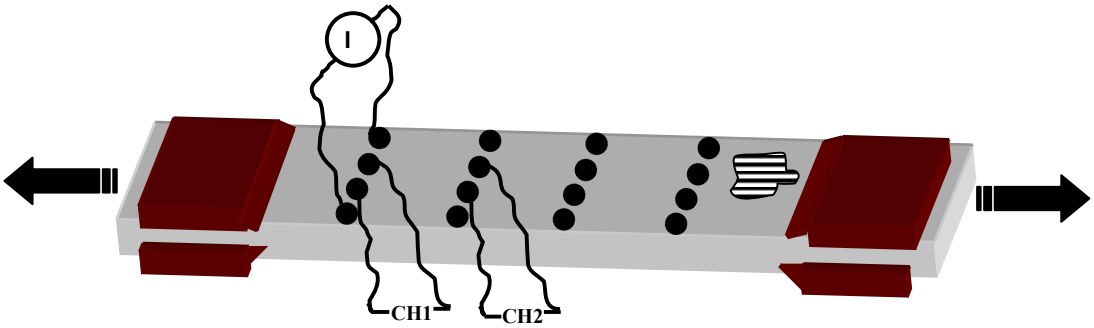

Figure 6. 7: Geometry of specimens subjected to mechanical loading; configuration C.

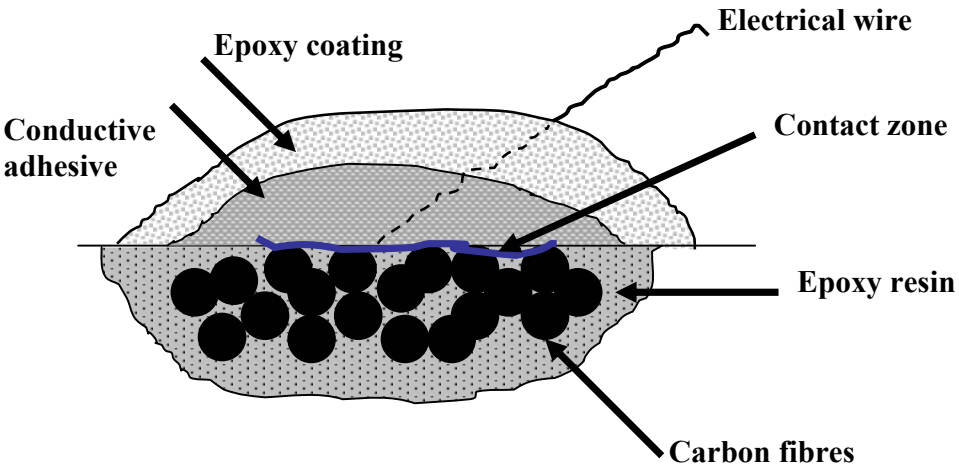

Figure 6. 8: Contact area for measuring electrical potential on the composite surface.

d) Configuration D

Resistance with current flow transverse to the fibres was also investigated with current introduced at the sample edges, using the sputtered layer technique (Figure 6. 9). Sputtering is done by ionising inert gas particles in an electric field, producing a gas of plasma. This is then directed toward the source or target, where the energy of these gas particles physically dislodges, or 'sputter off' atoms of the chromium or other source materials. A total thickness of 5 μm of chromium/gold was deposited. In these samples the current was introduced via Cr-Au-sputtered contacts of negligible contact resistance. The main difference with configuration C is that the current here is redistributed in greater surface area, taking into account the thickness of the composite as well. In addition, the two probe technique was employed, to measure the electrical potential.

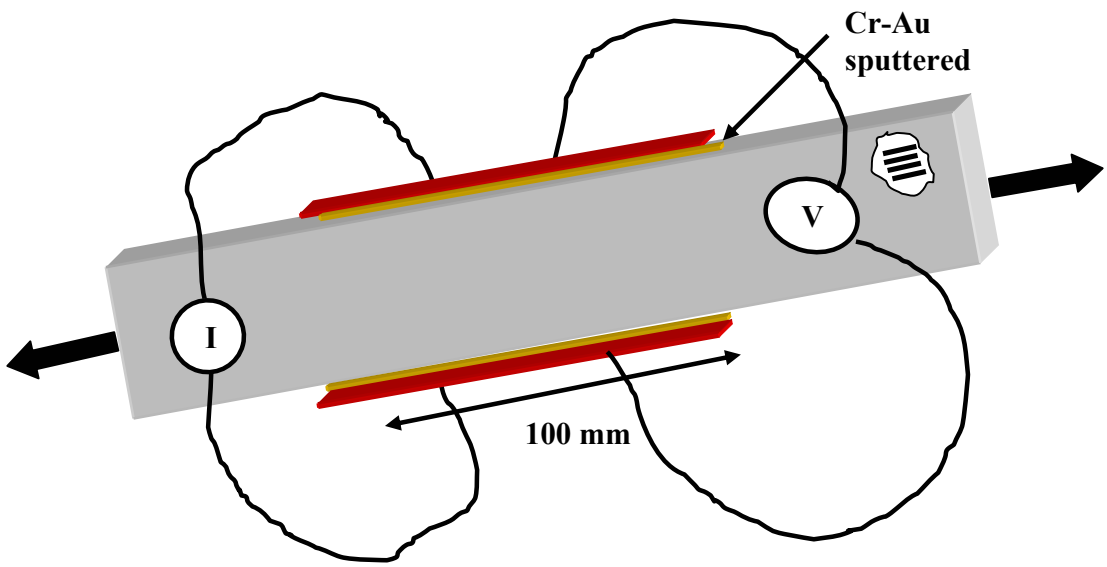

Figure 6. 9: Geometry of specimens subjected to mechanical loading; configuration D with sputtered contacts.

e) Configuration E

Finally, this configuration had sputtered current introduction electrodes created at the sample ends similar to configuration A, but with a two probe system for measurement of resistance (Figure 6. 10). In the potential measurements, not only the fibres located on the

top layers are taken into account, but also the fibres through the entire thickness of the composite.

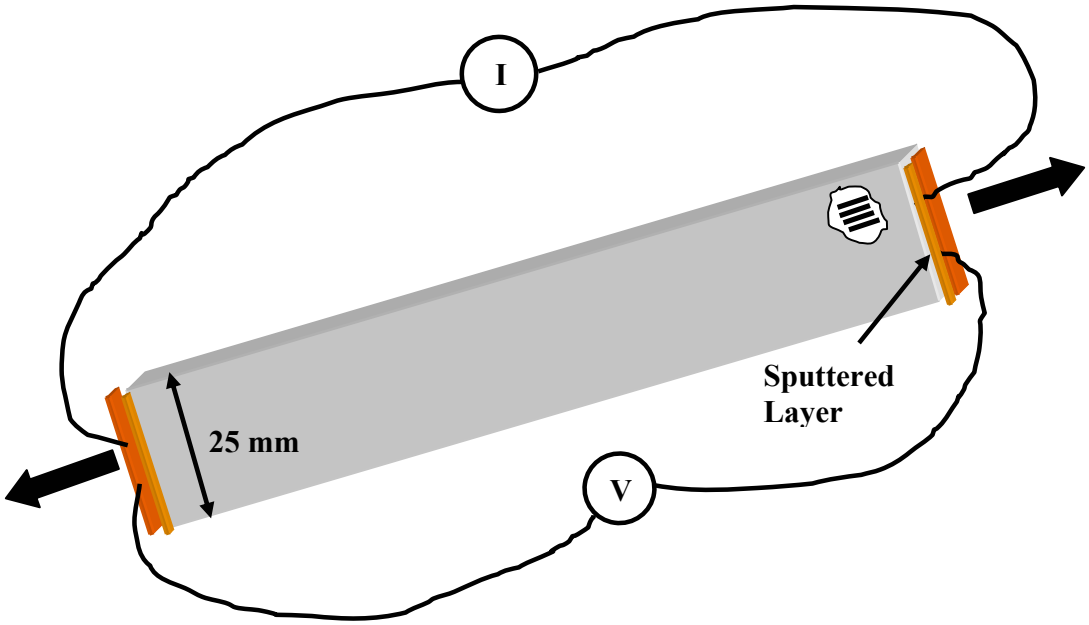

Figure 6. 10: Geometry of specimens subjected to mechanical loading; configuration E.

Also, since the potential probes are placed on the edges of the sample, current redistribution due to fibre misalignments away from the introduction area, (such as configuration A), is negligible.

It is possible to calculate the number of contact fibres in the contact spot. By assuming a cyclic area diameter of 5 mm and taking into account that the fibre diameter is 7 μm, the maximum number of fibres in contact would be approximately 714. However, the number of fibres which participate in the measured electrical potential will depend on the properties of the conductive adhesive and especially its viscosity, as explained later in Chapter 8, Section 8.1.

6.4.2 Specimens subjected to environmental loading conditions

a) Effect of Temperature

The specimens used in this investigation were strip formed unidirectional, cross ply and quasi-isotropic composites, with stacking sequences as shown in Table 6. 3. Their

geometric characteristics were identical to those samples used to investigate the effect of the mechanical strain. Fifteen samples were manufactured in order to investigate the effect of temperature on electrical potential. In all samples, the current was introduced on sample edges at fibre ends.

The dimensional characteristics of the samples are shown in Figure 6. 11. The concept of designing the electrodes was the same as for the samples used to investigate the effect of mechanical strain on electrical potential. In addition, a K-type thermocouple was placed on the surface of the each specimen, in order to measure accurately the surface temperature of the composite.

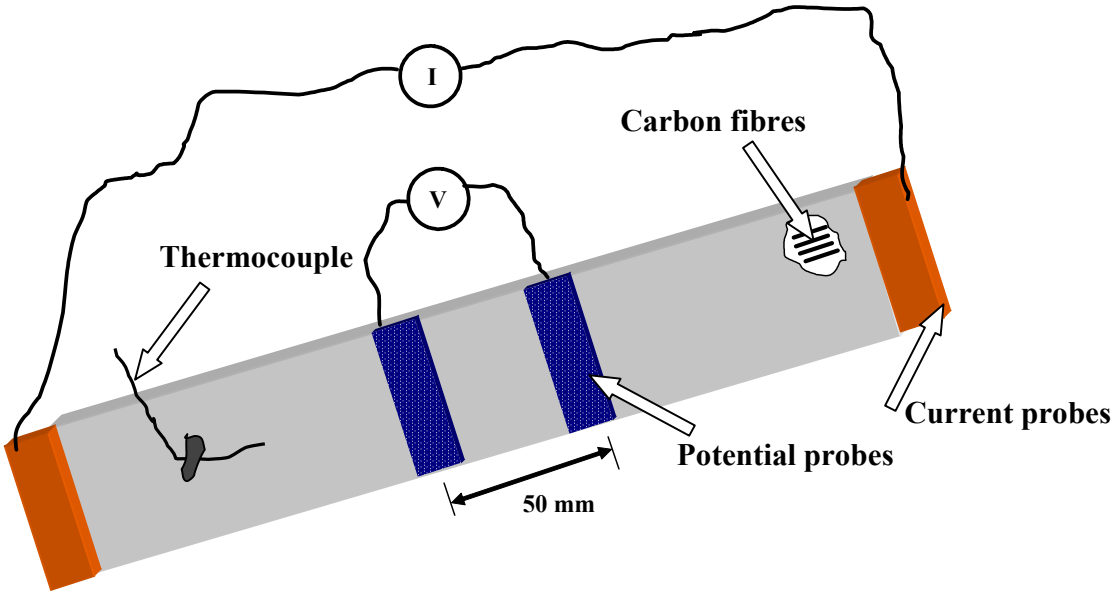

Figure 6. 11: Geometry of samples used for current introduction at the edges.

b) Effect of Water

Unidirectional samples, with fibres oriented in the 0° and 90° direction, dimension of 140 x 25 x 2 mm were used in this experimental study. The geometry of those specimens is represented in Figure 6. 4. The total number of samples was sixteen. All samples were immersed into distilled water at room temperature for a period of six months ensuring 100% surface water absorption. The specimens were prepared according to ISO 62:1999

standards. All specimens were dried in an oven and cooled down to room temperature before weighing them. Afterwards, they were immersed in distilled water in a plastic container and kept at a room temperature. After immersion for 24 hrs all specimens were removed from the container and the surface water was removed using a dry cloth; thereafter, all specimens were reweighed. This process was repeated for a period of seven days and then all specimens were submerged in the water until the end of the test period.

6.4.3 Tabs manufacturing

The tabs of the specimens were prepared from cross ply glass fibres reinforced polymer (GFRP) laminates. Their purpose was to electrically insulate the specimen from the machine grips during testing. The specimens had a thickness of 1 mm and length of 55 mm. The method used for bonding the tabs onto the composite had been found to be of significant importance in order to obtain the most efficient bonding. Initially, the surfaces of both the glass tabs and carbon samples were polished using a soft emery paper. The tabs were bonded to the specimens using Redux-420-NA. The following technique was applied to reinforce the bonding link. As shown in Figure 6. 12, the carbon specimens were placed on a metal sheet, among two bleeder sheets, aimed to constrain the movements of the samples.

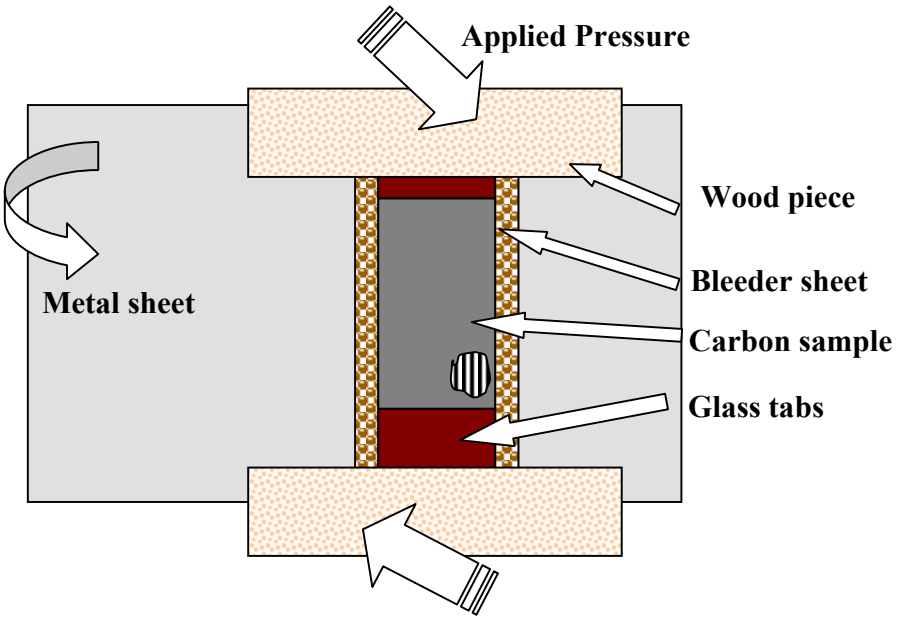

Figure 6. 12: Details of the technique used for manufacturing tabs for mechanical testing.

The glass tabs were placed afterwards on both the top and the bottom surface of the carbon samples; the whole set was then placed in a hot-pressure machine, manufactured by Foxwell Instruments, capable of applying heat and pressure simultaneously. The tabs were bonded on to the specimens using the same adhesive as previously, and cured at 80°C for 2 hrs, and 6 tonnes pressure. For homogeneous distribution, the pressure applied using pieces of wood, placed on the top of the tabs ensuring a good bonding, capable of withstanding loads exceeding 60 kN.

6.4.4 Investigation of potential fields in laminates subjected to dc current flow

Three cross ply and three quasi-isotropic plates were manufactured in order to investigate the distribution of electrical potential on the surface of the composite. The edges of all plates were cleaned and polished initially, as explained in Section 6.4.1, in order to remove any remaining, after manufacturing, broken fibres. The dimensions of all plates were 280 x 280 mm, and their thickness was 2 mm. The geometric characteristics of all plates are shown in Figure 6. 13.

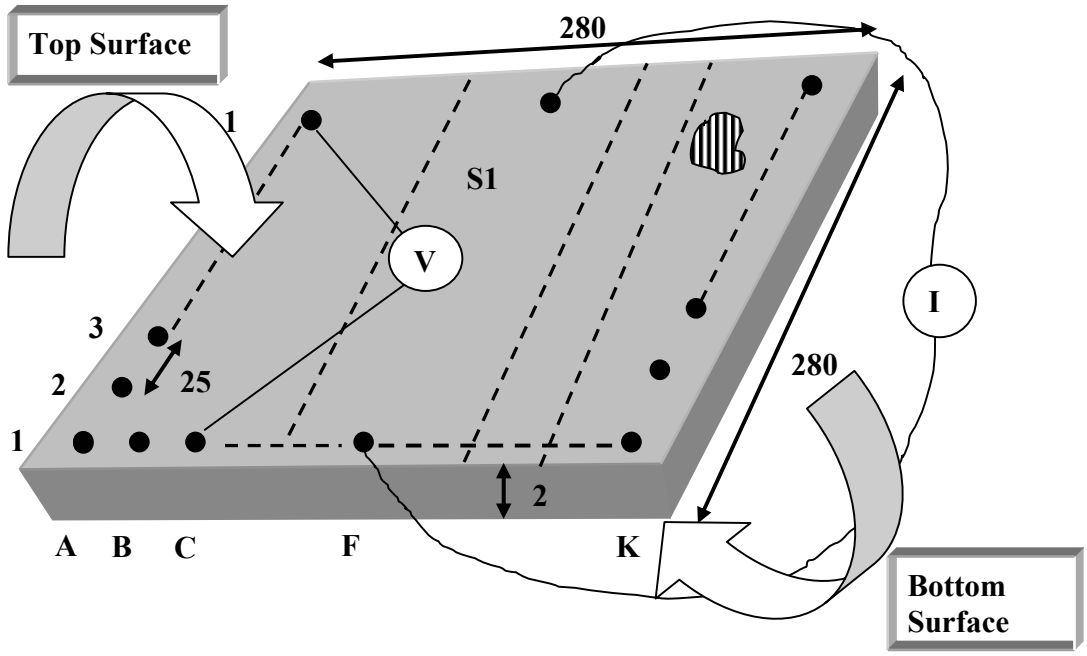

Figure 6. 13: Geometric characteristics and location of measurement probes for measuring potential distribution on composites plates.

On each panel, measurements of electrical potential were taken using arrays of probes positioned on the surface of the composite on a grid of 25 mm. The maximum number of probes used was 121. The manufacture technique of those electrodes was identical to that used in the specimens subjected to mechanical strain (Section 6.4.1).

For a suitable designation of the different current input it is suggested considering the 121 probes forming an 11 x 11 matrix in which a column is represented by the probes in the same line along the direction of the surface fibres. There are 11 columns denoted by A, B,….K, while the row is indicated by number 1, 2,….,11. The designation "S1" indicates the top surface which is the instrumented surface and "S2" is the bottom surface. Potential measurement probes and current introduction electrodes were confined to S1 or both S1 and S2. The same probe position designation system is used for both S1 and S2; for example, position A1S1 refers to a probe in the top left hand corner of the array on the top surface, and position A1S2 is the probe immediately opposite, to A1S1 on the other surface.

Each probe site was first abraded with emery paper in order to reveal the surface fibre. A thin copper wire was then placed accurately on the site, and held in place with silver paint. Each electrode was then covered by an epoxy coating.

In addition to potential measurement, some probes were used to introduce current into the laminate; the location of current electrodes was not fixed. Many different locations of current input/output pairs were chosen and their effect on the potential field was investigated for all different lay-ups.

The investigation of the potential field was also extended to damaged plates. The worst case situation would be complete penetration of the composite. In all the above panels holes of various diameters were created in different positions, as presented in Table 6. 5.

Table 6. 5: Summary of different size of holes created in composite plates.

Laminate Lay-up	***Hole Diameter (mm) ±0.2(mm)***
Cross Ply/Quasi-Isotropic	6
"	10
"	15
"	25
"	45
Cross Ply	45 + 15
Cross Ply	45 + 25 +15
Quasi-Isotropic	6 in various positions
"	25 + 15

The aim of these experiments was to investigate the optimum location of current probes in order to detect such severe form of damage. Each plate had either a single or a combination of holes. The effect of lay-up and positioning of current electrodes were two additional crucial parameters which have been investigated.

6.4.5 Specimens subjected to impact damage

Two cross ply and thirteen quasi-isotropic plates with dimension 280 x 280 mm and thickness of 2 mm were impacted, and the acquired data were used for the creation of a model relating the changes in electrical potential with the extent of the impact damage.

Early experiments of damage detection in the form of holes showed that potential changes can only extend to distance up to 40 mm from the damage centre, transverse to the current introduction line. As a consequence, 64 electrodes instead of 121 were placed

on the impacted or the bottom surface or in both simultaneously before impact occur. This is shown in Figure 6. 14.

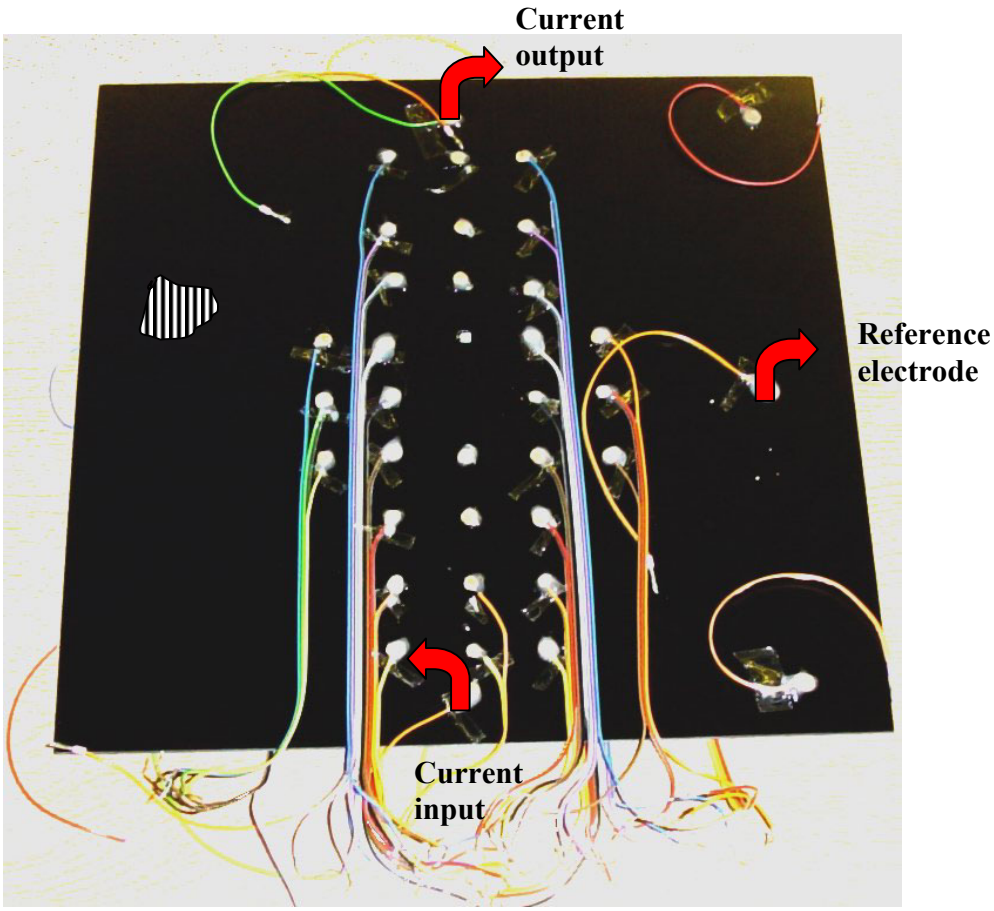

Figure 6. 14: Probe distribution on quasi-isotropic plate.

The current introduction probes were always placed on the mid point at each edge of the panel, with current flowing parallel to the surface fibre direction. A 100 mA current was introduced using a DC current calibrator. The reference probe was placed 100 mm away from the centrally located impact site, alternatively on the top or the bottom surface (Figure 6. 14).

The impact energies were varying between 2 J and 12 J. In the cross ply plates, all different energy impacts were contacted on the same plate. However, in the quasi-isotropic, different plates were used for each impact level. Table 6. 6 presents a summary of all impact energies for each lay-up.

Table 6. 6: Summary of the contacted impact energies on composite panels.

Laminate Lay-up	*Impact Energy (J)*
Cross ply/Quasi-isotropic	2
"	4
"	6
"	8
Quasi-isotropic	10
"	12

6.5 Mechanical Testing Equipment

A description of all the experimental set-up is given in this section. The main aim was to measure the electrical potential changes caused by mechanical strain, variations in temperature, and structural damage induced by impact and holes drilling. All the measurement parameters were acquired and recorded using a PC based data acquisition system. In all the experiments, a constant current source was used; the details of the equipment used, the measured parameters and their significance are discussed in the following sections.

6.5.1 Mechanical loading equipment

A schematic illustration of the experimental set-up and the electrical probes area on the composite surface are shown in Figure 6. 15 (a) and (b) respectively.

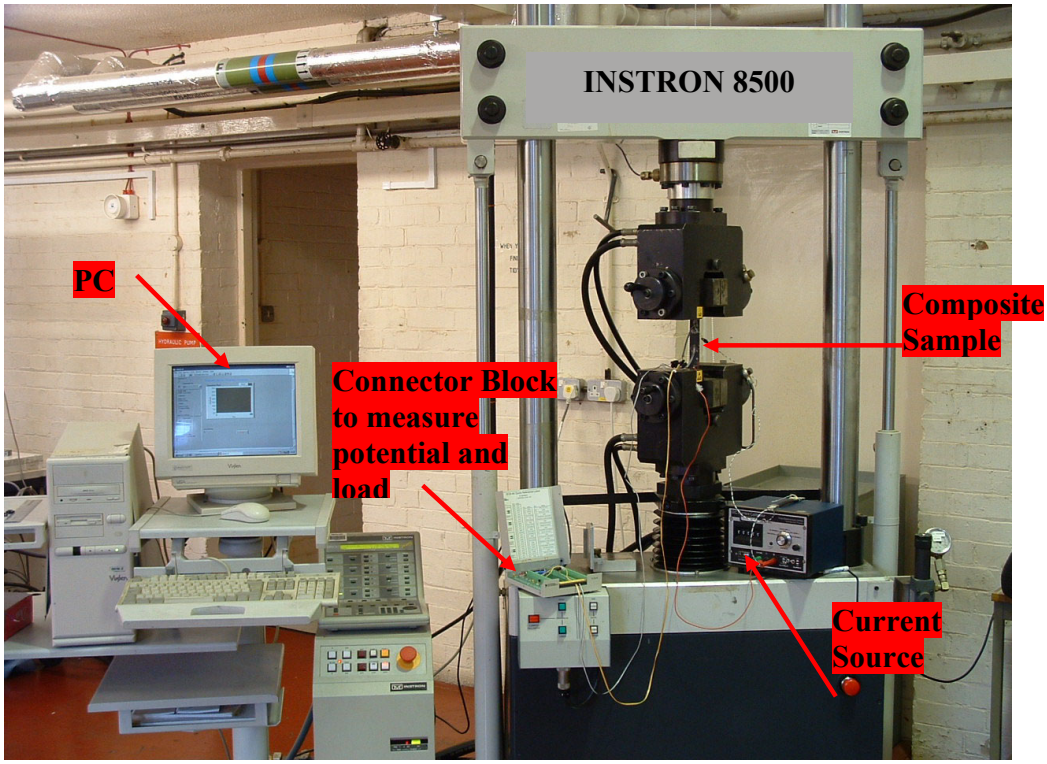

a)

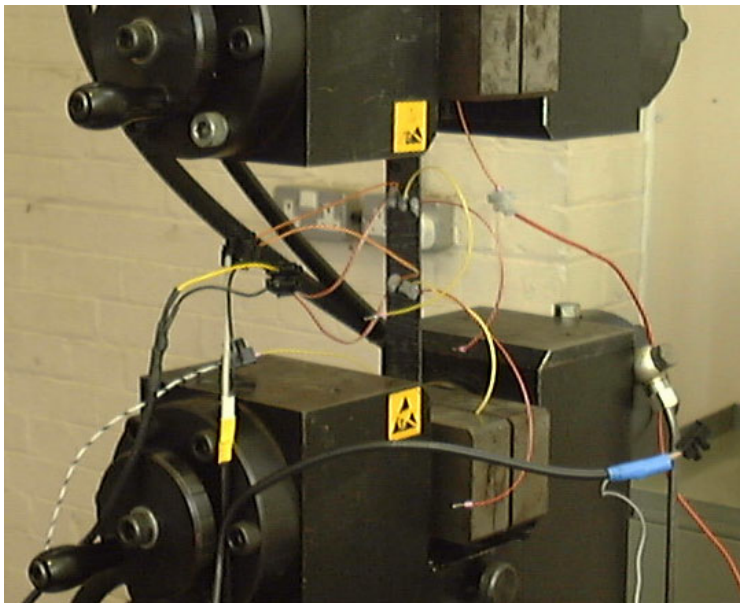

b)

Figure 6. 15: a) Photograph of the experimental set-up for mechanical loading testing b) close-up on the electrical probe area on the composite surface.

During the test, the electrical potential, load and strain were measured. An Instron 8500 series servo hydraulic machine was used for cyclic testing. The maximum dynamic loading carrying capacity was 100 kN and it could be measured with accuracy of ±0.4% for full scale loading. The maximum frequency of the test machine was 10 Hz; however, in most of the samples, a frequency of 0.1 Hz was used.

The Instron machine is capable of conducting cycling tests under both load and strain control. In the present study the machine was always under load control, and the values of load were directly recorded in the computer using lab-view data acquisition software. All tests were performed at ambient temperature.

6.5.2 Strain and electrical potential measurement methods

Direct measured and calculated strain values were used in this research. On selected samples the strain was measured using a dynamic extensometer, model 2620-602, manufactured by Instron. The maximum strain at 50 mm gauge length was 5%. The output of the extensometer was connected to the data acquisition system, so that the data were directly stored in the PC system. In other samples strain values were calculated from knowledge of the stress and the elastic modulus of the composite.

6.5.3 Current source

The function of the constant current source is to deliver a constant current through the specimen. The constant current source limits the amount of current flow. If constant voltage source used instead of constant current source, the voltage is limited and the current flow is unlimited. The main advantage from using constant current source is that from measuring potential drop, the resistance can be calculated using Ohm's law (equation 2.1). If the current varies, this cannot be done. An additional advantage is that due to the limited current flow the resistive heating due to Joule's effect is restricted.

The selection of current level flow through the samples is of significant importance and depends on various parameters such as sensitivity and resistivity heating effects; both are going to increase with increasing the amount of flowing current. The optimum selection

would offer a high sensitivity with the minimum heating effects. The effect of the latter is also enhanced by the increase in temperature during cycling.

Various researchers used different values of current levels; Schulte and Baron [92] have used 50 mA current and they reported no increase in temperature. A constant density current supply of 100 mA with accuracy of 6 μA manufactured by Time Electronics was used throughout this investigation. No further increase was attempted since it may affect the operation temperature of the silver paint. In unidirectional 90° samples the current source was unable to apply sufficient voltage at 100 mA due to the high resistance perpendicular to the fibres. Instead, a constant current of 10 mA was used.

The relevant specifications of the instrument are as follows:

Output:	0-100 mA in 5 ranges.
Accuracy:	±0.02% of setting, ±0.005% of range, ±2 nA
Voltage capability:	15V

6.5.4 Digital multimeters (DMM)

Digital multimeters convert analogue signals to digital information; a DMM, series 2000, manufactured by Keithley Instruments was used in this investigation to measure the electrical voltage in numerous samples. The high sensitivity and versatility of this instrument are some of its main features. It is fully programmable with 6½ digit resolution and in standard configuration it is capable of DC voltage measurements between 100 nV and 1 kV on six ranges with 0.002% accuracy. Due to its high input impedance (≥ 10 GΩ) the noise level is kept very low, increasing the sensitivity of the measurements. The DMM was used either for direct measurements or for calibrating and cross-checking the data acquisition system.

6.5.5 Data acquisition system (DAQ)

The data acquisition system comprises a PC-Pentium III 866 MHz, a data acquisition card, and connector block. Three different DAQ cards and connectors blocks were used in this investigation, depending on the application. A short description of the three boards is given below.

a) Data acquisition board for mechanical loading

The DAQ card used in this investigation was a four channel, NI-4452 card, manufactured by National Instruments. This board has 16-bit resolution and it is able of acquiring up to 204.8 thousand samples per second. This enables us to obtain a significant amount of data, even at very high testing frequencies such as 10 Hz. One of the major advantages of this card is that it can attain data simultaneously from all channels. This ability would eliminate any shift in phase between load and electrical potential during cycling, caused by the data acquisition system.

The input range varies from ±10 mV to ±42.4 V. For the input range used in this study (±100 mV) the error was as little as 3.05 μV. In addition the high input impedance (1 MΩ), contributes to low noise and distortion effects and makes possible high-accuracy measurements. A compatible connector block was used with this card, model BNC-2140, also manufactured by National Instruments.

b) Data acquisition board for impact testing

The National Instruments DAQ Card-AI-16XE-50 was used in the experimental series. This card is specially designed for lap-tops. This board has 16-bit resolution, sixteen analogue inputs, able of acquiring measurements from 64 channels, in single-ended mode. It does not obtain data simultaneously from all channels as the previous card, however, it scans all channels very fast and it is able of acquiring 20 thousands samples per second; the range of the input signal varies from ±0.1 V to ±10 V. In the present study, the measurement error was 30.5 μV.

A compatible terminal block was used with this card, the AMUX-64T, designed from National Instruments. This multiplexer block obtains either data from 64 channels in single-end mode or from 32 channels in differential form.

c) Data acquisition board for temperature change experiments

The DAQ card used for this experimental series was the PCI-6023E, manufactured by National Instruments. This board has 12-bit resolution acquiring measurements from 8 (single-end) or 16 (differential) channels, at speeds up to 200 thousands samples per second and the input range varies from ±0.05V up to ±10 V. The device measurement error was 48.8 μV. The connector block used was the SCB-68 which also had an IC temperature sensor for cold-junction compensation in temperature measurements.

6.5.6 Impact testing equipment

A Rosand instrumented falling-weight impact machine was used to conduct all the impact tests. A schematic illustration of the experimental set-up is shown in Figure 6. 16. All plates were impacted once with energies varying from 2 J to 12 J. The tester has the capability to prevent a second strike automatically; the drop on this tester is controlled by setting the velocity, the energy or the height. In these tests, the energy was set to the desired level. A hemispherical steel striker was used in all tests with a diameter of 10 mm.

Masses of 4.53 kg were used for impacts smaller than 8 J and 6.58 kg for impacts of 10 J and greater. All impacts occurred at distances of 0-10 mm from the centre of the plates. From the impact tester data various graphs can be plotted. Given the falling mass and choosing the energy, the required height is calculated. All tests were performed at ambient temperature.

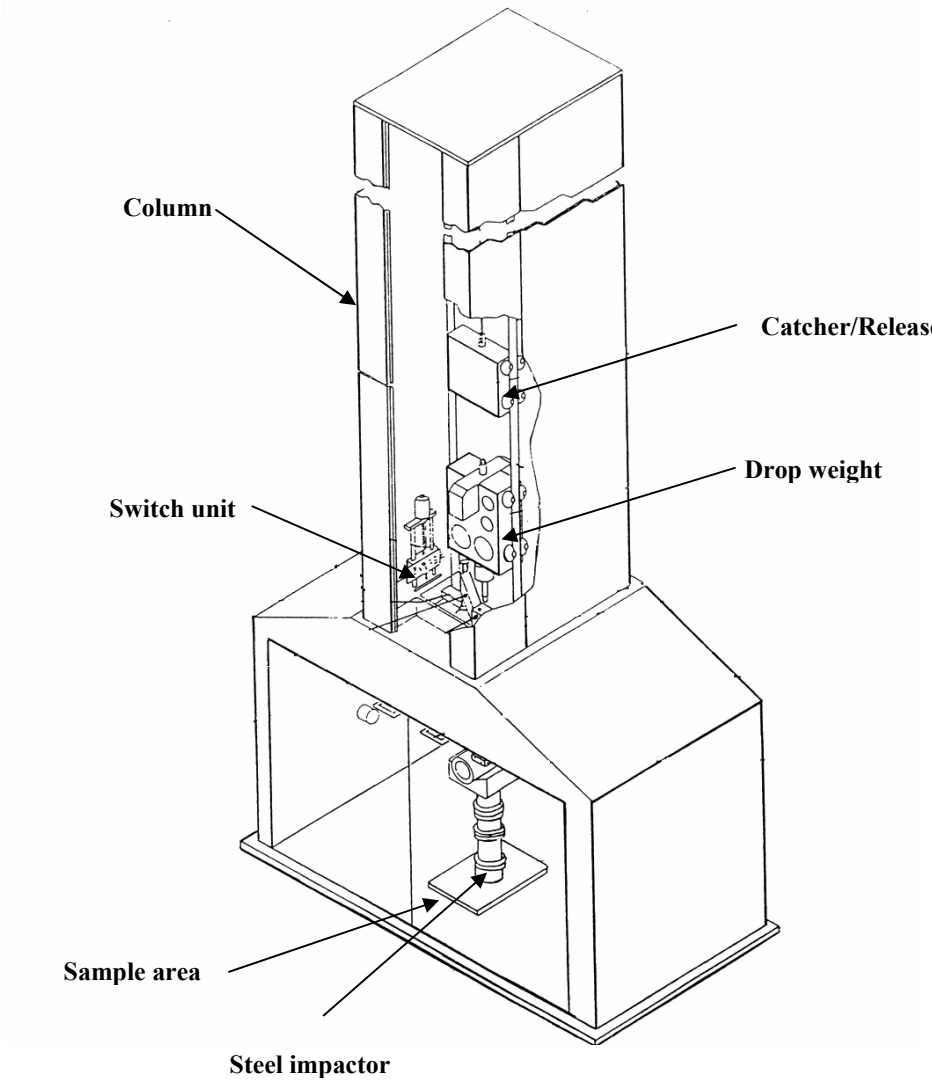

Figure 6. 16: Diagrammatic view of impact machine.

6.5.7 C-scan

All impacted plates were C-scanned with the pulse-echo technique to assess the quality of the laminates and to measure the damage level of the samples after impact. Ultrasonic testing is based on the investigation of sound waves propagated through the material. Ultrasonic techniques can derive information concerning structural features of the

material by observing the attenuation of either the scattered or reflected sound waves. The maximum resolution of the system used was 0.05 mm; a 10 MHz probe was employed and the resolution was set 0.50 mm.

The principle of this technique is demonstrated in Figure 6. 17. The specimens were immersed in water to transmit ultrasonic energy from the transducer to the test part, and a glass plate was used to reflect the signal.

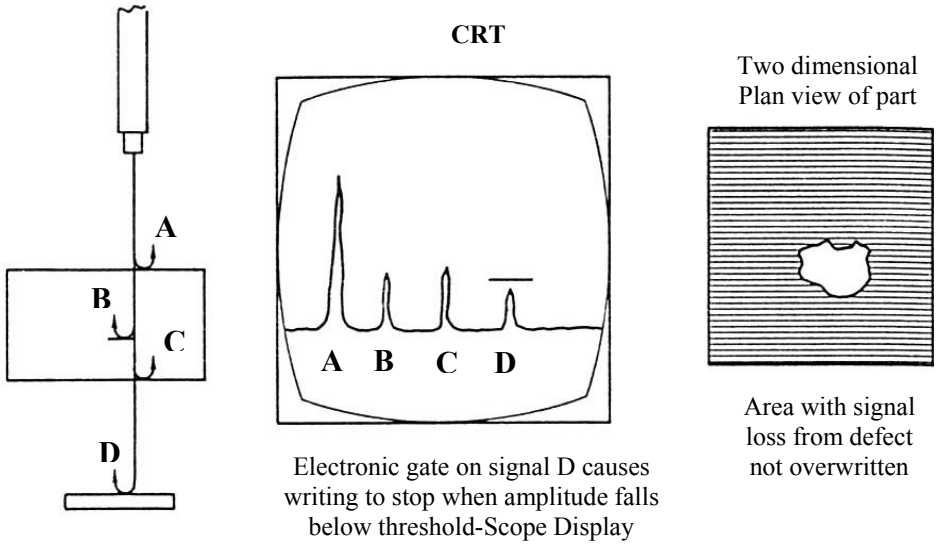

Figure 6. 17: Principle of C-scan technique.

Digital images of the damaged area were acquired and analyzed using commercial software. Damaged and undamaged areas are represented by different colours and the extent of damage was calculated by measuring the size of each area.

6.5.8 Temperature effect testing equipment

All the experiments were conducted using a Techne 500 series oven. The range of operating temperature is -70°C - 200°C. The minimum increase of temperature for this oven is 1°C and the temperature stability is ±1C while the maximum applied temperature on the specimen's surface was 90°C; any further increase would modify the properties of

the silver paint, affecting the potential measured values. Temperatures as low as -40°C were achieved using liquid Nitrogen. The liquid was stored in a steel Nitrogen vessel at -196°C under 1 bar pressure which was connected in the back side of the oven using a specially designed pipe.

The nominal temperature is referred to the one measured on the surface of the composite, and not inside the oven. All temperatures were measured using a welded-tip, K-type thermocouple, which was attached on the sample surface. The accuracy of this Nickel/Aluminium thermocouple is ± 2.5°C and the temperature range varies between -50°C and +250°C.

6.6 Test Programs

The laminate type, the testing mode and the fibre orientation are shown in Table 6. 7.

Table 6. 7: Samples and testing details.

Laminate Type	*Fibre Orientation*	*Type of Test*
UD	0° unidirectional	Cyclic/Temperature/Water
UD	90° unidirectional	Cyclic/Temperature/Water
CP	$[(0/90)_4]_s$	Cyclic/Temperature/Holes
QI	$[0_2/45_2/90_2/-45_2]_s$	Cyclic/Temperature/Impact/Holes

The same fibre type and resin was used throughout the investigation as covered in Section 6.3. Figure 6. 18 illustrates the coordinate system used for a unidirectional laminate. For all experiments, *Lab-view* program, designed by National Instruments was used for acquiring all data.

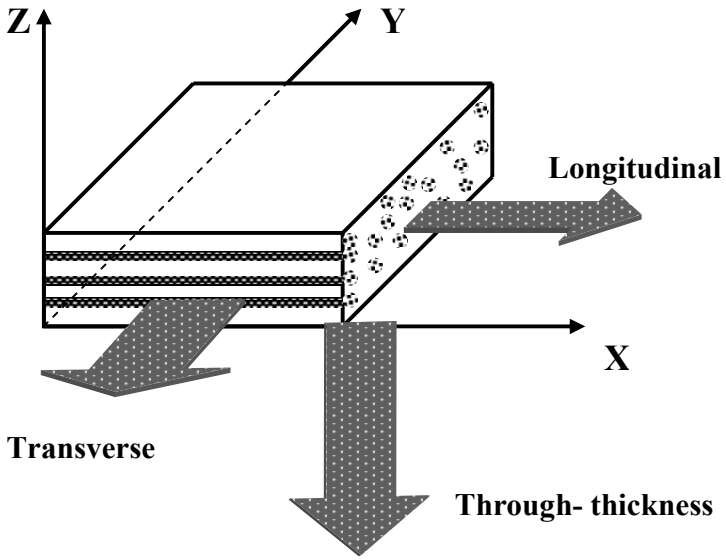

Figure 6. 18: Coordinate system used in this research study.

6.6.1 Mechanical loading

The purpose of conducting this experimental series was twofold; first, to establish a model predicting the current pattern within a composite structure, subjected to cyclic loading. This is important, considering that an in-service composite component is not only subjected to impact, but also to fatigue loads. Secondly, the knowledge of how the latter affects the distribution of electrical potential can give a better understanding of the effect of shock loads on composite structures.

Specimens in cyclic tests were subjected to different load levels and frequencies. For each lay-up, different current introduction and potential probe configurations were used. The details of the cyclic test programs are given in Table 6. 8. All samples were tested within the elastic region, enabling us to calculate the strain level using load data.

Table 6. 8: Details of mechanical loading tests.

Lay-up	*Max. Load (kN)*	*Max. Strain (%)*	*Frequency Levels (Hz)*
UD (0°)	22	0.3	0.05-0.1-0.5-1-3-7-10
CP	20	0.5	“
QI	11	0.5	“

The number of cycles varied from 500 to 1000; all specimens were monitored throughout cycling. Most of the specimens were tested at 0.1 Hz cyclic frequency. A phase shift was observed between electrical potential and mechanical strain. For that reason, different frequency levels were chosen in order to investigate whether the observed phase shift was due to current redistribution within the material or to capacitance. The maximum frequency was used was 10 Hz; however, the number of cycles at that level was limited to 250, to avoid overheating the sample.

A specially designed Lab-view program was used for acquiring the data. The main benefits were the ability to interfere directly in the acquiring process, such as increasing the number of obtained data, reducing the level of noise, changing the output and the input parameters during the experiment. By manipulating the scan rate and buffer size, the system could either be faster (acquiring more data) but more noisy, or vice versa.

6.6.2 Impact testing

The purpose of those experiments was to identify the sensitivity of the electrical potential technique to impact damage. For that purpose, different impact energy levels were selected, as explained in previous section. During the whole loading process, the potential values of 64 probes were monitored using the constructed DAQ system.

The potential was measured before and after impact. The Lab-view programme was designed to show a 3-D chart displaying real-time potential field change compared to the

unloaded status. However, all the contour plots of the potential distributions on the surface of each laminate were drawn using Matlab software.

6.6.3 Temperature effect testing

Temperature plays a critical role in electrical conduction of materials. The temperature dependent resistivity investigations will generate resistivity information about the physics of the conduction mechanism in the composite material. The purpose of this investigation was to investigate the behaviour of the electrical potential under pure thermal loads and to measure their effect in the percentage change of the conductivity compared to mechanical and impact loads.

A program was designed based on Lab-view for this experimental series. The designed program was able to acquire 10,000 values at a time and then to take the average of a hundred values; the scan rate was 2 scans per second.

The electrical potential was not measured continuously with temperature change. That could imply not sufficient time for the potential to stabilise in different temperature levels leading to unreliable measurements. In this investigation, however, the potential was measured at different temperature levels with a 10°C step.

7 POTENTIAL FIELDS

This Chapter presents the results from the investigation of the influence of current input location and stacking sequence on potential distribution fields in damaged and undamaged laminates. As discussed previously in Section 4.2.2, current flow processes in composites are complicated since the current flow depends on the fibre alignment and the number of fibre contacts in the transverse and through thickness directions.

Different current electrode configurations were initially studied in undamaged plates and the results are presented in Section 7.1. The analysis from the effect of damage in the form of holes of different sizes on the potential is presented in Section 7.2. Section 7.3 and Section 7.4 present the results of the effect of impact damage in cross ply and quasi-isotropic laminates respectively. Finally, the morphology of impact damage in quasi-isotropic laminates is presented in Section 7.5.

7.1 Potential Fields in Undamaged Plates

Two cross ply plates and two quasi-isotropic plates were manufactured. On each sample, measurements were taken of the electrical potential from 121 different points as shown in Figure 6. 13. The current electrodes and the potential probes were placed at distances of 20 mm and 40 mm respectively from the edges of the plates. No potential values were obtained at the current electrodes. For clarity, the surface on which the potential probes are placed is named **top** surface, and its opposite **bottom**.

Figure 7. 1 shows equi-potential representations for potential values, expressed in mV, for two undamaged cross ply plates. The horizontal axis represents the direction transverse to the top surface (0°) fibres and the vertical axis the direction parallel to the fibres. Visual inspection of the potential contours reveals that there are some common characteristics for the two cross ply laminates. In both plates, there are significant potential peaks near the current electrodes while the equi-potential field is almost flat elsewhere; the potential contours for both plates are also anti symmetric to the axis transverse to the fibres direction in the centre of the plate **(y=125 mm)**; half being positive and half being negative. Details for the creation of the contour plots are given in Appendix A, while the original potential data for all graphs are given in Appendix B.

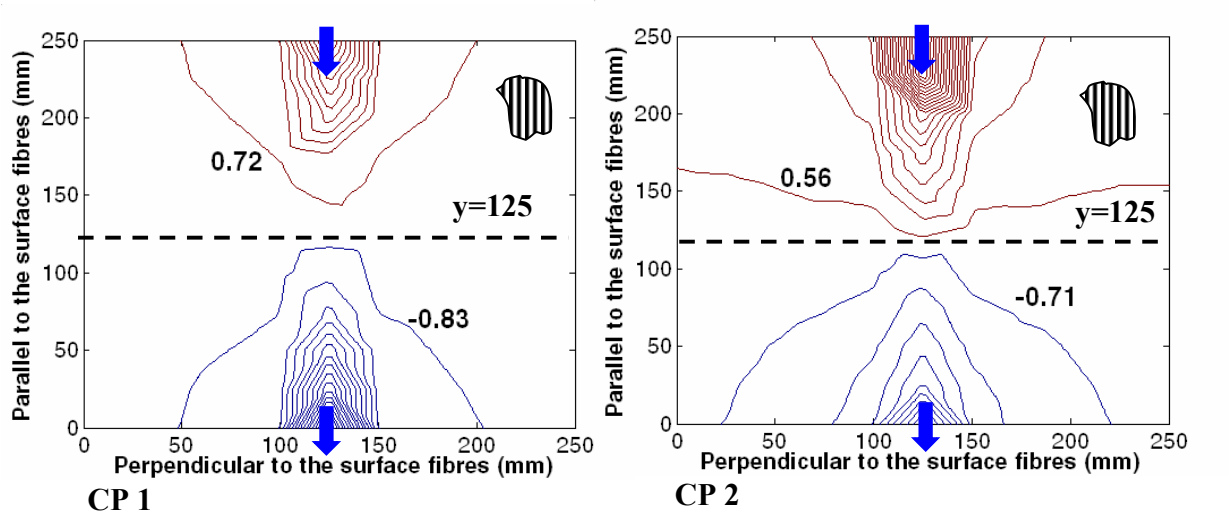

Figure 7. 1: Experimentally measured contour plots showing potential distribution on **top** surface of two cross ply laminates. Current introduction on **top** surface on mid point of horizontal perimeter edges.

These results are consistent with the theory for conduction process in composites; near the current electrodes, the high potential values can be attributed to the high current density, while elsewhere a drop of those values is expected, due to the dispersal of the current in the directions parallel and transverse to the fibres. The reduction is more abrupt in the transverse direction, due to the significantly higher electrical resistance, than the longitudinal. Quantitative analysis revealed that the two potential distributions agree up to 2.6% in potential values measured at probes on equivelant locations in the two plates, indicating the reproducibility of the contours in two separate samples.

Figure 7. 2 shows the potential drop along a section through the centre of the laminate parallel to the 0° fibre direction; three areas of potential change are observed. Initially, the potential decreases exponentially at the probes near the current electrodes, which correspond to the areas of the high potential gradients. In the second region a linear change of the potential values is observed reaching and crossing the area in the middle of the plates where the potential changes sign. This zone produces more flat potential contours as shown in Figure 7. 1. In the third region, an increase in the potential is observed which is more intense at the probes near the current output.

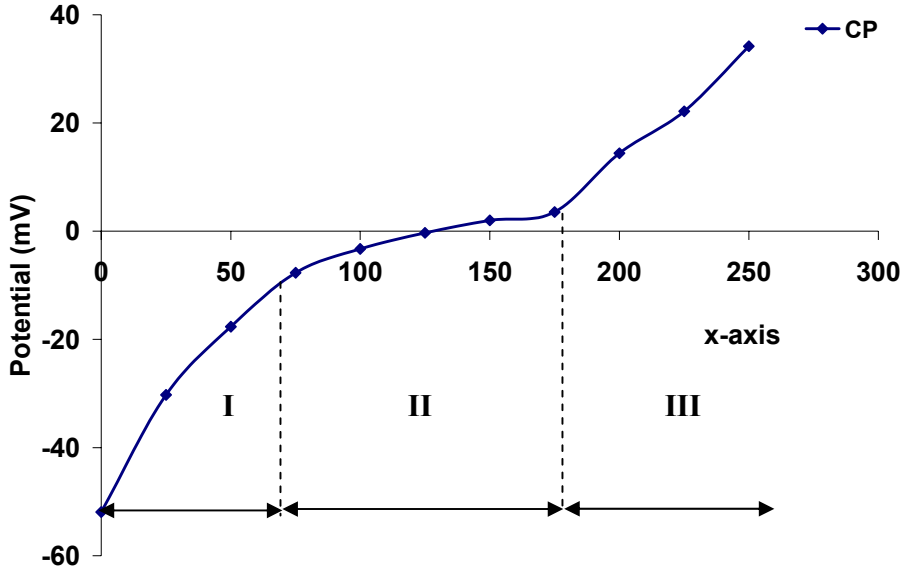

Figure 7. 2: Potential drop on the **top** surface along a section through the middle of the cross ply laminate, parallel to the 0° fibre direction; current electrodes on the **top** surface, on mid point of horizontal perimeter edges.

In Figure 7. 1, CP 2 plate, some asymmetry of the contour plots is observed at the areas where the potential changes rapidly and the contours have a more square than circular shape. This asymmetry arises from the asymmetry between the minimum and maximum potential values as measured experimentally. Ideally, these values should have the same magnitude but different sign. However, if the distances between the current input/output probes and the nearest potential measured probes are not exactly equal, the potential measurements will vary significantly due to the high potential gradient in that area, which affect the potential contours.

The position of the current introduction electrodes changes the field orientation significantly. Figure 7. 3 (a) and (b) show the potential contours for cross ply laminate where the current electrodes are located on the top surface on mid points transverse to the 0° fibres and on opposite diagonal to the laminate respectively.

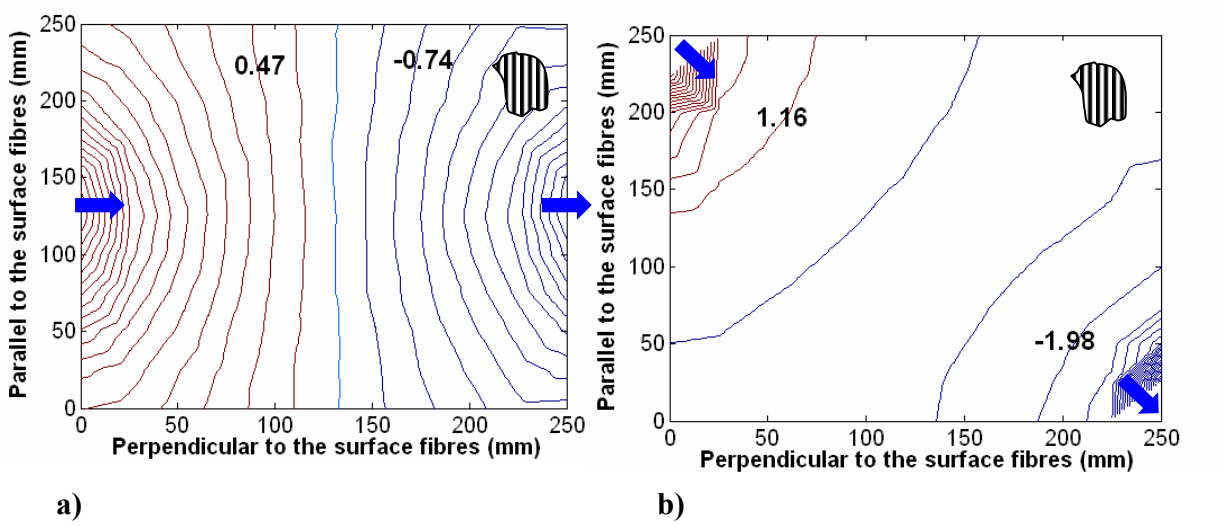

Figure 7. 3: Experimentally measured contour plots showing potential distribution on **top** surface of a cross ply laminate; current introduction on the **top** surface a) perpendicular to the fibre direction (A6S1/K6S1), b) diagonal to the fibres (A11S1/K1S1).

Similarly to Figure 7. 1, the potential contours are approximately perpendicular to the line joining the current input electrodes, without pronounced distortion towards the direction

of the top surface fibres. In this direction of current flow, equi-potential lines are parallel with carbon fibres on the top surface. Areas near the current electrodes are characterized from a high density of equi-potential lines, which gradually become more regular as they approach the middle of the plate.

However, as shown in Figure 7. 3 (a), when the current is introduced transverse to the fibres, the significant peaks in the potential values and asymmetry in the shape of the potential contours near the current input/output electrodes are not observed.

Figure 7. 4 shows that the potential drop, along a section transverse to the 0° fibres through the centre of the laminate, resembles qualitatively the one presented in Figure 7. 2 for a section parallel to the 0° fibres. A more quantitative analysis, however, would reveal some variations. The areas corresponding to regions I and II are reduced by 58% as a consequence of the higher transverse resistance, increasing the linearity of the potential change.

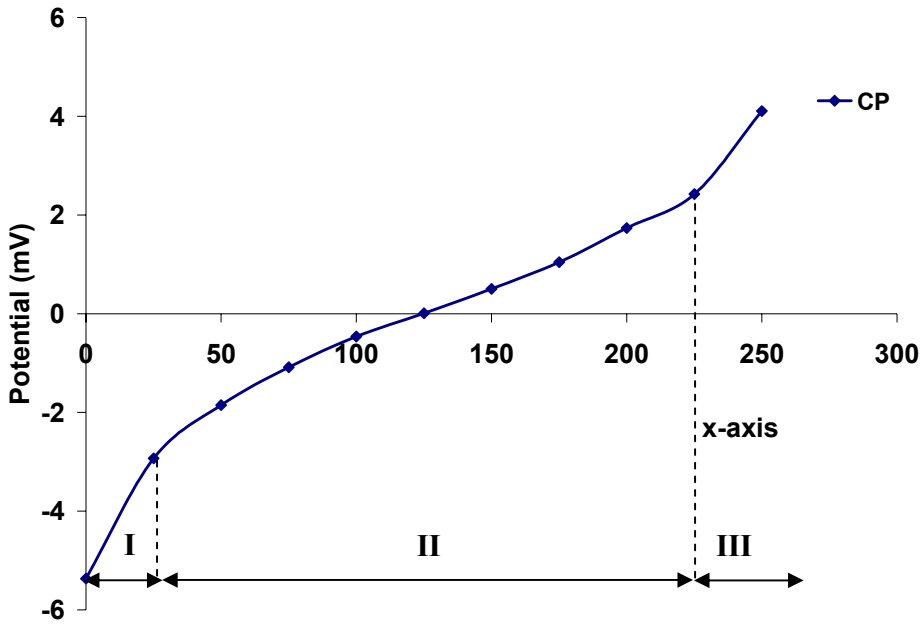

Figure 7. 4: Potential drop on the **top** surface along a section through the middle of the cross ply laminate, transverse to the fibre direction; current electrodes on the **top** surface on mid point of vertical perimeter edges.

The rate of the potential change remains constant in the areas I and III for both graphs. For the region II, however, Figure 7. 4 reveals that the rate in potential change for current introduction transverse to the 0° fibre direction is more than a double the rate when the current is introduced parallel to the 0° fibres. The faster attenuation of the potential values in the first case comes also as a consequence of the high transverse resistance, which tends to minimize the amount of current flowing away from the current source, transverse to the fibres. More even potential distributions are obtained when the current electrodes are placed on the opposite surface of the laminate.

Figure 7. 5 (a), (b) and (c) show the potential fields for undamaged cross ply plate with the current electrodes placed on mid points of horizontal, on opposite diagonals and perpendicular perimeter edges on the bottom surface of the laminate respectively. When the current input is on the bottom surface, it will have to flow via fibre-to-fibre contacts through thickness to reach the top surface of the surface. The electrical resistance in that direction is more than 10,000 times greater than in the longitudinal direction (Chapter 4). As a consequence, the electrical potential values will be very much reduced and the high potential gradients near the current electrodes, as observed in Figure 7. 1, will be diminished.

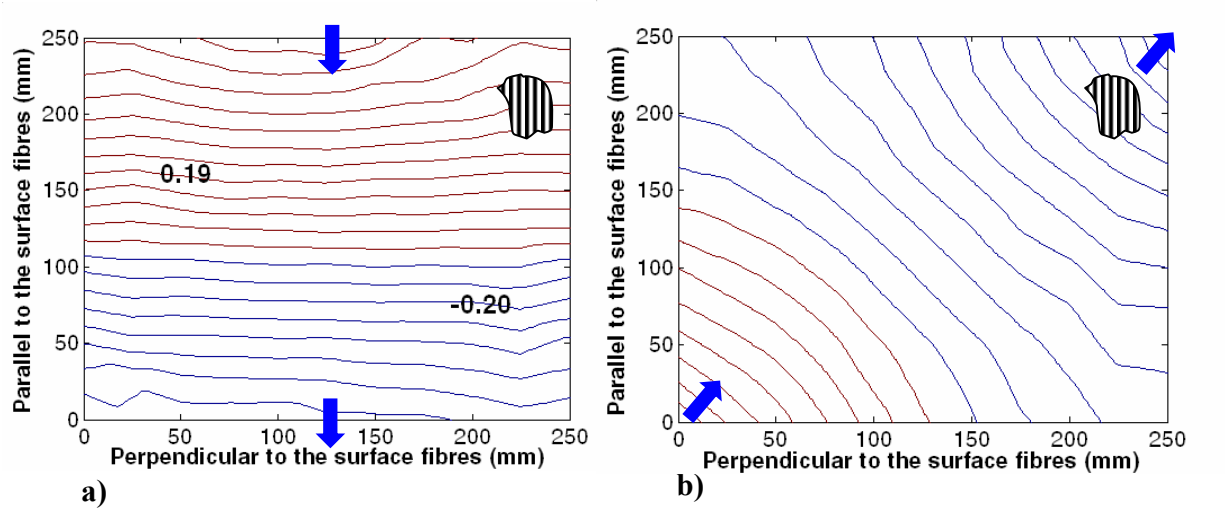

Figure 7. 5: Experimentally measured potential distribution on top surface of a cross ply laminate. Current introduction bottom surface, a) on mid point of horizontal perimeter edges (F1S2/F11S2) b) on opposite diagonals (A1S2/K11S2).

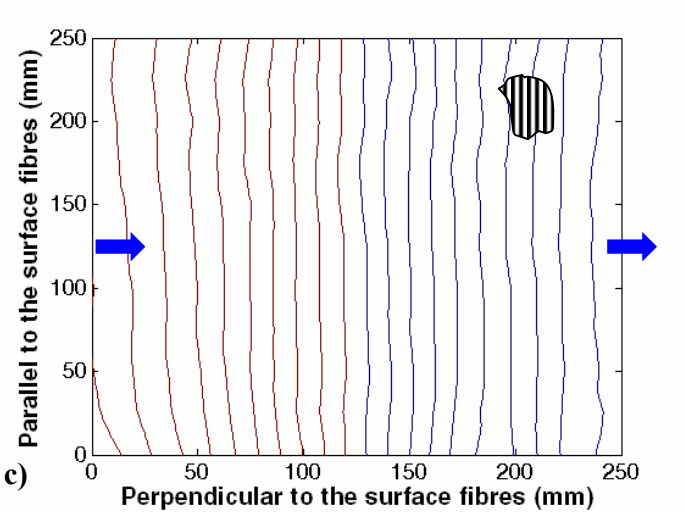

Figure 7. 5 (continued)**:** Experimentally measured potential distribution on **top** surface of a cross ply laminate. Current introduction **bottom** surface, c) surface on mid point of perpendicular perimeter edges (A6S2/K6S2).

For all graphs in Figure 7. 5, the equi-potential contours are perpendicular to the line joining the current input electrodes, without a pronounced distortion towards the direction of the 0° fibres. Similar observations were obtained when the current was introduced on the top surface. This indicates that the equi-potential plots are not affected by the current electrodes position. In the cross ply plate the underlying lamina will be 90° to the surface fibres. The overall symmetry of the contours suggests that despite the great electrical anisotropy of individual laminae, the presence of layers of differing orientation with electrical conductivity between them produces potential fields which in two dimensions are similar to electrically isotropic material. The position of the current introduction electrodes changes the field orientation significantly. This can be seen in situations where the current electrodes are located on the top or on the bottom of the plate.

Figure 7. 6 presents the potential distribution patterns in undamaged quasi-isotropic plates. Similar to the cross ply plates, the potential contours are oriented almost perpendicular to the line joining the current input points, with a small rotation towards the 45° orientation of the ply underneath the surface lamina. There is a slight departure from this picture at the edges of the laminate where distortion occurs, most probably due to edge effect; the position of the current probes influences the orientation of the potential contour plots.

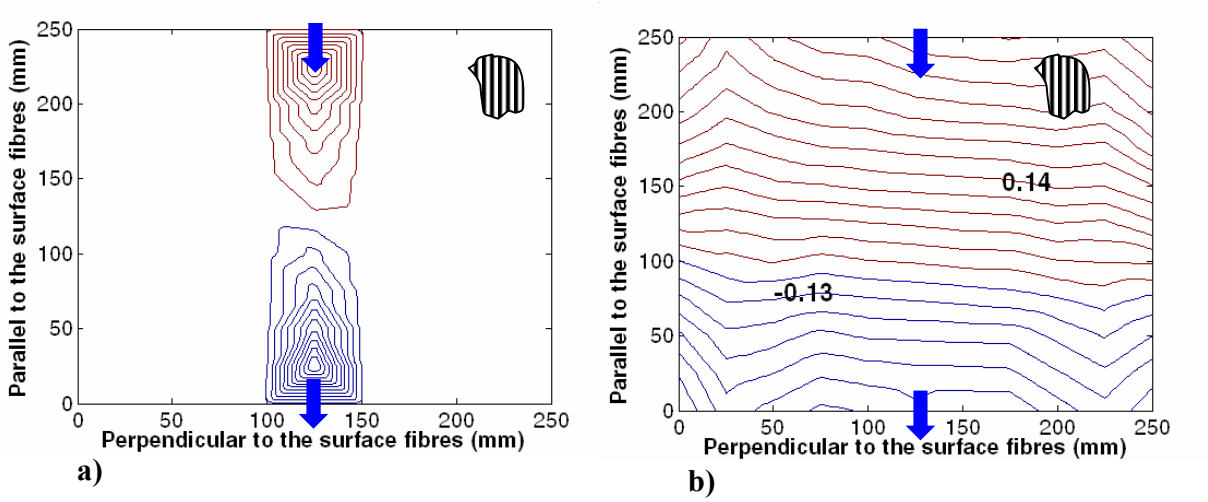

Figure 7. 6: Experimentally measured potential distribution on **top** surface of quasi-isotropic laminate; current introduction a) **top** surface, on mid point of horizontal perimeter edges b) **bottom** surface on mid point of horizontal perimeter edges.

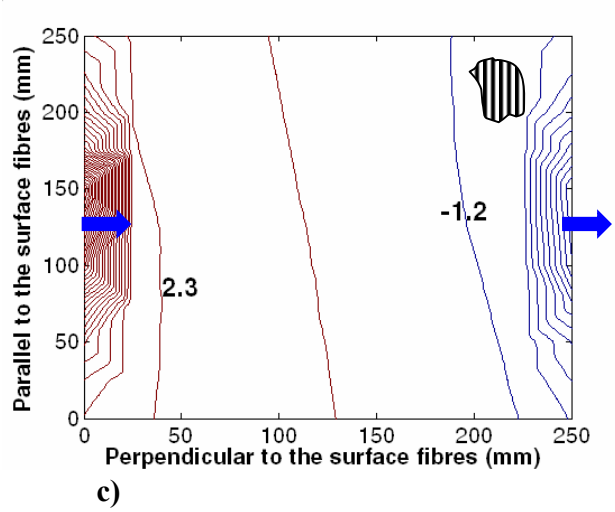

Figure 7. 6 (continued): Experimentally measured potential distribution on **top** surface of quasi-isotropic laminate; current introduction c) **top** surface on mid point of perpendicular perimeter edges.

A comparison between Figure 7. 3 (a) and Figure 7. 6 (c) would reveal that in both CP and QI laminates potential peaks appear near the current introduction electrodes. In CP plate, however, the potential contours extent up to the centre of the laminate as opposed to the quasi-isotropic plate in which the contour are mainly extended around the current input points. This is because in the CP plate the underlying lamina, 90° layer, still has an active role in the current flow process, and it will carry the current transverse to the fibres while in the QI plate, the 90° layer is below the 45° and its contribution in the conduction process is less significant than in the CP plate. The comparison of Figures 7. 6 (a) and (b)

shows the contrast in potential distribution produced by introducing the current on the top and bottom surface.

7.2 Potential Fields in Plates with Holes

Holes were introduced in all the above plates in order to study the optimum location of the current electrodes for damage detection. Various diameter holes were drilled as shown in Table 6. 5. Figure 7. 7 and Figure 7. 8 present the potential contours and potential difference contours, for cross ply plates drilled in the middle with holes diameter of 15 mm and 25 mm respectively. The current input positions are half way along the horizontal perimeter edges on the top surface, with the current flowing parallel to the 0° fibre orientation. The potential values are measured on the top surface and they are displayed in mV.

The potential difference contours, represent equal values of potential change from before the insertion of the hole (Figure 7. 1) compared with after. As it can be seen, the introduction of a hole will not affect the potential contour significantly, and no indication of damage is obtained. However, the potential difference contours can indicate the position of the damage on the laminate.

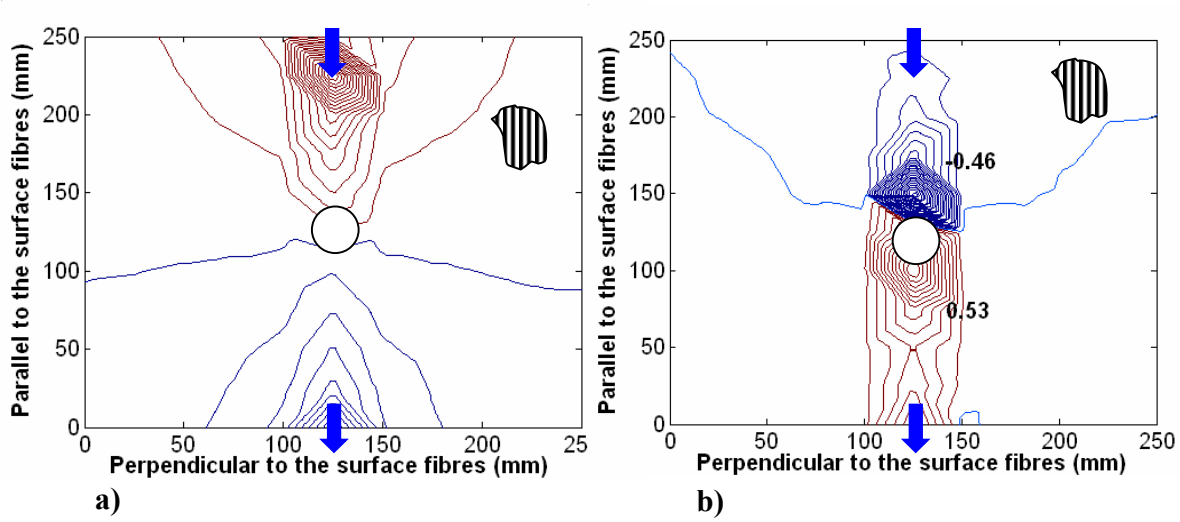

Figure 7. 7: Cross ply plate with a 15 mm hole in the middle: a) experimentally measured contour plot on **top** surface, b) potential difference contour plot; current introduction on the **top** surface on mid point of horizontal perimeter edges.

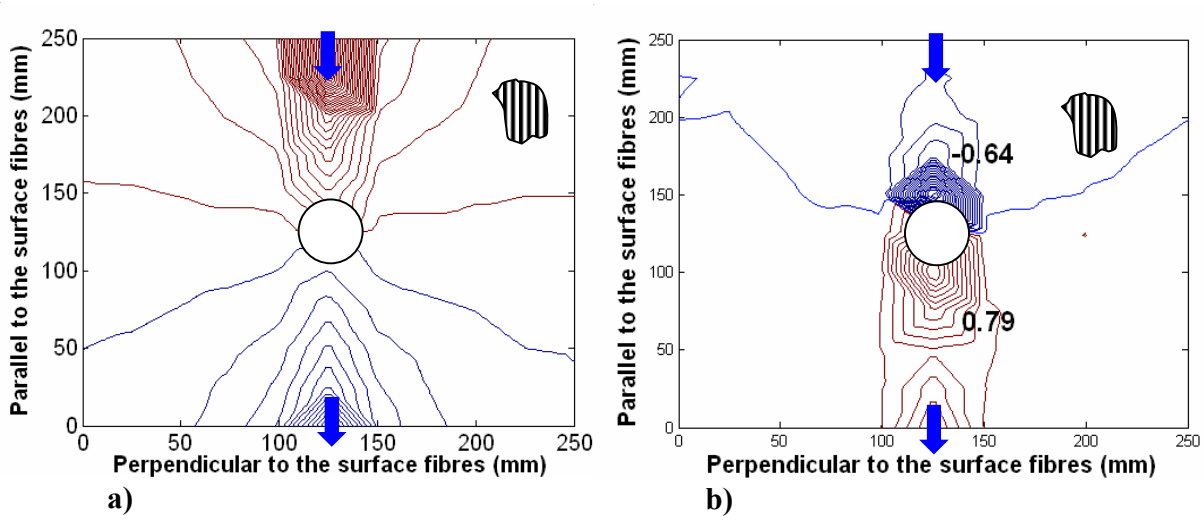

Figure 7. 8: Cross ply plate with a 25 mm hole in the middle: a) experimentally measured potential contour plot on **top** surface, b) potential difference contour plot; current introduction on the **top** surface on mid point of horizontal perimeter edges.

For both hole diameters, the greatest change occurs in two bands on each side of the hole, extending in a direction parallel to the 0° fibres and towards the current introduction electrodes. Potential changes greater than 2% were found at distances up to 100 mm and 110 mm from the centre of the 15 mm and 25 mm holes respectively. The maximum relative potential changes were found to be 95% and 122 %, for the above holes, respectively. The region of greatest change occurs at a point on the line connecting the current input electrodes, adjacent to the perimeter of each hole.

Despite the long length parallel to the fibre direction where detectable changes in potential achieved, in the transverse direction changes in potential greater than 2% are only achievable at distances up to 25 mm from the damage centre. This is because the current will flow in the transverse direction only via fibre-to-fibre contact, reducing the amount of current reaching at points in a distance from the main current flow line and so lowering the detectable potential changes.

The observed asymmetry around the hole region, as shown in the potential difference contours in Figure 7. 7 and Figure 7. 8, can be attributed to the differences in the magnitude of the potential values on the probes near the input/output electrodes as explained previously, in Section 7.1.

The position of the current electrodes will significantly affect the damage detection. Figure 7. 9 and Figure 7. 10 present potential contours and potential change contours for laminates with 25 mm and 45 mm holes in the centre respectively.

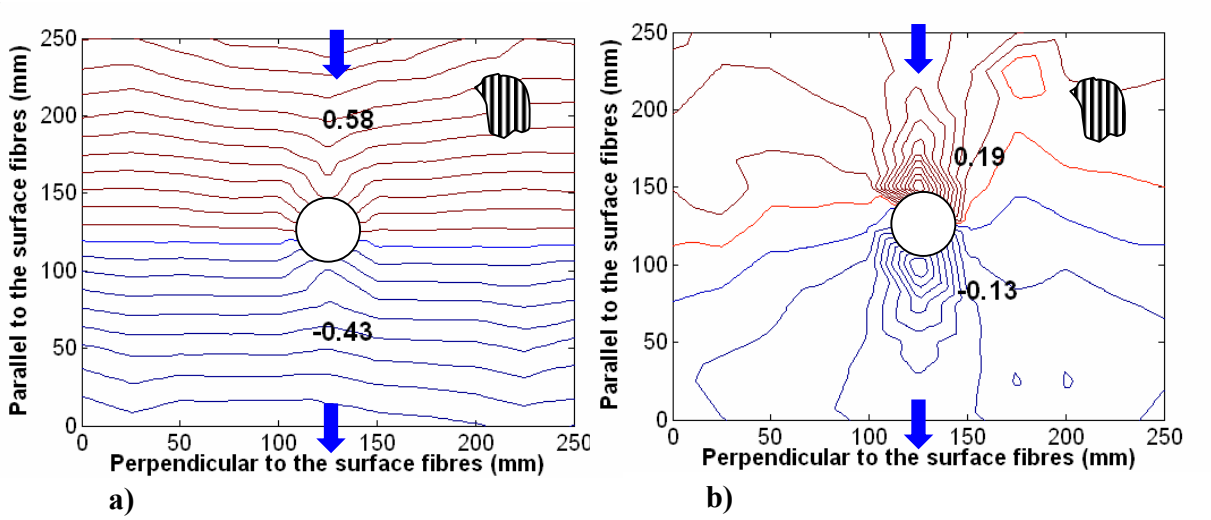

Figure 7. 9: Cross ply plate with a 25 mm hole in the middle: a) potential contour plot on **top** surface, b) potential difference contour plot; current introduction on the **bottom** surface on mid point of horizontal perimeter edges (F1S2/F11S2).

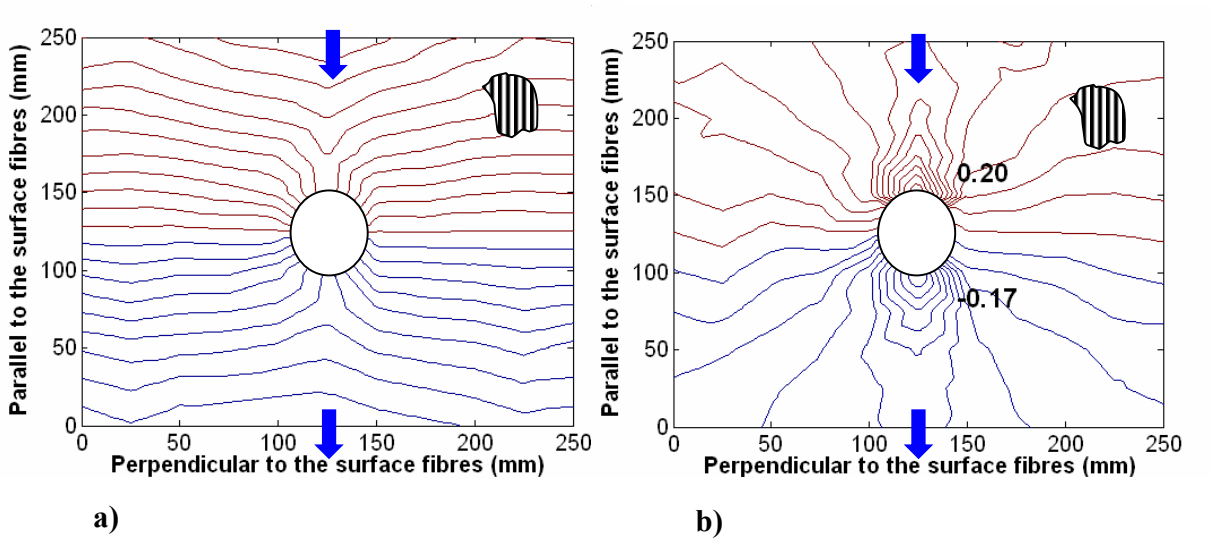

Figure 7. 10: Cross ply plate with a 45 mm hole in the middle: a) potential contour plot on **top** surface, b) potential difference contour plot; current introduction on the **bottom** surface on mid point of horizontal perimeter edges (F1S2/F11S2).

The current electrodes are placed on mid points and parallel to the 0° fibres on the bottom surface, while the potential measurements are taken on the top. The local field distortion around the hole may be seen, directly from the potential contour without having to plot the potential differences; this is due to the current conduction processes.

When the current input is on the bottom surface, it will have to flow via fibre-to-fibre contacts through thickness, to reach to top surface of the plate where the potential measurements probes are located. Its path within the composite structure will be significantly affected by any disorders between the layers, reflecting these changes on the measured potential values on the top surface.

The magnitude of potential values measured on the top surface will be relevant to the magnitude of potential changes arising from damage. This is because when the current is introduced on the bottom surface, a very small portion of it will reach the top surface due to very high resistance through the thickness direction. As a consequence, the distortion of the potential field around the damage can be seen directly by plotting potential contours instead of plotting potential change contours.

This is not the case, however, when the current in introduced on the top surface as demonstrated in Figure 7. 7. In this case the current remains on the top surface, because of the small longitudinal resistance as compared to the transverse or through thickness. Due to its high density, the measured potential values near the current electrodes will overcome any potential changes due to damage, preventing damage detection. The location and size of damage can only be revealed, considering the potential change which will then only be comparable with potential changes arising from the actual damage.

The contour plots of potential change are similar to those observed when the current is introduced on the top surface. The distorted area extends in a direction parallel with the 0° fibres and towards the current introduction electrodes. The region with the greatest change is adjacent to the perimeter of each hole. Figure 7. 11 shows the percentage of the potential change that was measured for different size holes. The disturbances around the hole, transverse to the 0° fibre direction are very limited. The graph X-axis represents a

section across the middle of the plate and parallel to the 0° fibre direction and the Y-axis the relative percentage potential change. The largest change occurs at the site adjacent to the 45 mm hole, showing a value approximately three times greater than that corresponding to the 15 mm hole. The maximum percentage change for the case of the 15 mm hole is about 98%, and 281% for the case of 45 mm hole.

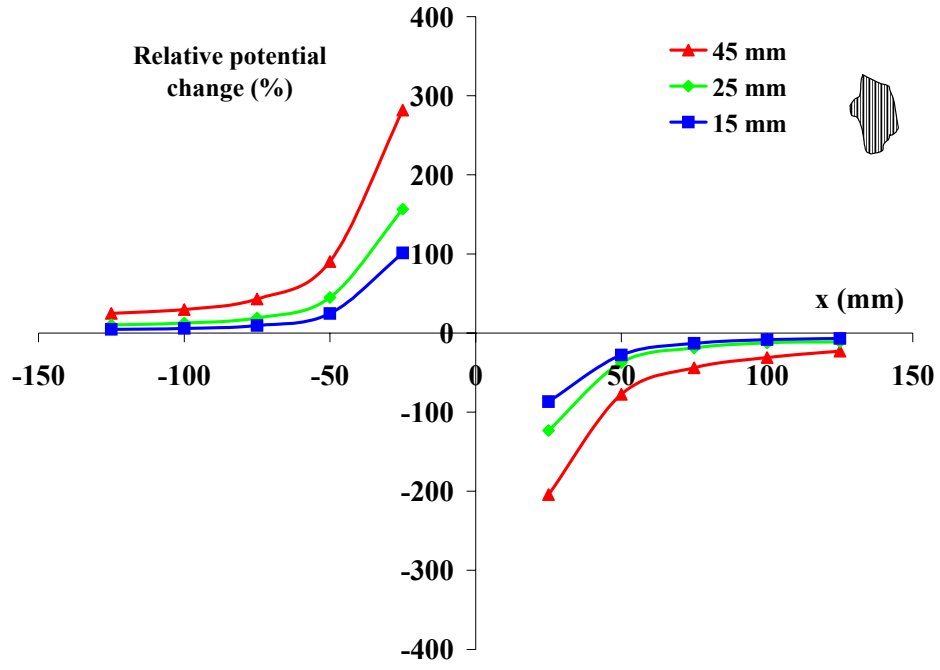

Figure 7. 11: Relative percentage potential change for a cross ply plate due to the presence of holes; current electrodes on **bottom** surface, potential measurements on **top** surface.

The distance from the hole over which the potential is significantly changed is roughly the same as the hole diameter on each side. Changes at a greater distance than this are less than 10% of the original value; there are some small changes extending over all of the remaining area of the plate.

Changing the current input probes to a location midway along the vertical sides of the laminate reduces the sensitivity to damage. As shown in Figure 7. 12 and Figure 7. 13, no indication of damage was found in laminates having holes in the centre with diameter of 15 mm and 25 mm respectively.

The potential difference values, as shown in Figure 7. 12 (b) and Figure 7. 13 (b), are tiny changes at the noise level of 8 μV. It seems therefore unlikely to detect delamination caused by impact, with the above current electrodes configuration, since holes are more severe form of damage.

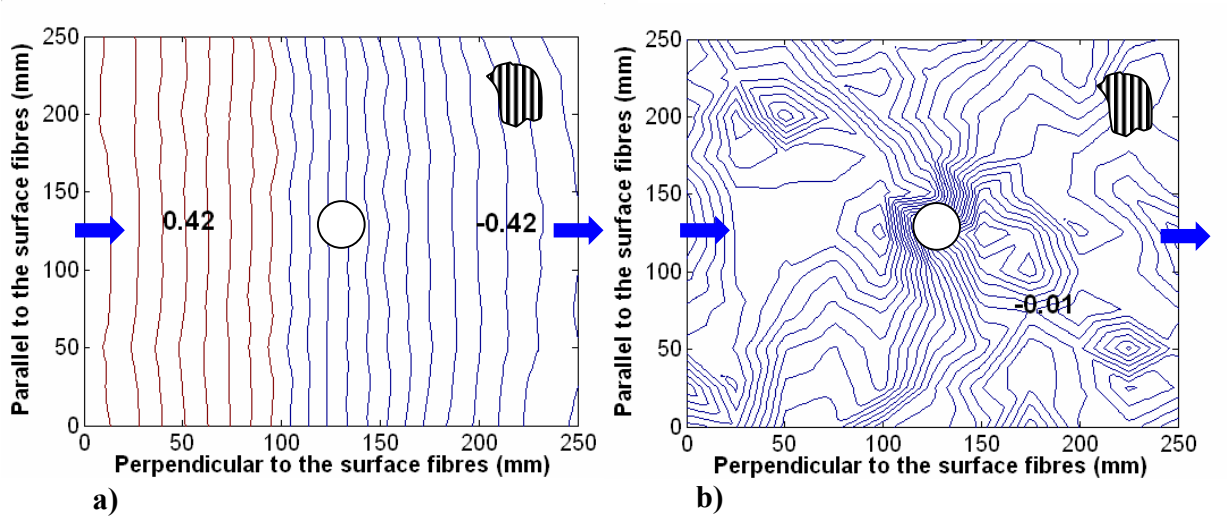

Figure 7. 12: Cross ply plate with a 15 mm hole in the middle: a) experimentally measured potential contour plot on **top** surface, b) potential difference contour plot; current introduction on the **bottom** surface on mid point of perpendicular perimeter edges (A6S2/K6S2).

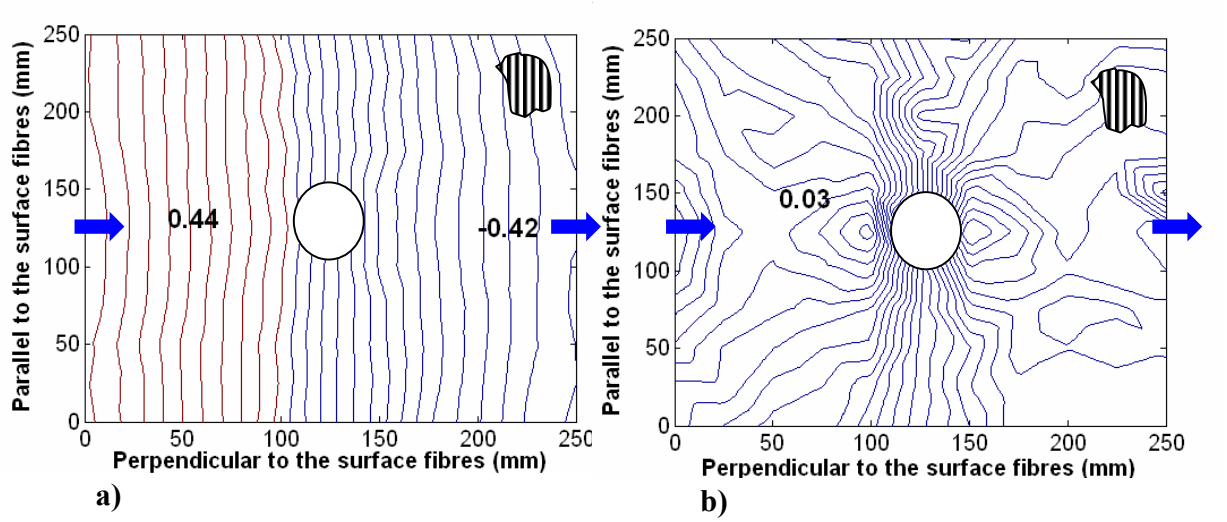

Figure 7. 13: Cross ply plate with a 25 mm hole in the middle: a) potential contour plot on **top** surface, b) potential difference contour plot; current introduction on the **bottom** surface on mid point of vertical perimeter edges (A6S2/K6S2).

Summarizing the results presented so far in this Chapter it can be said that potential contours are significantly affected by the location of the current electrodes. When current is introduced on the top surface, where the potential is measured, the potential distribution is characterized by peaky values near the current probes, followed by flatter distribution towards the centre of the laminate. However, when the current electrodes are positioned on the bottom surface, more diffuse potential contours obtained, and the potential values are lower. Regardless of the position of the current, it was found that the potential contours tended to be perpendicular to the line joining the current input electrodes. The stacking sequence of the composite structure does not affect significantly the potential distribution patterns.

Damage, in the form of holes, is detectable when the current flow is parallel to the 0° fibre direction. When the current electrodes are located on the top surface, the location of the damage can only be revealed by subtracting the potential values before the insertion of the hole, from the values after. However, when the current probes are placed in the bottom surface, a disturbance in the potential contour is observed directly by measuring the potential after the hole is inserted. In both cases, the potential difference contour plots are extended mainly in the direction parallel to the fibres towards the current introduction electrodes. The maximum value of change is greatest adjacent to the 45 mm hole with a value approximately three times that observed at the side of the 15 mm hole.

When the current introduction electrodes are positioned transverse to the fibres direction, the sensitivity of this technique drops significantly so that even holes with diameter of 25 mm cannot be detected clearly. For that reason it is concluded that the optimum configuration for damage detection is placing the current electrodes in the direction parallel to the surface fibres, on the bottom surface.

7.3 Impact Damage in Cross Ply Plates

The current introduction probes were located on the mid points on the bottom surface, parallel to the 0° fibre direction. The damage produced by the impacts was measured quantitatively using an ultrasonic C-scan. Typical picture is shown in Figure 7. 14 (a).

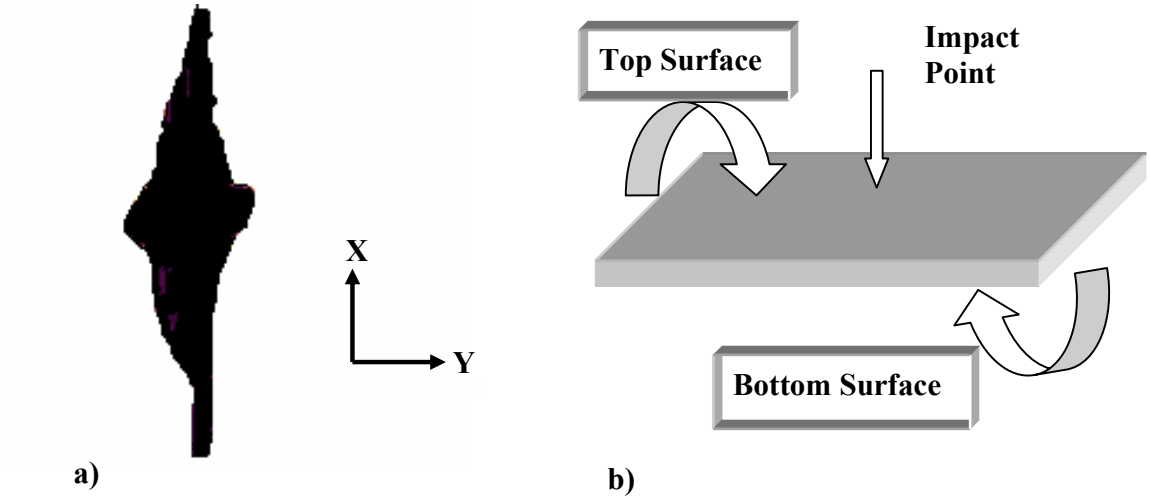

Figure 7. 14: (a) Outline of impact damage size as revealed using C-scan for cross ply plate, (b) designation of top, bottom surface.

For 4 J impacts, the shape of delamination was circular with a radius of 9 mm. For 6 J and 8 J, extension of the delamination in the fibre direction of the 0° ply was detected. All delaminated areas produced by the impacts are as shown in Table 7. 1. It can be seen that increasing the impact energy the damage area increases. For these plates, all impacts were on the same point, in the centre of the laminates. For better designation, the impacted surface is named **top** surface, and the opposite **bottom** (Figure 7. 14 (b)).

Table 7. 1: Damage extent under various impact energies.

Impact Energy in Joules (J)	***Damage size (X*Y) mm, X axis parallel to fibre direction and Y transverse to the 0° fibres***
2	0
4	18 x 18
6	43 x 26
8	89 x 36

7.3.1 Potential fields in impact damaged cross ply plates

Figure 7. 15 shows the potential field measured after impact of 8 J on a cross ply laminate. Based on the results for damage detection revealed for the laminates with holes, the current electrodes were placed on the bottom surface, and the potential was measured on the top surface. The local field distortion around the impact damage zone can be seen.

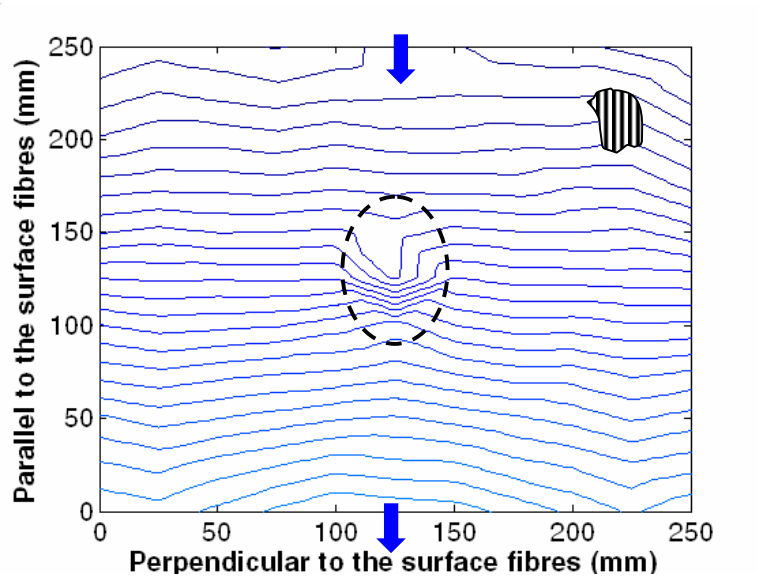

Figure 7. 15: Distortion of potential field after impact of 8 J on cross ply laminate; potential measured electrodes on the **top** surface, current electrodes on the **bottom** surface.

The current will flow through the whole thickness of the laminate, in order to reach the top surface where the potential is measured. Structure imperfections such as those caused by impact damage will affect the current path and these changes will be reflected in the potential measurements on the top surface. There is no significant change in potential for 2 J and 4 J energy impacts, even though there was some back face splitting visible after 4J; detectable changes in potential began at 4 J. Figure 7. 16 shows a two dimensional plot of the percentage changes in potential, resulting from the impact plotted as a function of distance from the impact centre along the fibre direction.

There is a correlation between the potential changes and the largest projected area as revealed by C-scan. A peak in the percentage change is found at 25 mm distance from the centre of impact, extending in the direction of the fibres. Potential changes greater than 5% were found at distances up to 100 mm followed by a decline to changes of a few percent, achieved at greater distances from the centre of impact. The maximum potential percentage change was found to be 40% for a 6 J impact and 60% for an 8 J impact for 36 mm and 89 mm diameter delamination.

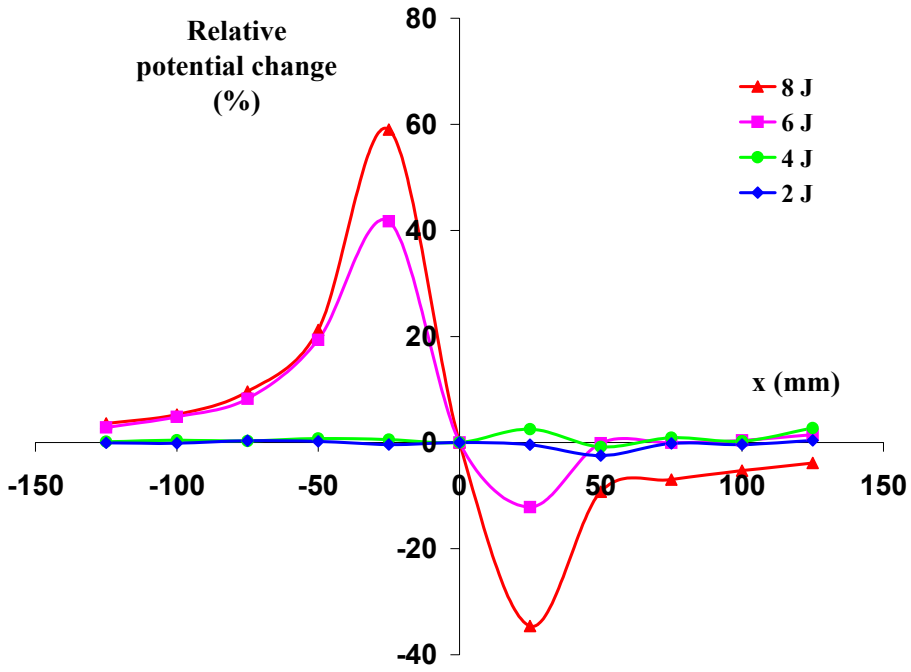

Figure 7. 16: Percentage relative potential change along the middle of a cross ply plate and parallel to the **top** surface fibres; measured electrodes on the **top** surface, current electrodes on the **bottom** surface.

At distances of 125 mm from the centre of the damage site, potential changes were at 3.8%. This suggests that a network of probes of spacing 100 mm could detect whether damage had occurred.

In the direction transverse to the fibres, the maximum potential changes rose up to 22% at distances 25 mm from the impact site, followed by significant reduction up to 4.3% at

distances 50 mm from the impact centre. The extent of the potential changes in the current flow direction is much greater than in transverse direction because a very small portion of the current will flow transverse to the fibres, due to high electrical resistance, reducing significantly the potential values.

7.4 Impact Damage in Quasi-Isotropic Plates

The investigation of the effect of impact damage on electrical potential in cross ply plates (Section 7.3), was conducted using a single cross ply plate subjected to different impact energies on the same spot (centre of plate). That creates an issue of accumulating damage especially at elevated impact energies, questioning the actual effect of each individual impact size on the potential changes and in extent the sensitivity of this technique to impact damage. As a response to this demand a series of experiments were conducted on distinct plates, each one subjected to one impact.

All plates were instrumented on the top surface, *(configuration 1)*, and the bottom surface, *(configuration 2)*, with 32 electrodes (Figure 6. 14), in order to measure potential distribution across the plate. In configuration 1 the current electrodes were placed on the top surface while in configuration 2 they were positioned on the bottom surface. In both configurations, the current flow was always along the 0° fibre direction. All plates were ultrasonically C-scanned after impact to measure the size of impact damage.

Table 7. 2 shows the sizes of all the measured delaminations for the different impact energies. The X represents the length of delamination parallel to the fibres and Y the width.

Table 7. 2: Damage size measured for different impact energies using C-scan.

Panel Designation	***Impact Energy (J)***	***Damage Size (X * Y) mm^2***
1	2	19 x 11
2	4	34 x 15
3	6	50 x 25
4	8	74 x 23
5	10	111 x 28
6	12	135 x 29

Figure 7. 17 shows the damage areas revealed by the ultrasonic C-scan for all impacted plates. The shape of the delaminations was roughly elliptical with the major axis extending parallel to the 0˚ direction of the outer fibre layer. The smallest measured damage area was 19 x 11 mm for the 2 J impact, and the biggest was 135 x 29 mm for the 12 J impact.

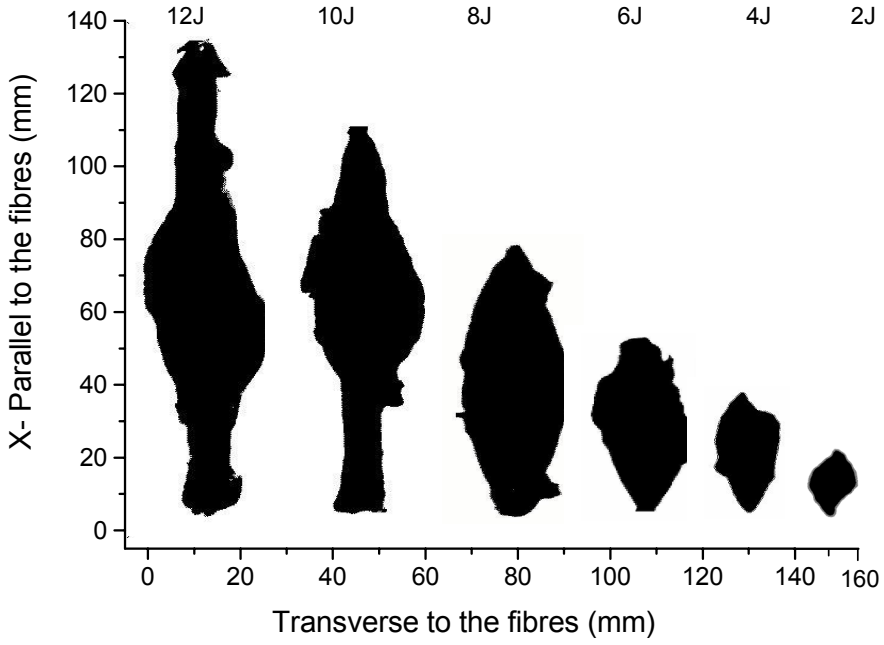

Figure 7. 17: Outlines of impact damage size as revealed using C-scan for quasi-isotropic plates.

Figure 7. 18 (a), (b), show the potential distribution before and after the 10 J impact. The current electrodes and the potential probes were located on top surface. In order to illustrate more clearly the percentage changes in potential, the data are represented in 3-D contour plots instead of 2-D; there is little obvious potential change in the composite plate, because of the large variation in potential within an individual plate. However, by plotting contours of equi-change in potential it can be seen where the damage is located, (Figure 7. 19 (a)). Figure 7. 19 (b) represents potential changes for the same impact but for current/potential probes located on the bottom surface. It can be seen that in both Figure 7. 19 (a) and (b), there are large changes in potential around the damage zone. However, the measured potential changes in the immediate damaged area when the probes are placed on the bottom surface, are more than three times greater than when they are positioned on the top surface, although they do not extend as far spatially.

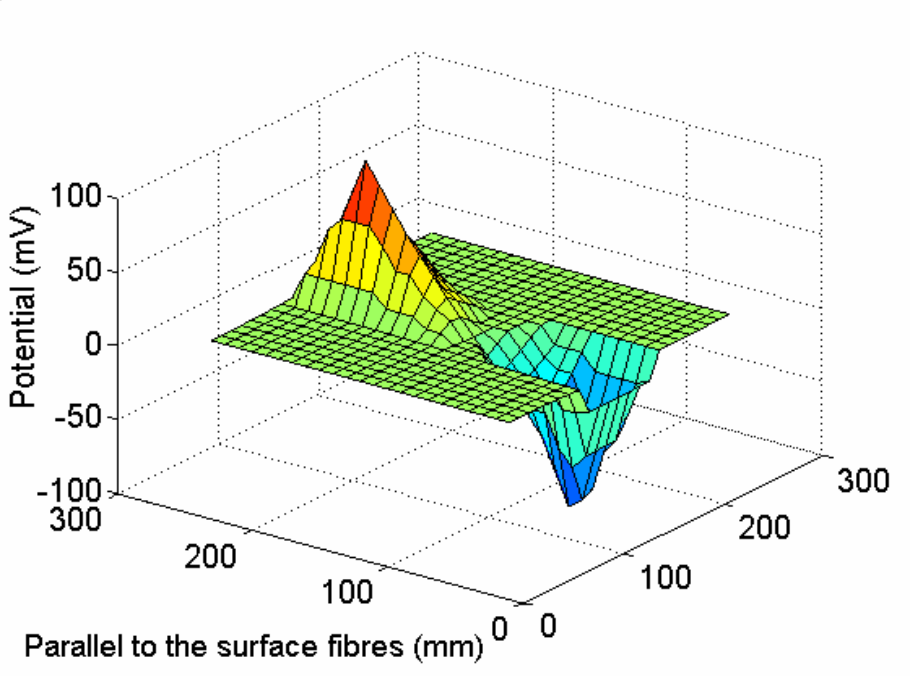

a)

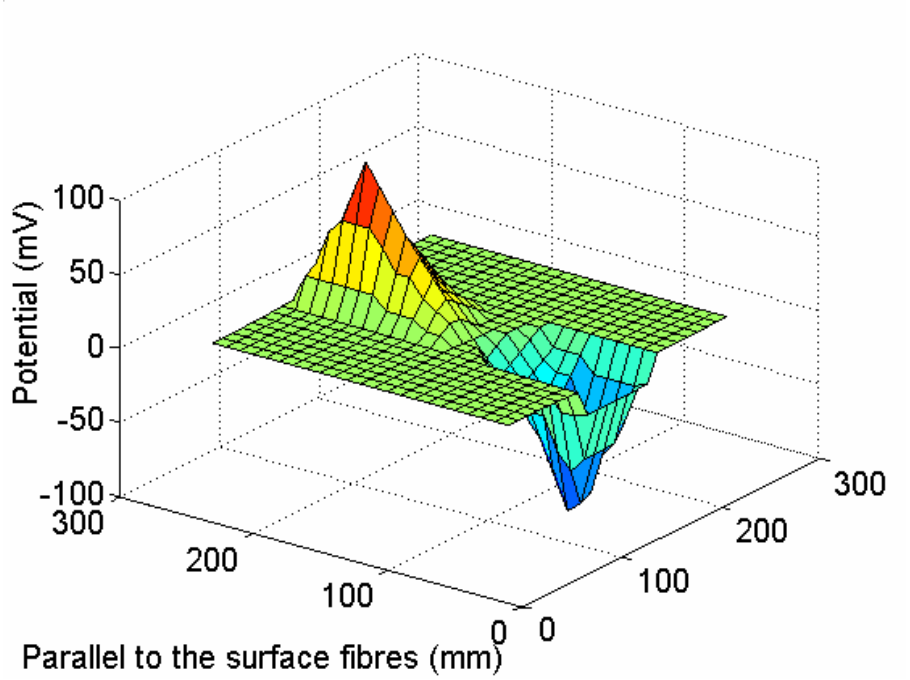

b)

Figure 7. 18: Plots of a) potential distribution on the **top** surface before 10 J impact, (b) potential distribution after 10 J impact; current electrodes/potential measurements on the **top** surface.

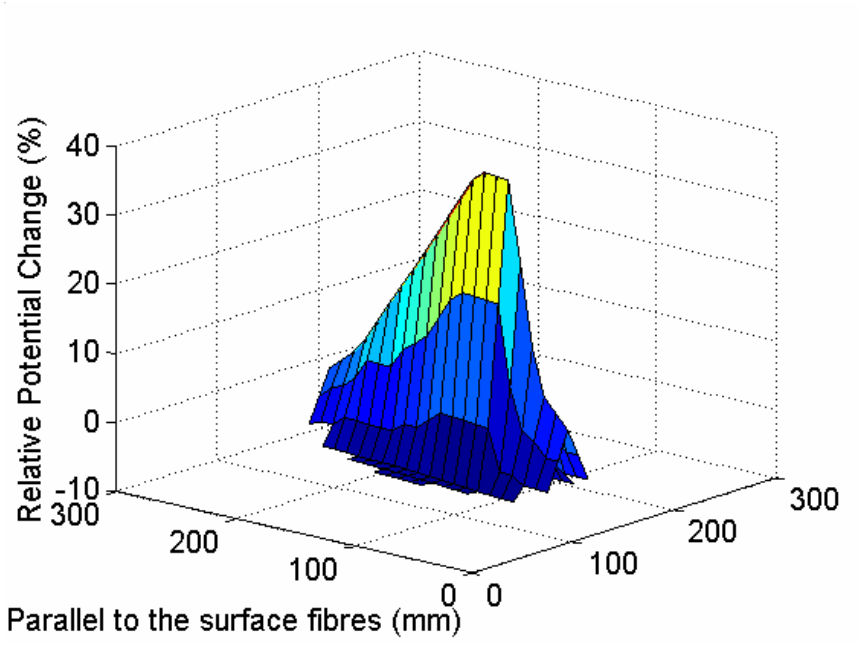

a)

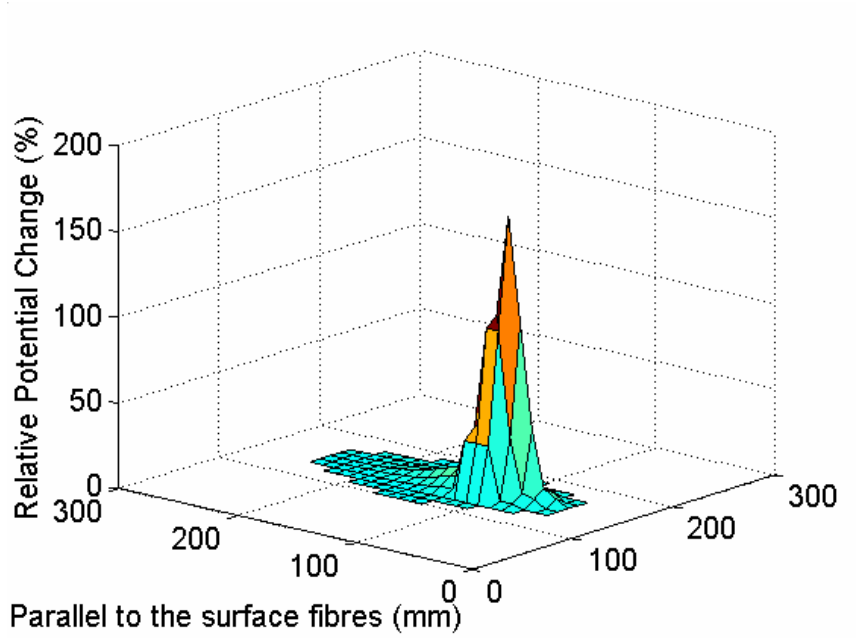

b)

Figure 7. 19: Plots of percentage potential change after 10 J impact a) for current electrodes/potential measurements on **top** surface (b) for current electrodes/potential measurements on the **bottom** surface.

Figure 7. 20 and Figure 7. 21 show typical examples of 3-D contour plots of percentage potential differences caused by impact damage for plates subjected to impacts between 2J and 12J for configuration 1. The main potential disturbances are located in the area

around the impact site and extended parallel to the fibre direction. The size of peak potential changes increases with impact energy.

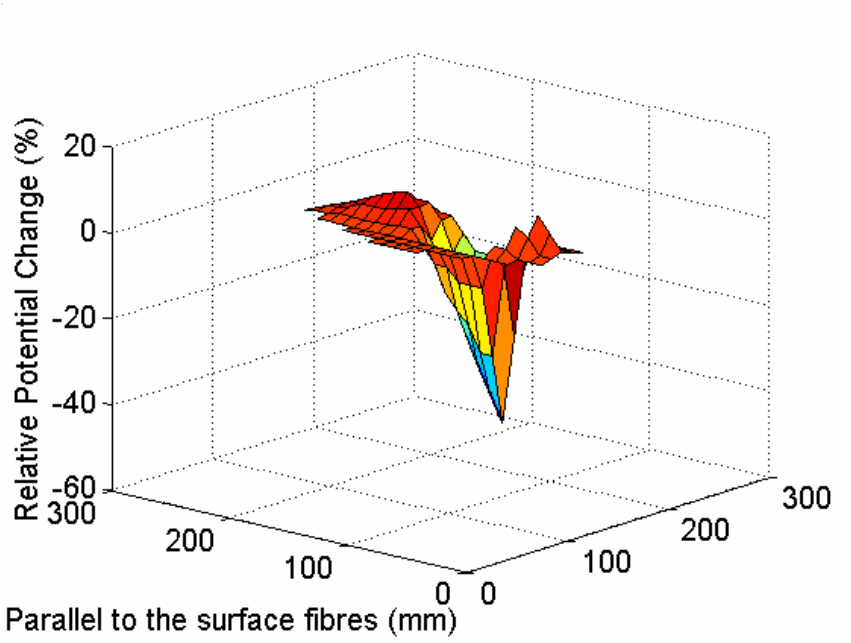

a)

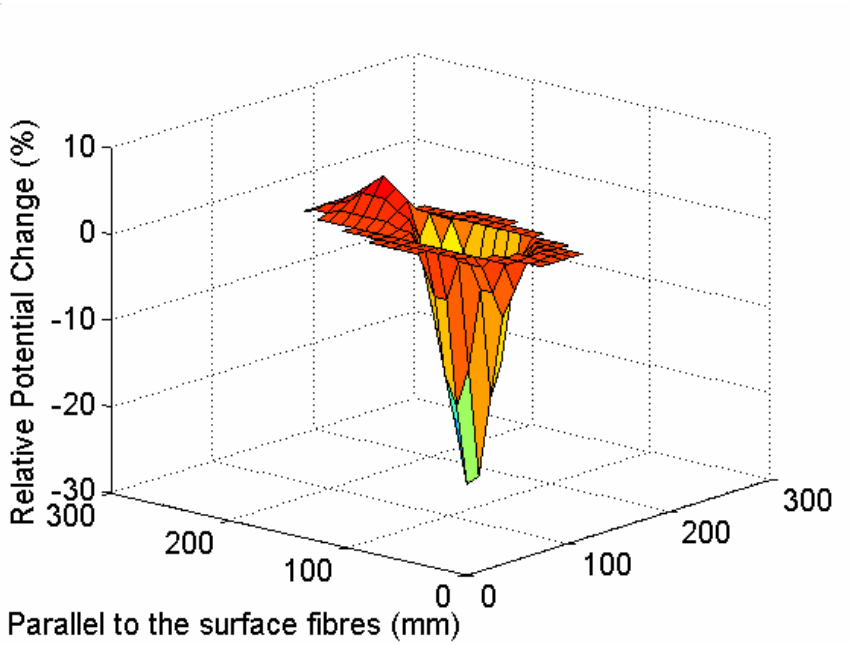

b)

Figure 7. 20: 3-D illustration of potential percentage difference after a) 12J and b) 8J impact; current electrodes/potential measurements on the **top** surface of the plate.

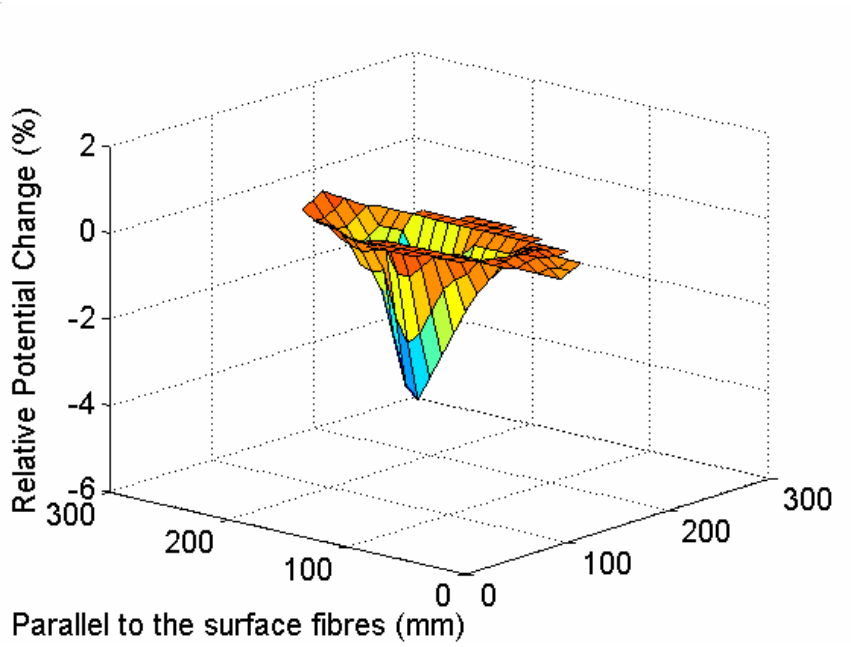

a)

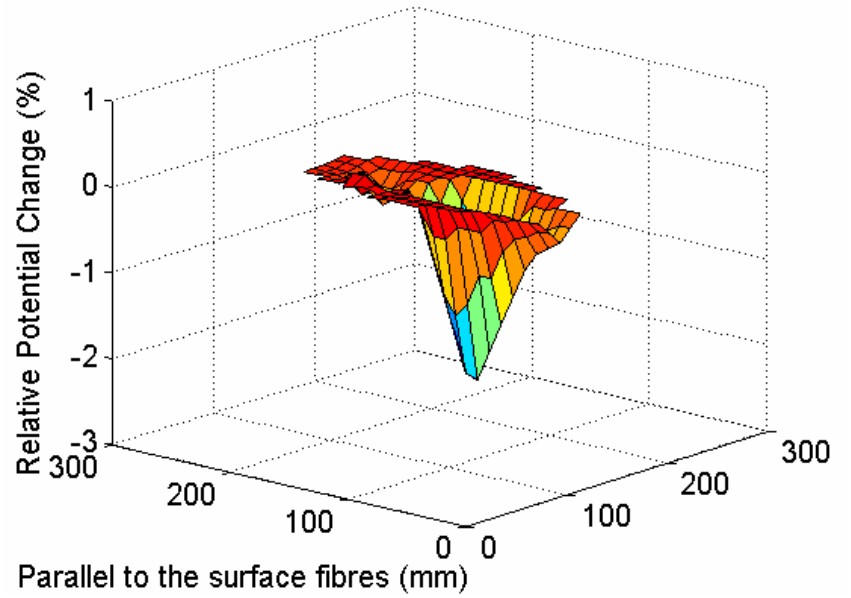

b)

Figure 7. 21: 3-D illustration of potential percentage difference after a) 4 J and b) 2 J impact; current electrodes/potential measurements on the **top** surface of the plate.

Figure 7. 22 and Figure 7. 23 also present 3-D contour plots of percentage potential differences caused by impact damage for plates subjected to impacts between 2 J and 12 J for configuration 2. Similarly to configuration 1, it can be seen where the damaged area is. However, the potential changes are significantly more intense than in configuration 1,

even for the small energy impacts. This is because both the current/potential probes are located on the bottom surface, where the major damage occurs. The majority of the current will remain on the bottom layer, due to the very low longitudinal resistivity of the fibres, giving very high values of the electrical potential on the measured probes. Since the damage is more severe than in the top layer, the potential changes are expected to be greater.

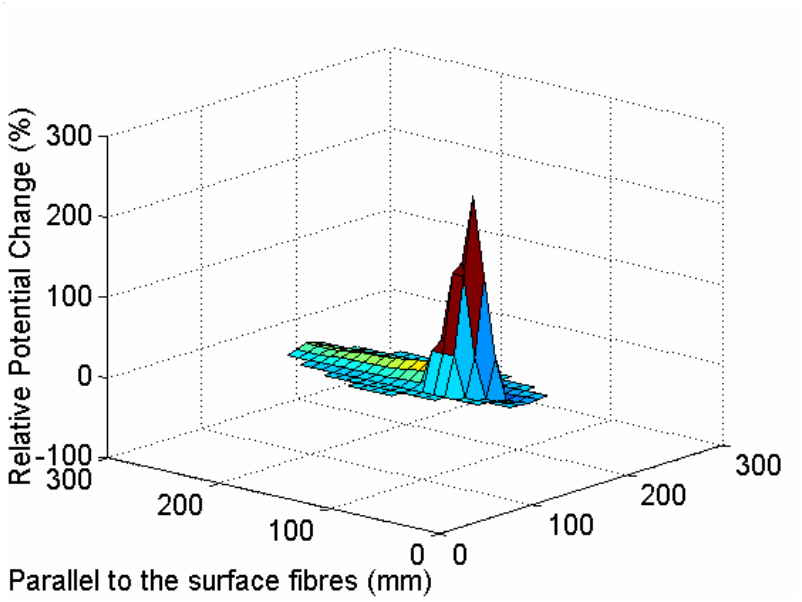

a)

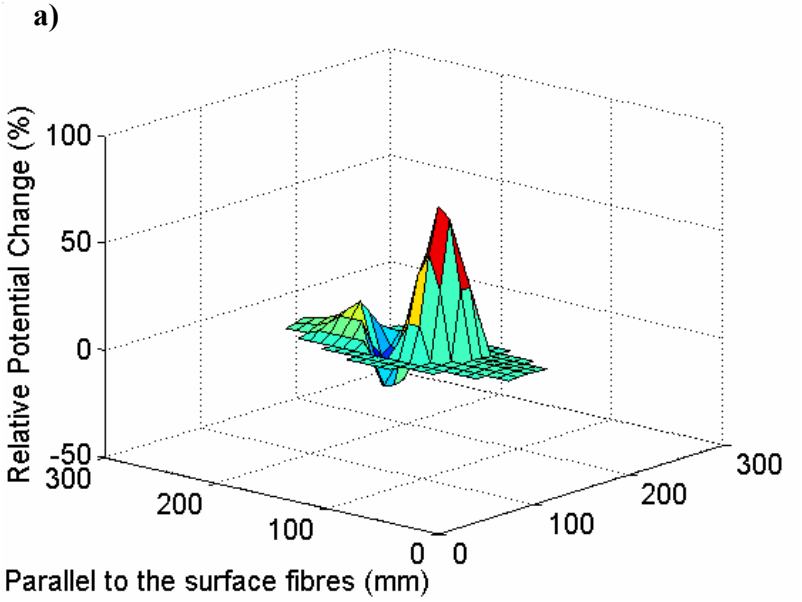

b)

Figure 7. 22: 3-D illustration of potential percentage difference after a) 12 J and b) 8 J impact; current electrodes/potential measurements on the **bottom** surface of the plate.

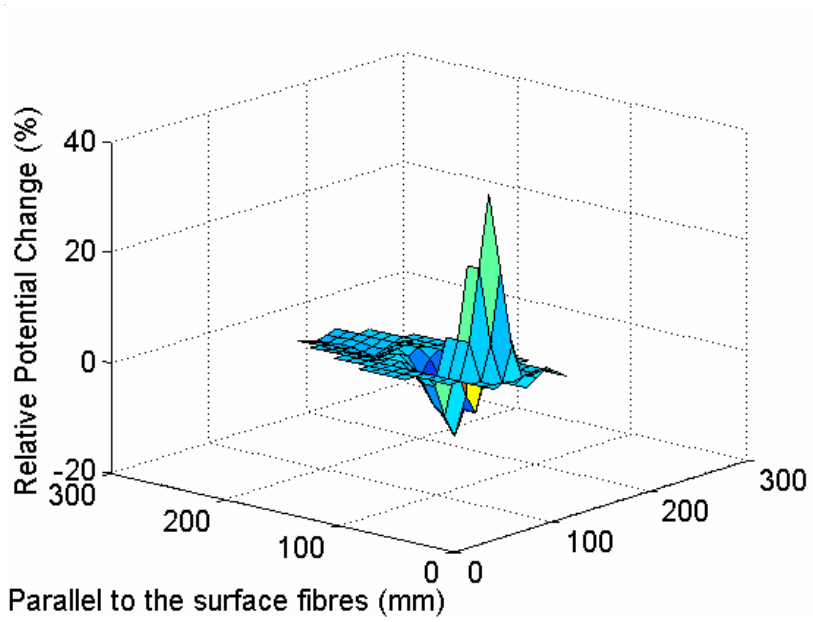

a)

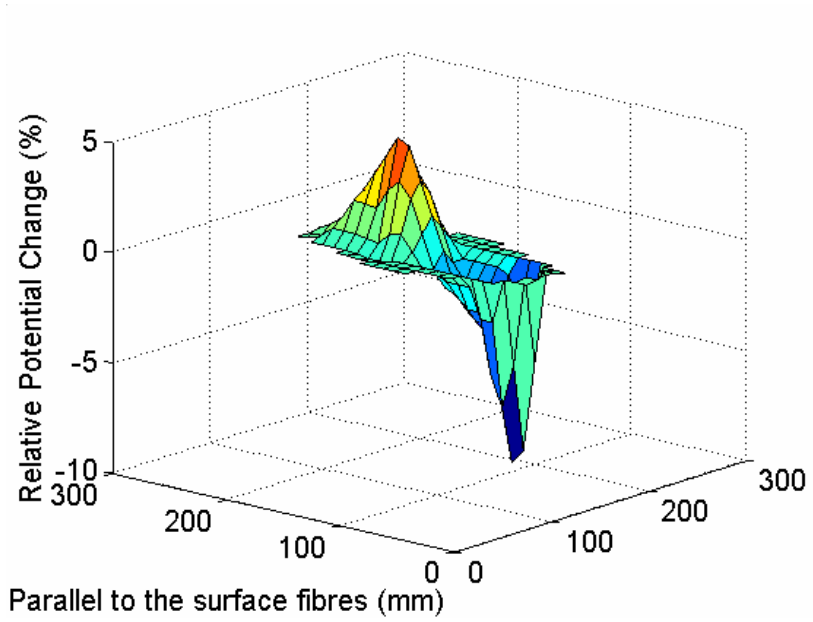

b)

Figure 7. 23: 3-D illustration of potential percentage difference after a) 6 J and b) 2 J impact; current electrodes/potential measurements on the **bottom** surface of the plate.

Figure 7. 24 shows the relation between contours of equi-potential change, and the positions of maximum extent of damage for the 12 J impact in the longitudinal and transverse directions, for current/potential probes located on the top and bottom surface

respectively. The "footprint" of detectable potential change is significantly larger in both transverse and longitudinal directions than the C-scan measured damage size.

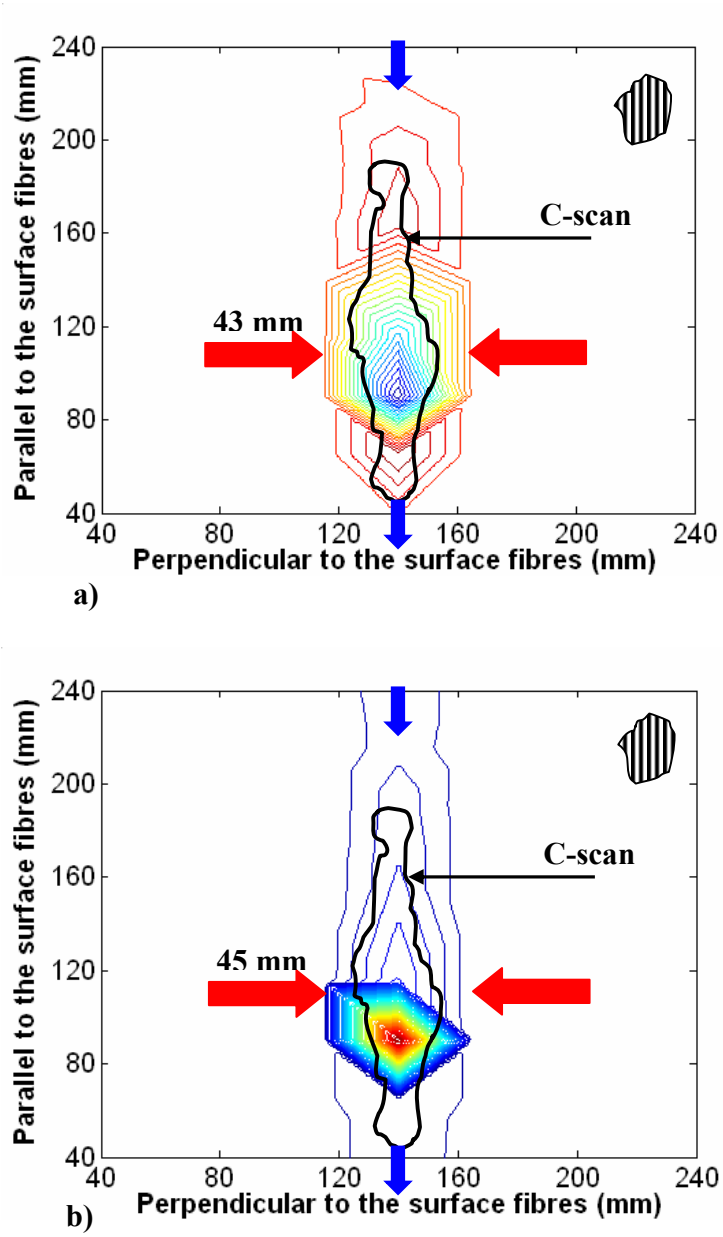

Figure 7. 24: Correlation between potential change contours for 12 J impact, and maximum damage extent as measured by C-scan; a) current electrodes/potential measurements on the **top** surface 1 b) current electrodes/potential measurements on the **bottom** surface.

It is believed that there are two reasons for this discrepancy. Firstly, the mesh grid used for measuring the electrical potential is wider than the one used in C-scan leading to

reduction in the accuracy and greater dispersal of the measurements and secondly, the software used for the equi-potential plots is based on curve fitting. This implies that the lines may extend even further than the actual measurements in order to fit all the data. In C-scan method, however, the graphical representation is obtained based on the actual experimental readings. The potential change corresponding to the maximum length of the C-scan measured damage area is about 10% for configuration 1 and 13% for configuration 2.

Figure 7. 25 and Figure 7. 26 show the influence of maximum damage extent (length) on the maximum change in potential, and also on the size of the region where the potential change was greater than 2% for configurations 1 and 2 respectively. The points in both figures were obtained based on experimental data rather than contours. The maximum change in potential increases little up to a damage length of up to 40 mm for configuration 1; after this point there is a much greater rate of increase in potential. The extent of the region of detectable potential changes increases approximately linearly with the size of the damaged region up to a damage length of 110 mm for configuration 1.

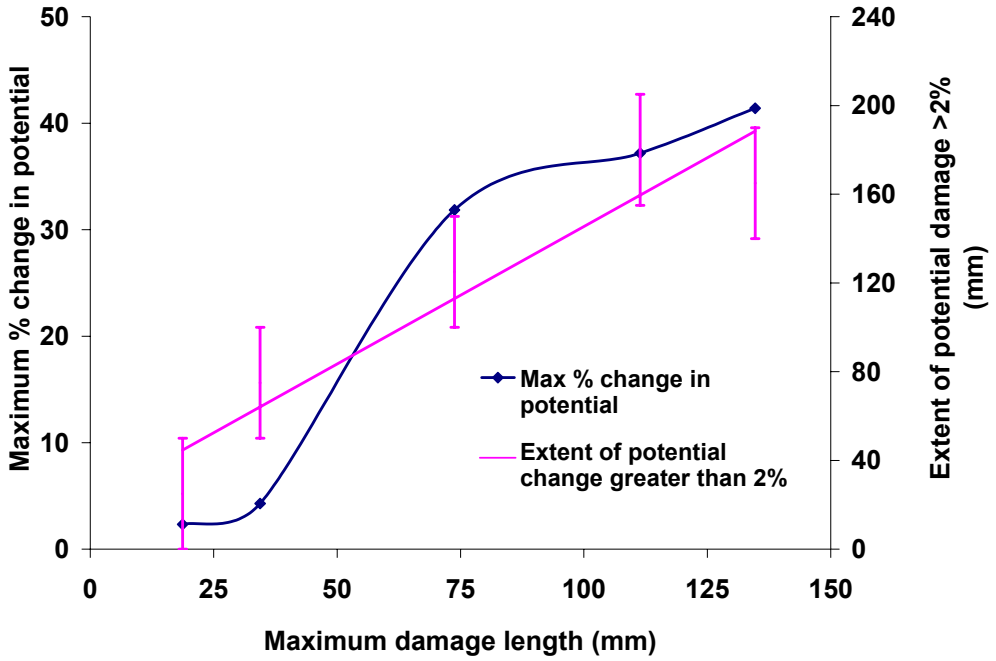

Figure 7. 25: Maximum potential change and extent of detectable potential change against maximum damage size as revealed by C-scan; current/potential probes on the **top** surface.

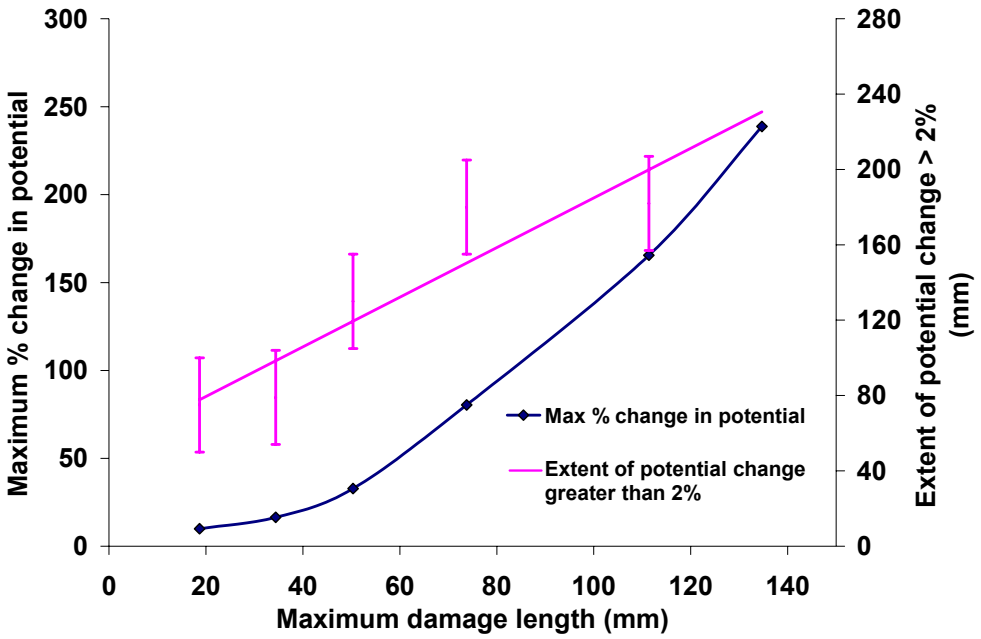

Figure 7. 26: Maximum potential change and extent of detectable potential change against maximum damage size as revealed by C-scan; current/potential probes on the **bottom** surface.

Above this damage length there are some evidences of saturation. Up to this point, the region of detectable potential change is roughly double the size of the delamination length measured by the C-scan. In configuration 2, (Figure 7. 26), the maximum change in potential increases monotonically with the size of the damaged region up to a damage length of about 140 mm.

7.5 Morphology of Impact Damage

An investigation was conducted on the extent of impact damage and in particular delaminations, within the quasi-isotropic composite panels. All laminates were sectioned parallel and transverse to the direction of the top surface fibres, near or at the impact point. The damage profile was pictured and the length of delamination damage in each layer was measured. For this investigation, samples around the impacted area were cut from each panel; they were encapsulated in Triofix filled acrylic resin and polished as described in Section 6.4.1. Typical pictures of the damage morphology in a section parallel and transverse to the fibres of the top surface under the impact point are shown in Figure 7. 27, Figure 7. 28 for 4 J impact and Figure 7. 29, Figure 7. 30 for 12 J impact.

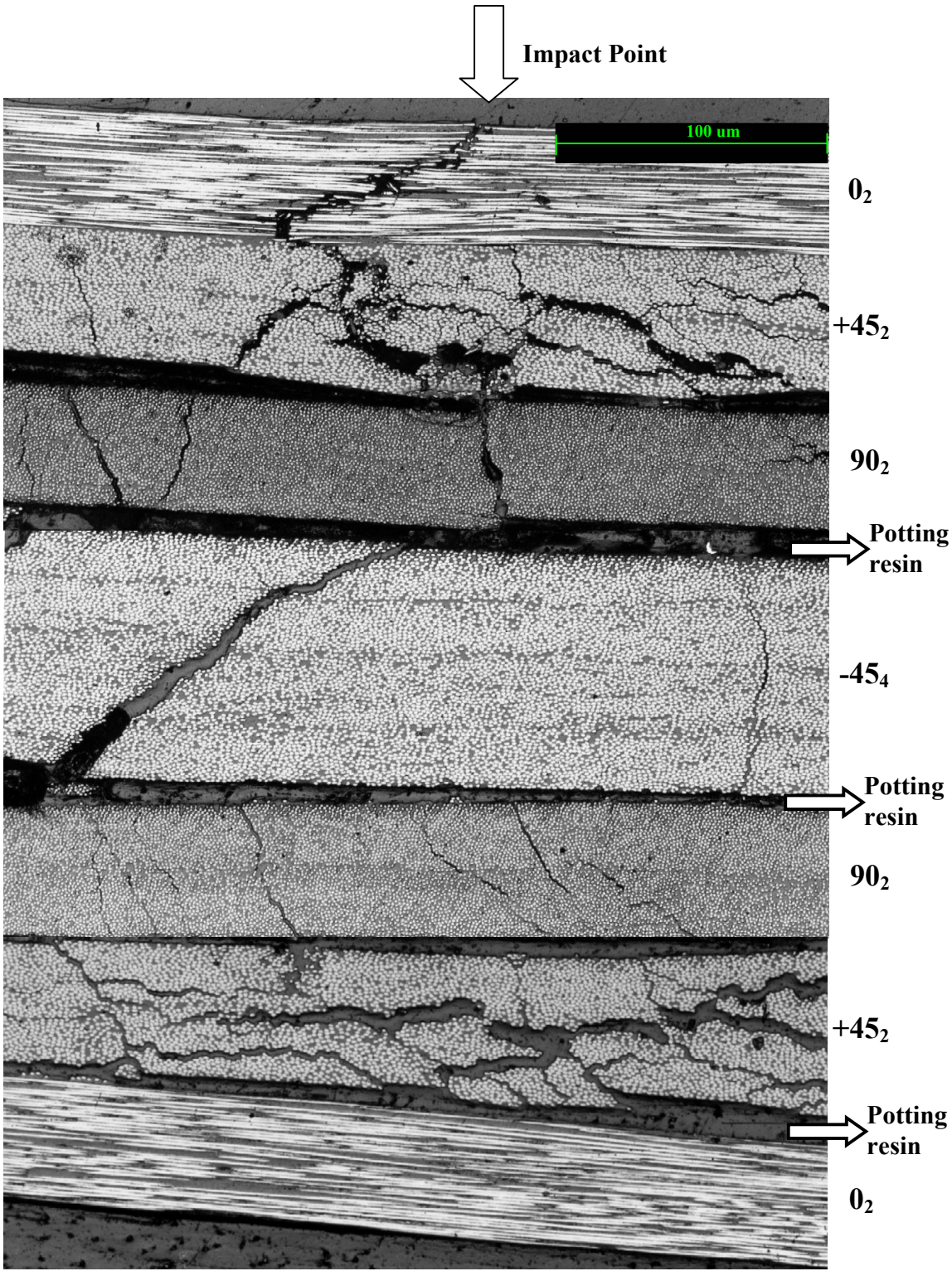

Figure 7. 27: Damage pattern in a quasi-isotropic plate after 4 J impact; section parallel to the fibres on the **top** surface, at the impact point.

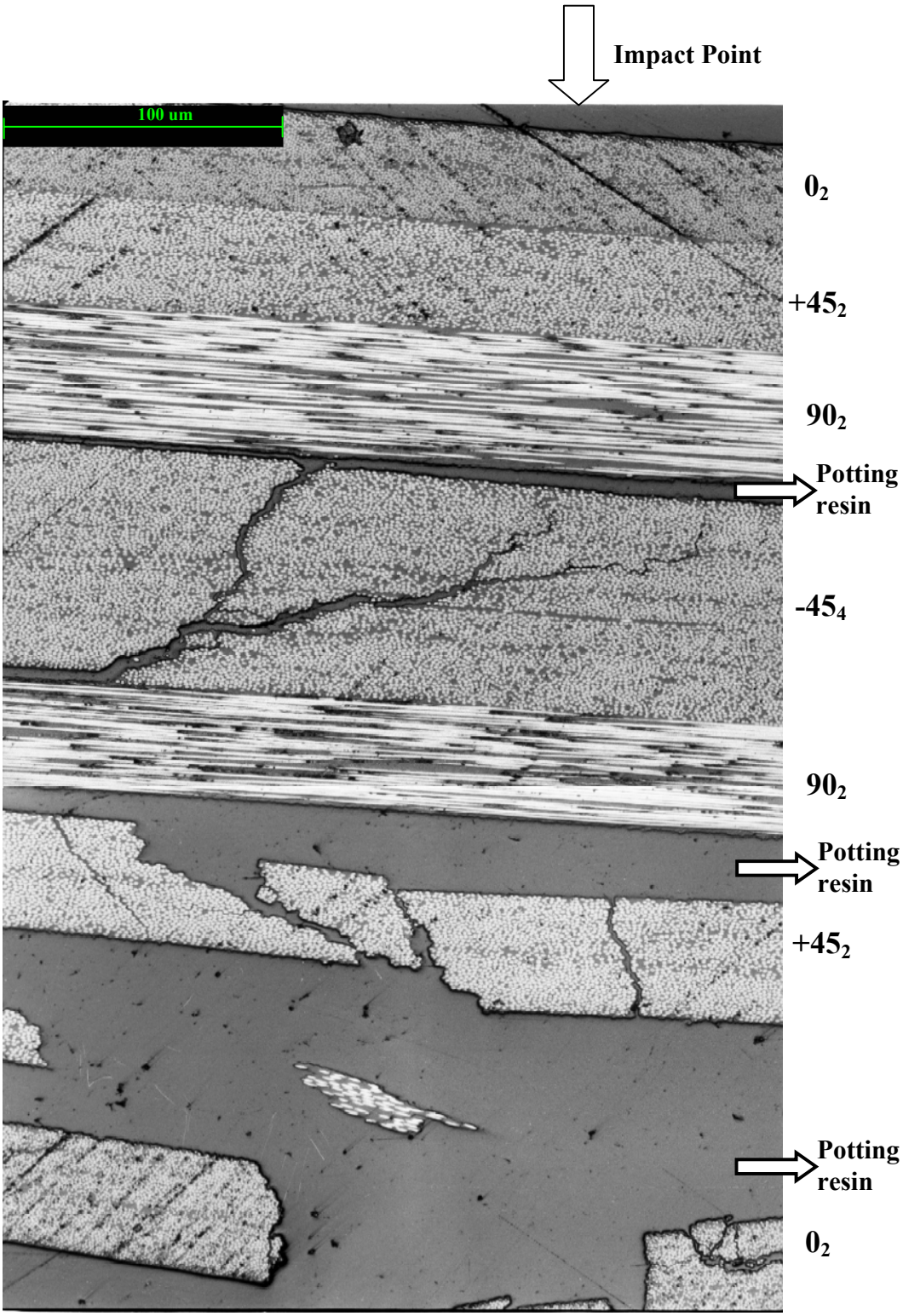

Figure 7. 28: Damage pattern in a quasi-isotropic plate, after 4 J impact; section transverse to the fibres on the **top** surface, at the impact point.

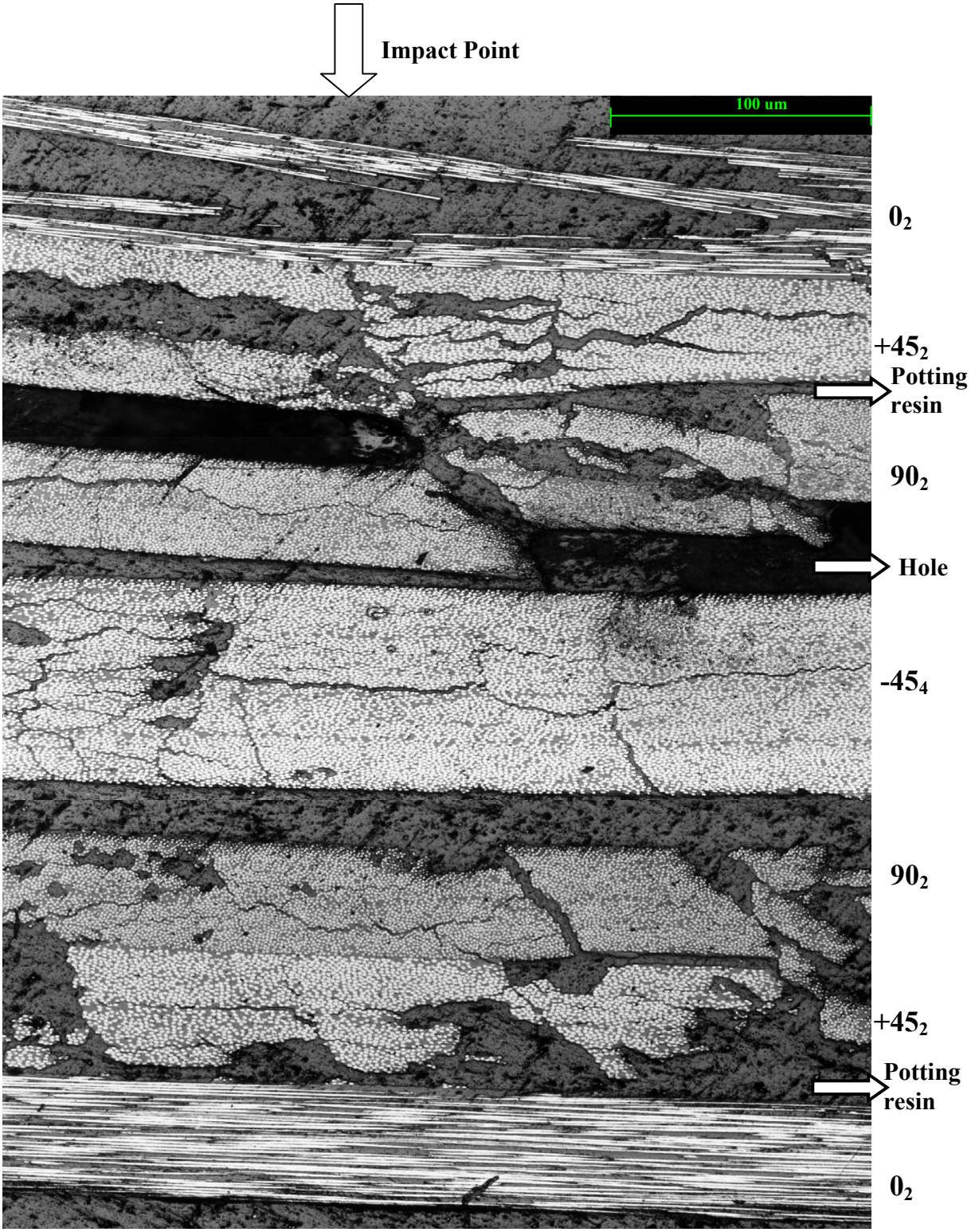

Figure 7. 29: Damage pattern in a quasi-isotropic plate, after 12 J impact; section parallel to the fibres on the **top** surface, at the impact point.

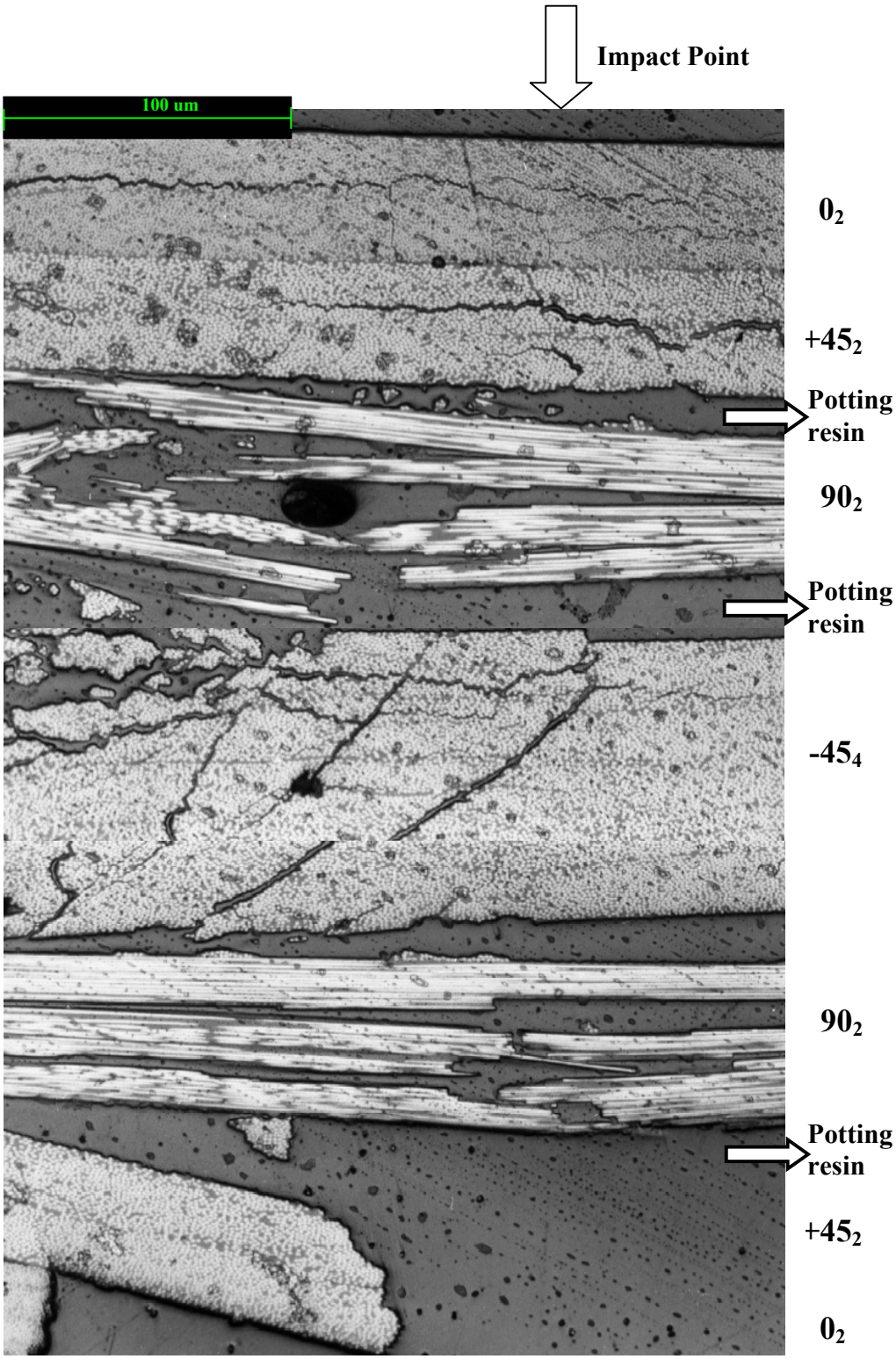

Figure 7. 30: Damage pattern in a quasi-isotropic plate, after 12 J impact; section transverse to the fibres on the **top** surface, at the impact point.

The layers near the top surface are mainly characterized by delaminated areas between neighbour plies and in some cases broken fibres while the damage near the bottom is characterized by more severe debonding between adjacent layers and more intensive fibres breakages. The selected Figure 7. 27 and Figure 7. 29, which depict the damage outline within the laminate at the impact point in a section parallel to the fibres at the top surface, are not well representative of the severe damage which occurs at the bottom layers. Maps of the damage pattern in all plates are shown in Figure 7. 31 and Figure 7. 32, for sectioning longitudinal and transverse to the direction of the top surface fibres (0°) respectively.

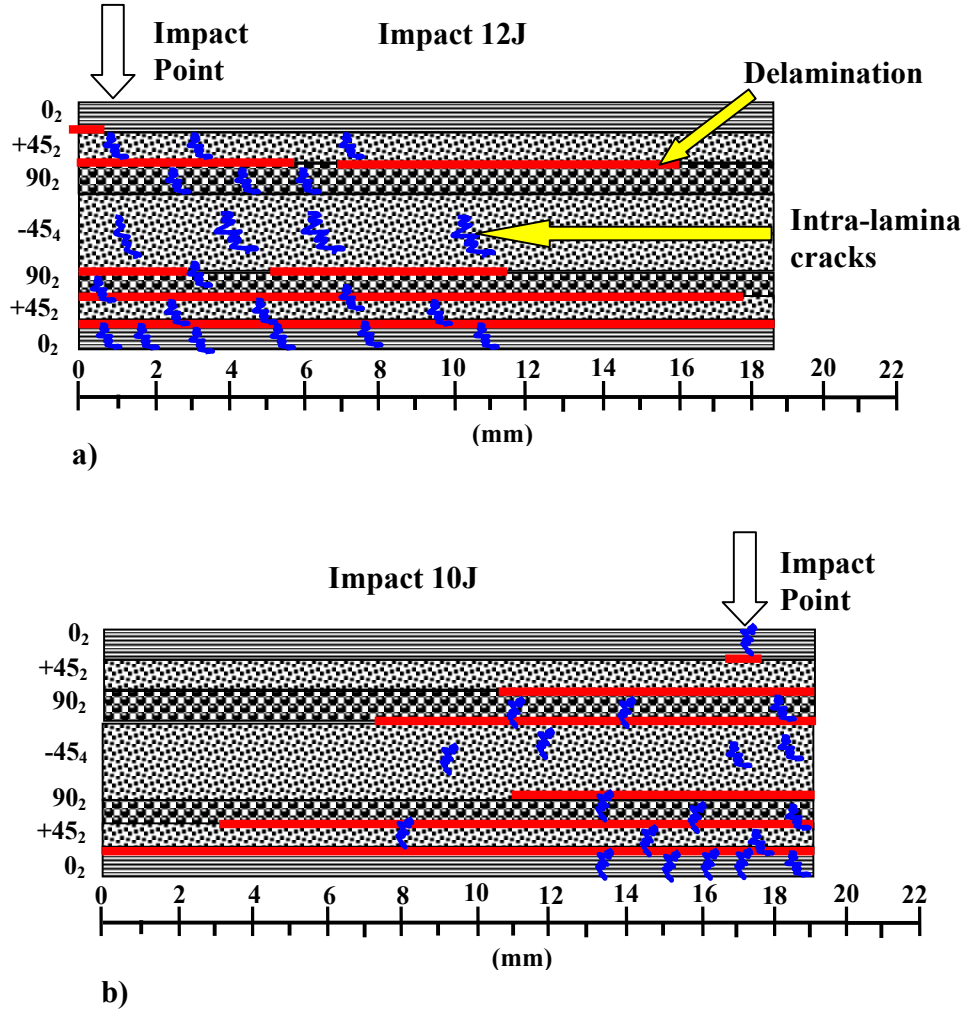

Figure 7. 31: Damage pattern after a) 12 J, b) 10 J; section parallel to the direction of the fibres on the **top** surface.

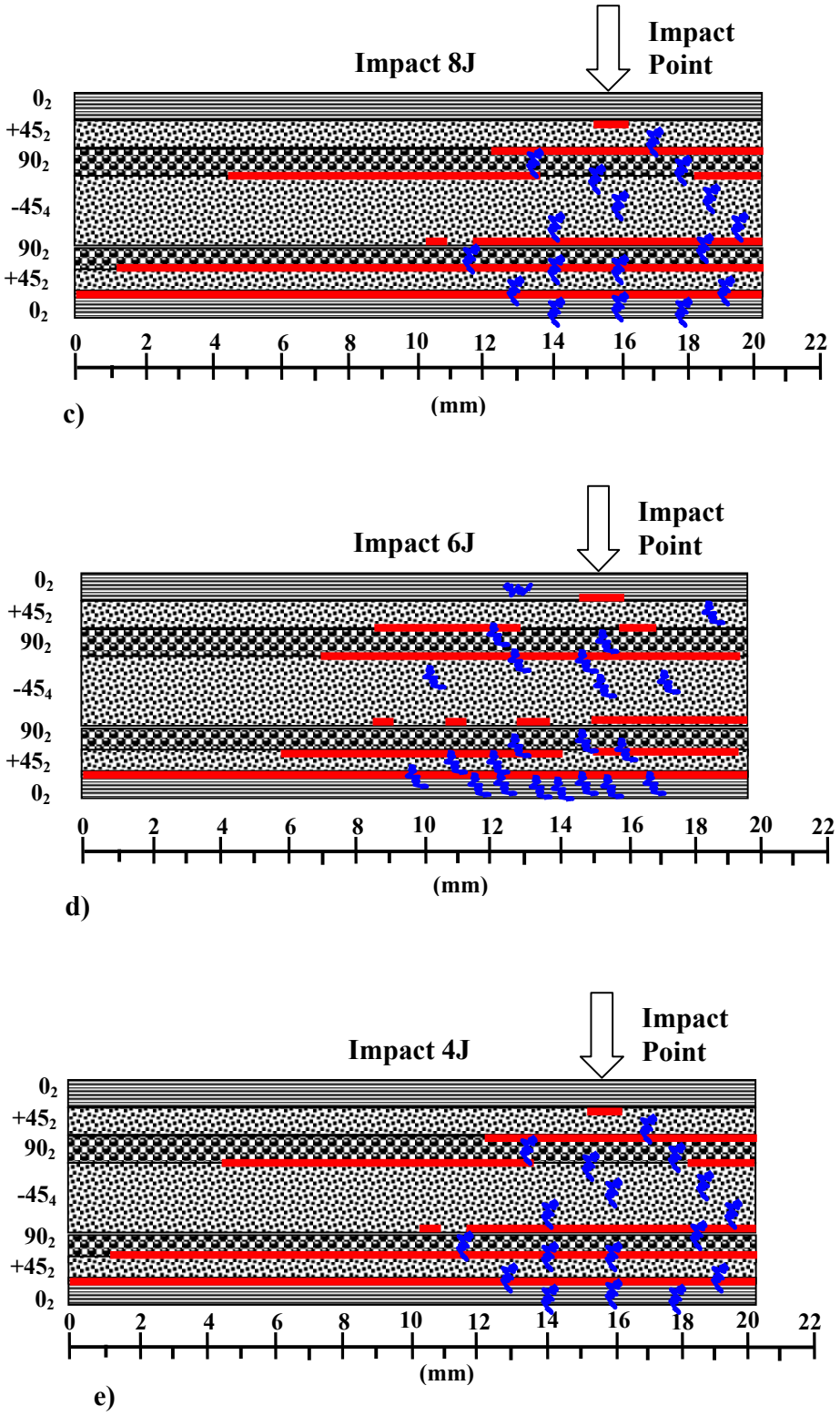

Figure 7. 31 (continued): Damage pattern after c) 8 J, d) 6 J and e) 4 J impact; section parallel to the direction of the fibres on the **top** surface.

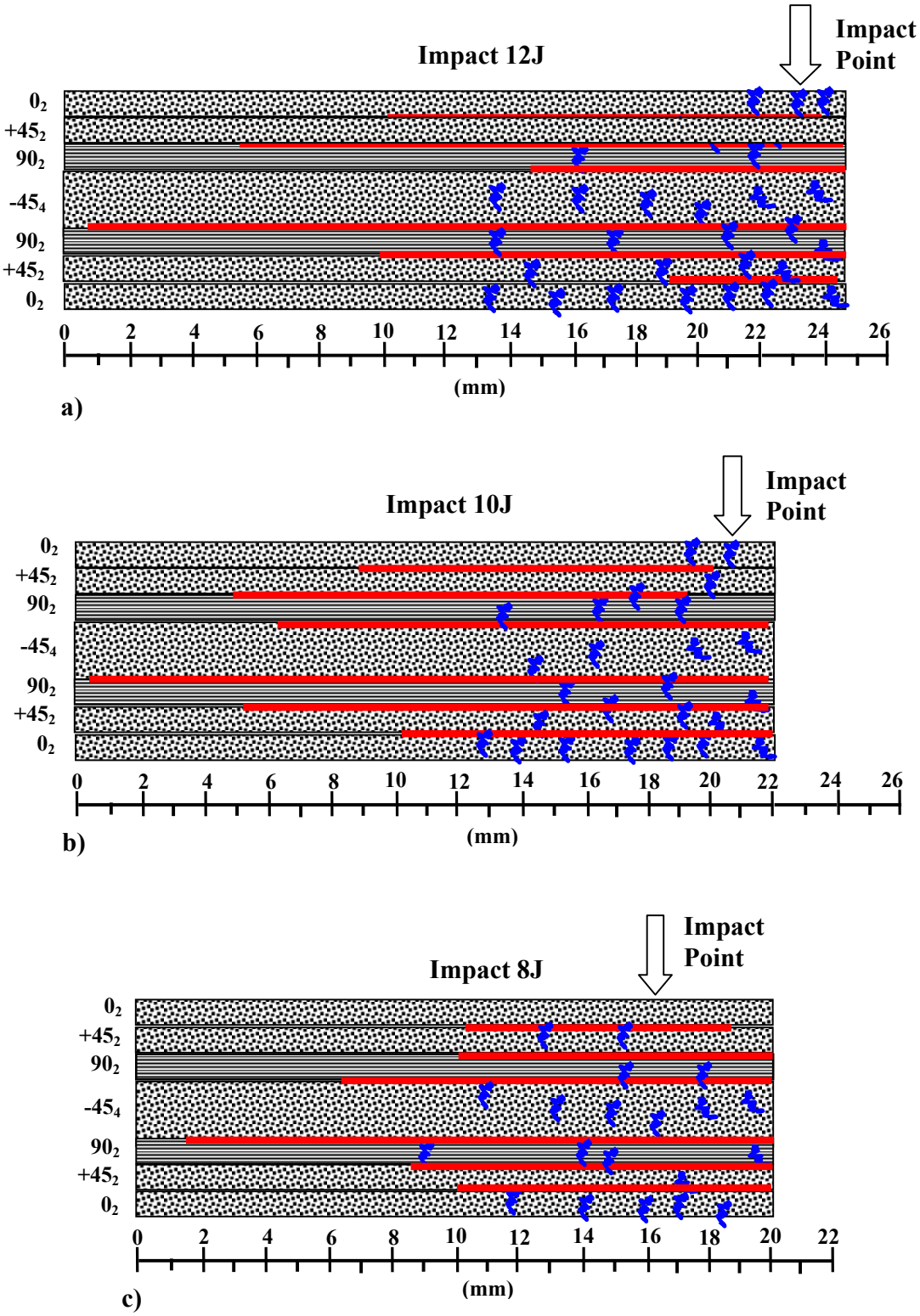

Figure 7. 32: Damage pattern after a) 12 J, b) 10 J, c) 8 J; section transverse to the direction of the fibres on the **top** surface

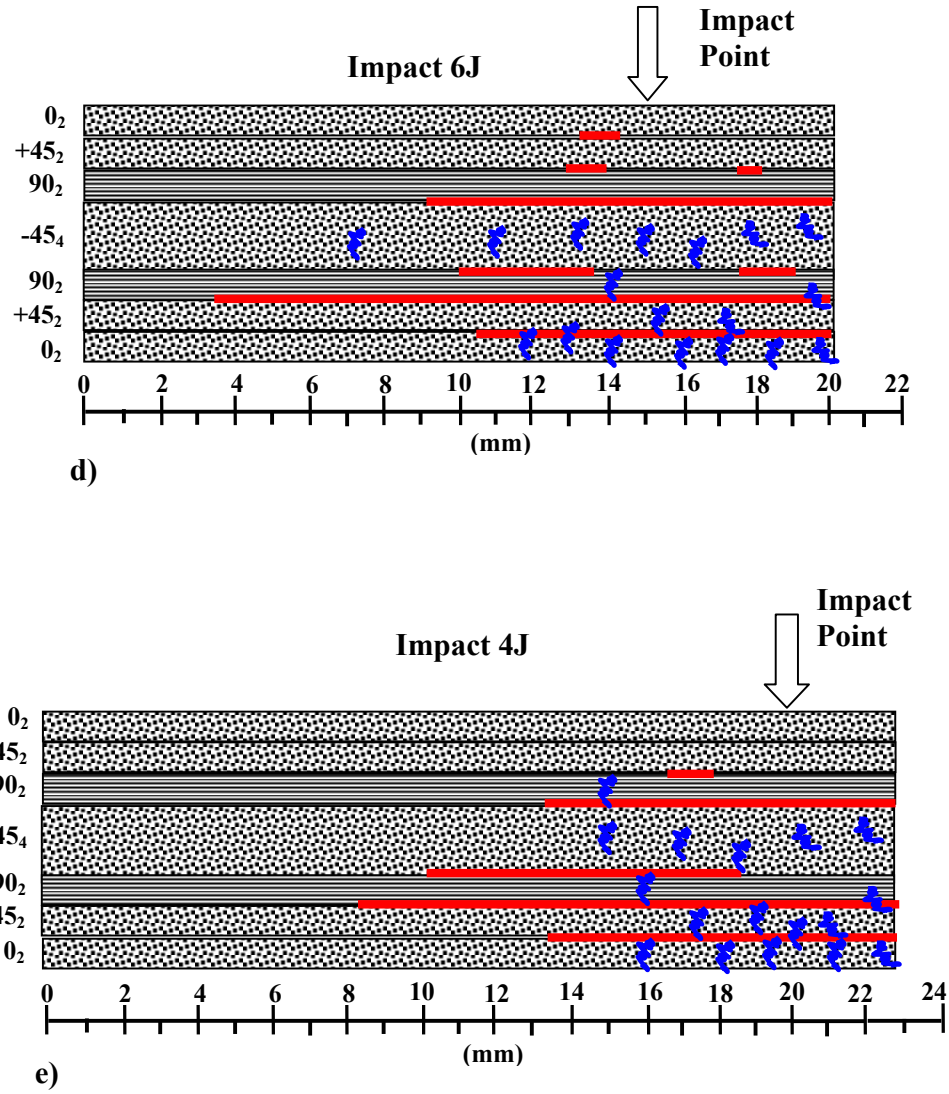

Figure 7. 32 (continued): Damage pattern after d) 6 J and e) 4 J impact; section transverse to the direction of the fibres on the **top** surface

Both Figure 7. 31 and Figure 7. 32 demonstrate the complexity of the damage pattern associated with different impact energies; however, there are some general characteristics which can be attributed to all plates. The higher impact energies such as 12 J and 10 J are associated with the development of intra-lamina cracks, matrix cracks and delaminations in all layers. The number and the area of those cracks at the layers closer to the top

surface are smaller than in the layers in the middle or at the bottom surface. Plies near the bottom surface are also subjected to major fibre breakages, as the sectioning demonstrated.

For smaller impact energies, the intra-lamina cracks do not extent in all layers but they are concentrated at the middle and bottom layers. The dominant damage form at the layers near the top surface is delaminations, which mainly extend in the area around the impact point. A detailed view of the extent of delamination damage in each layer for all impact energies is shown in Figure 7. 33 and Figure 7. 34, for sectioning parallel and transverse to the 0˚ direction fibres respectively. Delamination damage follows a similar pattern to the fibre breakage one. As the longitudinal sectioning demonstrates, the major delamination length along the 0˚ direction fibres (longitudinal) is observed at the layers near the bottom surface, and can be attributed the maximum bending stresses exceed these layers [130]. The transverse sectioning, however, revealed that the major length of delaminations in the direction transverse to the top surface fibres is found at the layers in the middle of the plate, where significant matrix cracks and shear stresses are developed [129].

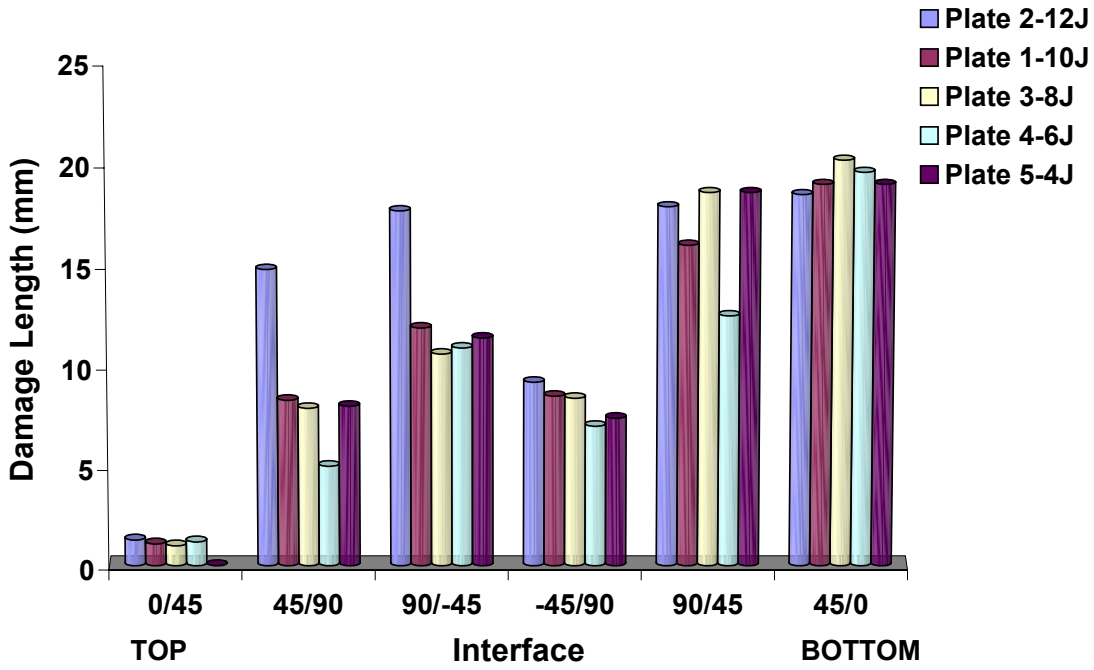

Figure 7. 33: Damage length at each layer along a section parallel to the 0˚ direction fibres (longitudinal).

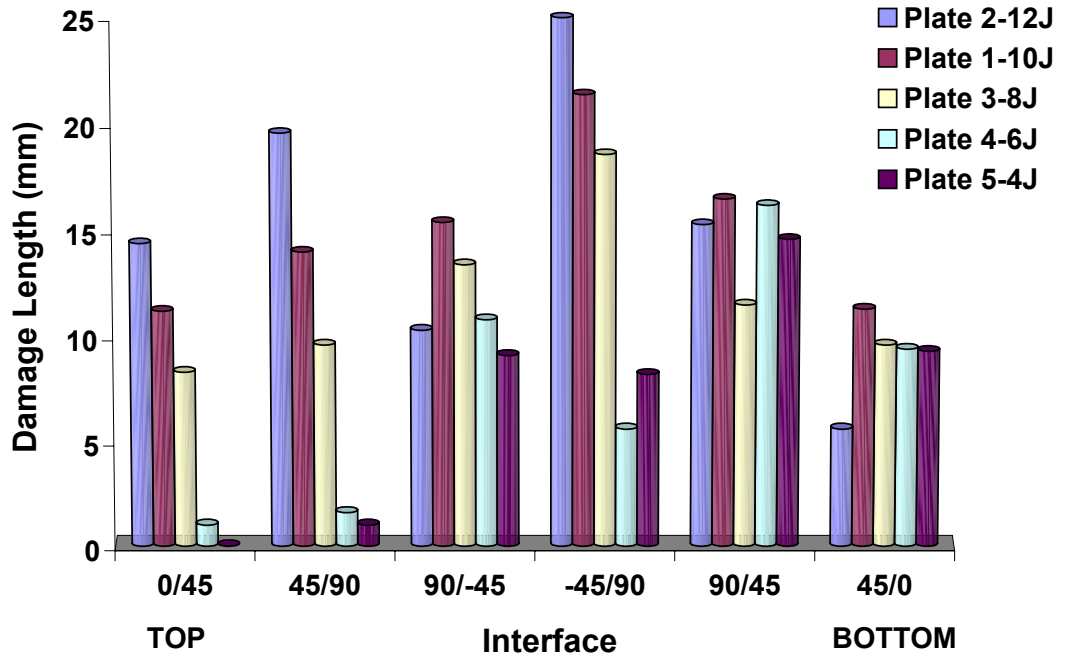

Figure 7. 34: Damage length at each layer, along a section transverse to the 0˚ direction fibres (perpendicular).

Table 7. 3 finally summarizes the results obtained after sectioning, presenting the maximum extent of delamination damage in each plate, in the directions parallel and transverse to the top surface fibres, for each impact energy. In Table 7. 3, is also shown the damage size as obtained using C-scan. These two results cannot be compared directly, because the C-scan measurements corresponds to the maximum projected damage area, which is the ensemble of all delaminations within the plate, whereas the results presented after sectioning corresponds to two individual layers; one with the maximum delamination length parallel to the fibres and the other with the maximum delamination length in the transverse direction. In addition and referring to the layers which exhibit the biggest impact damage, only a part of the impact damage is shown because of the difficulty in sectioning in two directions.

Table 7. 3: Damage size measured for different impact energies using microscopy and C-scan.

Impact Energy (J)	***Maximum Damage Size Measured Using Microscopy (X * Y) mm^2***	***C-Scan Damage Size (X * Y) mm^2***
4	19 x 15	34 x 15
6	19.6 x 16	50 x 25
8	20.2 x 19	74 x 23
10	19 x 21	111 x 28
12	18.5 x 25	135 x 29

Summarizing the results from the impact experiments it can be said that detectable potential changes arising from impact damage were measured, for various impact energies on cross ply and quasi-isotropic laminates. The magnitude of those changes is strongly dependent on the configuration of the current electrodes and potential measurements probes. Potential changes up to 41% were measured after 12 J impact when current electrodes and potential probes were positioned on the top surface of the laminate. Similarly to holes induced damage, the extent of those changes was mainly parallel the 0° fibres direction rather in the direction perpendicular. The sectioning of the impacted plates revealed that potential changes based on this current/potential probes configuration mainly arise from delaminations located near the top layers.

For current electrodes/potential probes located on the bottom surface, potential changes up to 238 % were measured. The metallographic investigation revealed that these changes are mainly sensitive to fibre breakages and fibres split in addition to delamination damage.

8 EFFECT OF EXTERNAL PARAMETERS

Measurements have been made of the effect of mechanical strain, temperature and humidity, on potential distributions and electrical resistance in both unidirectional and multidirectional carbon fibre epoxy laminates. The effects of current flow direction and technique for current introduction on piezo-resistance have been studied in detail.

This Chapter is organized as follows: In Section 8.1 a detailed review is given of the effect of mechanical strain on the electrical potential based on experimental observations for unidirectional and multidirectional samples. Section 8.2 presents the results from the microscopy investigation of the interface carbon fibres/conductive adhesive used for introducing the current. Finally, the effect on the electrical resistivity of environmental factors, such as temperature and water, are presented in Sections 8.3 and 8.4 respectively.

8.1 Effect of Mechanical Strain on Electrical Potential

The electrical response of unidirectional, cross ply and quasi-isotropic CFRP laminates subjected to cyclic mechanical strain has been investigated (Table 6. 3). The details of all samples testing programs and configurations used are given in Section 6.4. A number of different current input and current measurement configurations were examined on samples in order to investigate the current processes within a unidirectional and multidirectional composite laminate.

Data are presented as plots of electrical potential and strain vs time and as plots of relative potential change, ΔV/V vs strain. Apparent gauge factors (GF) values were calculated from the expression:

$$GF = \frac{\Delta V}{V_{\min} \Delta \varepsilon} \qquad (8.\ 1)$$

where ΔV and V_{min} are the range of potential change and the minimum potential respectively, and Δε is the strain range; in all cases, minimum strain was very close to or at zero.

8.1.1 Unidirectional samples-configuration A

In this configuration the current flows parallel to the fibres, with current introduction on sample edges at the fibre ends (Section 6.4.1, Figure 6.4). Figure 8. 1 and Figure 8. 2 show potential changes measured at the sample surface for current inputs attached via silver paint and carbon cement. The use of silver paint resulted in a positive change of the electrical potential with mechanical strain as shown in Figure 8. 1. This contradicts investigations from other researchers who found only negative piezo-resistance change with applied strain [54], [104], [106], [108]. When carbon cement is used for current input, however, negative potential changes are observed with increasing strain.

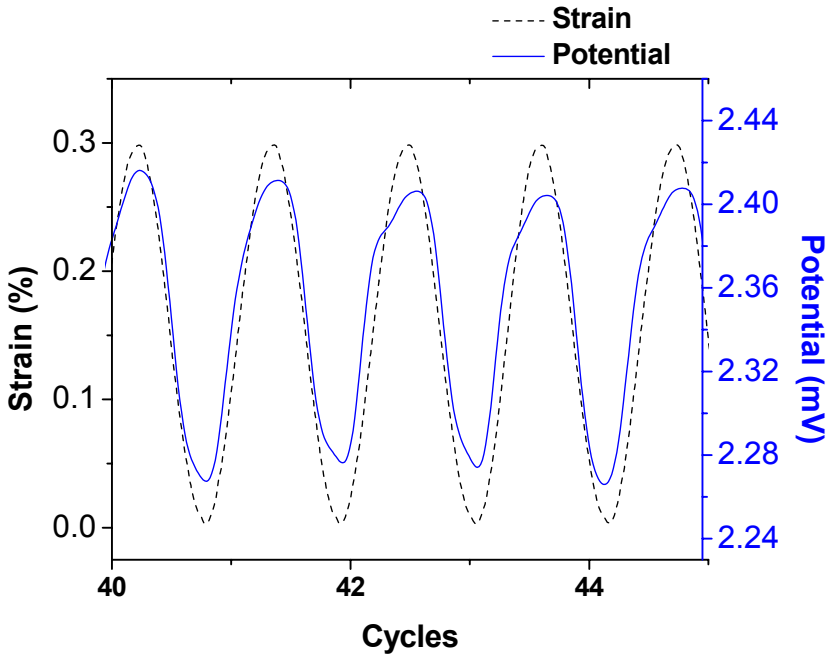

Figure 8. 1: Plot of potential and strain vs time for configuration A; silver paint current introduction at sample ends.

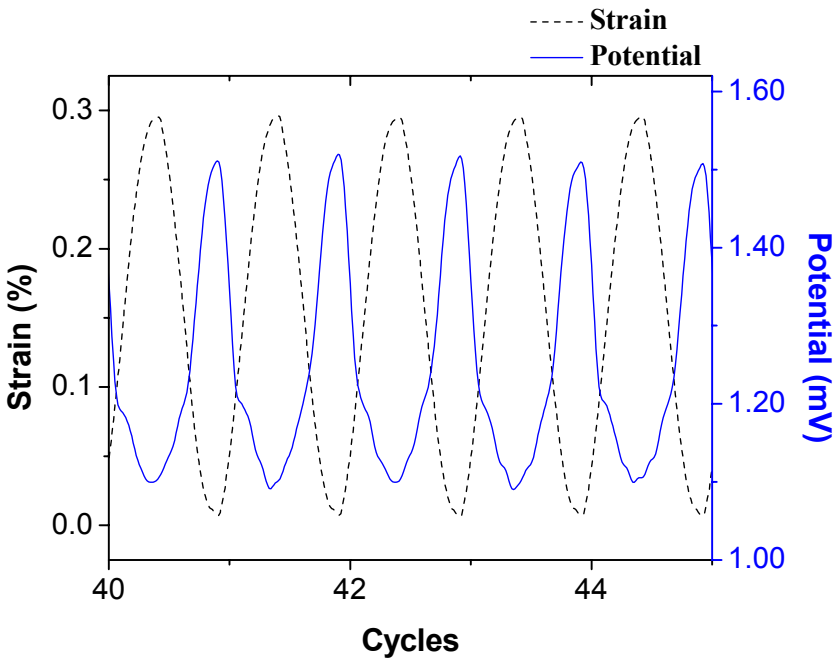

Figure 8. 2: Plot of potential and strain vs time for configuration A; current introduced using carbon cement.

The potential difference at zero strain was found to be up to 40% less than that found with silver paint; this reduced further with increasing strain. The out-of-phase shift of mechanical strain with the changes in electrical potential was measured 180°, corresponding to negative piezo-resistivity. The in-phase response is understandable and expected, because the resistance along the stress direction changes proportionally with the elongation of the fibres.

Plotting ΔV/V vs strain instead of time for the data in Figure 8. 1 and Figure 8. 2 produces the curves shown in Figure 8. 3 and Figure 8. 4. This shows the relationship between strain and fractional potential changes. It suggests the relation between strain and fractional potential is positive for silver paint and negative piezo-resistance for carbon cement. The observed non linear changes imply changes in GF with increasing strain. For the current leads attached with silver paint, the gauge factor was 20.6, while when carbon cement used, a negative piezo-resistance with a gauge factor of -89 was measured. A summary of gauge factors for all configurations is given, in Table 8. 1, at the end of this section.

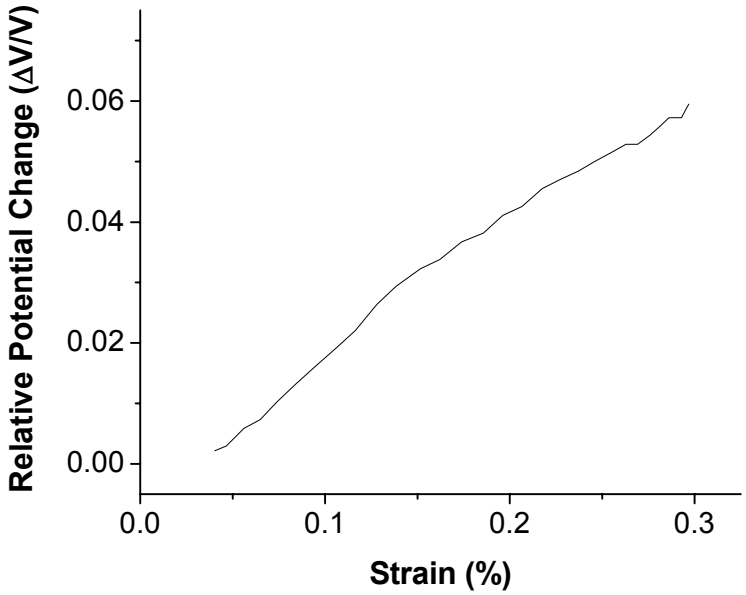

Figure 8. 3: Relative potential change vs applied strain for a single half cycle; data from Figure 8. 1.

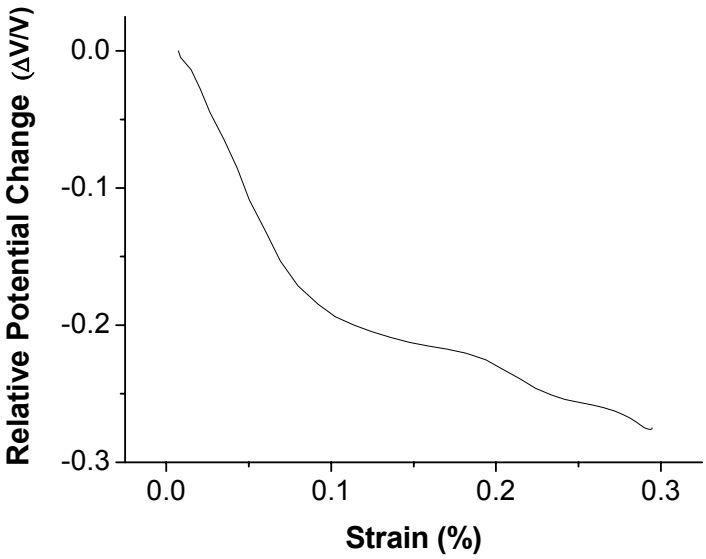

Figure 8. 4: Relative potential change vs applied strain for a single half cycle; data from Figure 8. 2.

The effect of changing the applied cyclic strain frequency over a range, from 0.05 Hz to 10 Hz, was also investigated. No effect on either the phase relation or the output of the potentials was found.

8.1.2 Unidirectional samples-configuration B

In this configuration the current is introduced on individual points on the surface of the sample, flowing parallel to the fibres direction (Section 6.4.1, Figure 6. 6). This configuration was created in order to investigate the extent to which the absence or reduction of current in carbon fibres, affects the measured potential in relation to the strain. Potential changes measured in channel 1 (CH 1) and channel 2 (CH 2) are shown in Figure 8. 5 (a) & (b).

An in-phase potential response to strain was found in CH 1 (positive piezo-resistance) while negative piezo-resistance was seen in CH 2. The gauge factors were 5.36 for CH 1 in the line of the current, and – 3.27, for CH 2.

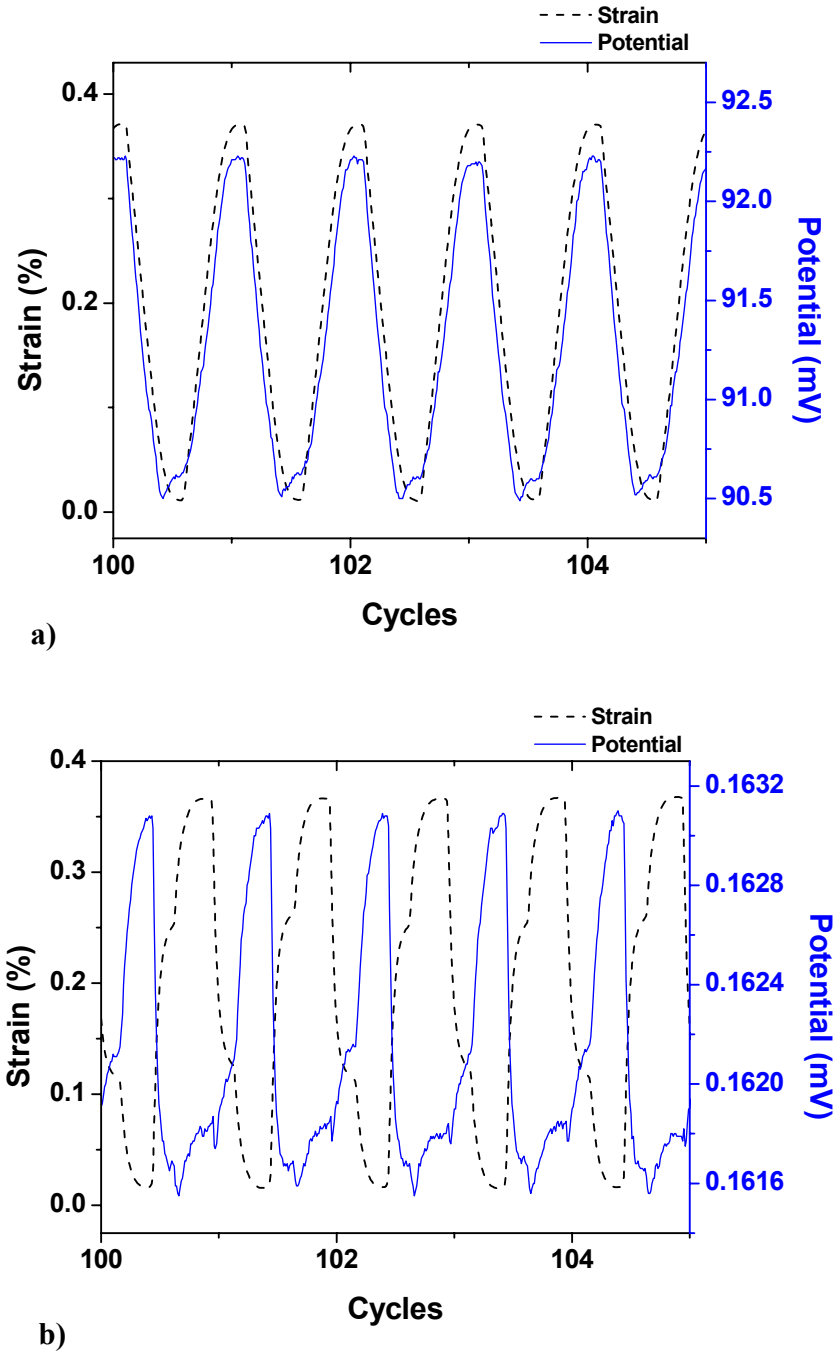

Figure 8. 5: Applied strain and potential vs time for sample in configuration B; (a) CH 1, (b) CH 2.

In CH 1 the measured potential values at zero strain are considerably greater by a factor of over 40 than for configuration A, and for CH 2, they are a factor of 14 smaller; this is due to the very high concentration of current in the line connecting the current electrodes.

In configuration A, the current was introduced over 50 mm^2 surface area and it was spread throughout the sample while in configuration B, the current was introduced via a single point on the specimen's surface, and resulted in a high local concentration in the longitudinal direction only. This is because transverse resistivity is a factor of over 10^4 greater than the longitudinal, and it will not disperse transversely to the fibres. For the same reason, the current reaching the CH 2 measurement points, displaced 6 mm laterally from the line of current introduction, will be very small and will result in small values of potential.

8.1.3 Unidirectional samples-configuration C

This configuration had the same series of probes, as in configuration B, but arranged transversely, perpendicular to the line of the fibres, in order to measure potential changes in this transverse direction (Section 6.4.1, Figure 6. 7). The strain was applied parallel with the fibres. The potential response to the applied strain cycles in the two channels was identical and in-phase as shown in Figure 8. 6. This shows that the potential output is very high, a factor of 100 greater than in configuration A, and a factor of 2-3 greater than the point introduction of current with current flowing along the fibres.

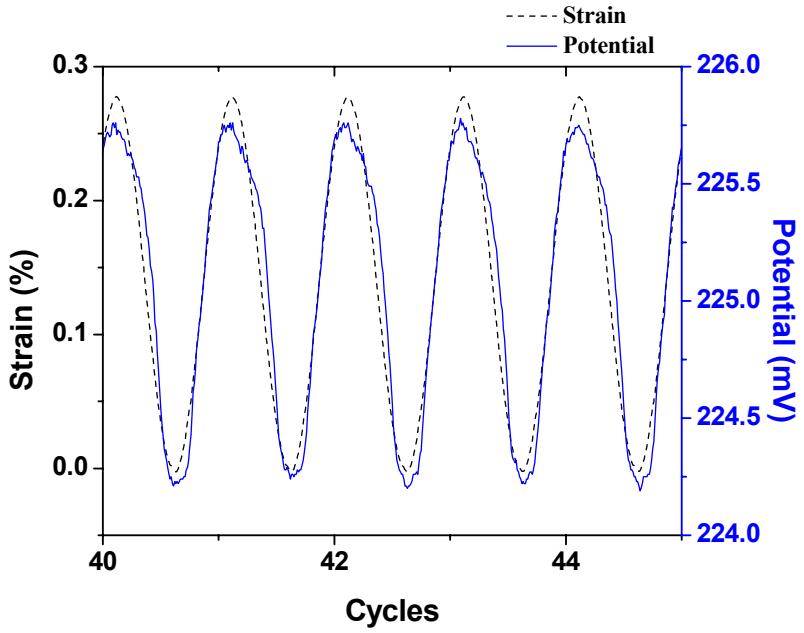

Figure 8. 6: Strain and measured potential vs time for configuration C.

In this formation, the current will disperse laterally from the introduction point, parallel with the fibres, along the entire length of the sample, as this is an easy conduction path. Figure 8. 7 shows that the fractional potential response to applied strain is positive throughout cycling. The GF can be calculated as +2.47.

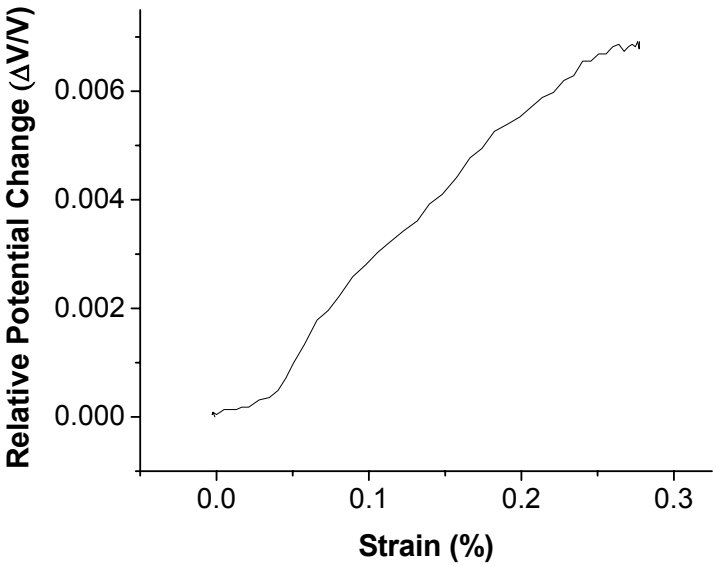

Figure 8. 7: Relative potential change vs strain for single half cycle; configuration C.

8.1.4 Multidirectional laminates

The potential responses to applied strain were always similar in cross ply and quasi-isotropic lay-ups for all electrode configurations. The response of cross ply and quasi-isotropic samples in configuration A is shown in Figure 8. 8 (a), and (b) respectively. The piezo-resistive response is always positive for both carbon cement and silver dispersion adhesives to introduce the current. This contradicts investigations from other researchers who found negative piezo-resistance [105], [110]. The values of GF were 5.76 for cross ply and 1.21 for the quasi-isotropic.

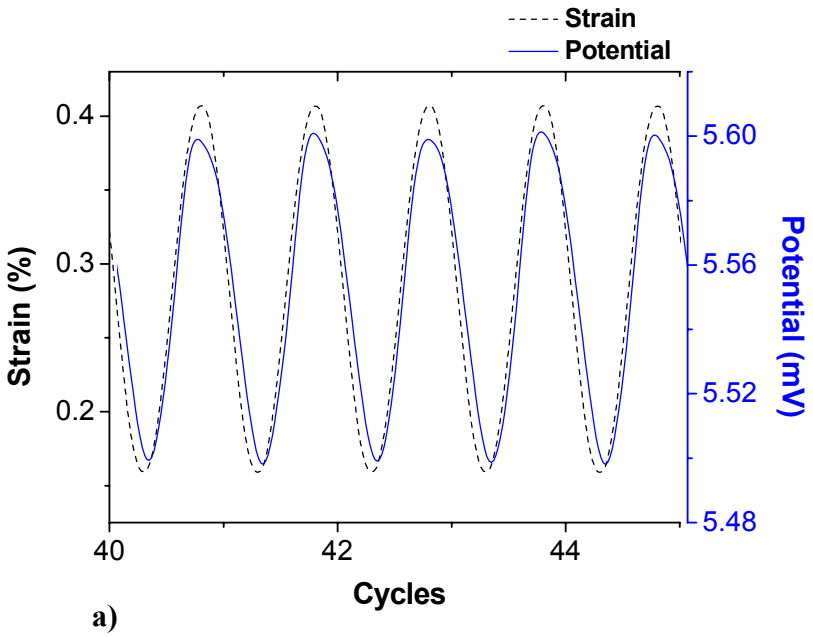

a)

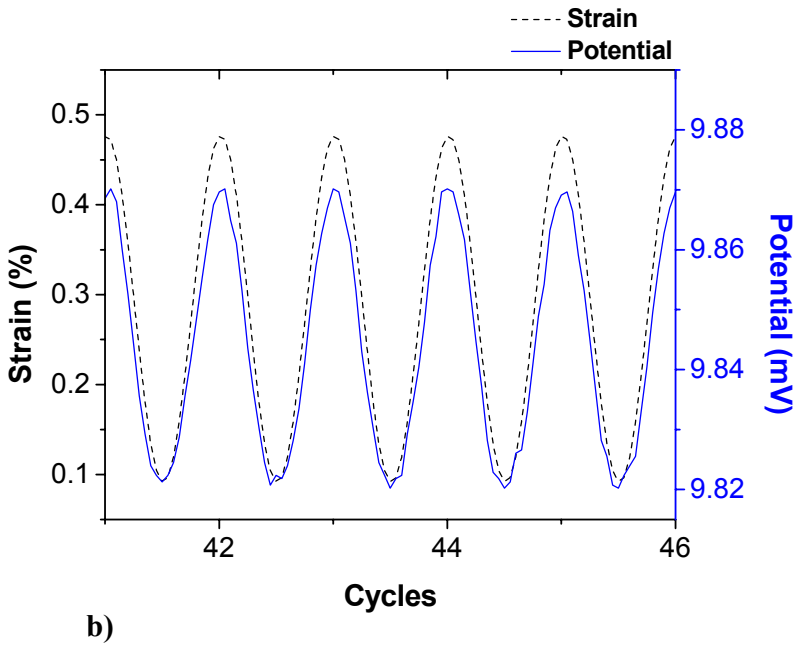

b)

Figure 8. 8: Strain and potential vs time for a) cross ply and b) quasi-isotropic laminate; configuration A using carbon cement as conductive adhesive.

In configuration B (Figure 8. 9), with point introduction of current along the surface fibres, both CH 1 and CH 2 exhibited positive piezo-resistivity, for the cross ply samples, with the potentials always being in-phase with the applied strain. The size of the potential for CH 1 was over 200 mV, and for CH 2 was 0.56 mV while the GF was 10.8 for CH 1 and 11.2 for CH 2. Similar behaviour was observed for the quasi-isotropic specimens.

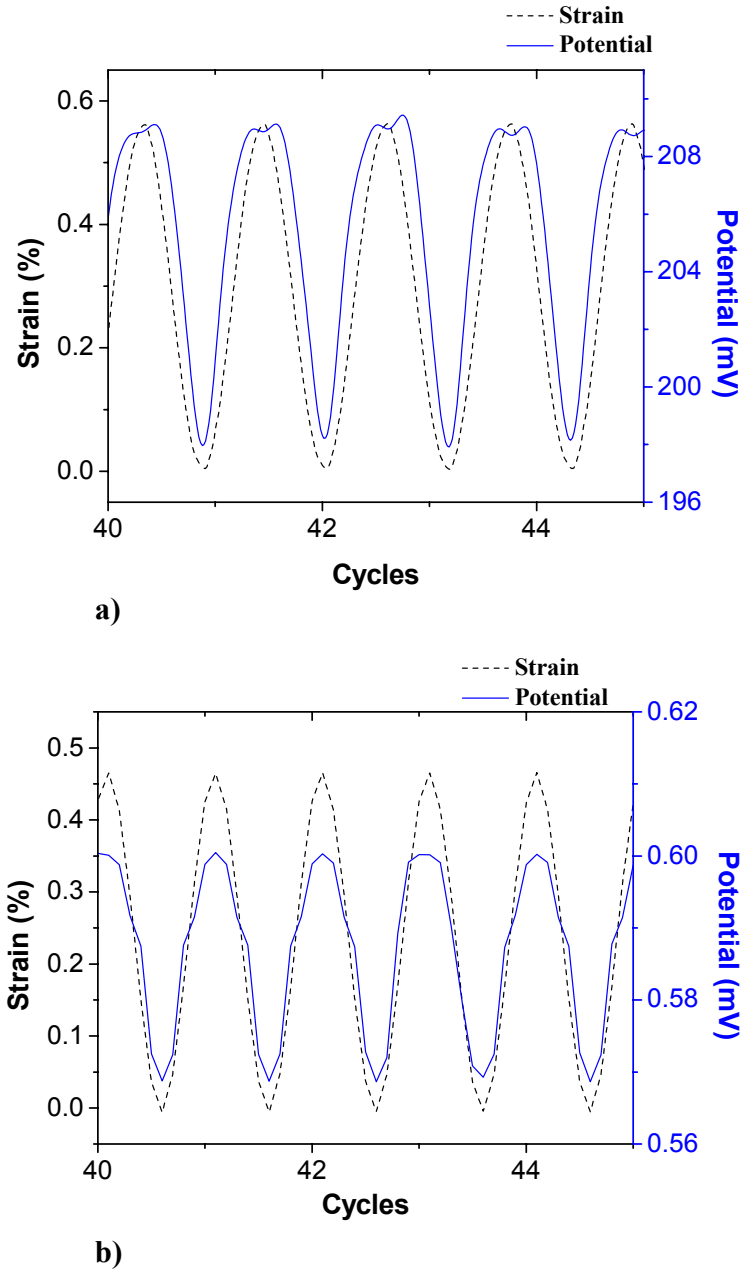

Figure 8. 9: Strain and potential vs time for cross ply laminate, configuration B; (a) CH 1, (b) CH 2.

In configuration C, both cross ply and quasi-isotropic lay-ups showed negative piezo-resistivity in the potential response. This is shown in Figure 8. 10 (a) and (b) respectively. The size of the potential differences in samples was moderate at 7.5 mV and the gauge factor was -7.1 for cross ply laminates.

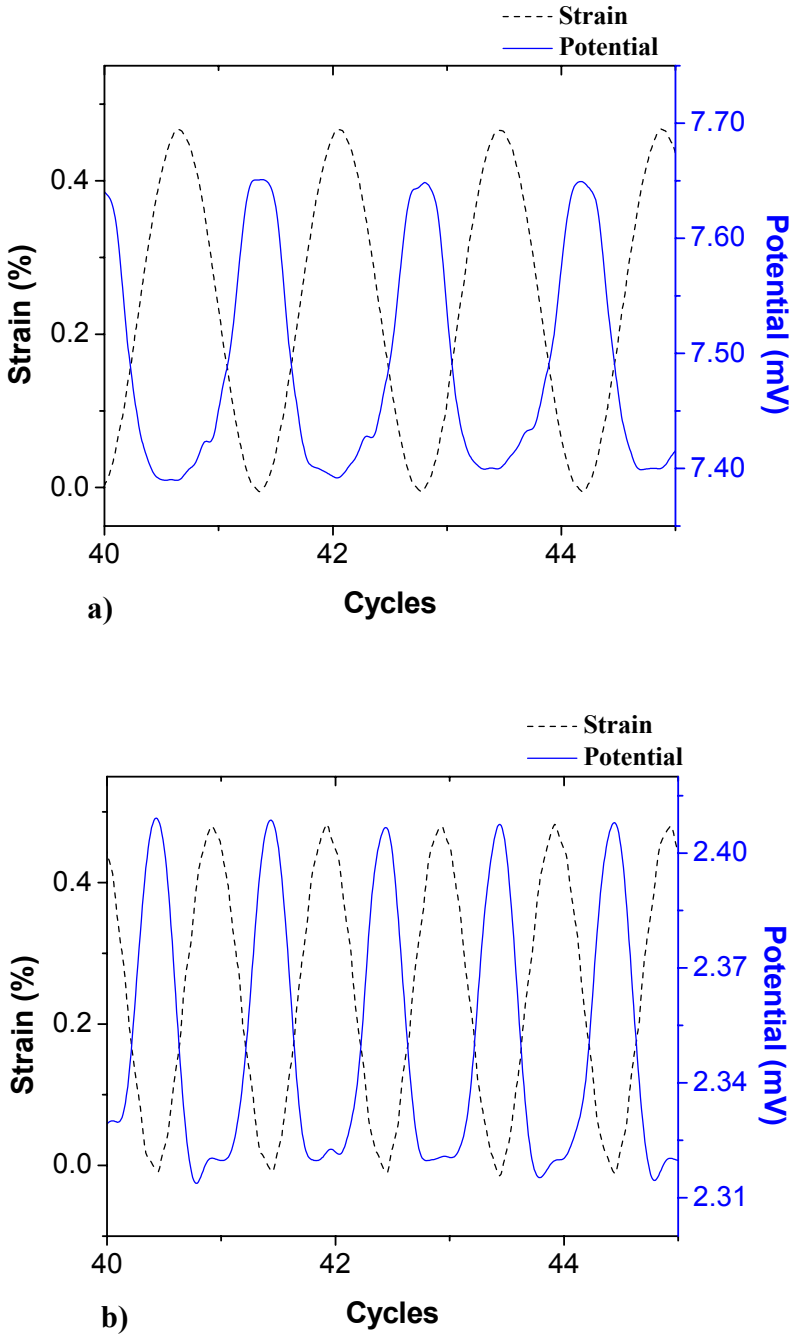

Figure 8. 10: Strain and potential Vs time for a) cross ply and b) quasi-isotropic laminate; configuration C.

Table 8. 1: Summary of potential and gauge factors observations.

Electrode configuration		***Unidirectional***		***Cross Ply [0,90]***	
		Zero strain Potential (mV)	***Gauge Factor (GF)***	***Zero strain potential (mV)***	***Gauge factor***
Configuration A	Current electrodes bonded with silver epoxy	4.37	+3.6	N/A	N/A
	Current electrodes bonded with silver dag	2.26	+20.6	5.5	5.76
	Current electrodes bonded with carbon cement	1.5	-89	N/A	N/A
Configuration B	Channel 1; in line with current	90.5	+5.3	198	+10.8
	Channel 2; displaced laterally	0.16	-3.27	0.57	11.1
Configuration C	All electrodes silver paint	224	2.4	7.4	-7.1

8.2 Microscopy Investigation of Electrode Bonding

As mentioned in Section 8.1, the use of silver paint and carbon cement as adhesives mediums for introducing current, led to positive and negative piezo-resistance changes respectively, with applied strain. An investigation was conducted using microscopy on the interface between the composite and the adhesive, in order to retrieve more information about the contact area for the two adhesives.

Four samples were manufactured for each conductive adhesive, dimension of 25 x 10 x 2 mm. All samples were polished. The main aim of mechanical polishing was to subject the samples to different levels of abrasion to expose only the carbon fibres and abrade epoxy resin from the interface. All specimens were encapsulated in Triofix filled acrylic resin and graded using carbide papers of four different grid levels. The final stage was the final polishing of the samples using a commercial colloidal silica/alumina with diameter of 0.05 μm.

Typical pictures of the bond lines of carbon cement and silver dag interface between are shown in Figure 8. 11 and Figure 8. 12 respectively. It can be seen that the silver dag bond line has a continuous bond with the carbon fibres; however, the carbon cement bond contains areas of porosity and poor bonding. As a result, the current is not distributed homogeneously into the composite and not all the fibres carry the same amount of current which presumably affects the change of the potential with strain.

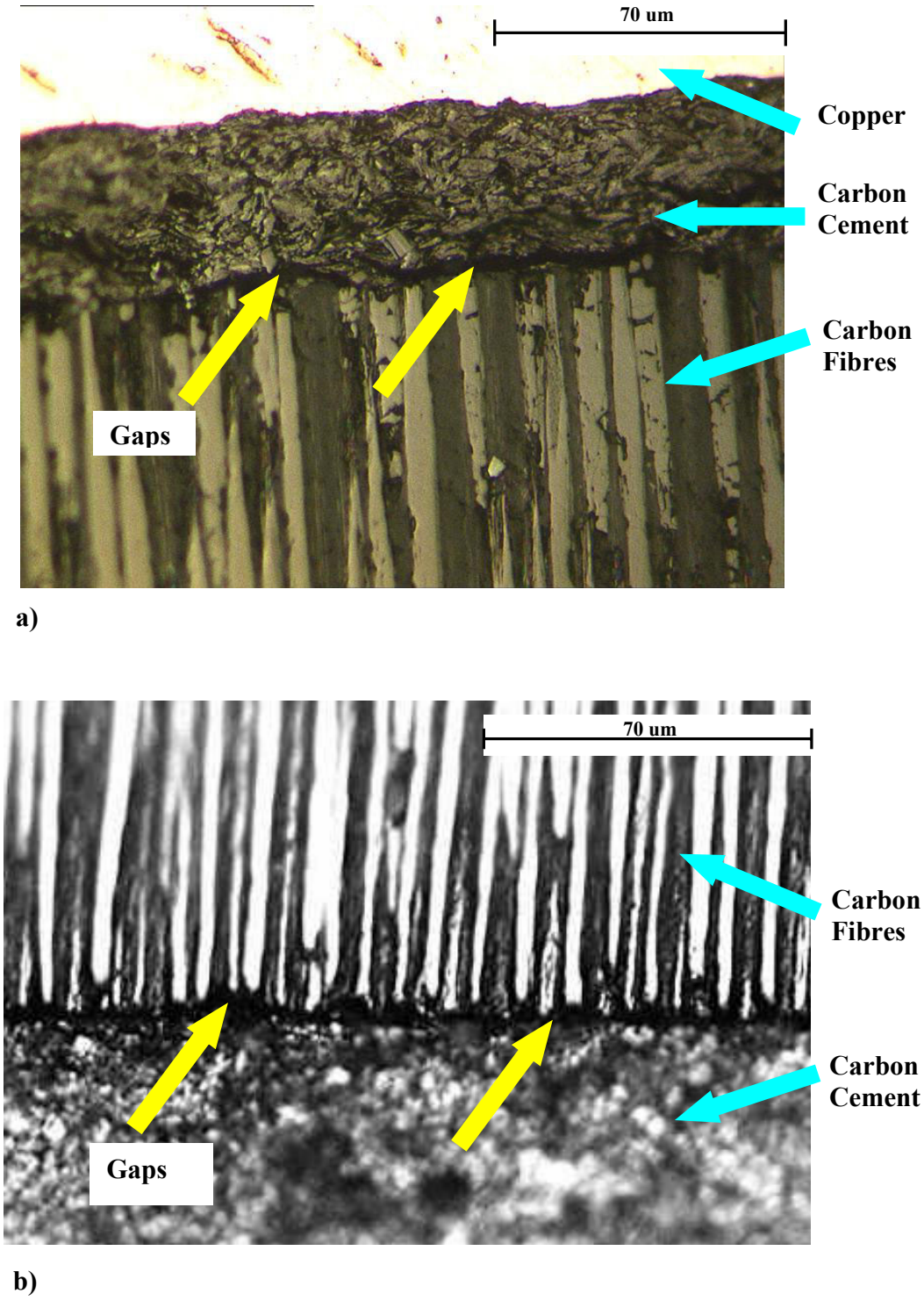

Figure 8. 11: Section through carbon cement current introduction contacts, for two different samples, showing the gaps in the contact region.

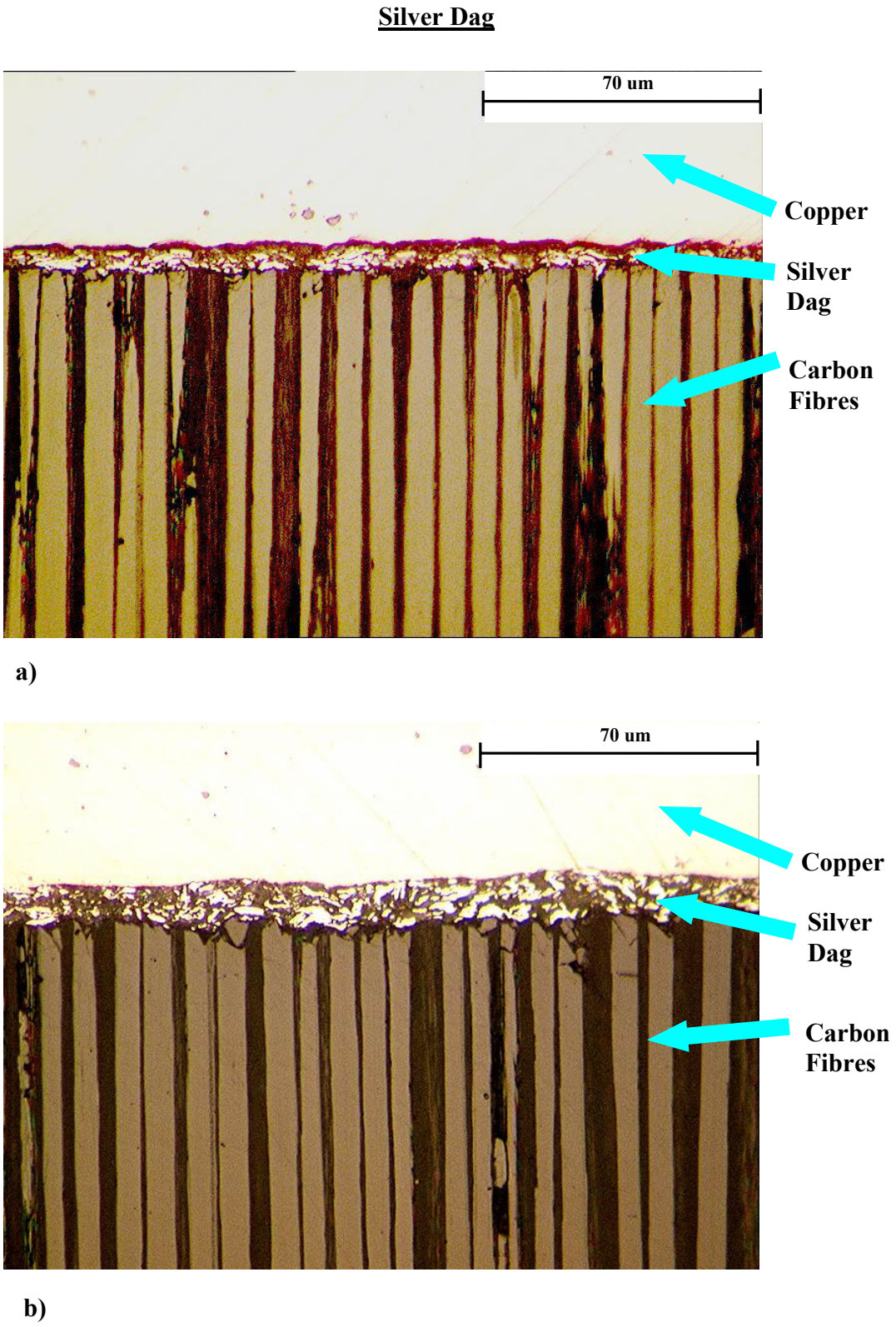

Figure 8. 12: Section through silver dag current introduction contacts, for two different samples.

8.3 Temperature Effect on Electrical Resistivity

The effect of various temperatures on electrical resistivity, in unidirectional and multidirectional laminates was investigated. The aim of this research work was to study qualitatively the general behaviour of the electrical resistivity, at low and high temperatures, but most importantly to quantify and compare the magnitude of the potential percentage changes with these caused by impact damage and mechanical strain. The latter has been overlooked by previous researchers who investigated the electrical behaviour of CFRP laminates (Chapter 4). All the details about the experimental set-up, stacking sequences and software for obtaining data are given in Chapter 6, Sections 6.4.2, 6.5.8 and 6.6.3.

8.3.1 Unidirectional Specimens

Figure 8. 13 shows the change of the electrical resistivity with temperature for unidirectional samples with the fibres aligned in the 0° direction; the current electrodes are positioned on the edges of the samples at the fibre ends.

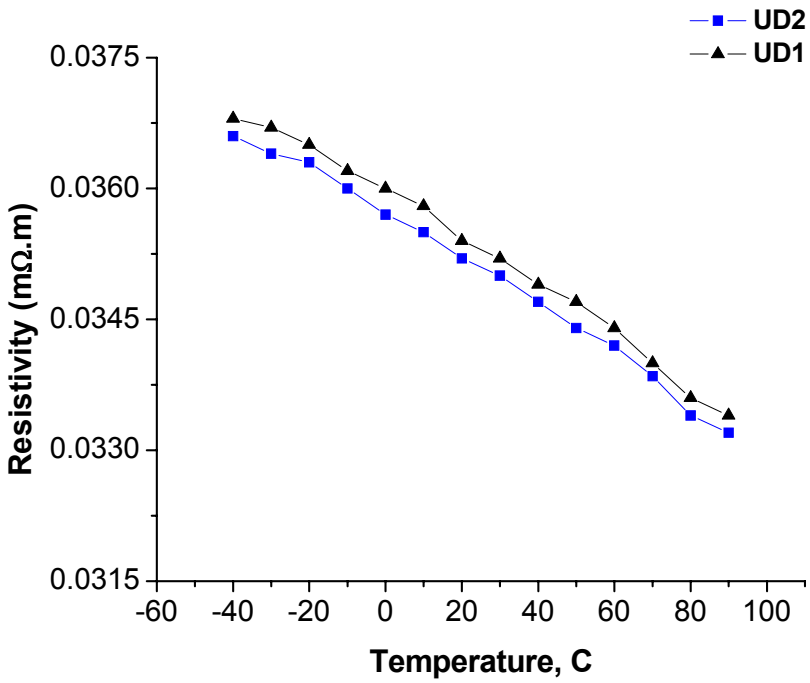

Figure 8. 13: Change of electrical potential with changing temperature for unidirectional samples, with current introduced at the edges of the composite at the fibre ends.

The potential decreases, approximately linearly, with increase of the temperature from the very lowest temperatures to the highest. This behaviour is similar to that observed in intrinsic semiconductors (Section 2.5). These findings are in agreement with the temperature behaviour of T300 carbon fibres as reported by the manufacturer [42] and contradict the results presented by Thiagarajan [33], who found an increase in electrical resistivity, as temperature elevates.

The values of temperature coefficient of resistivity (TCR) are shown in Table 8. 2.

Table 8. 2: Experimentally measured temperature coefficient of resistivity of CFRP.

	UD	***CP***	***QI***	***T300 fibres***
Temperature Coefficient of Resistivity *10^{-5} mΩ.m/°K	-2.65	-3.8	-5.12	-1.02

As can be seen, the TCR of the composite samples is of the same order of magnitude as the TCR of single T300 fibres. This similarity in the longitudinal resistivity behaviour of unidirectional CFRPs and their constituent fibres suggests that the longitudinal properties are fibre dominated.

8.3.2 Multidirectional Specimens

The temperature dependent electrical resistivity results for cross ply and quasi-isotropic samples are shown in Figure 8. 14 and Figure 8. 15 respectively. The electrical resistivity linearly decreases with increasing temperature.

This behaviour is similar to the unidirectional samples, indicating that the stacking sequence of the composite samples does not influence the dependence of the electrical potential on temperature.

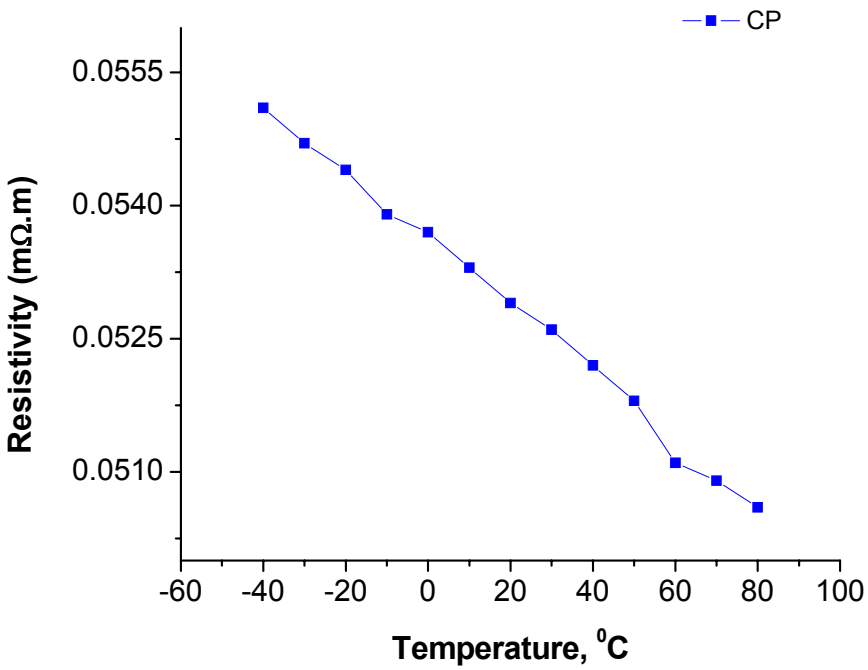

Figure 8. 14: Change of electrical potential with changing temperature for cross ply samples, with current introduced at the edges of the composite at the fibre ends.

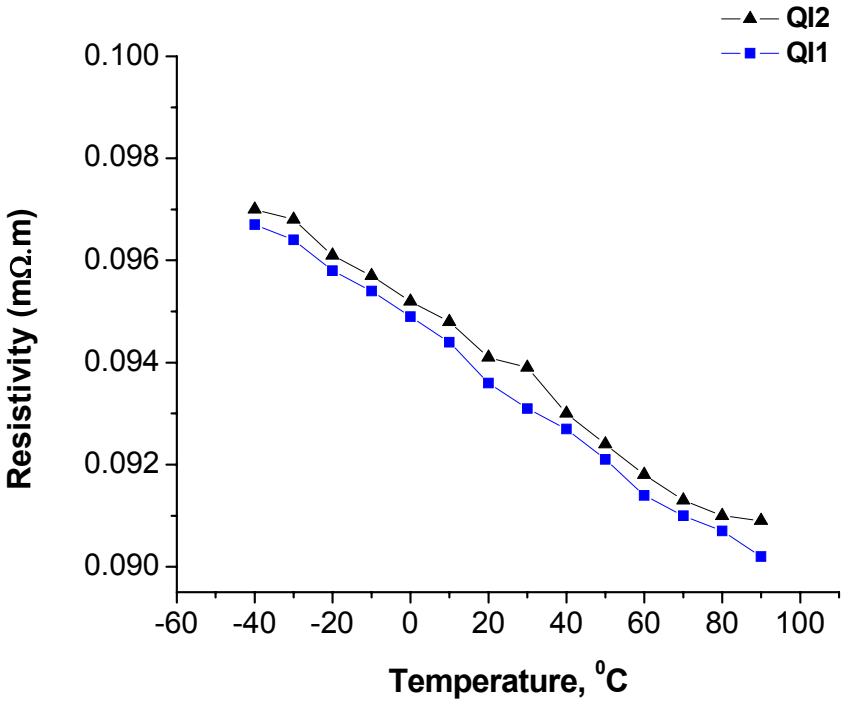

Figure 8. 15: Change of electrical potential with changing temperature for quasi-isotropic samples, with current introduced at the edges of the composite at the fibre ends.

8.4 Water Effect on Electrical Potential

The effect of water on the electrical potential was the second of the environmental conditions studied in this research study. Unidirectional samples, with the fibre oriented in 0˚ and 90° direction, were immersed into distilled water at room temperature for a period of six months (Section 6.4.2). The thickness of all samples was 2 mm. The current introduction probes were placed on the edges of the specimens, and the measurement potential probes were positioned on the surface. Based on experimental results from other researchers [150], such a long period under the water, would ensure 100% weight saturation, at least on the surface of the samples where the potential is measured.

For all samples, both current and potential probes were immersed into the water. The potential was measured before and after the specimens were immersed and the potential difference was recorded. Table 8. 3 summarizes all findings.

Table 8. 3: Experimental findings after immersion into distilled water for a period of eight months.

No of Sample	*Initial Potential (mV)*		*Final Potential (mV)*		*Percentage Change*	
	UD-0	*UD-90*	*UD-0*	*UD-90*	*UD-0*	*UD-90*
1	1.85	3.56	1.82	3.86	-1.2	8.5
2	2.68	3.89	2.65	4.28	-0.8	10
3	2.73	2.19	2.70	2.35	-1	7.1
4	2.77	2.48	2.74	3.01	-1.1	8.5

A decrease in potential values was observed for all unidirectional samples with the fibres aligned in the 0˚ direction and an increase of potential for the samples with the fibres aligned in the 90° direction. To correlate the obtained results with similar investigations from other researchers, changes in potential can be interpreted in resistance or resistivity changes following equations (2.1) and (2.2). The range of resistance changes varied

between -0.89 % and -1.2 % for the longitudinal. The transverse resistance was increased up to 10%. Similar observations are also reported elsewhere in the literature [36], [89].

Summarizing the results presented in this chapter it can be said that the response of electrical potential to mechanical strain in unidirectional and multidirectional composites is significantly affected from the current input configurations. Inhomogeneous current introduction led to situations where increasing mechanical strain produce decrease of potential change. The conduction processes also significantly affect the sign and the size of the GF. There is a significant difference between the behaviour of unidirectional and multidirectional samples. In the first case it was possible to convert a negative GF, when carbon cement was used as adhesive for introducing the current, to positive when silver paint was used. For the multidirectional samples, however, positive changes of the GF were observed for using either conductive adhesive. The importance of the inhomogeneous current introduction on the electrical potential was not investigated by others researchers, raising questions of whether their results and theories [54], [104], [105], [106], [110], for conduction mechanisms in CFRPs, should be considered reliable.

The electrical resistance, and so the electrical potential, also responded to changes in environmental conditions, such as temperature and water. A reduction was observed in electrical resistance of unidirectional and multidirectional samples, with temperature increasing from -40 °C up to 90 °C. A reduction in electrical potential was also monitored in unidirectional samples with the fibres aligned along the 0° direction after immersion in water for a period of six months. For unidirectional samples with the fibres aligned along the 90° direction, however, an increase of the electrical resistance was observed.

9 NUMERICAL ANALYSIS

The complexity of the current processes in unidirectional and multidirectional laminates, required the development of numerical models, firstly to obtain a good understanding of the 3-D conduction processes in composite plates, and secondly to know how mechanical strain and damage, in the form of delaminations, located at various positions within the structure, would affect the potential distribution on the outer surface of the sample.

This Chapter is constructed as follows. Sections 9.1 and 9.2 refer to the basic principles of finite element analysis, and the assumptions, encountered in the model developed in this study. The development of mesh sizes in unidirectional and quasi-isotropic laminates are described in Sections 9.3 and 9.4 respectively while Section 9.5 presents the effect of mechanical strain on potential distributions in unidirectional samples. In Section 9.6 potential distributions in undamaged cross ply and quasi-isotropic laminates are shown. Finally, the results from the development of models predicting the effect of delaminations on potential distribution on quasi-isotropic laminates are presented in Section 9.7.

9.1 Finite Element Model

Finite Element Analysis (FEA) is a process which can simulate stress, fluid flow or electrical fields on a structure. Finite Element Modelling (FEM) divides the structure into a grid of elements which form a model of the real structure. Each of the elements is in the form of a simple shape (such as square or triangle) for which the finite element program has information to write the governing equations in the form of a matrix. These elements are connected by nodes that have degrees of freedom.

For the model developed in this study, the governing equation is described by Ohm's law for flow of electrical current, as shown in equation (9.1).

$$J = \sigma^E E \qquad (9.1)$$

where J is the electrical current density (current per unit area), σ is the electrical conductivity matrix, and E is the electrical field intensity defined as:

$$E = -\frac{\partial V}{\partial x} \qquad (9.2)$$

where ∂V is the electrical potential. Since a potential rise occurs when a charged particle moves against the electrical field, the direction of the gradient is opposite to that of the electrical field.

In the finite element (FE) code, the matrix of governing equation for each element is computed at the nodes of each element, forming the final solution matrix; the principles behind finite element modelling have been documented in many text books [151], [152], [153], [154].

A coupled electrical-thermal-mechanical element model has been developed to analyse the resistance spot welding process of electronic chips [151] and composite sheets [155].

To the author's knowledge, limited finite element work has been conducted on the effect of impact damage on electrical potential in composite structures [156]. The present numerical analysis aims to establish an accurate and reliable finite element model, which is able to predict the conduction process, in unidirectional and multidirectional, damaged and undamaged composite laminates.

The electrical conduction mechanism of CFRP is a 3-D process and 3-D models can more accurately describe those processes. Finite element analysis can simulate the electrical potential distribution in composite plates under a given current load and boundary conditions. The analysis is limited by computer performance, mainly the amount of available memory and process speed for achieving the calculation. The amount of memory needed is a function of the storage method and increases with the number of nodes. The calculation time depends on the algorithm used, the number of processors and it increases with the number of nodes in the model.

The main objectives of this research study were first to model the potential distributions in undamaged plates; this includes the effect on the electrical potential of different stacking sequences, such as cross ply and quasi-isotropic plates, and different current input/output configurations. The second objective was the introduction of delamination damage within the composite structure. Apart from the effect of size of those delaminations on the electrical potential, other critical parameters were also investigated such as their position (in-plane and through the thickness) in relation to the current input/output probes. Finally, the effect of mechanical loading on electrical potential in unidirectional laminates was initiated and modelled.

The geometry and 3-D mesh of the laminates were defined using I-DEAS_9 software [152], which is a general purpose CAD based drafting system. The reasons leading to the selection of this package were firstly its powerful drawing capabilities, compared to other similar available packages, and secondly because of its capability to interface with specialized programs for numerical analysis of electrical potential distributions, such as ABAQUS 6.2 [151]. All groups of nodes and elements created on I-DEAS, were input in ABAQUS, which was used for finite element calculations.

The latter was found to be the most suitable for this model. This is mainly because of the immense range of available elements, which allow the user to select the ones which better fit to the problem, and secondly because its commands enable the user to better simulate the current process in the model, defining crucial parameters such interlaminar electrical conductance, and electrical properties of each layer. A coupled thermal-electrical model, provided by ABAQUS was used as an example for the development of the present model. The thermal part of it was not considered and therefore was not included in this research.

9.2 Numerical Model-Assumptions

The formulation of almost all numerical models is based on assumptions which are taken in order to simplify a complex practical problem and take a more tractable approach. The selection of those assumptions is essential, since the outcome of the analysis is strongly dependent on them. The main assumptions used in the present research are:

1. A unidirectional composite was modelled as a series of orthotropic brick elements, as shown in Figure 9. 1. The axis parallel to the fibre direction was modelled as x-axis, and y, z simulated the transverse and through thickness direction respectively.
2. The current flows between adjacent layers via interface nodes, (Figure 9. 1). Conduction processes occur in three dimensions; parallel and perpendicular to the fibres. The through thickness and transverse conductivity were assumed to be equal.
3. The properties of all elements are determined by the properties of the constituent materials and the volume fraction.
4. Although the rest of this thesis uses electrical resistivity, electrical conductivity (conductivity = 1/resistivity) was used in the model. This was because delaminations at the laminate interfaces can be modelled easier giving zero value in conductivity, whereas use of resistivity would result in requirement for infinite values.

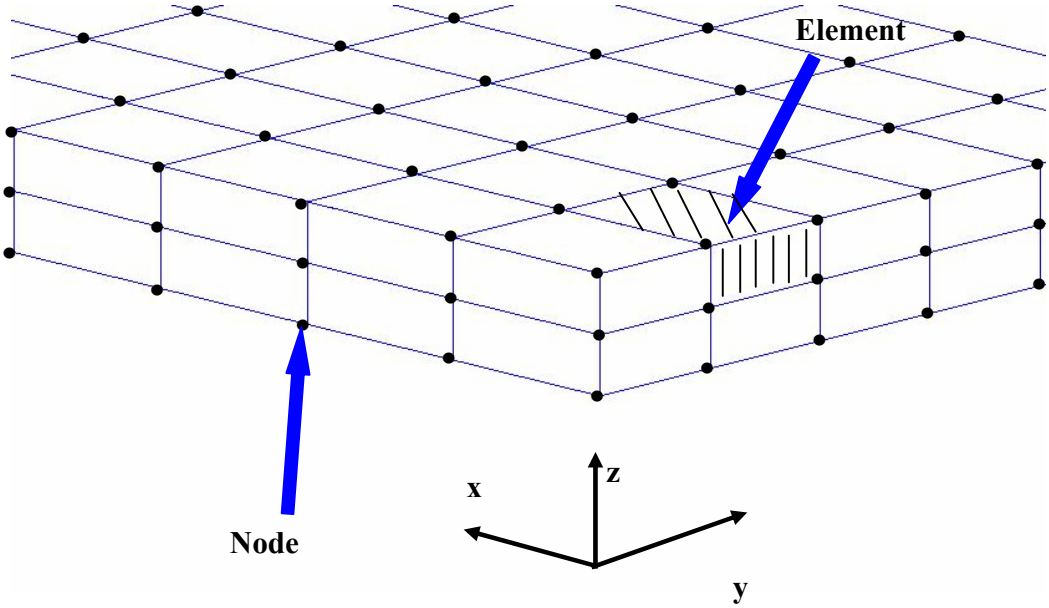

Figure 9. 1: Schematic representation of element types and nodes used in the numerical analysis study.

The same assumptions were used throughout the finite element investigation. As discussed previously, one of the benefits of using ABAQUS is its ability to modify some of the most crucial parameters affecting the electrical conduction processes. Such parameters are the electrical conductivity of each layer in all 3-D directions and the interface electrical conductance between layers with different fibre orientations; the numerical values of those were obtained based on experimental data.

9.2.1 Electric field equation:

The electrical field in the plate is governed by Maxwell's equation of conservation of charge and the electrical current flowing at the interface between two surfaces is modelled as:

$$J = g(V_A - V_B) \qquad (9.\ 3)$$

where J is the electrical current density flowing across the interface from point A on one surface on point B on the other, V_A and V_B are the electrical potential on opposite points

on the surfaces and *g* is the electrical conductance at the interface; both points A and B corresponds to nodes.

The various layers in a multidirectional laminate were simulated by defining the orientation and electrical properties of those elements. Delaminations were defined by separate groups of elements and the interface electrical conductance between adjacent groups was set equal to zero. The interlaminar electrical conductance in undamaged areas was given an experimentally measured non-zero value. The current was introduced on individual nodes on the outer layer, and the boundary conditions on electrical potential degrees of freedom were also defined on those nodes. The output of the model was the electrical potential values obtained for every node located on that layer.

In this study, two finite element models were constructed. One was concerned with unidirectional laminates and the other with multidirectional. Different mesh sizes were used for each model as discussed later in Section 9.3 and Section 9.4 respectively.

9.2.2 Numerical analysis parameters

Material Options:

Composite material electrical properties were modelled with orthotropic conductivity, whose values were precise in each simulation batch and taken from experimental measurements. The electrical properties were active in this coupled thermal-electrical analysis; all mechanical behaviour material options (such as elasticity and plasticity) were ignored.

Current Load:

Concentrated current was applied on single nodes in each simulation. Input locations were on outer surfaces, either on the same surface, where the potential was measured, or on the opposite surface; the current magnitude was 100 mA.

Boundary Conditions:

The boundary conditions used to prescribe the electrical potential and the temperature degrees of freedom at the nodes. In each simulation, the output current electrode was used to define the boundary condition node, in which the potential was zero.

9.3 Development of Finite Element Mesh in Unidirectional Samples

In this finite element study, the mesh size was developed for modelling potential distributions in unidirectional samples. The dimensions of the specimens were 280 x 25 x 2 mm. The samples were modelled using 3-D solid elements, type DC3D8E. This type of elements is an 8-node linear brick and is specialized for coupled thermal-electrical analysis as proposed by ABAQUS [151]. These elements were selected because the solution in a coupled thermal-electrical analysis requires the use of elements that have both temperature (11 degrees of freedom) and electrical potential (9 degrees of freedom) as nodal variables. Each sample had a thickness of 2 mm, represented by three elements in the through thickness direction.

As shown in Figure 9. 2, the current was introduced via two node contacts (points 1 and 2) on a line parallel with 0° surface fibres. The current electrodes were positioned at 90 mm distance from the specimen's edges, along the fibre direction and 5 mm in the transverse direction. The potential values obtained for all nodes positioned along the current flow line, between points 1 and 2. The mesh size was optimized for the directions parallel and perpendicular to the fibres.

For the finite element model, the electrical characteristics of the ply were defined. The experimental values of longitudinal and transverse resistivity (0.028 and 220 mΩ.m respectively) were used as input parameters into the modelling file. These values were obtained experimentally as is described later in Chapter 10, Section 10.1.1. The through thickness resistivity of the layer was considered to be homogeneous and equal to the transverse unidirectional ply resistivity.

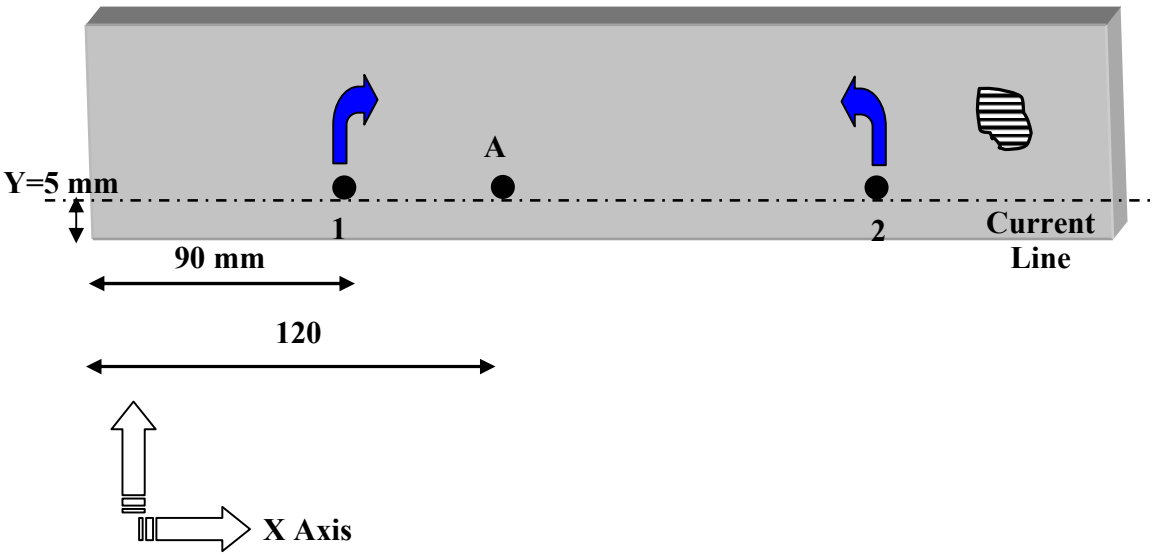

Figure 9. 2: Graphical representation of the profile of unidirectional samples used for developing the mesh size.

9.3.1 Mesh development

Table 9. 1 presents the different length elements used for this investigation. The length of each element in the direction perpendicular to the fibres (X-direction) was kept constant and equal to 1.25 mm while in the through thickness direction (Z-direction) the length was 0.67 mm.

Table 9. 1: Various element lengths used for mesh development in the direction parallel to the fibres, in unidirectional samples.

Element Length (mm)				
Longitudinal direction, x-axis	3.75	2.5	1.25	0.625
Transverse direction, y-axis	1.25	1.25	1.25	1.25
Thickness direction, z-axis	0.67	0.67	0.67	0.67

Figure 9. 3 shows the effect of different mesh sizes, in the longitudinal direction, on potential values. The graph X-axis, represents a section parallel to the fibre direction and along the main current flow. The Y-axis represents the potential values. The 'Mesh 3.75 mm' corresponds to element length of 3.75 mm while 'Mesh 0.625 mm' to element length of 0.625 mm. It can be seen that for mesh size less than 1.25 mm, little change in potential values is observed. This value was taken as the optimum value and was used for the numerical analysis of the potential response of unidirectional samples to mechanical strain.

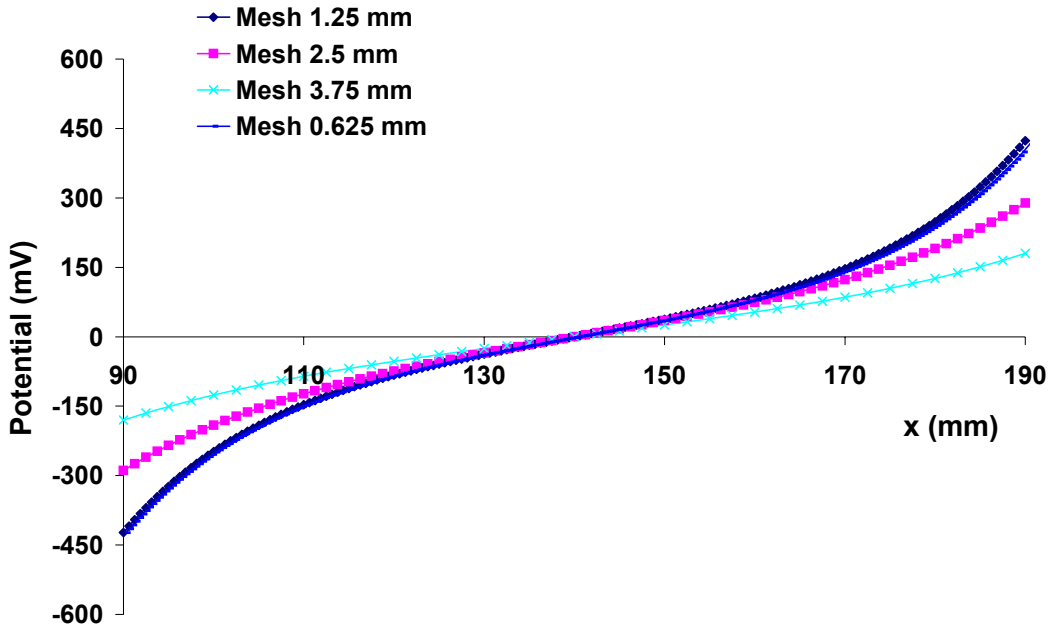

Figure 9. 3: Numerical simulation of the effect of various mesh sizes on the potential distribution along a section parallel to the fibre direction, for unidirectional samples; Current input/output points on the surface, parallel to this section.

The trend of potential values vs mesh size is shown in Figure 9. 4 for point A, located at distance 30 mm from the current introduction probe, along the current flow line. As can be seen, the reduction of the element length leads to a reduction in the gradient of potential values curve.

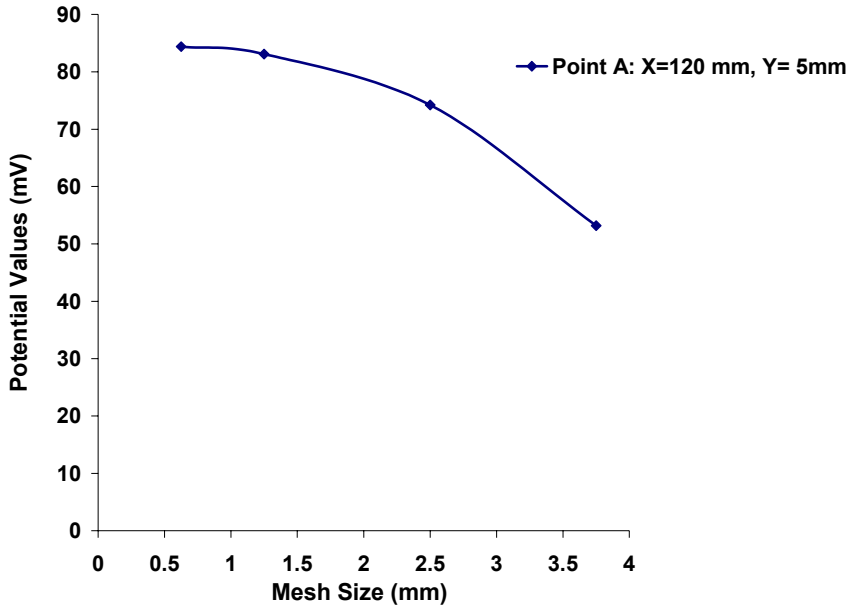

Figure 9. 4: Potential values trend for different mesh sizes, in unidirectional samples at point A.

Similarly to the longitudinal direction, the mesh size was also defined in the direction transverse to fibres. The lengths of each element in the longitudinal and through thickness directions were kept constant and equal to 1.25 mm and 0.67 mm respectively. Table 9. 2 shows the different length elements used for this investigation.

Table 9. 2: Various element lengths used for mesh development in the direction perpendicular to the fibres, in unidirectional samples.

Element Length (mm)				
Longitudinal direction, x-axis	1.25	1.25	1.25	1.25
Transverse direction, y-axis	3.75	2.5	1.25	0.625
Thickness direction, z-axis	0.67	0.67	0.67	0.67

Figure 9. 5 shows the effect of different mesh sizes on potential values. The graph X-axis, represents a section transverse to the direction of the fibres (at the point A shown in Figure 9. 2) while the graph Y-axis represents the potential values. The designation of the various mesh sizes is the same as stated previously. It can be seen that mesh density less than 1.25 mm has a negligible effect on potential values; this value of mesh was used in the subsequent numerical analysis.

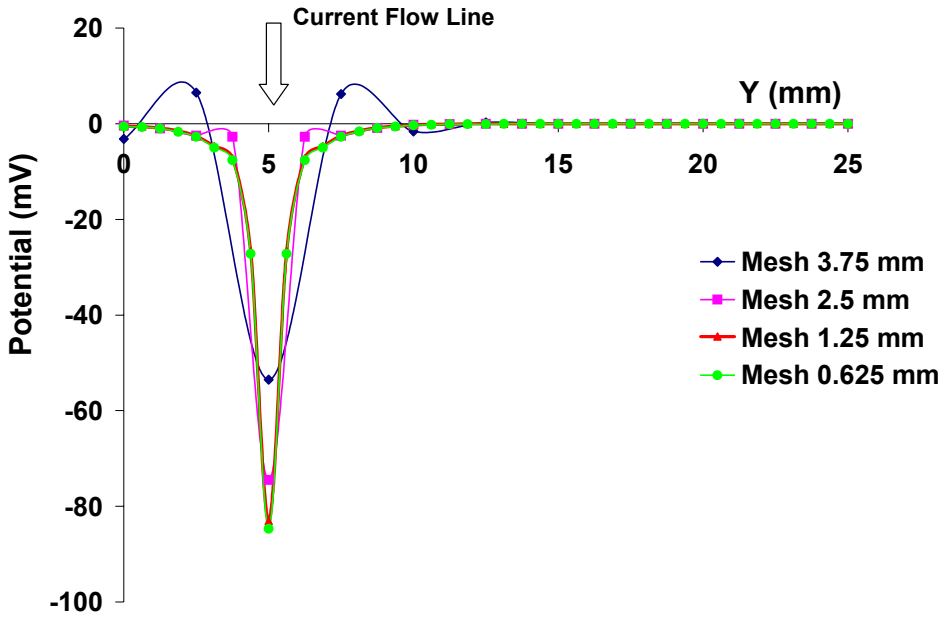

Figure 9. 5: Numerical simulation of the effect of various mesh sizes on the potential distribution along a section transverse to the fibre direction, for unidirectional samples; Current input/output points on surface, perpendicular to this section.

9.4 Development of Finite Element Mesh in Multidirectional Laminates

Two different models were constructed for developing the mesh in multidirectional laminates. The main difference between them was the number of elements used, and the aspect ratio of each one of those, which were found to be very crucial parameters in terms

of convergence between experimental and numerical results. For a suitable designation of those models, it is suggested considering as **Model-A**, the model with the high aspect ratio of elements, and **Model-B**, the model with the very small aspect ratio of elements.

For clear designation, the term 'Top surface' refers to the instrumented with probes surface for measuring the potential distribution while 'Bottom surface' refers to the opposite surface (Figure 9. 6).

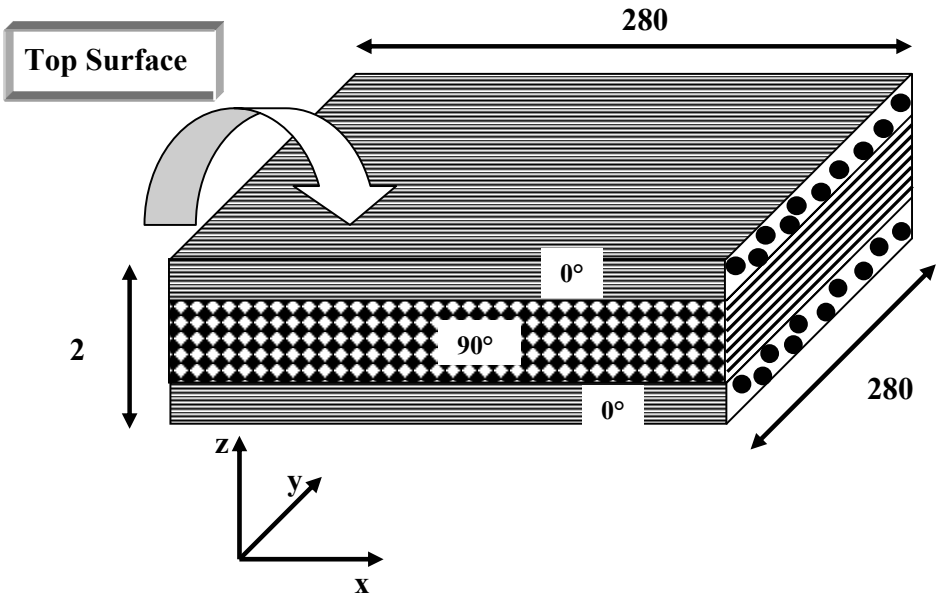

Figure 9. 6: Sample and axis system.

9.4.1 The mesh

a) Model-A

The laminates were modelled using the same type of element as for the unidirectional samples (Section 9.3). The potential distribution was calculated for the undamaged $[(0/90)_4]_s$ and $[0_2/45_2/90_2/-45_2]_s$ laminates; a general view of the origin and axis directions, in relation to the 0° and 90° direction fibres is given in Figure 9. 6. All dimensions are in millimetres.

The dimensions of the plates were 280 x 280 x 2 mm. Each ply had a thickness of 0.25 mm represented by three elements dimension of 10 x 10 x 0.083 mm, as shown in Figure 9. 7, and it was defined by 11,303 nodes and 6,672 elements. For a multidirectional laminate of the same dimensions and a lay-up where the orientation changes at each ply, the total mesh would include 90,424 nodes and 53,376 elements. For the finite element model, the electrical characteristic of the ply and the configuration of the current input were defined. The through thickness resistivity of the layer was considered to be homogeneous and equal to the transverse unidirectional ply resistivity of 310 mΩ.m [157]; however, along the fibre direction the resistivity is equal to 0.022 mΩ.m [157]. These resistivity values were measured on quasi-isotropic plates experimentally [157] and although are different than those quoted in Section 9.3 for unidirectional samples, the former were used in this model in order to compare directly the numerical with the experimental results for the quasi-isotropic laminates.

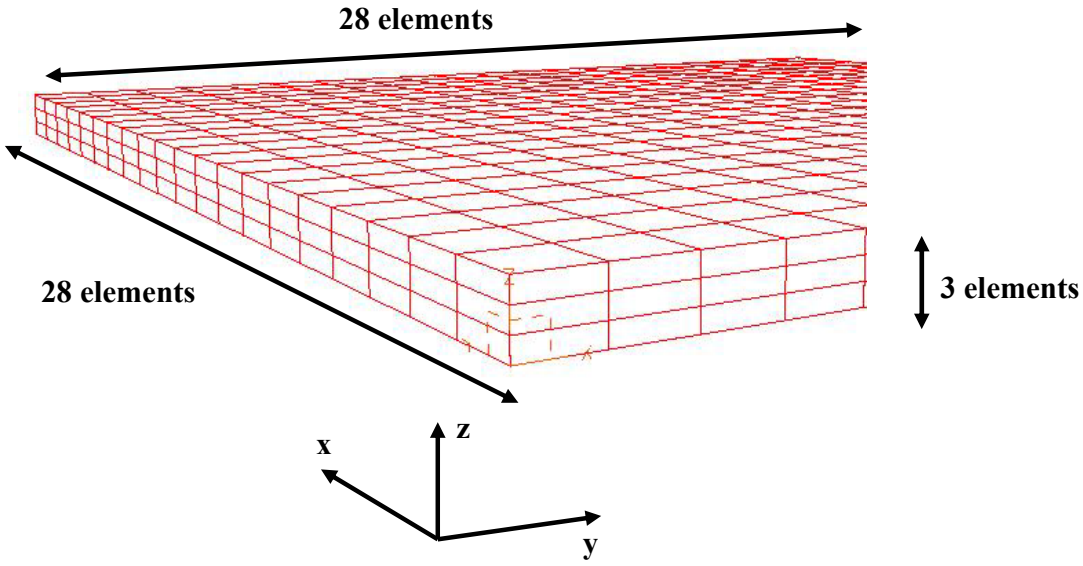

Figure 9. 7: Mesh representation of a ply of the quasi-isotropic laminates.

For the above laminates, the contact between two plies of different fibre orientation generates an electrical resistance at the interface which can be represented by the interface conductance [157]. The measured interface conductance per unit area, between 0/90 and 0/45 layers is given in Table 9. 3. For reasons of simplicity and because of the

small difference in value between interface 0/90 and 0/45 it was assumed that the conductance of all interfaces in the $[0_2/45_2/90_2/-45_2]_s$ laminates are equal to the values corresponding to 0/90 interface [157].

Table 9. 3: Experimental values of the electrical parameters used in the finite element model [157].

Specimens	***$[(0/90)_4]_S$***	***$[0_2/+45_2/90_2/-45_2]_S$***
Interface	0/90	0/45 ≡± 45/90
Longitudinal Conductivity σ_0 $(m\Omega.m)^{-1}$	45.4 (± 18%)	45.4 (± 18%)
Transverse Conductivity σ_{90} $(m\Omega.m)^{-1}$	0.0032(± 6.4%)	0.0032 (± 6.4%)
Interface Conductance per unit area G (S/m^2)	125	287

The accuracy of the model will be highly dependent on the aspect ratio and angle of distortion of the elements. Aspect ratio is defined as the ratio of the length of one dimension to another, which ideally should not exceed more than 5:1 [151], while the distortion angle of the elements should not be less than 45° or greater than 135° [151]. In this model, no attention was paid to the aspect ratio and distortion angle relating to the elements used, which were 120:1 and smaller than 45° respectively.

As a consequence, the predicted potential values gave a significant error compared to the experimental results, when the experimental value of interface conductance was used; the discrepancy between numerical and experimental values was 48.5% for the cross ply and 43.2% for the quasi-isotropic laminates. The numerical results were correlated with the experimental values when the interface conductance was set equal to 0.0125 S/mm^2 for the quasi-isotropic plate, which is almost 50 times greater that the experimentally measured value of 0.000287 S/mm^2, and 0.125 S/mm^2 for the cross ply, 1000 times greater than the experimentally measured. This discrepancy can be attributed to the high aspect ration and distortion of the elements that were used.

b) Model-B

In this investigation, only quasi-isotropic plates were modelled, having lay-up and dimensions as shown previously. The same type of elements were used as in Model-A; however, their aspect ratio was significantly improved from 33:1 to 5.6:1, improving simultaneously the distortion angle of the elements, in an effort to eliminate the problem with the great discrepancy in the potential values for the numerical simulations and the experiments.

Initially, it has been attempted to significantly increase the mesh. The number of elements was greater than 260,000 per laminate, raising significant problems of computer capacity. To overcome them, the number of elements through the thickness of each ply was reduced to one from three; all other electrical properties of each layer, were kept the same as in Model-A. Table 9. 4 shows the different length elements used for this investigation.

Table 9. 4: Various element lengths used for mesh development in, in quasi-isotropic laminates.

Element Length (mm)				
Longitudinal direction, x-axis	7	3.5	2.8	1.4
Transverse direction, y-axis	7	3.5	2.8	1.4
Thickness direction, z-axis	0.25	0.25	0.25	0.25

A comprehensive study was made on the effect of mesh size on potential values; this is shown in Figure 9. 8, for various selected mesh sizes. The X-axis, represents a section through the middle of the plate, parallel to the fibre direction and along the main current flow while the Y-axis represents the potential values. The ‘Elements length = 7 mm’ corresponds to the purest mesh size, which includes 40 elements in the directions parallel and transverse to the fibres, and the ‘Elements length = 1.4 mm’ to the richest mesh which includes 200 elements.

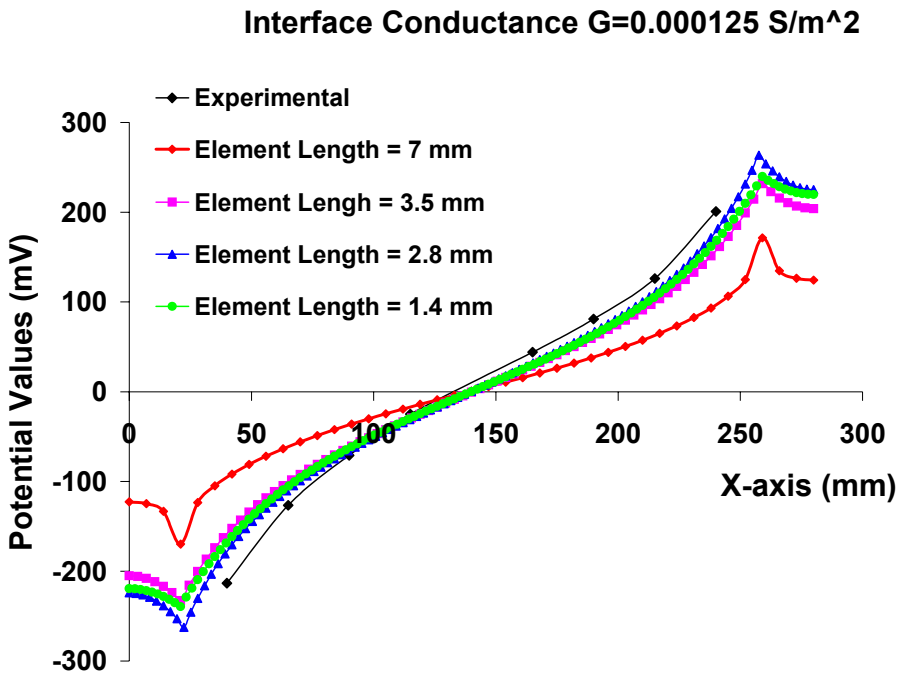

Figure 9. 8: Numerical simulation of the effect of various mesh sizes on the potential distribution on the **top** surface of quasi-isotropic laminate, along a section through the plate centre, parallel to the fibre direction, for quasi-isotropic plates, for front-surface instrumentation; Current electrodes on mid points on **top** surface, parallel to this section.

The 'Elements length = 2.8 mm' correlates the numerical and the experimental results while there is a little improvement beyond that for smaller element lengths; this value was taken as the optimum value and was used for the results reported in this study for both undamaged and damaged laminates.

9.5 Potential Response of Unidirectional Samples to Mechanical Strain

In this study, the response of the electrical potential to mechanical strain was investigated. This finite element analysis attempted to model experimental observations related to strain induced changes in potential distribution on the surface of a unidirectional CFRP sample with surface point introduction of current. The geometrical

details of the samples and the electrical parameters of the models are given in Section 9.3. Each sample is represented by elements dimension of 1.25 x 1.25 x 0.67 mm; it was defined by 19,572 nodes and 13,920 elements.

As demonstrated in Figure 9. 2, the current was introduced via two node contacts on a line parallel with 0° surface fibres. Pairs of potential measurement probes 40 mm apart were arranged either along the current flow line (Points A and B) or at 2.5 mm and 3.75 mm away from the current line (Points C and D) as illustrated in Figure 9. 9.

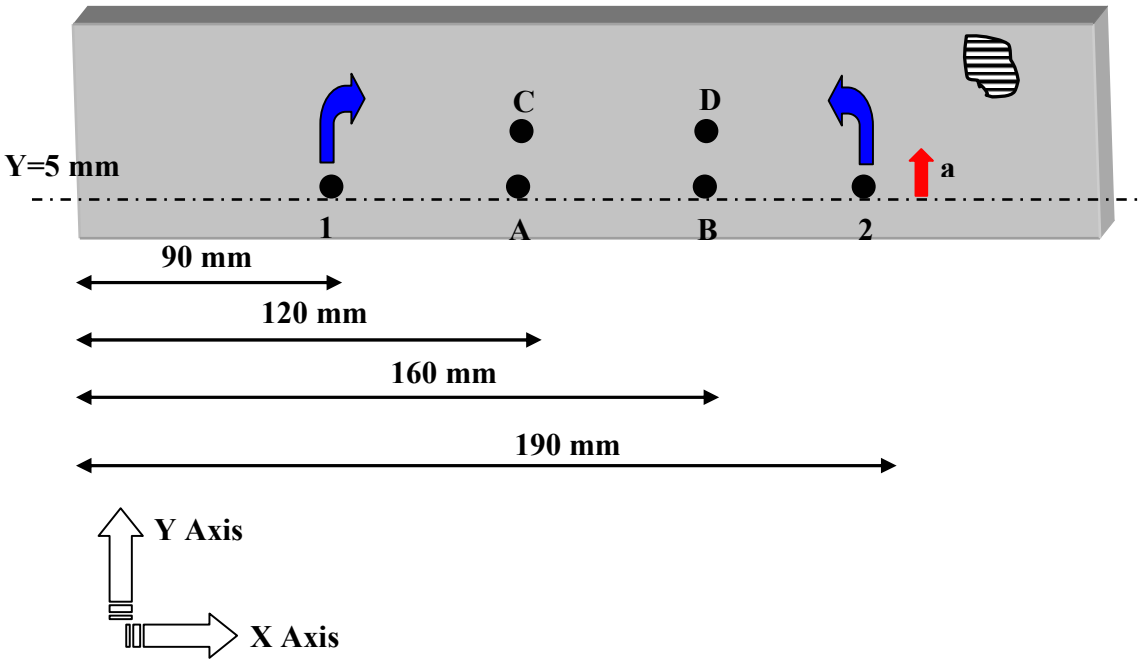

Figure 9. 9: Graphical representation of the profile of unidirectional samples used in numerical simulations.

The distance between the current electrodes was 100 mm and the distance between the potential probes 40 mm respectively. The laterally displaced distance from the current flowing line is symbolised with ***'a'***. The numerical model simulated the response of electrical potential on the top surface at three levels of mechanical strain: 0, 0.15% and 0.3%. For 0.15% and 0.3% strain, the resistivity values were modified by application of

the uniform current gauge factors as measured, using configurations D and E, of 1.75 longitudinal and 2.7 transverse.

Figure 9. 10 shows a calculated potential field at zero strain, for surface point introduction of current in unidirectional CFRP. A very local distribution of potentials is observed, around the line of current flow, as a consequence of non-homogeneous current introduction. Elsewhere there is an equi-potential field of small values of potential difference. The significantly lower electrical resistance parallel to the fibres than in transverse direction will result in a non-homogeneous current distribution on the plate, constraining the current flow transverse to the fibres in a very narrow distance, approximately 5 mm. The potential values at the current electrodes were approximately 330 mV while at the points A and B were of the range of 15 mV.

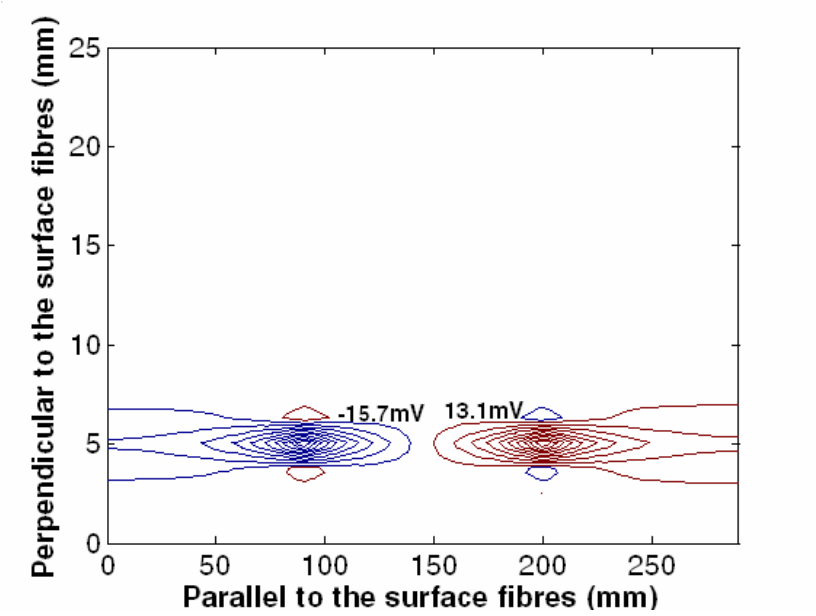

Figure 9. 10: Potential distribution in unidirectional laminate resulting from point current input at the surface.

Due to the extremely high anisotropy of electrical resistance, an abrupt reduction of current flow in the direction perpendicular to the fibres is expected, resulting in significantly reduced potential difference values at very small distances from the line of current flow.

The numerical calculations, which produced the potential distribution shown in Figure 9. 10, were repeated by changing the values of resistivity in the direction longitudinal and perpendicular to the fibres. Once the calculations had been performed for strain values of 0.15% and 0.3%, potential readings at points A and B were recorded and values of potential difference were calculated. The values of potential change with mechanical strain were converted into gauge factor using equation (9.1).

Table 9. 5 presents the results from the numerical analysis for potential differences between A-B points and C-D points; the apparent trend of gauge factors for strains of 0.15% and 0.3% is shown in Figure 9. 11.

Table 9. 5: Finite element simulation of the response of the electrical potential to mechanical strain.

Strain / ***a (mm)***	***0%***	***0.15%***	***0.3%***	***GF (Numerical)***	***GF (Experimental)***
0 (CH1)	92.5 mV	92.9 mV	93.8 mV	4.6	5.3
1.25 (CH2)	3.45 mV	3.53 mV	3.58 mV	12.5	
2.5 (CH2)	1.54 mV	1.55 mV	1.58 mV	8.6	
3.75 (CH2)	1.01 mV	1.00 mV	0.989 mV	-6.6	-3.26

For the points A and B in line, the potential difference increases with mechanical strain, and the predicted GF of 4.6 is in close agreement with the experimentally measured value of 5.3.

For potential measurements between points displaced laterally from the line of current flow (points C-D), the GF increases with mechanical strain for distances up to 2.5 mm. This behaviour can be attributed to the fact that when the current is introduced on individual nodes, its density is extremely high and the nearby nodes are affected; a portion of the current will then flow from those as well, at zero strain.

However, the absolute values are reduced due to the faster increase of the transverse resistance perpendicular to the fibres, than in longitudinal, and the subsequent reduction of current flow transverse to the fibre direction.

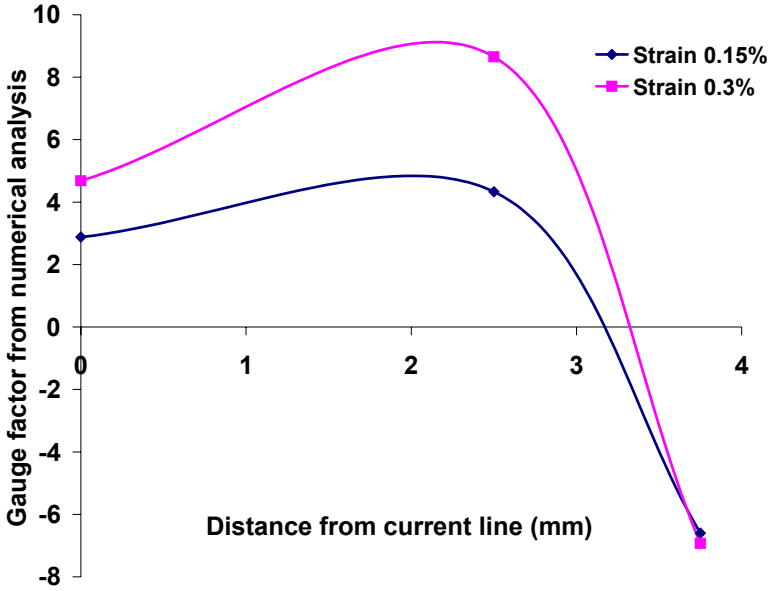

Figure 9. 11: Plot of numerically calculated gauge factor vs distance from line of current introduction showing how it changes over the surface of the composite.

A negative gauge factor is predicted at distance 3.75 mm from the current flow line. At this distance, the potential values are very much decreased, and this is the limit where we get non-zero potential values. The gauge factor for potential measurements at points C and D was calculated to be -6.6 as opposed to -2.6 gauge factor measured from the experiments.

Figure 9. 12 shows the calculated and experimentally measured relation between $\Delta V/V$ and applied strain for channel 1 (CH 1) and channel 2 (CH 2) positions (Section 8.1.2). The agreement with CH 1 is exceptional while in CH 2 there are differences; these may be due to the resolution and accuracy of the numerical calculation. The values of potential and potential change at this point are very small and percentage errors may be significant; nevertheless the trend of both lines is towards negative values of $\Delta V/V$.

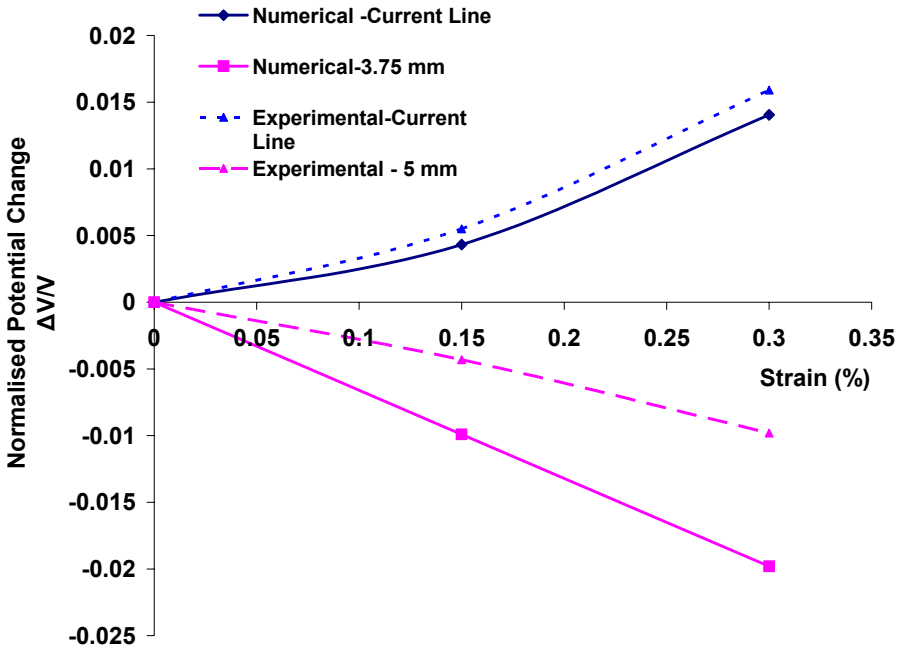

Figure 9. 12: Plot of normalised potential change (ΔV/V) vs applied strain for experimentally measured data and numerically calculated, for channel 1 and channel 2; configuration B.

The numerical analysis demonstrated that changes in local current and resistance conditions will affect the values and the sign of apparent and subsequently intrinsic gauge factors. Both numerical and experimental configurations showed that positive gauge factors are the result of increased current density along the current flow line, while the negative ones appeared to be the result of current reduction at the points displayed laterally from the line of current flow. In either case, this can be attributed to the faster increase of the transverse electrical resistance than of the longitudinal.

9.6 Calculated Potential Fields on Multidirectional Laminates

In this finite element study, potential distributions were simulated on undamaged multidirectional plates. The mesh and the electrical characteristics of the model are given in Section 9. 4.

Figure 9. 13 and Figure 9. 14 show the potential distribution fields on cross ply and quasi-isotropic laminates. The current electrodes are located on the mid-points on the bottom surface, along the top surface fibre direction (0°).

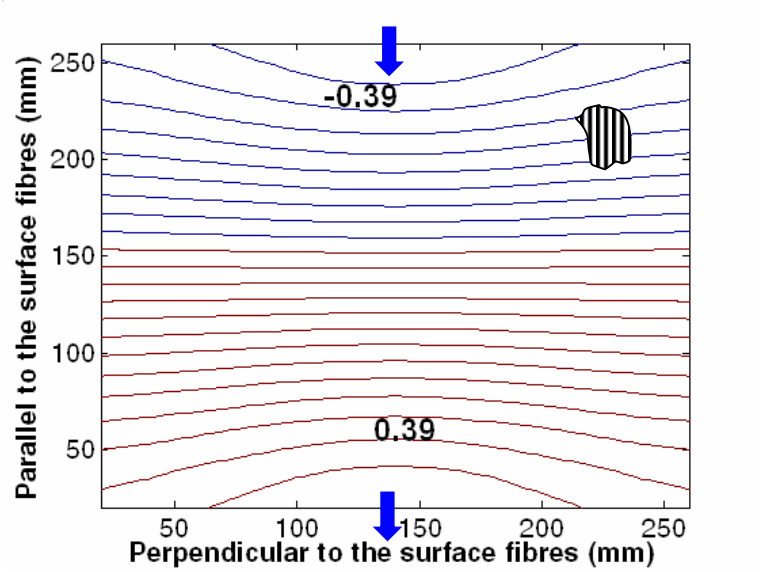

Figure 9. 13: Numerical simulation of potential distribution on **top** surface of undamaged cross ply laminates. Current introduction is on **bottom** surface, on mid point of horizontal perimeter edges.

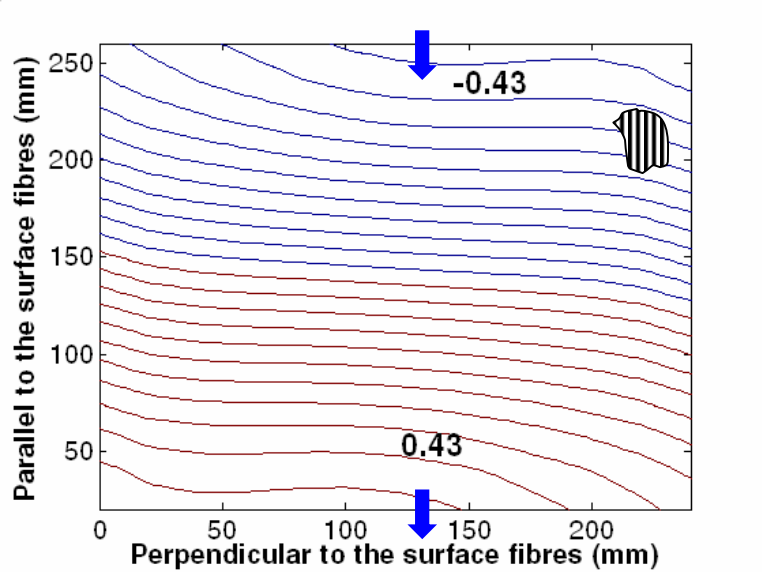

Figure 9. 14: Numerical simulation of potential distribution on **top** surface of undamaged quasi-isotropic laminate. Current introduction is on **bottom** surface, on mid point of horizontal perimeter edges.

The similarity between the two distributions and the experimental ones (Section 7.1, Figure 7. 5 (a) and Figure 7. 6 (b) respectively) can be seen with the exception of the experimentally measured distributions, at the left and right hand edges. The orientation of the potential contours with respect to the line joining the current input and output electrodes is also almost identical (approximately 90° to the line), with a slight rotation towards the orientation of the 45° layer immediately underneath the outermost lamina for the quasi-isotropic laminate. Quantitative measurements reveal that the finite element simulations of potential values and those measured experimentally agree up to 3.7 %. Potential values measured at probes positioned at the same location in the two plates, indicating the accuracy and the credibility of the numerical model.

9.7 Modelling of Delamination Damage in Quasi-Isotropic Laminates

A finite element study on the effect of delaminations inside the $[0_2/45_2/90_2/-45_2]_s$ laminates has been done. The objective was to simulate different damage sizes and locations with two different input/output configurations and to find their effect on the potential field and the level of potential change compared to an undamaged plate. The mesh size was based on Model-B, and it was refined around the delaminated area in order to improve accuracy as shown in Figure 9. 15.

The damage was modelled as a single delamination in order to investigate the sensitivity of the model in small size damage and to compare individual delaminations at separate layers with those extended throughout the structure; delaminations were simulated by modifying the surface interaction at the delamination location. The electrical interaction between two plies was defined equal to 0 S/mm^2 along the surface corresponding to the delamination. Experimentally the propagation of a delamination is in the fibre direction of the lower ply opposite to the impacted site in relation to the interface, and the shape of the delamination is often elliptical due to its substantial propagation [158].

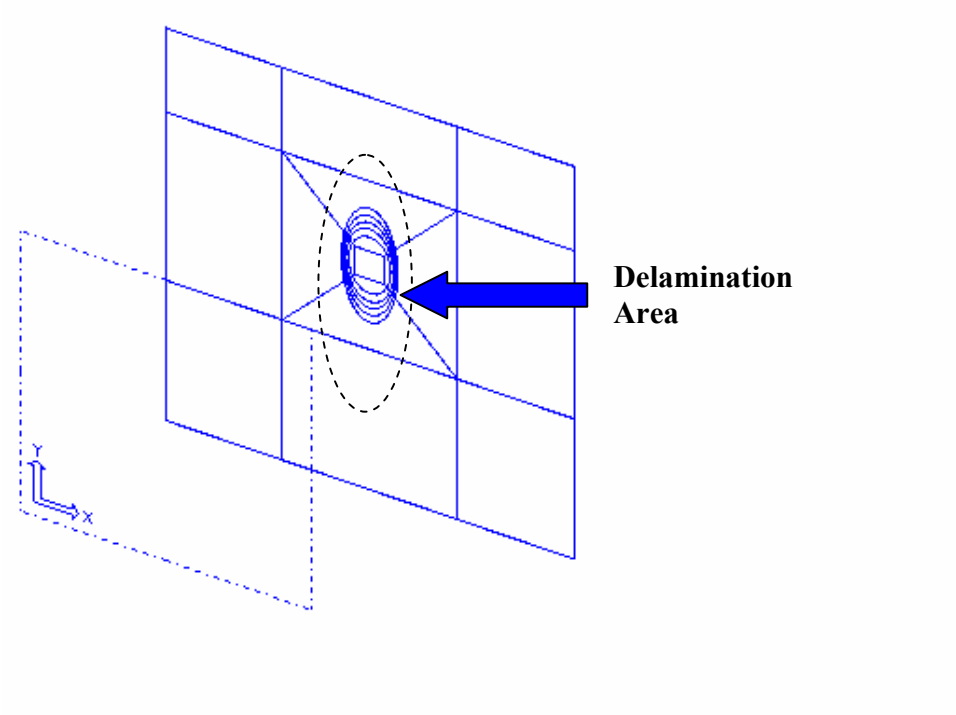

Figure 9. 15: Finite element meshing in the quasi-isotropic plates with refined mesh around delaminated area.

The damage sizes as shown in Table 9. 6 were modelled. The x-axis represents the direction parallel to the fibres (0° direction) and y-axis the direction transverse (90° direction); for each delamination, an individual group of nodes and elements was created.

Table 9. 6: Dimensions of delaminations modelled in the numerical analysis.

Size of Delaminations		***Position-Interface***
x-axis (mm)	***y-axis (mm)***	Centre-0/45
20	20	Centre-0/45
40	28	Centre-0/45
50	32	Centre-0/45
60	34	Centre-0/45
70	36	Centre-0/45
80	38	Centre-0/45

Figure 9. 16 presents the shape of different delamination configurations defined at the first from the top interface 0/45 in the centre of the laminate; this interface is the most sensitive to delamination damage.

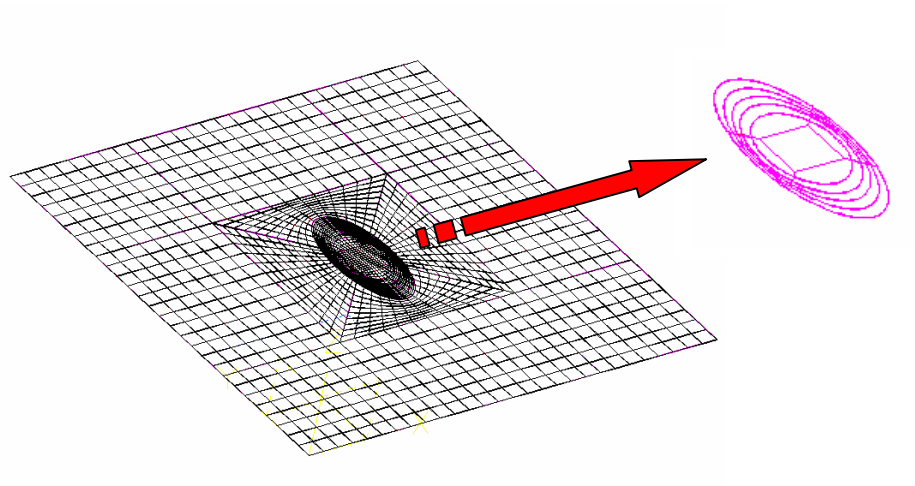

Figure 9. 16: Different delaminations embedded within the composite structure.

9.7.1 Current flow along the fibre direction

The first input/output configuration had current introduction probes situated on the top face and aligned parallel to the 0° direction fibres, along the symmetrical axis of the plate. Figure 9. 17 shows the calculated potential field on the top surface of a QI laminate, before and after a delamination is introduced between the first and second layers. There is little obvious potential change in the composite plate, because of the large variation in potential within an individual plate.

The difference between current input on top and bottom surface can be seen by comparing Figure 9. 14 and Figure 9. 17. The second picture is characterized by two high potential peaks, near the current input/output nodes where the current density is high, while elsewhere the contour distribution is flat. This behaviour was also observed for the experimental configurations (Section 7, Figure 7. 6 (a). In Figure 9. 14, however, these peaky areas disappear, because the potential values are very much reduced.

The high electrical resistivity through the thickness will significantly reduce the current reaching the top surface and so the potential values.

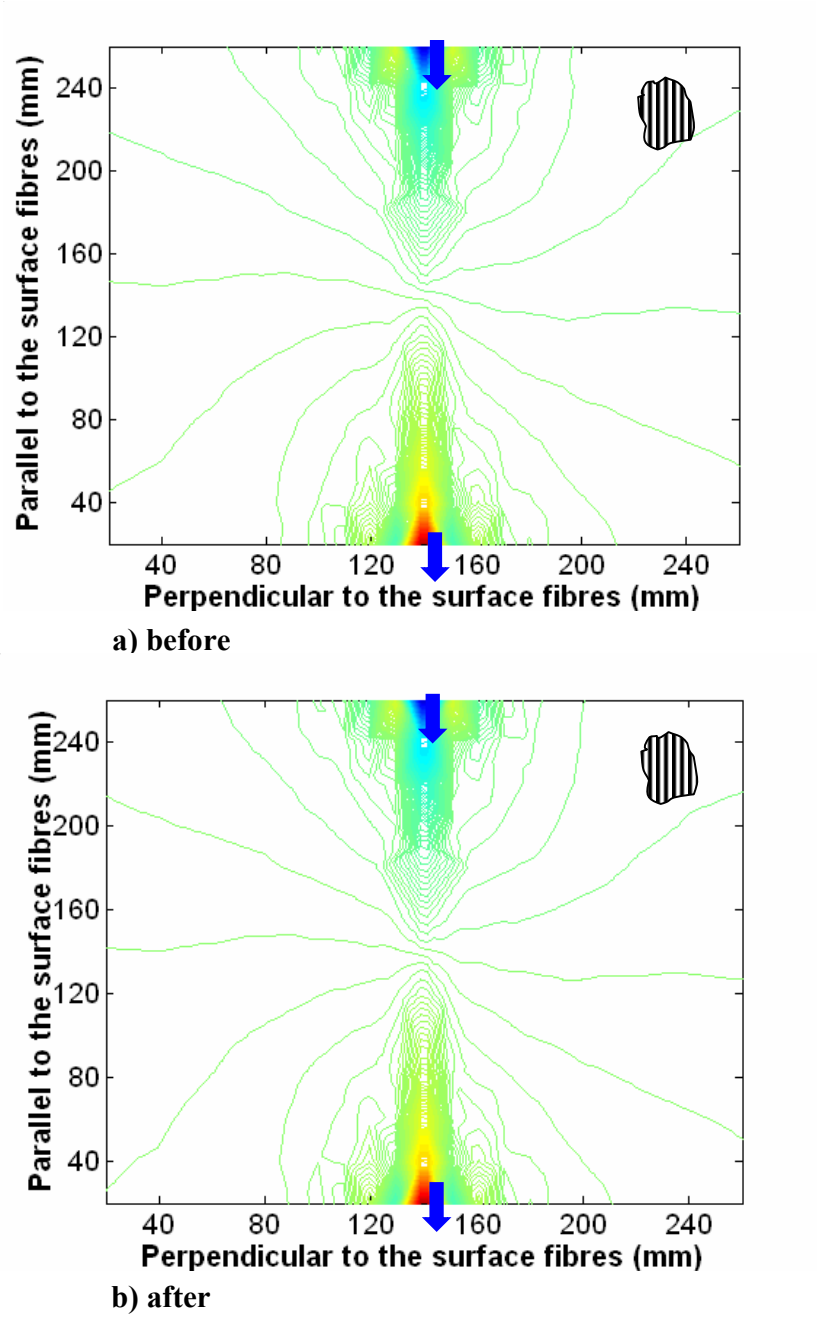

Figure 9. 17: Calculated potential distribution on **top** surface of quasi–isotropic laminate, a) before and b) after delamination is introduced between first and second layer in the centre of the laminate; current input on **top** surface, mid point of horizontal edges.

Indications of damage could be obtained by producing contour plots of equi-potential change. Figure 9. 18 (a) and (b) show the calculated equi-potential change contours produced by single delaminations of size 38 x 80 mm and 20 x 20 mm sizes respectively, located between the first and second plies.

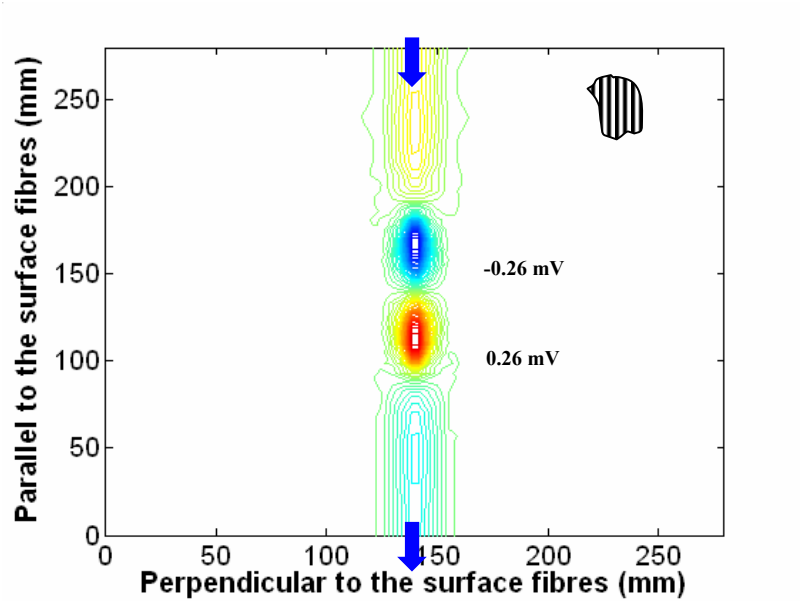

a)

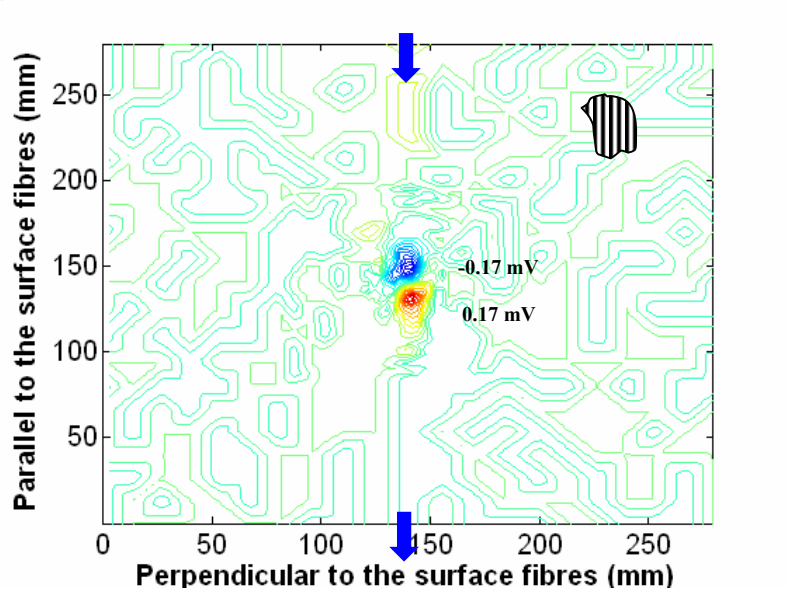

b)

Figure 9. 18: Calculated contours of potential change on **top** surface of quasi-isotropic laminate relative to the undamaged state, after creation of single delamination a) 38 x 80 mm and b) 20 x 20 mm between first and second ply, in the centre of the plate area; current input/output on **top** surface, mid point of horizontal edges.

The current input is on mid point of horizontal edges, on the top surface. The boundary of the delamination is shown in this figure, superimposed on the contour plot in the centre of the laminate. Plotted in this way, the delaminations always have a characteristic two lobed appearance, with the centre of each lobe located at the delamination boundary. In Figure 9. 18 the contour lines away from the centre of the laminate are tiny potential change values at the noise level, and do not indicate any damage in those areas.

One lobe represents a positive potential change peak, the other a negative potential trough. As was the case in the experimentally generated plots of this type, the regions of potential change extended out considerably beyond the boundaries of the delamination. In this theoretical simulation the region of potential change extended to the edge of the laminate. In the direction perpendicular to the top surface fibres, the region of disturbance extended only as far as the boundary of the delamination itself.

In general cases the changes are small, but compared to the potential values before delamination, the percentage change is relatively high and depends on the size and location of the delamination. For current introduction at the mid-points, on the top surface and parallel to the 0° fibres, the potential change ranges from 1% to 32% of the undamaged value, for delaminations between first and second ply, located in the centre of the plate.

Figure 9. 19 shows the contour plot of potential change for delamination dimensions of 38 x 80 mm, located 60 mm from the centre of the plate parallel to the 0° fibres, between first and second ply; current input is on the top surface, at mid points parallel to the 0° fibres. When the centre of the delamination is moved by 60 mm from the centre of the plate, the percentage changes become from 18% to 59%, 1.2% to 28% and 5% to 30% for the minimum and maximum delamination size. These numbers are for movements parallel to the fibre direction, perpendicular to the fibre direction and at 45° to the fibre direction. These results indicate that when the delamination centre is shifted from the middle of the plate parallel to the fibres and towards the input/output probes, the sensitivity to damage increases.

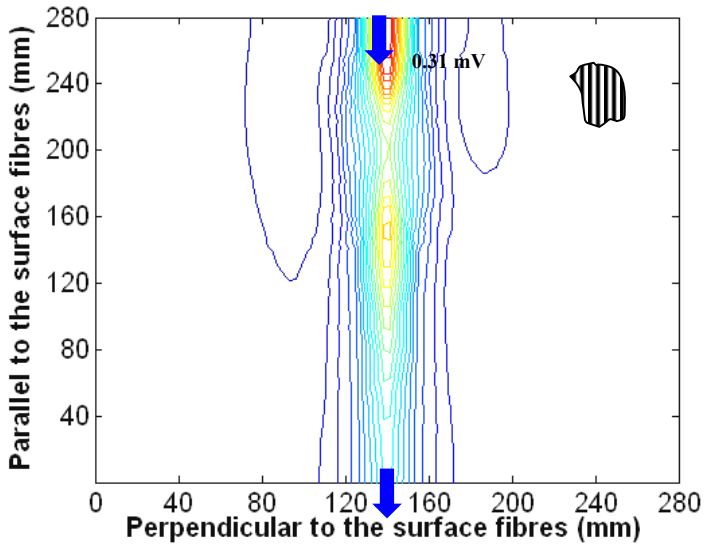

Figure 9. 19: Calculated contours of potential change on **top** surface of quasi-isotropic laminate relative to the undamaged state, after creation of single delamination 38 x 80 mm placed 60 mm from the centre of the plate parallel to the fibres, between first and second layer; current input/output on **top** surface mid point of horizontal edges.

This outcome was expected, since the potential values closer to the input/output probes are greater than in the middle, producing greater potential changes due to the existence of a delamination.

9.7.2 Effect of current electrodes location on damage detection

With current input on the bottom surface, and current probes same as previously, on the mid-points parallel to the fibres of the top layer, it is predicted that there will be no potential disturbance around the damaged site, as Figure 9. 20 demonstrates; this is achievable only if the contour plot of potential difference is plotted. Experimentally, however, a potential disturbance for this configuration was observed (Figure 7. 15). It is believed that this due to the fibre breakage of the external 0° ply in the bottom surface, parallel to the line connecting current electrodes. In the model any other damage form in the plate has not been considered apart from pure delamination within various layers.

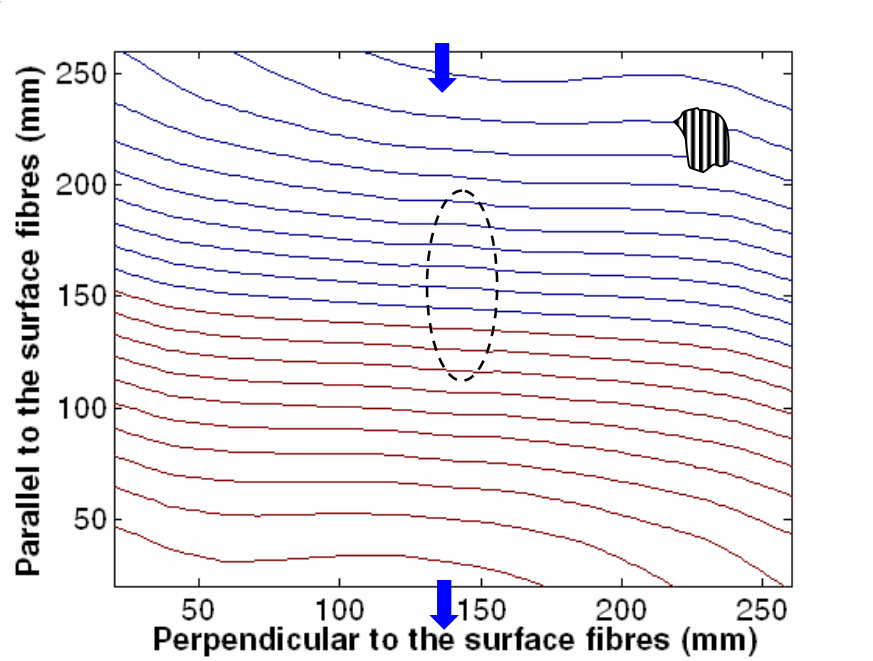

Figure 9. 20: Calculated contours of potential distribution on **top** surface of quasi-isotropic laminate relative to the undamaged state, after creation of single delamination 38 x 80 mm at the centre, between first and second layer; current input/output on **bottom** surface mid point of horizontal edges.

Changing the current input probes to a location midway along the vertical sides of the laminate it was found that even the biggest delamination could not be detected. This is shown in Figure 9. 21, which shows the potential contour and potential change contour for laminates with delamination dimensions of 38 x 80 mm located between the first and second layer from the top, in the centre of the plate. The current is introduced on top surface.

The calculated potential changes were up to 0.2% of the initial value. Changes of that level may interfere with the device measurement error and therefore may not be detectable. Similar observations were also observed for damage in the form of holes (Section 7. 2, Figure 7. 12).

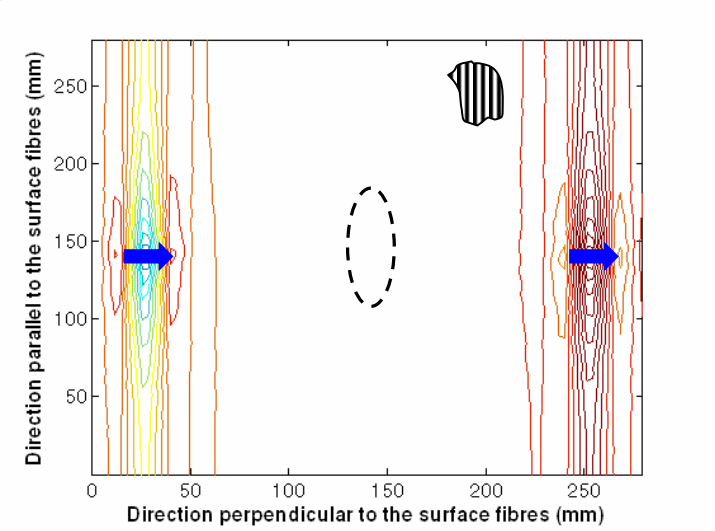

a) potential distribution

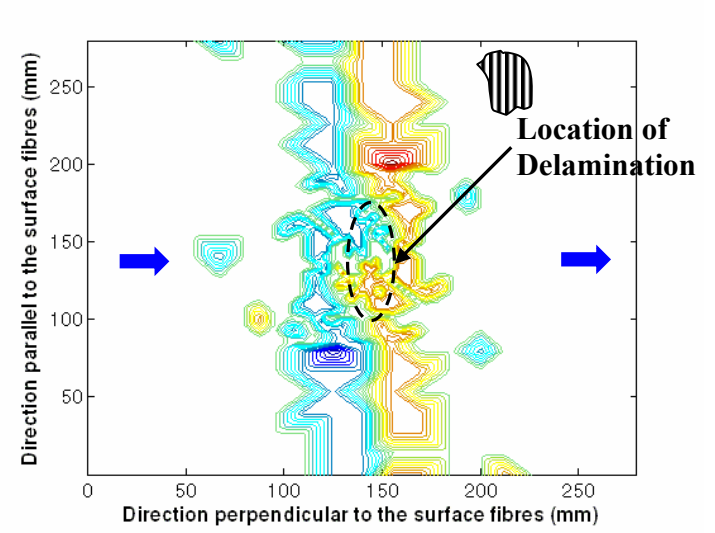

b) potential change distribution

Figure 9. 21: Calculated contours of a) potential distribution and b) potential change distribution on the **top** surface of quasi–isotropic laminate, after delamination, dimension of 38 x 80 mm, is introduced between first and second layer from the **top,** in the centre of the plate; current input on **top** surface, mid point of vertical edge.

9.7.3 Effect of though thickness position of delamination on electrical potential fields

New numerical models were constructed in order to evaluate the effect of delamination position through thickness on potential fields. Various size delaminations, as shown in

Table 9. 6, were initially placed between the second and third layer from the top surface, and then at the interfaces of all layers through thickness. All delaminations were positioned in the centre of the laminate as shown in Figure 9. 22. The current was introduced on the top surface, along the fibre direction on the mid points of horizontal edges.

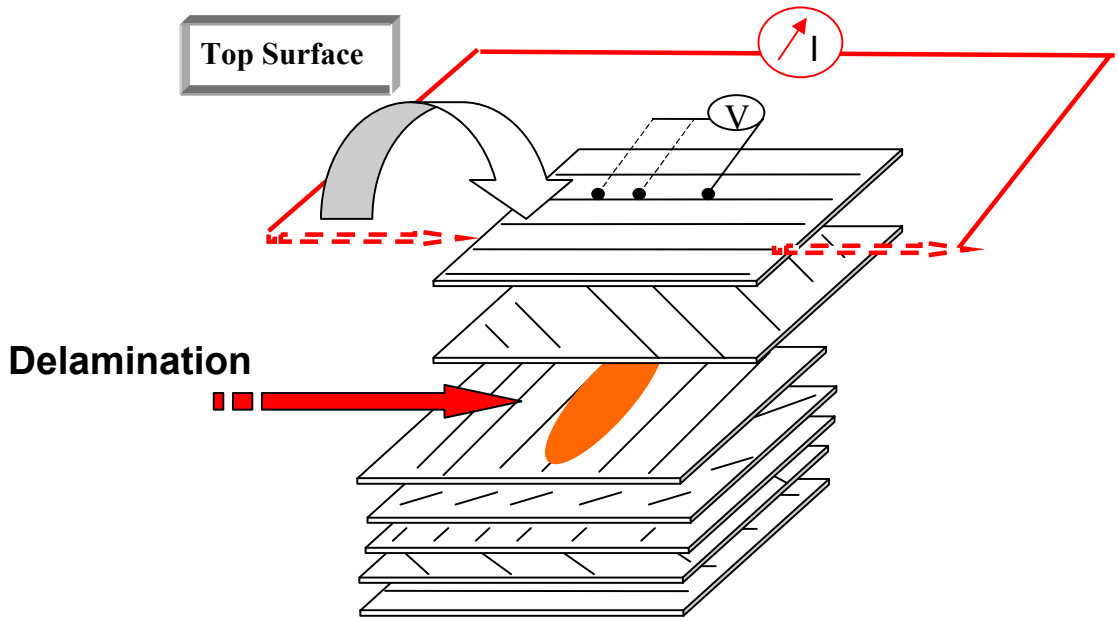

Figure 9. 22: Delamination located between second and third layer in a quasi-isotropic laminate.

Figure 9. 23 simulates potential difference fields for delamination dimension of 38 x 80 mm, located between the second and third layer from the top surface. As it can be seen the delaminated area may still be recognisable; however, the relative potential change is only 0.55% of the undamaged value, in contrast to the value of 32% which was found when the delamination was located between the first and second layer. Potential changes of that range appertain to the error of the measured device and therefore it seems unlikely to be experimentally detectable. Potential differences in areas away from the delaminated area, are tiny changes at the noise level and arise from the contour plotting software.

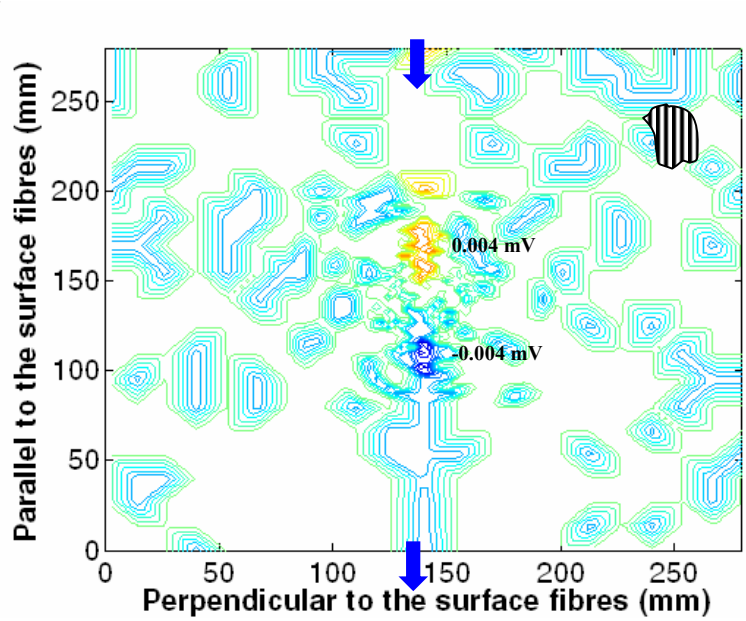

Figure 9. 23: Calculated contours of potential change on top surface of quasi-isotropic laminate relative to the undamaged state, after creation of single delamination 38 x 80 mm between second and third ply, in centre of the plate area; current input/output on **top** surface mid point of horizontal edges

For the same current configuration as above, no potential disturbances were observed for delamination located between third and fourth layers. When delaminations are extended in all layers through the thickness direction, the potential values remain almost the same as when delamination was introduced between the second and third layers. This indicates that only the delaminations close to the top surface, where the potential measurements are taken, are detectable rather than delaminations located in the middle of the structure.

9.7.4 Correlation between numerical and experimental results

Figure 9. 24 shows the influence of maximum damage extent (length) on the size of the region where the relative potential change was greater than 2% for the numerical and experimental results; the latter corresponds to the results obtained for current/potential probes situated on the top surface. The numerical analysis demonstrated that the extent of the region of detectable potential changes increase, approximately, exponentially up to a

damage length of up to 50 mm and then linearly with the size of the damaged region throughout the remaining damage length. The region of detectable potential change as demonstrated by the numerical analysis is from 3.4% to 25% greater than the size of the delamination length measured by the C-scan, as opposed to the experimental results in which the region of detectable potential is roughly double the C-scan measured values.

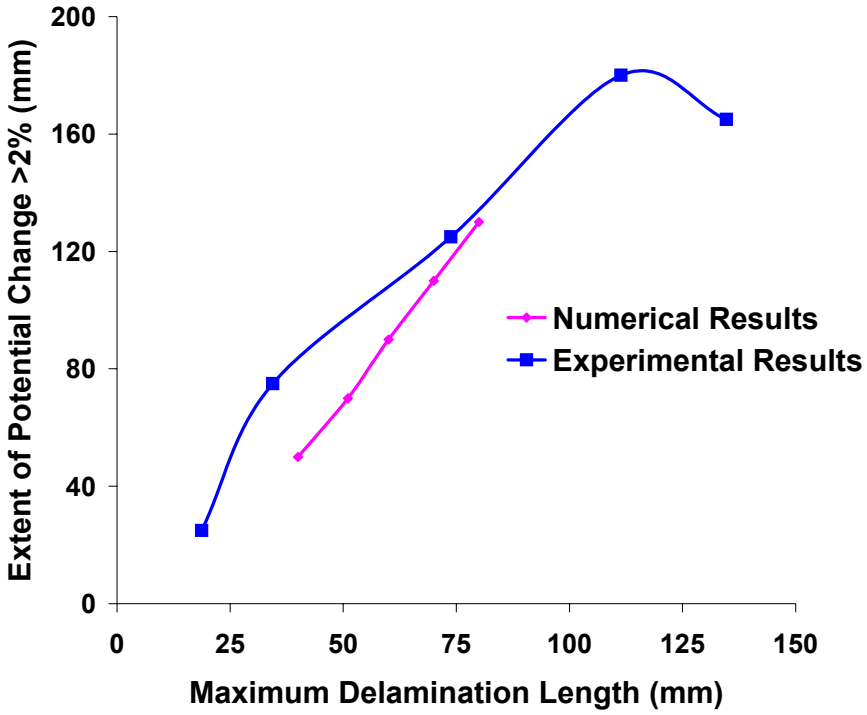

Figure 9. 24: Extent of detectable potential change against maximum damage size as revealed by numerical and experimental results; current electrodes/potential probes on **top** surface, mid points of horizontal edges.

As the damage length increases, the curve of the simulated results approaches the experimental curve and tends to be identical for damage length up to 80 mm. The differences to the experimental results are due mainly to the fact that the numerical results are based on modelling a single delamination, located between two individual layers, while the experimental results include the effect of more than one delamination,

located on various layers and position, and the effect of other damage forms such fibre breakages.

Summarizing the results presented in this chapter it can be said that the developed numerical models successfully predicted potential distributions on unidirectional and multidirectional laminates. In unidirectional samples, positive and negative gauge factors were found. Both were caused by transverse resistance increasing faster than longitudinal resistance on application of strain in conditions of non-uniform current flow. The numerical calculations were in agreement with experimental observations.

The mesh size and the distortion angle of the elements were found to be crucial in terms of conversion between experimental and finite element results for the multidirectional laminates; factors affecting the sensitivity of the models are the location of delaminations and current electrodes. Delaminations located near the measurement surface cause significant potential changes; however, negligible potential differences were found when they are extended through the thickness of the structure. This indicates that the sensitivity of the model in detecting delamination damage located inside the composite structure is very much limited.

The sensitivity of the model is also reduced when the damage is not parallel with the current flow. This is due to the high transverse resistance which will limit the amount of current reaching the damaged areas away from the current flow and as a consequence the predicted potential values will be small, compromising damage detection.

10 DISCUSSION

This Chapter summarises the main observations obtained from the experimental and numerical results. The main points of this research work are discussed guiding the reader through the actual meaning of the results. The issue of representing numerical potential contours in undamaged and damaged plates is also addressed. There were some difficulties in modelling potential distributions, raised from the high anisotropy in electrical conductivity (1:10000), in the directions parallel and perpendicular to the fibres direction. Nevertheless, the finite elements simulations provide strong evidence of the sensitivity of this technique to delaminations located at various interfaces.

This Chapter can broadly be divided into four Sections. The effect of mechanical strain on electrical potential is discussed in Section 10.1. The effect of current introduction on the electrical potential using various conductive adhesives is discussed in detail and how these can affect the response of potential to mechanical strain. Section 10.2 refers to the results from the effect of environmental conditions such as temperature and humidity on the electrical potential. The results from potential distribution in undamaged plates are discussed in Section 10.3. The results from the impact experiments and numerical simulations of delaminations are discussed in Sections 10.4 and 10.5 respectively, together with the effect of the position of the potential measured probes analysis; the correlation between the finite element analysis and experimental results is presented. Finally Section 10.6 compares the potential changes obtained from impact damage, with changes in potential due to mechanical strain, temperature and humidity.

10.1 Effect of Mechanical Strain on Electrical Potential

Conduction processes in unidirectional and multidirectional laminates under mechanical strain were investigated in this research work. A number of people, for instance Thiagarajan, Chung and Cho, have worked on this topic (Section 4.5). In their studies they report positive or negative piezo-resistance with GF values ranging from 2.16 [93] up to 37 [108]. The contradiction among their results, and the lack of a well established and justified model, led to further research study on this topic. This work has shown that regions of poor bonding and hence poor conductivity in current input, produce situations where increasing strain produce decreases in potential difference. These changes are reflected in GF changes in terms of both its size and its sign depending on the direction of current flow relative to the fibre direction and on whether point or area introductions of current are used. Non uniform current introduction, produced variously by local point introduction of current, or use of viscous adhesives producing intermittent contact, resulted in a wide range of apparent gauge factors ranging from 20.6 to -89. There is a significant difference between the behaviour of unidirectional laminates and multidirectional laminates. In the case of unidirectional material, the adhesive used for introducing the current directly affects the sign of the gauge factor, switching it from positive, when silver paint is used, to negative when carbon cement is used. For multidirectional laminates, however, the usage of different adhesives made no difference. Negative values of piezo-resistivity were obtained in the following circumstances.

1. unidirectional laminate; current introduced using carbon cement, flow parallel with the fibres, measurement parallel with fibres.
2. unidirectional laminate; current introduced on sample surface at a point, flow parallel with the fibres, measurement location displaced laterally from the points of current introduction.
3. multidirectional laminate; current introduced at point on sample surface, flow transverse to surface fibres.

It was possible to convert a positive GF to a negative one by deliberately creating an in-homogeneous current introduction using silver paint to make intermittent contact. All other values of gauge factor were positive, but of size varying from 1.7 to 20.6.

10.1.1 Ideal conduction processes in unidirectional samples

The value of GF when current was introduced at the fibre ends using a sputtered contact in a two probe system was measured. Those measurements correspond to configuration E (Section 6.4.1) and they were taken by Dr. C Wei at Cranfield University. Figure 10. 1 shows relative potential change measured at the sample ends plotted against strain for three cycles of strain applied to the sample. The data are almost linear with little hysteresis and the nominal gauge factor is calculated as 1.75. The calculated value of resistivity for this configuration was 0.028 mΩ.m, in close agreement with theoretical resistivity values for 60% volume fraction composites of T300 carbon fibre, which was 0.022 mΩ.m [56]. The value of 1.75 for the gauge factor is towards the lower end of the range of values [159] quoted for CFRP, and it is close to those quoted for similar carbon fibres [23].

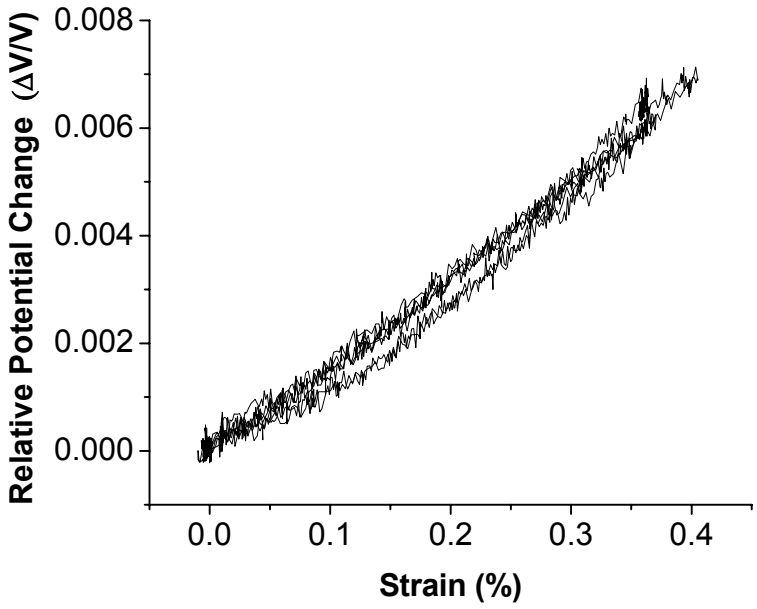

Figure 10. 1: Plot of relative potential change vs applied strain throughout three strain cycles for configuration E.

These low values can be regarded as the true values for piezo-resistance, because they approximate to the values of pure carbon fibres. The sputtered electrodes will join all the fibres together with a low resistance path at each end, and the value of resistivity measured demonstrates negligible contact resistance. There will be uniform current flow with all fibres carrying equal current, the potential being measured across the entire known current. Changes in potential should only be due to the dimensional changes of the fibres themselves, which would increase the electrical resistance of the fibres assuming no changes in resistivity, (as described in Section 3.2.3).

The transverse potential response or configuration D, which was also investigated by Dr. C Wei, is plotted in Figure 10. 2. It shows positive piezo-resistance with a GF of 2.7 while the zero-strain resistivity transverse to the fibres can be calculated as 220 mΩ.m. Analogous behaviour in through thickness piezo-resistance with applied strain for unidirectional samples is also reported elsewhere [108]. Similarly to the longitudinal direction, the sputtered edge electrodes will create a uniform current path and may be regarded as accurate. All other apparent piezo-resistive values have their origin in conduction and measurement processes not represented by this ideal situation.

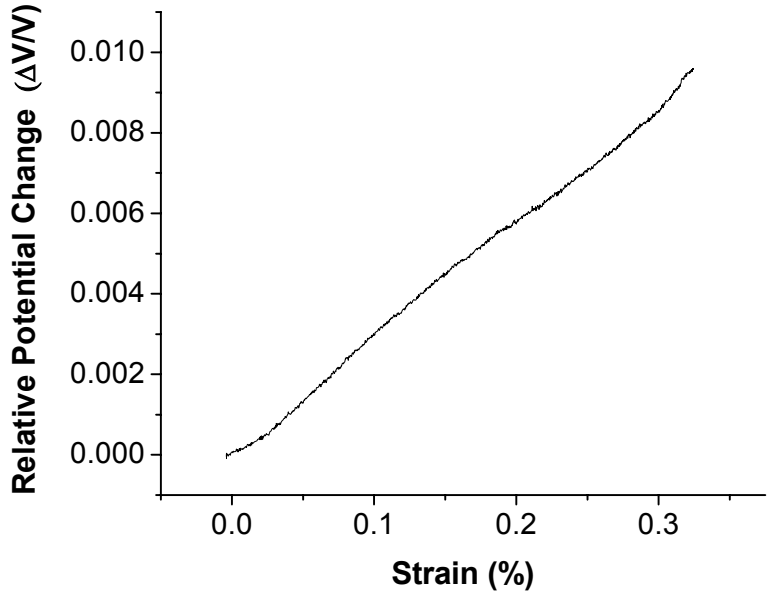

Figure 10. 2: Relative potential change vs strain for single half cycle; configuration D.

10.1.2 Real conduction processes in unidirectional samples

In unidirectional CFRP, current flow is a complicated and 3-D process. Changes in the number of fibres involved in the local conduction route and current flow lateral to the fibre direction significantly affect the conduction processes. A poor conductive medium for introducing current would contribute in an inhomogeneous current distribution within the sample; this would continue throughout the sample length due to the large anisotropy of resistivity, resulting in the reduction of current carrying fibres. Thus under non uniform current conditions, surface electrode measurements will reflect local conditions at the surface only, and may not be representative of internal currents and potentials. A simple calculation using the experimentally values for longitudinal and transverse resistivity (Section 10.1.1) demonstrates that for uniform current flow parallel to the fibres, the potential difference between the fibre ends 280 mm apart is achieved in only 0.1 mm for current flow transverse to the fibres. This suggests that if the current is introduced at fibre ends of the sample the conductive medium must assure a uniform distribution on a scatter range significantly less than 0.1 mm. Subsequently, and assuming that the through thickness electrical resistivity is of the order of the transverse, the potential measurements on the sample's surface will reflect processes occurring at 0.1 mm depth.

The present work has shown that regions of poor bonding produce situations where increasing strain produce decreases in potential difference. Carbon cement appears to be an ineffective current introduction medium. The poor contacts made using this medium may be seen visually in micro-sections taken of the contact area for silver paint and for carbon cement electrodes. These are shown in Figure 8. 11, where large gaps in the interface region can be seen for the carbon cement example. This will lead to the inferred inhomogeneous current distributions. Potential changes out of phase with applied strain are also found where the current input is out of line with the measurement probes; current at the measurement probe site must cross from fibre to fibre in this situation. Changes in potential difference between two adjacent electrodes during load cycling cannot be

interpreted only in terms of potential or resistance changes. They may be caused by local current changes and resistivity changes as well.

In a situation such as the experimental one where a constant current is applied to the sample ends, the total current passing through the sample must remain constant. However, if the distribution of current at the points of introduction and exit is inhomogeneous, then mechanical strain applied parallel to the fibres will change the local currents, as fibres enter or leave the conduction process. This will change the potentials measured by surface electrodes in either a positive or negative direction, depending on whether the number of fibres involved in the local conduction process is increasing or decreasing.

If current distribution at the point of entry and exit is homogenous then, as there will be equal potentials in adjacent fibres, for current flow along the fibres there will be no or negligible current flow across the fibre-to-fibre contacts, and the material should behave as a homogeneous conductor.

This situation is created only for current introduction at the fibre ends (at sample edges), and positive piezo-resistance is observed. This arises because straining fibres along their length will reduce their diameter via Poisson contraction, as well as shifting the fibre-to-fibre contact positions slightly, reducing the number of contacts and decreasing the contact area for transverse conduction; this effect is illustrated in Figure 10. 3.

The transverse resistivity will be increased, causing a positive transverse piezo-resistive effect in response to longitudinal strain (configuration C and D). The changes in contact distribution will change current paths and local current values as strain is applied. Those changes in current will be additionally intensive because of variations in the through thickness resistivity, resulting in additional current paths within the structure which will be reflected on the samples surface.

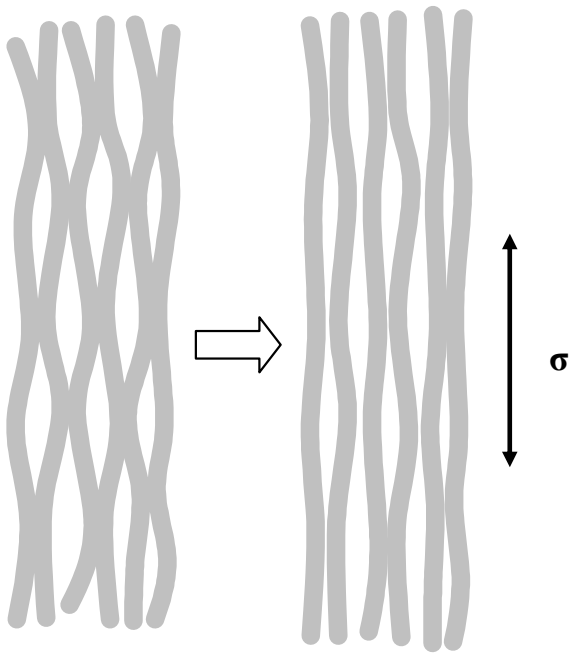

Figure 10. 3: Schematic diagram showing fibre crimp and the effect of longitudinal strain on the distribution of fibre contacts.

Point surface introduction of current will always result in inhomogeneous current distributions as the experimental and finite element configurations demonstrated. Positive gauge factors measured for potential measurements along the current flow line and negative for potential measurements at points displaced laterally from the line of current flow (configuration B). This is the result of a balance of the current portion flowing parallel and perpendicular to the fibres. By applying longitudinal mechanical strain, the electrical resistance parallel to the fibres will increase, and for constant imposed current the potential difference increases. The current flow, however, will not be constant in the direction transverse to the fibres. Although the resistance between the points displaced laterally from the current flow line will increase, the different values of gauge factors measured for the direction parallel (1.75) and transverse (2.7) to the fibres will impose the constant current to be reduced at the points placed laterally from the current line leading to negative piezo-resistance. The additional current will be transferred to the

points positioned along the current flow line, contributing to positive piezo-resistance. Due to extremely high electrical anisotropy of electrical resistivity, 1:10000 for the directions parallel and perpendicular to the fibres, abrupt changes of electrical potential are expected, at very small distance from the current flow line; this was highlighted by the numerical results, Figure 9. 10.

The decrease in potential values with applied strain for configuration A and current introduced via carbon cement was measured at 30%. This reduction is significantly greater than the one in configuration B for channel 2. Even if the longitudinal gauge factor was zero, with a transverse gauge factor of 2.7 and a strain of 0.3%, the maximum resulting decrease in transverse current would be less than 1%. Decreases of transverse current of 20-30% would require transverse gauge factors in the region of 20-30, and these have not been observed in surface measurements.

One difference between configuration A with intermittent edge contacts produced by carbon cement and configuration B is that conduction processes in the latter are confined to the surface layers. In configuration A, the current is introduced across the entire thickness, and conduction processes in the thickness as well as the width have to be considered. It may be that transverse current flow in the through thickness direction may have gauge factors of the required size, caused by the different volume fractions of fibres in the inter-ply region.

10.1.3 Multidirectional samples

The presence of layers in the directions of 45° and 90° forms a totally different and more complicated than in the UD samples, current network. As illustrated in Figure 8. 9, the potential changes are in phase with the applied mechanical strain despite the use in configuration B of a current path with current flow transverse to the surface fibres. The schematic electrical circuit relevant to cross ply or quasi-isotropic laminates under configuration B is shown in Figure 10. 4. The current introduction points are named as “a” and “c”. In this situation, the 90° or 45° plies below the surface 0° plies form a low resistance bridge, R_3^L in parallel with the transverse resistance, R_1^T.

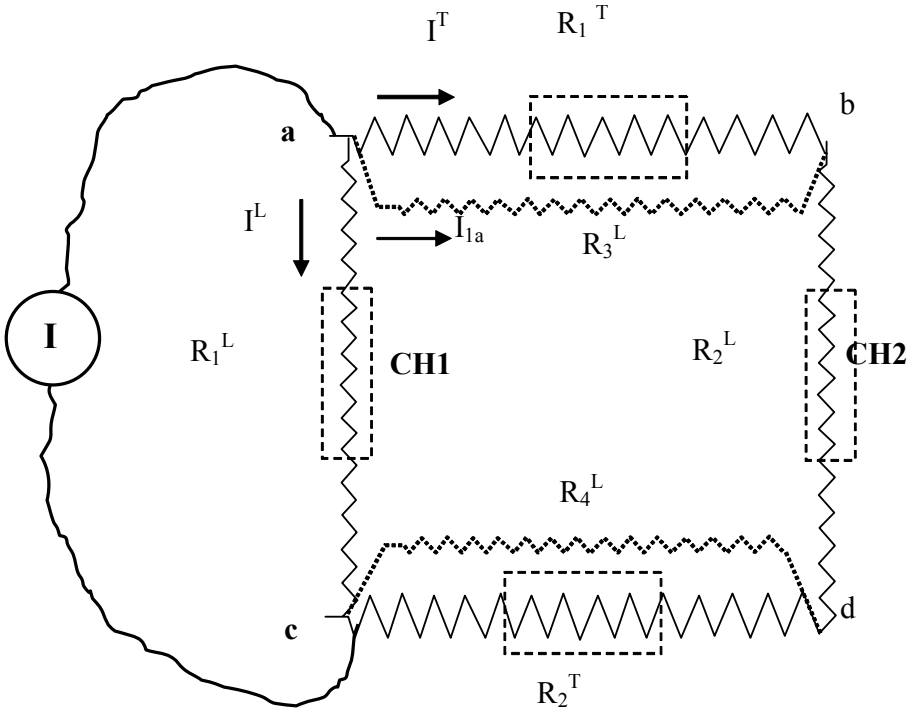

Figure 10. 4: Schematic current network showing the effect of off-axis plies on the conduction process in multidirectional laminate.

The off-axis layers effectively short circuits current flow perpendicular to the fibres and allows a more equal potential field. The current can flow easier in the transverse direction reaching the points placed laterally to the line of current flow, (CH 2). As a consequence the potential distribution on the surface of multidirectional laminates is uniform with an almost equi-potential field, even when point surface introduction of current.

Potential changes were also in phase with the applied mechanical strain for continuous current introduction at fibre ends, despite the use of carbon cement as adhesive, as shown in Figure 8. 8 (a). The effects of inhomogeneous current introduction caused by carbon cement are nullified by the action of the off-axis plies which take the majority of the transverse current. Thus, uniform current flow in all directions can take place via low resistance conduction along fibres, and conduction from fibre to fibre. The cause of the negative piezo-resistivity need not contribute significantly to the potential changes.

The exception to this behaviour is configuration C, current flow transverse to the surface fibres (Figure 8.10 (a)). This sample exhibited negative piezo-resistivity, in contrast to the unidirectional behaviour for this configuration. At zero strain, the off-axis plies will be contributing to the current flow and they significantly reduce the potential values from those found in unidirectional laminate. When strain is applied, the Poisson effect will reduce fibre diameters for axial plies, and will subject off-axis plies to compressive strain parallel to their length. This could act in the opposite direction to the mechanism suggested in Figure 10. 3, increasing inter-ply contact, improving the current flow in the internal layers and reducing the measured potentials on the exterior layer, leading to negative piezo-resistivity.

10.2 Effect of Environmental Conditions on Electrical Potential

10.2.1 Effect of temperature

The temperature dependence of the longitudinal resistivity was investigated. The results presented in this research work are similar to those obtained by other researchers, who reported a decrease in longitudinal resistivity with increasing temperature, for different graphite polymer composites [119], [160], [15], [17]. The behaviour depicted in Figure 8. 13, and Figure 8. 15, is similar to all types of carbon fibres with T_{HT}< 2500°C (Figure 3. 6), which act as semiconductors and they have a negative temperature coefficient of electrical resistivity. The results presented in this research study showed an 8% decrease of longitudinal electrical resistivity as the temperature varied within a range of 140°C. The decrease in electrical resistance with increasing temperature is predominantly due to an increase in the concentration of electrons and holes. As the temperature increases more thermal energy is available to excite electrons from the valence to the conduction bands.

Thiagarajan [33], however, obtained a positive temperature coefficient for the same type of fibre and resin system used in this investigation, concluding that the behaviour of the CFRPs is similar to metals. He also reports that the longitudinal properties of UD samples are fibre dominated; if this is the case though, a negative temperature coefficient of

electrical resistivity should be expected, because the fibre type used in both investigations is Torayca T300, a standard modulus high strain PAN fibre with T_{HT}<2500˚C. As explained previously, this type of carbon fibres experiences a decrease in resistivity with increasing temperature (Section 3.2.2). Only graphite and more perfect pyrolytic fibres (with $T_{HT}\geq$ 3000°C) have a positive temperature coefficient. This arises from the fact that due to their almost perfect crystal structure they behave as metals in which the carrier mobility decreases with rising temperature.

The introduction of off-axis layers, such as in multidirectional laminates, does not influence the response of electrical potential to temperature. This is because the intrinsic longitudinal thermal behaviour of composites is mainly dependent on the physical properties of the carbon fibres. The measured reduction of electrical potential with increasing temperature was 8% for cross ply and 5% for quasi-isotropic samples.

The TCR of cross ply and quasi-isotropic samples was found to be greater than the TCR of unidirectional specimens. It is believed that this is due to the conduction processes within the composite. In unidirectional samples, as discussed in Section 10.1, an inhomogeneous introduction of current at the fibre ends, due to poor conductive medium, would persist throughout the specimen as a result of the large anisotropy of electrical resistivity. This would contribute in the reduction of the number of the fibres which participate in the conduction processes. In multidirectional samples, however, the off-axis plies will distribute the current in the directions parallel and perpendicular to the fibres, increasing the number of the current carrying fibres leading to a faster decrease of electrical resistivity with increasing temperature than in unidirectional samples.

10.2.2 Effect of water

The effect of water absorption on electrical potential was investigated in unidirectional samples. As presented in Section 8.4, all samples were immersed into distilled water for a period of six months. The results revealed a decrease in longitudinal resistance varying from 0.9%-1.2% and an increase for transverse resistance within the range of 8.5-10%. The experimental procedure followed by the author, did not comply directly with any

standard rule for water saturation in CFRP composites. Further experiments, however, conducted by Dr Wei at Cranfield University in conditions according to ISO 62:1999 standards, revealed 1% decrease in longitudinal resistance. This close agreement with the results obtained by the author confirmed that the six months immersion of the samples into water, led to 100% surface weight saturation of the specimens and therefore the obtained results were credible.

Decrease in longitudinal resistivity with water absorption is reported elsewhere in the literature [36], [89]. The negligible changes in longitudinal electrical resistance are expected as the resistance of the water which is absorbed either by the matrix or the interface regions, does not affect the overall resistance significantly. This is because the electrical resistivity of the water is 6.1×10^{5} Ω.cm [161], approximately 3×10^{4} times greater of CFRP transverse resistance, and 1.9×10^{8} times greater of CFRP longitudinal resistance.

In contrast to the results presented for the longitudinal resistance, the transverse resistance was increased (up to 10%). This change can be attributed to the conduction processes and flux of electrons in a composite structure in relation to the water absorption by the matrix. In real composites, unlike ideal composites, the carbon fibres form a rather complex network of fibre-to-fibre contacts. Current can flow through the paths formed by the fibres and the matrix preserves the role of holding the fibres in contact, maintaining the contact pressure between two or more contacting fibres. Belani [89] suggests that an increase in the electrical resistance on moisture absorption arises from a decrease in fibre-to-fibre contact pressure. He supports this theory based on experimental observations made by Panizza [162], who reports an increase in the length of unidirectional CFRP composites with absorption of water when exposed to different environments, just as if the specimens are subjected to mechanical strain perpendicular to the fibre direction. This strain affects the contact pressure between two or more contacting fibres, resulting in a change in the effective length of the conducting path and thus giving values of electrical resistance in the transverse direction, which increases with increasing levels of moisture.

10.3 Potential Fields in Undamaged Plates

The potential distribution was measured on the top surface of cross ply and quasi-isotropic undamaged laminates. To the knowledge of the author, there has not been a methodical and analytical investigation of the complex patterns of potential distributions in multidirectional composite laminates, despite that a numerous of researchers attempted to correlate damage development [92], [94], [103], [111], and location [114], [118], with changes in electrical potential or resistivity. This research study revealed that the position of the current input/output electrodes, significantly affects the potential contours. It was possible to turn a highly anisotropic electrical field, to a pseudo-isotropic field by only changing the location of the current electrodes. As it will be discussed in Section 10.4, this has a significant effect in determining the location of damage.

Two different configurations were studied; the first had the current introduction located on the top surface, where the potential measurement probes were also placed. The second had the current introduction positioned on the bottom surface, while the potential probes were still placed on the top.

a) Current probes on the top surface, potential measurements on the top surface

Regardless whether the current flows parallel or transverse to the top surface fibres (0° direction) this configuration is characterized by peaky potential values near the current electrodes, due to the increased current density, followed by flatter distribution towards the centre of the laminated as shown in Figure 7. 1 and Figure 7. 3 (a). These maxima, however, are significantly greater when the current is introduced parallel to the fibres direction, than when it is introduced transverse to the fibres. The justification lies to the current flow processes on the surface of lamina. As shown in Figure 10. 5, and expressing the ratio of resistivity as ratio of electrical resistance following equation (2.2), when the current **(I_0)** is introduced along the fibre direction (0°) on the top surface of the plate, (Points A & B), the high electrical anisotropy between the longitudinal resistance R_0 and transverse resistance R_{90} (1:10000) will force the majority of the current to flow along their length rather than in the transverse direction **(I_{90})**. The changes in current

distribution on the lamina's surface will be mirrored to the measured potential values as shown in Figure 7. 1 and Figure 7.3 (a).

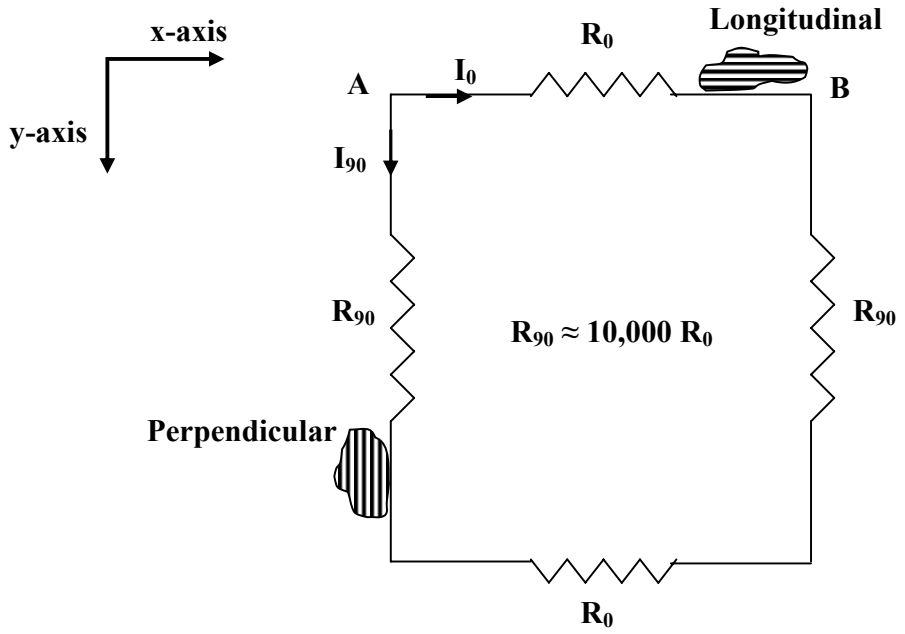

Figure 10. 5: Electric analogue of current distribution in the direction parallel and perpendicular to the 0° direction fibres.

Independently of the position of the current electrodes and current flow in relation to the direction of the fibres, it was found that in both cross ply and quasi-isotropic laminates the potential contours were approximately perpendicular to the line joining the current input electrodes. The stacking sequence of the composite structure, does not affect significantly the potential distribution patterns.

b) Current probes on the bottom surface, potential measurements on the top surface

More diffuse potential distributions are obtained for this configuration than in the previous case, for current flow along the fibres (0°). The same concept for current flow processes developed in case (a) can be applied here, assuming that the values of transverse and through thickness resistance are equal. As shown in Figure 10. 5, for current introduction along the fibre direction, the significantly higher values of the

through thickness resistance than the longitudinal, will radically reduce the amount of current reaching the top surface, where the potential measurements are taken. As a consequence the potential values will be very much decreased (more than 5,000 times) and the high potential peaks near the current electrodes will be eliminated.

Similarly to case (a), the potential contours are perpendicular to the line joining the current input/output electrodes. There is no pronounced distortion towards the direction of the fibres for the cross ply laminates. However, this is not the case for the quasi-isotropic plates, where a small rotation towards the 45º of the ply underneath the surface lamina.

Generally for case (a) it can be said that both cross ply and quasi-isotropic laminates seem to produce a highly anisotropic electrical field following the electrical anisotropy in electrical resistivity, with significant elevation in potential values around the current electrodes. In case (b), however, the high resistance perpendicular to the fibres in a single lamina is effectively eliminated by adjacent misorientated plies which transfer the electrical current through the thickness of the lamina nullifying the anisotropy of individual plies. Hence a much more isotropic distribution of laminate resistance is achieved.

For current/potential probes location such as in case (a), the calculated and experimental potential distributions for undamaged laminates (Figure 9. 17 (a) and Figure 7. 6 (a) respectively), showed good agreement in the middle of the plate. There was a difference close to the plate edges, which may have simply been a consequence of inadequate numbers of measurement electrodes in the region close to the edges where potential fields will be changing most rapidly. For probes configuration corresponding to case (b), the numerical and experimental potential contours were in agreement throughout the plate (Figure 9. 14 and Figure 7. 6 (b) respectively). Both experimental and calculated fields showed a rotation of the equi-potential contours towards the underlying 45° ply in QI laminates. This supports the view that the finite element simulation gave a good representation of potential distributions in these materials.

10.4 Potential Fields in Damaged Plates

A small number of researchers have attempted to correlate potential or resistivity changes to damage in CFRP composites. The majority of these studies was concerned with fibre breaks or delaminations due fatigue [93], [96], [103], [104]. Other researchers attempted to develop models to predict the location of delamination based on experimental measured potential values. None of them, however, used potential disturbances to detect and measure the extent of damage arising from impacts. The present study established a qualitative and quantitative model, able to demonstrate the effect of impact damage on electrical potential in relation to the position of the current electrodes, and potential measurement probes. The experimental observations were also supported by the development of numerical models for predicting the effect on electrical potential of various size delaminations, in relation to their position within the composite structure.

Current input location does significantly influence potential contours; this influence extends to the equi-potential change fields produced by holes, impact and delamination damage. The extent of the potential change fields and their size appear to be both dependent on the current input location, and whether the electrodes are on the same side as the measured field or on the opposite surface. In some configurations damage was detectable with one current location and almost undetectable with another. This suggests that current switching to provide alternative current locations will be important in practical damage detection systems based on this principle. The main current/potential probe configurations for damage detection are discussed in this section.

a) Current probes on the top surface, potential measurements on the top surface

This configuration applied for detecting damage caused by the creation of holes, in cross ply plates, and impact in quasi-isotropic laminates. All plates were impacted on the top surface and the current flow was parallel to the fibres aligned in 0˚ direction (external ply). The insertion of holes significantly affects the potential change distributions, as shown in Figure 7. 7 (b). The region with the greater change is the nearby to the

perimeter of each hole. Two holes diameter of 15 mm and 25 mm were drilled. The largest potential change measured was 122% of the undamaged value and it was found for the greater size hole. Potential changes greater than 10% were found approximately at distance same as the diameter of each hole extended along the 0˚ direction fibres. The sensitivity of damage detection was significantly reduced perpendicular to the fibres. Potential changes greater than 2% were measured at distances of 25 mm from the centre of the hole.

A quantitative study of the sensitivity of the electrical potential technique to impact damage has shown that the electrical potential responded well not only to the significant damage caused by a 12 J impact, but also to small damage, dimensions of 11 x 19 mm, caused by a 2 J impact. Figure 10. 6 shows the potential changes for all impacts with respect to potential values in the undamaged plate, for a section through the impact point, parallel to the 0° fibre direction.

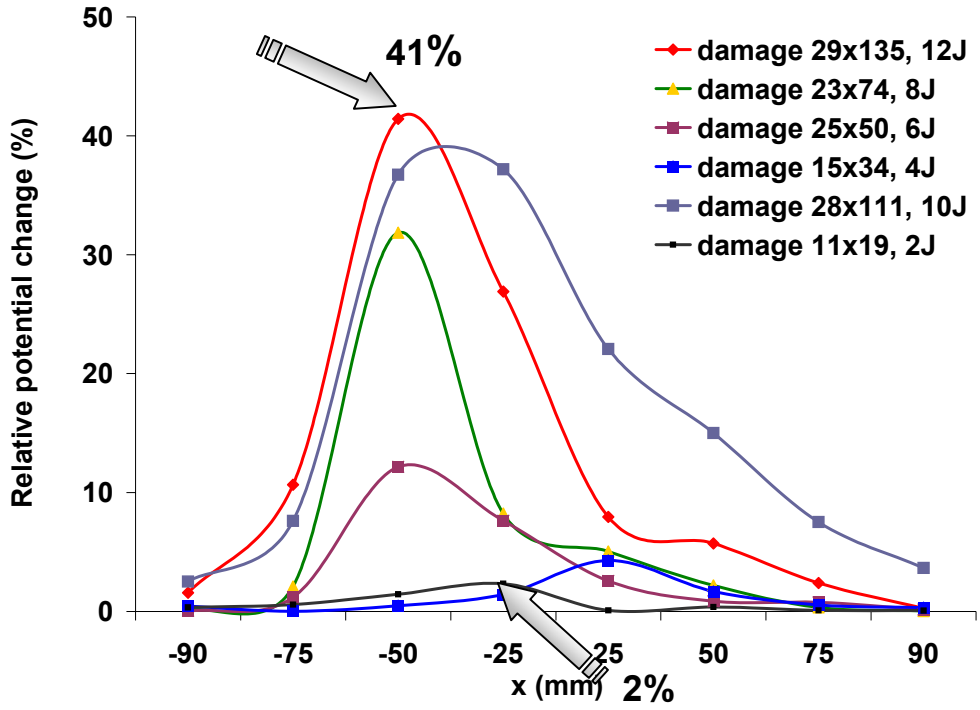

Figure 10. 6: Relative potential change along a section through the damage centre, parallel to the fibre direction, for quasi-isotropic plates; Current input/output on the **top** surface, parallel to this section, potential measurements on the **top** surface.

The greatest change in potential was up to 41% of the original value; this was recorded 50 mm away from the impact site, parallel to the 0° fibre direction. At distances of 80 mm from the damage centre the changes reduced to less than 5% of the original value while after 4 J and 2 J impacts there were only small changes, 4% and 2% respectively, around the damage zone.

Despite the long length parallel to the fibre direction, detectable changes in potential achieved in the transverse direction only 43 mm away from the damage site detectable changes in potential are achievable (Figure 7. 24 (a)).

The experimental data shown in Figure 7. 16 , Figure 7. 25 and Figure 10. 6 reveal that in both cross ply and quasi-isotropic laminates, the peak changes in potential occur at distance about 25-50 mm to one side of the centre of the impact event. These increase slowly at first with increased damage extent, but after 50 mm damage length the rate of increase becomes much greater (Figure 7. 25). It may be that this change is associated with a change in delamination morphology, such as an increase in the number of delaminations, rather than an increase in the extent of a single delamination.

It is interesting to note that the size and spatial extent of the potential disturbances reflect the extent of the damage as revealed by the C-scan (Figure 7. 24 (a)). Parallel with the surface fibres (0˚) the potential changes extend the greatest distance, as does the delamination damage while perpendicular to the surface fibres, the damage width is only 10-43 mm and this is the approximate extent of the potential disturbances greater than 10%. This incongruity can be attributed firstly to the higher grid mesh of the C-scan and secondly to the graphical representation of the potential values which is based on curve fitting, as explained in Section 7. 4.

From the point of view of detectability damage, one of the most important measurements is the distance from the damage that detectable changes in potential can be measured. This research work demonstrated that this distance is approximately double the maximum extent of delamination for current flow along the fibres (Figure 7. 25). That distance sets

an upper limit to the spacing between potential measurement probes in a real measurement system. There may be alternative configurations of current and potential probes position, which increase even further the spacing between potential probes. Increased sensitivity of the system is one way in which this aspect could be improved.

b) Current probes on the top surface, potential probes on the bottom surface

This configuration was used for detecting damage caused by the creation of holes and impact in cross ply plates. Damage in the form of hole appears to have a major influence on the potential field, as shown in Figure 7. 11. The region with the greatest change is adjacent to the perimeter of each hole. The potential change at the site adjacent to the 25 mm hole was approximately twice as much as that of the 6 mm hole. The maximum change percentage for the 15 mm hole is about 101% and 281% for the 45 mm hole. The distance from the hole over which the potential is significantly changed is roughly the same as the hole diameter on each side. Changes at a greater distance than this are less than 10% of the original value while there were some small changes extending over all of the remaining area of the plate. This testing demonstrates that detectable potential changes (greater than 2%) were found at distances about three times of the hole size.

Impact experiments in cross ply plates were also showing potential changes where damage occurred. The potential changes were related to the damage size as revealed by C-scan measurements. Small energy impacts, with literally no delamination damage produced very small potential changes. These changes were within the experimental error. Larger energy impacts, however, produced potential changes up to 60% of the undamaged value for damage extending 89 mm in the direction parallel to the fibres and 43 mm in the transverse direction. Potential changes greater than 3% were found at distances up to 50% of the damage size.

c) Current probes on the bottom surface, potential measurements on the bottom surface

This configuration investigated the effect of impact damage on potential distributions. The same quasi-isotropic plates as in case (a) were used. The impact point was on the top

surface, and the current flow parallel to the fibres aligned in 0˚ direction on the bottom surface. The outline of the potential changes were not much different than this in case (a), however, the actual size of the change was significantly different.

As shown in Figure 10. 7 the maximum potential change was 238% (for the 12 J impact) and was located 50 mm away from the centre of the plate, parallel to the 0° fibre direction. At distances of 90 mm from the damage centre the changes reduced to less than 9% of the original value. After 4 J and 2 J impacts, there were still changes 16% and 5% respectively, around the damage zone (50 mm away from impact centre). Similar to that in case (a), in the transverse direction only at 45 mm a distance from the impact site, potential changes were achievable (Figure 7. 24 (b)). The experimental results shown in Figure 10. 7 and Figure 7. 26 demonstrate that the maxima in potential changes occurs about 20-50 mm to one side of the centre of the impact event. These increase approximately exponentially with the damage size.

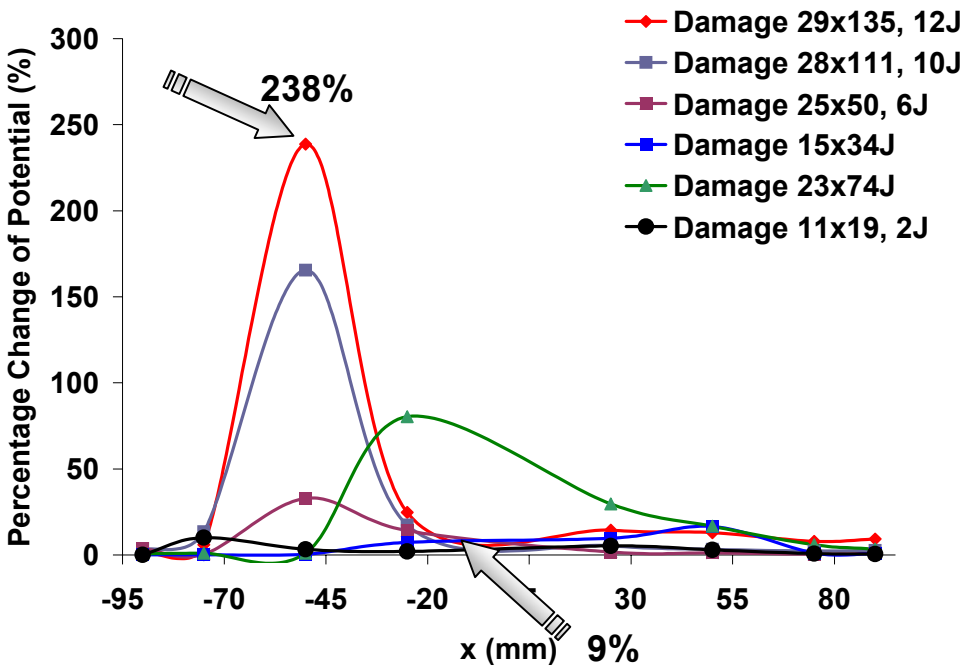

Figure 10. 7: Relative potential change along a section through the damage centre, parallel to the fibre direction, for quasi-isotropic plates, for configuration B; Current input/output on the **bottom** surface, parallel to this section, potential measurements on the **bottom** surface.

10.5 Numerical Analysis of Potential Fields in Damaged Quasi-Isotropic Laminates

Modelling of the effects of delamination damage will be a more difficult task than modelling the potentials in undamaged laminates. This is because real impact damage areas consist of networks of linked multi layer delaminations with associated fibre breaks [163]. These will be difficult to represent, and they are significantly different in their effect on potential distributions than the single delaminations modelled so far in this work. In addition, even for single delaminations, the discontinuities at the delamination boundaries will be a more difficult test of the model than the uniform fields of the undamaged laminates.

In this study numerical simulations were developed for current electrodes located on the top surface and potential measurements also on top surface. Refined meshes have been used to represent delaminations, and the optimum mesh sizes have been developed to get accurate representation of the potential fields.

The contours of equi-potential change surrounding impact damage are shown in Figure 7. 24 (a), (experimental), and Figure 9. 18, (finite element), are superficially similar although they differ in detail. In both simulated and experimental distributions, the potential changes are concentrated in a region elongated along the surface fibre direction (0°). For the experimental configuration, this region appears to extend perpendicular to the fibres at distances greater than the actual measured damage size as discussed in Section 7. 4. This is not the case for the numerical simulations, where the potential changes are extended to the borders of delaminations.

The numerical simulations of delaminations showed that the potential changes were of the same magnitude as in case (a), where current electrodes and potential probes are located on top surface.

As shown in Figure 10. 8 and Figure 9. 18 (a), there is a characteristic two lobed appearance to the region in which there is a maximum and minimum point of potential change.

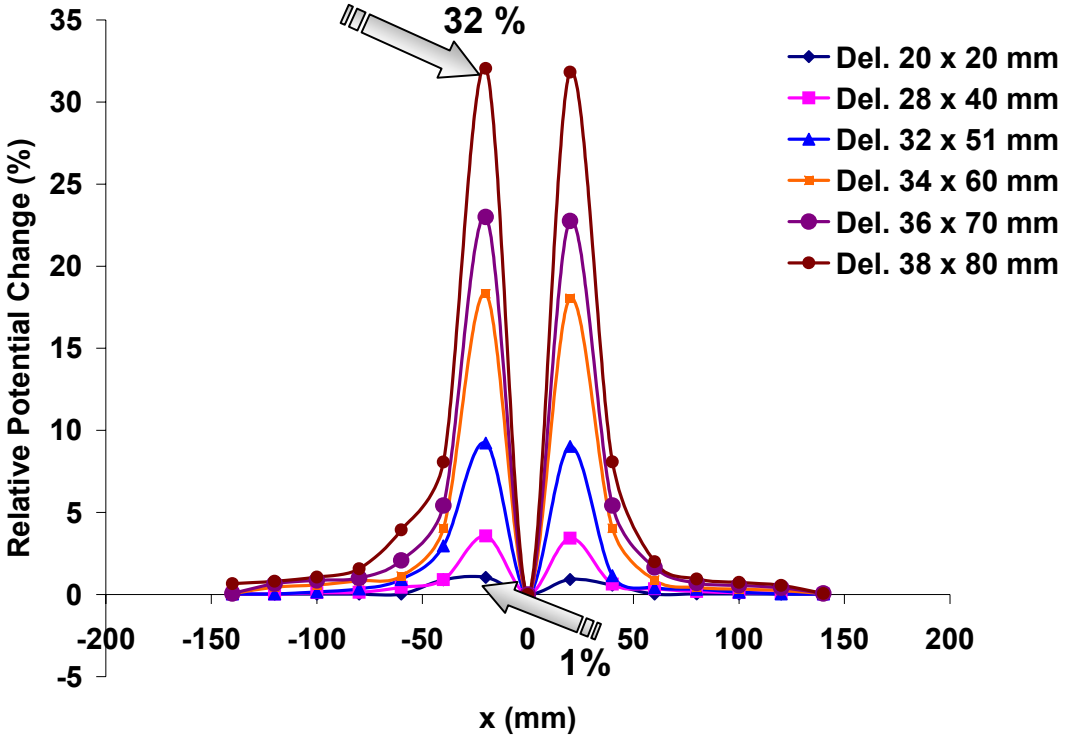

Figure 10. 8: Numerical simulation of relative potential change on **top** surface due to different delamination sizes, along a section through the damage centre, parallel to the surface fibre, for quasi-isotropic plates; Current input/output on the **top** surface, parallel to this section**.**

This symmetry is not apparent in the experimental distributions (Figure 10. 6). The explanation for this is threefold. Firstly, in the experimental configurations, the impact damage may not be distributed symmetrically around the impact point. Secondly in some plates, the impact point was slightly shifted from the centre of the plate; the latter was the case for the 12 J, 4 J and 2 J impacts where the impact point was not in the centre of the plate but approximately 10 mm displaced from the middle of the plate, parallel to the surface fibres. This would affect the potential field on the top surface in relation to the impact point. Thirdly, the selection of the reference point in the numerical simulations was in the same line crossing the centre of the delamination, perpendicular to the fibres.

In the experimental configurations, however, the reference point was not always in the same line with the impact site.

The numerical simulation demonstrated the maximum potential change was 32%, for the greatest delamination, dimension of 38 x 80 mm, and the maximum distance for detectable potential changes greater than 4% was 75 mm away from the delamination centre. This particular configuration, with the current/potential probes positioned on the top surface, takes more consideration of the damage closer to the surface of the plate which is mainly related to delaminations as shown in Figure 7. 31 and Figure 7. 32.

A comparison between numerical and experimental potential changes for similar damage size reveals some sizeable differences as shown in Figure 10. 9. The results obtained from case (a) for 8 J impact and damage size 74 x 23 mm (74 mm along the 0˚ fibre direction and 23 mm in the transverse). The maximum potential change was 31% and the potential changes were extended 80 mm away from the impact centre.

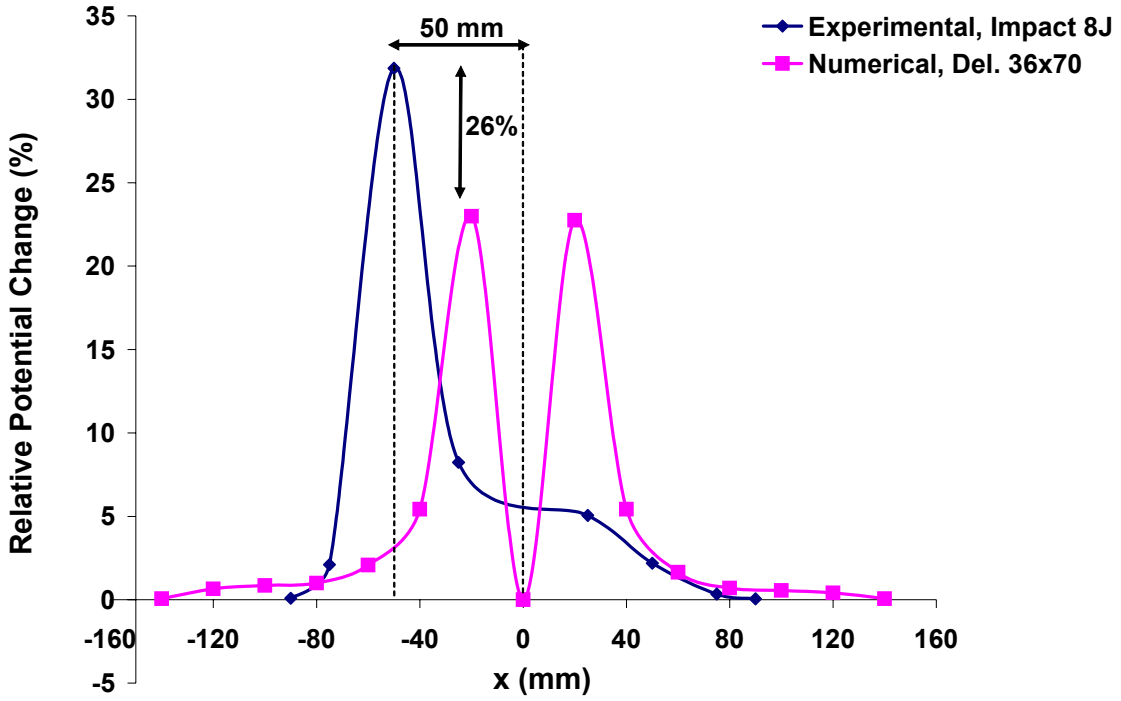

Figure 10. 9: Correlation between numerical and experimental results for same damage size; current electrodes **top** surface, potential measurements **top** surface.

The closest numerically simulated damage size was a delamination 70 x 36 mm located between the first and second interface from the top surface. This simulation demonstrated that the maximum potential change was 23% and potential changes greater than 4% were extended 75 mm away from the delamination centre.

The 26% discrepancy between numerical and experimental results was expected. The metallographic analysis of the 8 J impacted plate showed that the greater extent of delamination between the first and second interface was in the direction transverse to the 0˚ direction fibres, with a measured length of 8.3 mm, while along the fibre direction the delamination was extended only 1 mm.

The results obtained from the numerical calculations in contrast to the experimental, were referring for elliptical shape delamination with the greater axis extending parallel to the 0˚ fibres. This difference would have an effect on the obtained potential values for this particular probes configuration, where both current electrodes and potential probes were positioned on the top surface, very close to the first delaminated interface.

As shown in case (c), Section 10.5, with the current/potential probes located on the bottom surface, the potential changes were not of the same magnitude as for the numerical simulations. This is due to the fact that in this configuration the fibre breakages, which are more severe on the bottom side of the plate, are taken into account as the metallographic analysis showed (Figure 7. 30), rather than the individual delaminations within the structure or closer to the top surface. The finite element analysis gives a much clearer view of the results obtained experimentally for probes located in the top surface, indicating that if the potential measured probes are located on the top surface, delamination detection close to the boundary surface is achievable.

However, when the probes are positioned on the bottom surface, pure delamination damage is not detectable, since the potential changes will be significantly affected by the fibre breakages on the bottom layers.

The conducted experiments were inadequate to produce a single delamination in the middle of the plate without fibre breakages (Figure 7. 31) and as a consequence, no results were obtained for this type of damage. However, numerical simulations revealed that a single delamination located in the middle of the plate, cannot be detected regardless of its size. The threshold distance through the thickness, in which internal damage in the form of delamination can be detected is between the second and third layer and only for delaminations with size greater than 36 x 70 mm while the maximum measured potential changes varied just below 1% around the delaminated area.

These observations were confirmed by the metallographic analysis. Figure 10. 10 shows the influence of maximum damage extent on the maximum change in potential, for the three layers closer to the top surface, as measured by transverse sectioning.

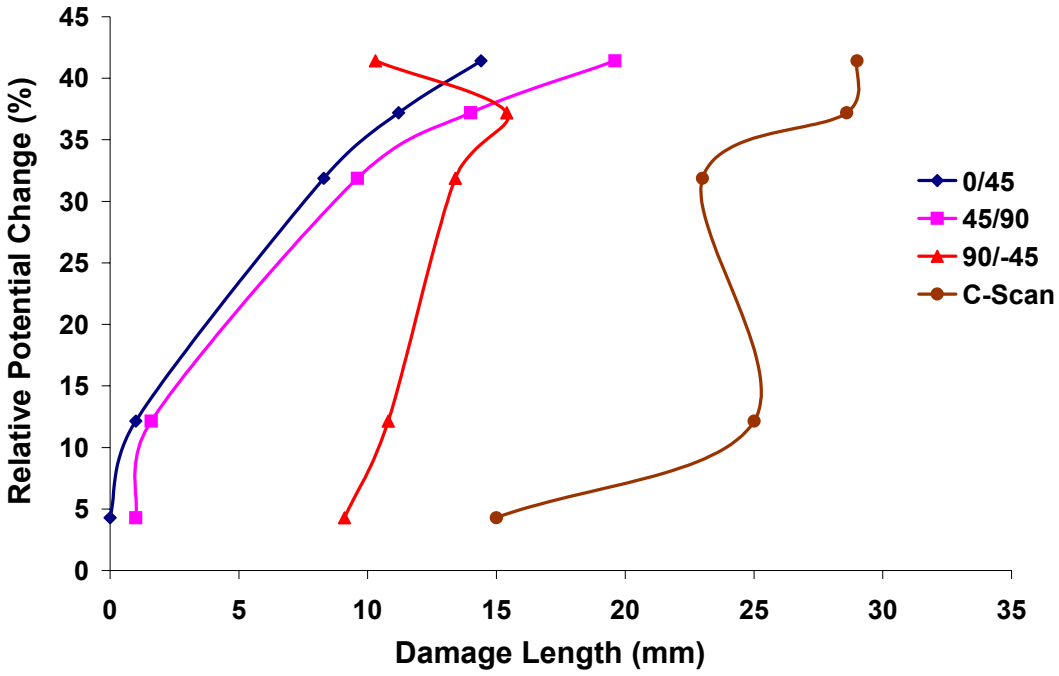

Figure 10. 10: Maximum potential change against maximum damage size as revealed by transverse sectioning, for the three top layers; current electrodes on **top** surface, potential measurements on **top** surface.

The current electrodes and the potential measurements probes are located on the top surface. The potential change values are the same as in Figure 10. 6 and they are taken with potential measurements and current electrodes on the top surface. On the same plot it also appears the damage extent in transverse direction as measured using C-scan. The bullets on each curve correspond to 4 J, 6 J, 8 J, 10 J, 12 J energy impacts. As can be seen, there is an excellent correlation between potential changes and damage extent for the 0/45 and 45/90 interfaces, which are closer to the top surface. More questionable, however is the correlation for the interfaces as we move further from the top surface (90/-45 interface). There is also very little correlation for the C-scan measured damage, which is the projection damage of all layers. These results indicate that the threshold distance through the thickness of the laminate to which delaminations can be detected, for the above current/potential probes configuration, is between second and third layer.

The influence of maximum damage extent on the maximum change in potential, for the bottom layers, as measured by transverse sectioning is shown in Figure 10. 11.

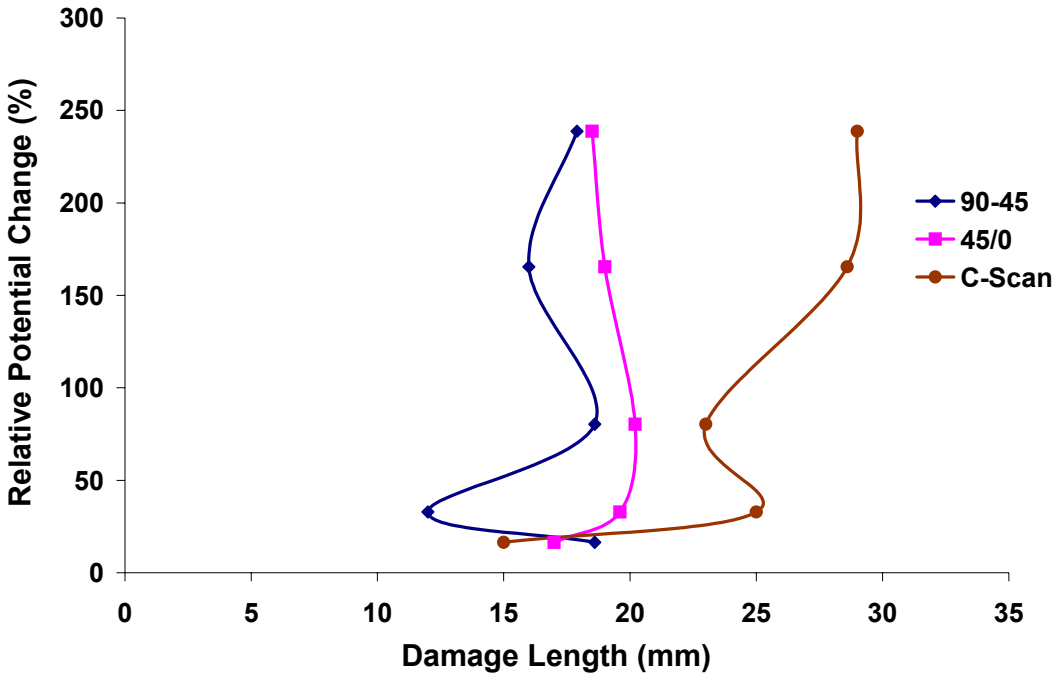

Figure 10. 11: Maximum potential change against maximum damage size as revealed by transverse sectioning, for the two bottom layers; current electrodes on **bottom** surface, potential measurements on **bottom** surface.

The current electrodes and the potential measurement probes are located on the bottom surface. As can be seen, there is a reasonable correlation between the C-scan damage area and the extent of damage on the bottom layers. This indicates that the projected damage area, as revealed by C-scan, is mainly associated with damage occurring on the bottom layers rather than the top; this would explain the little association of the C-scan damage with the damage occurring on the top layers as shown in Figure 10. 10.

10.6 Damage Sensing Using Electrical Potential Techniques

The performance of the electrical potential method as a damage sensing technique was demonstrated in this Thesis. The challenges of this research work were many, since this is a relatively unexplored method. The developed experimental configurations and finite element simulations attempted to answer practical questions such as whether it is possible to detect damage, what is the sensitivity of this technique to damage and which are the factors that may affect it. These key questions were approached on the basis of investigating a very serious drawback of CFRP composites, which is their susceptibility to impact damage.

The aim of this Thesis has never been to commercialize this technique. The insufficient time and facilities combined with financial restrictions would never allow such radical development. This suggests that after this work was completed, there are still many unanswered questions and many practical unsolved problems to be solved, as explained later. The scope of this research work was to understand and apply the principle which governs this technique on a practical problem, such as impact damage, and build a rigid base and model for further development of this method for structural health monitoring of composite structures.

As demonstrated in this Thesis, damage in the form of delaminations or fibres breakages can be detected using the electrical potential method. External devices were not used, eliminating the concerns over reliability of sensing and actuation devices, or the durability of bonds between the service and the host. Unlike techniques based on

transient emissions from damage events, changes in electrical potential are permanent and as a consequence the technique does not have to be permanently active. Measurements before and after a damaging event are all that it is required. The ability to detect damage is significantly influence by the current flow processes within the laminate.

Various configurations for current introduction and potential measurements were studied in order to detect damage. The contour plots were plotted based on potential values acquired from a network of probes, positioned in a grid of 25 mm. The contour lines at points between two probes were plotted based on linear interpolation of the potential values at the neighbour probes. The distance of 25 mm may appears to be relative large for interpolation of potential values, however, in any practical application it would be difficult to reduce the distance more. In addition, as discussed in Section 10.4, the selected grid of probes was able to define the boundaries of potential field around the C-scan projected damage zone. The noise level of the potential measurements was measured 8μV; this level was found to be significantly smaller (approximately 10 times) than the potential values and potential change values used for producing the contour plots, for current introduction parallel to the 0° fibres direction. This would enhance the credibility of those contours.

However, in the case where the current flow is perpendicular to the fibres (Figure 7. 12), the potential changes values were measured approximately 10 μV. These values are in the noise level raising questions of the reliability of the potential change contours. The trustworthiness of the equi-potential plots based on experimental values may further be enhanced from the strong agreement with the contours produced by numerical simulations, as discussed in Section 10.3. The creation, however, of a numerical model simulating potential fields in CFRP composites, was found to be a very demanding task, because of the large anisotropy in the electrical properties of the materials in the directions parallel and perpendicular to the fibres.

The experimental observations and finite element models led to the conclusion that delaminations and/or fibre breakages were detectable only for current flow along the fibre direction of the ply, on which the potential measurements are taken. Damage caused by impact was detected by placing the current/potential measurement probes either on the top or bottom surface. The selection of the surface would be determined by the type of damage to be detected, e.g. if delaminations located near the top surface are to be detected, the current/potential probes should be placed on that surface. Potential changes up to 41 % were measured after 12 J impact on a 2 mm thick laminate.

The extent of the region of detectable potential changes greater than 10% was 75 mm from the impact centre. This suggests that a network of probes of spacing 75 mm could detect whether damage had occurred. For the same impact energy and current probes/potential measurements on the bottom surface, potential changes up to 238% were measured. These measurements encountered potential changes arising from delamination and fibres splits or breakages near the bottom layers. The extent of the region of detectable potential changes greater than 10 % was 95 mm from the impact centre, suggesting a network of probes spaced 95 mm along the fibres for detection.

The sectioning of the impacted laminates and the finite element simulations revealed that single delamination, located in the middle of the composite plate, would not be detected by measuring the potential changes on either surface. In addition, a probe network spatially displaced at distances of more than 22 mm from the impact on both sides, perpendicular to the fibres would not be able to detect potential changes greater than 10%. These latter observations are some of the most significant drawbacks of this method.

The impact experiments were conducted at room temperature and without applying any mechanical loading on the structure. These conditions, however, may not correspond to the functional conditions of a composite part, which may be subjected simultaneously to cyclic loading and impact in humid environments at low or high temperatures. The potential change errors induced by those external parameters are compared in Table 10. 1.

Table 10. 1: Comparison of the potential change due to external parameters.

External Factors	***Measurement error***	***Temperature***	***Water***	***Mechanical Load***	***Impact Damage***
Percentage Change in Potential Values	3.0 μv (constant for all measurements)	0.5 %/°C	-1.0 %	1.5 % for each 0.1% strain	41%-238%

The potential changes due to water absorption are taken from measurements on unidirectional samples. It is believed that quasi-isotropic samples behave similarly since the resin, which absorbs water is the same in both systems. The potential changes due to mechanical strain are taken from Figure 10. 1. It is assumed linear elastic behaviour of the material up to 0.5% strain. Finally the effect of temperature is based on the measurements for quasi-isotropic samples.

If the potential changes caused by parameters such as 100% water absorption, 10°C temperature difference and 0.5% mechanical strain are summarized, the relative potential changes to unloading conditions at room temperature and dry environment will be 13.5%. The value of the induced error is negligible if a configuration with the current electrodes and potential measurements on the bottom surface is considered. On the other hand, it may influence potential measurements taken in order to detect delamination close to the top surface. These measurements would require current electrodes/potential measurement on top surface and the induced error would approximately be 1/3 of the values related to impact damage, reducing significantly the sensitivity of the method and raising issues of the reliability of the results. A spatial probe network of less than 75 mm spacing along the fibres direction would be required for accurate measurements.

Despite some practical difficulties related to the manufacture of probes as well the reduction of their number, the electrical potential technique is a very promising method for on-line impact damage detection of composite structures. There are still questions to be answered related to the time required for application and its flexibility in complex composite structures. The answers may well be the object of a future research. Alternative strategies for interrogation of the contact probe network should be investigated. Strategies have to be evaluated for optimum accuracy and resolution of impact damage sites, together with minimum number of contacts. Development of neural networks for prediction of damage location has to be considered. The results and the numerical models presented in this Thesis may very well be the technical and scientific ground to plant new ideas and improve the technical aspects of this method.

11 CONCLUSIONS-FUTURE WORK

This chapter is concerned with the conclusions and future work. Each section of this thesis has formed the basis for publications in conferences and journal. The majority of the results reported in this thesis are published elsewhere (page iv).

In this chapter, the major conclusions from the investigations reported in this thesis are divided into separate sections based on the chapter sequence. Sections 11.1 to 11.7 present the major conclusions. A vision of the perspectives of the electrical potential technique as a damage sensing tool in real applications is given in Section 11.8.

11.1 Test Methods

- An experimental set-up was developed based on digital acquisition system in order to investigate the response of electrical potential to impact damage, mechanical strain and temperature. The noise level of the system was 8 μV or 0.9 % of the maximum measured potential value.

- The developed system performed well giving clear indications of location and extent of impact damage.

11.2 Potential Distribution Fields

- Potential measurements on the surface where the current is introduced led to very peaky potential distributions near the current electrodes. For current introduction on the opposite surface, smoother potential distributions were obtained.

- The location of the current introduction electrodes changes the potential field orientation significantly. The contours of potential distribution are approximately perpendicular to the line joining the current input electrodes, without a significant pronounced distortion towards the direction of the fibres.

- Investigations of the potential distribution on cross ply and quasi-isotropic laminates have shown an almost identical potential field on their surface. This implies that the stacking sequence of the laminate does not have any significant effect on the contour patterns.

11.3 Effect of Damage on Electrical Potential - Holes

- The potential change contours are extended mainly in the direction parallel to the surface fibres towards the current introduction electrodes rather than in the transverse.

- Damage could be detected with current electrodes were positioned parallel to the top surface fibre orientation. When current is introduced perpendicular to the fibres, damage can be detected only for holes with diameter greater than 25 mm.

- Damage induced by holes showed extensive potential changes reaching up to 281% of the potential values for undamaged plate. Changes greater than 10% were measured at distances 100 mm from the centre of the hole, for current electrodes positioned on the bottom surface parallel to the 0° fibres while the potential measurements were taken on the top surface while perpendicular to the surface fibres, the damage width is only 50 mm.

11.4 Effect of Impact Damage in Quasi-Isotropic Plates on Electrical Potential

- Potential distributions after impact damage depend on the damage extent, and current input locations. The size of potential changes and the extent of the region of detectable potential changes, increase with increasing damage area.

- Potential changes up to 41% of the undamaged values were measured when potential and current probes are located on the top surface and up to 5% at distances 80 mm from the impact centre. These changes are generated from the existence of delamination at the layers near the top surface.

- Potential changes up to 238% were found when probes are located on the bottom surface. At distances 80 mm from the impact centre potential changes up to 9.2% were measured. These changes can be attributed to the extensive fibre breakages at the bottom surface.

- For all impact experiments it was found that the width of detectable potential changes, transverse to the fibres, was approximately 43 mm.

- Current input locations which result in the current flowing perpendicular to the surface fibres, result in little or no alteration of potential around the delamination, and as a consequence the latter cannot be detected.

11.5 Response of Electrical Potential to Mechanical Strain

- Unidirectional CFRP samples with uniform current introduced at the fibre ends, strained parallel to the fibres exhibit positive piezo-resistance with a gauge factor of 1.75. Uniform current introduction perpendicular to the fibres also produces positive piezo-resistance with a gauge factor of 2.7. These values reflect strain-induced changes due to fibre dimensional changes.

- Unidirectional samples with non uniform current flow, produced by intermittent contact at the sample ends, or point introduction of current on the sample surface, produce a range of apparent negative gauge factors from -89 to +20.5.

- Anomalous values of piezo-resistance are associated with changes in both local resistance and current during straining, under conditions of non uniform current distribution. Under these conditions, measurements of strain induced changes in potential between two points cannot be interpreted as changes in local resistance alone. Gauge factors calculated from such measurements reflect mechanically induced changes in current flow, rather than material properties.

- In multidirectional laminates strained parallel to the surface fibre direction, with current flowing parallel with the fibres, the off-axis plies provide a low resistance transverse current path and promote homogeneous current distributions. This results in positive piezo-resistivity.

- Finite element simulation of the response of electrical potential to mechanical confirmed the experimental data, demonstrating that in phase change of potential with strain is due to elastic behaviour of fibres. However, out of phase change is due to inhomogeneous distribution of the electrical current and dimensional changes as well.

11.6 Response of Electrical Potential to Temperature and Humidity

- The electrical potential in the longitudinal direction decreases as the temperature increases. The stacking sequence of the composite sample does not affect this behaviour.

- The water immersion experiments showed that the electrical resistance along the fibre direction is almost unaffected by the water absorption. Resistance transverse to the fibre direction increases because of a decrease in fibre-to-fibre contact pressure.

11.7 Numerical Simulations-Impact Damage

- Studies of numerically calculated potential distributions on the surface of the laminates showed good agreement with impact results when potential/current probes are on the top surface. Potential changes up to 32% were detected and detectable potential changes greater than 2% were found at distances 75 mm from the centre, along the 0° fibre direction.

- Potential changes greater than 4% were found at distances in excess of 75 mm from the damage centre. However, transverse to the fibres the damage width extends till the borders of delaminations.

- The threshold distance, through the thickness direction, for detection of delamination damage is between the second and third layer. This was also confirmed by a metallographic analysis of the impacted plates.

- No detectable changes were found for delamination located in the centre of the plate, for current introduction configuration transverse to the 0° fibre direction.

11.8 Future Work

Based on the results obtained in this project it seems that the electrical potential technique for damage detection is very promising. There are, however, a number of unsolved issues that need to be further explored. Some areas of future research are listed below:

1. Exploration of new methods for improving the sensitivity of this technique to damage located in the direction perpendicular to the current flow line.
2. Damage detection of artificial delaminations located at the interfaces of individual layers within the composite structure.
3. Investigation of the effect of thickness of the laminate on electrical potential for impact damage detection.
4. Usage of remote probes, instead of hand manufacturing, could significantly reduce the preparation time for applying this technique.
5. Development of a neural network, enabling the accurate prediction of damage level for various sizes of impacts and locations.

The 3-D finite element model presented in this Thesis can be developed further for more accurate representation of potential fields in composites. The numerical model should address the problem of the very large anisotropy of the electrical properties in the direction parallel and perpendicular to the fibres direction. Nevertheless, the finite element analysis could by employed for further study of the effect of different size delaminations, on the electrical potential. The damage can be placed in various positions within the composite structure and in relation to the current introduction probes. All these configurations can significantly reduce the time and the cost for applying the electrical potential technique and contribute in the optimisation of the probes network. An important aspect of this analysis, however, that has to be addressed is the transverse sensitivity and the effect of fibre breakages on the potential.

The most critical application of this technique, however, would be its usage as damage sensing tool for on-line Structural Health Monitoring of composite structures. The distinction between the influence of mechanical or environmental effects (such as strain, temperature, humidity) and impact damage on electrical potential, as developed in this Thesis, sets a threshold in the level of the sensitivity of this technique enabling further predictions related to the damage tolerance of the composite components. These studies could be the basis for application of this technique on a real structure subjected simultaneously to impact-mechanical and environmental loads, and recording the electrical potential response.

REFERENCES

[1] Jones F.L, *'The physics of electrical contacts'*. The Clarendon Press, Oxford, 1957

[2] Blatt F.J, *Physics of electronic conduction is solids'.* McGraw-Hill book company, New York, 1969

[3] Llewellyn J. F, *'The physics of electrical contacts*', Oxford, 1957

[4] Jiles D, *'Introduction to the electronics properties of materials'*, Chapman & Hall, New York, 1994

[5] Hummel R.E, *'Electronics properties of materials. An introduction for engineers'*, Springer-Verlag publications, Berlin, 1985

[6] Vincent Del Toro, *'Electrical engineering fundamentals'*, Prentice-Hall international editions, second edition, New Jersey, 1986

[7] James F Shackelford, *'Introduction to materials science for engineers'*, Prentice Hall, fourth edition, New Jersey, 1996

[8] Jonassen N, *'Electrostatics'* Chapman & Hall, New York, 1998

[9] Wei G, Nigel M.S, *'An introduction to electronics and ionic materials'*, World Scientific, Singapore, 2000

[10] Callister D.W, *'Materials science and engineering; an introduction'*, Wiley International, sixth edition, New York, 2003

[11] Jones I.P, *'Materials science for electrical and electronic engineers'*, Oxford, 2001

[12] Kraus J. D., Carver K. R., *'Electromagnetics'*, McGraw-Hill, second edition, 1973

[13] Matthews F. L, Rawlings R. D, *'Composite materials: Engineering and science'*, published by Woodhead Publishing Limiting, Cambridge, 1999

[14] Whyatt O. H, Hughes D. D, *'Metals, Ceramics and Polymers'*, Cambridge University Press, London, 1974

[15] Johnson W, *'The structure of PAN based carbon fibres and relationship to physical properties'*, In: Watt W and Perov B. V (ed), Strong Fibres, Handbook of composites, North-Holland publications, Volume 1, pp 389-443, 1985

References

[16] Fitzer E, Manocha L. M, *'Carbon Reinforcements and Carbon/Carbon Composites'*, Springer, 1988

[17] Saunders G. A, *'Electron transport in graphites and carbons'*, In: Blackman L. C. F (ed), Modern aspects of graphite technology, Academic Press, London, 1970

[18] Hyer M. W, *'Stress analysis of fibre-reinforced composite materials'*, McGraw-Hill, Singapore 1988

[19] Perret R, Ruland W. J, *'The microstructure of PAN-base carbon fibres'*, J. Appl. Cryst, **3,** pp 525-532, 1970

[20] Johnson D. J, *'Structure-property relationships in carbon fibres'*, J. Phys. D: Appl. Phys, **20**(3), pp 286-291, 1987

[21] Diefendorf R. J, Tokarsky E, *'High-Performance carbon fibres'*, Polymer Engineering and Science, **15** (3), pp 150,159, 1975

[22] Guigon M, Oberlin A, Desarmot G, *'Microtexture and structure of some high-modulus, PAN-base carbon fibres'*, Fibre Science Tech, **20**, pp 177-198, 1984

[23] Dresselhaus M. S, Dresselhaus G, Sugihara K, Spain I. L, Goldberg H. A, *'Graphite fibres and filaments'*, Springer Series in Materials Science, Vol. 5, 1988

[24] Mrozowski S, *'Electronic properties and band model of carbons'*, Carbon **9**(2), pp 97-109, 1971

[25] Watt W, Perov B. V*' Strong Fibres, Handbook of composites'*, Handbook of composites, Volume 1, 1985

[26] Robson D, Assabghy F. Y. I, Ingram D. J. E *'Some electronics properties of polyacrynonitrile-based carbon fibres'*, Journal of physics D: Applied Physics, **5**(11), pp 169-179, 1972

[27] Robson D, Assabghy F. Y. I, Ingram D. J, *'An electron spin resonance study of carbon fibres based on polyacrylonitrile'*, Journal of physics D: Applied Physics, **4**(9), pp 1426-1438, 1971

[28] Shido A, *'Studies on graphite fibre'*, Report 317, Government Research Institute, Osaka-Japan, 1961

[29] Fischbach D. B, Komaki, *'Electrical resistance of carbon fibres'*, Extended abstracts 14th Biennial Carbon Conference, Pennsylvania State University-USA, pp 191-204, 1979

[30] Bright A. A, Singer L. S, *'The electronic and structural characteristics of carbon fibres from mesophase pitch'*, Carbon, **17**(1), pp 59-69, 1979

[31] Lovell D. R, *'A comparison of available fibres'*, In: Carbon fibres technology, uses and prospects, edited by The Plastics and Rubber Institute, London, pp 39-47, 1986

[32] Tahar M. Z, Dresselhaus M. S, Endo M, *'Size effects in electrical properties of benzene-derived graphite fibres'*, Carbon **24**(1), pp 67-72, 1986

References

[33] Thiagarajan C, *'Smart characterisation of damage in carbon fibre reinforced composites under static and fatigue loading conditions by means of electrical resistivity measurements'*, PhD Thesis, Cranfield University-UK, 1995-1996

[34] Chung D. D. L, *Carbon fibre composites'*, Butterworth-Heinemann publications, Boston-USA, 1994

[35] Soule D. E, *'Magnetic Field Dependence of the Hall Effect and Magnetoresistance in Graphite Single Crystals'*, Physical Review, **112**(3), pp 698-707, 1958

[36] Pan G, Muto N, Miyayama, M, *'Humidity sensitive electrical resistivity of carbon fibres'*, Journal of Materials Science Letters, **12**, pp 666-668, 1993

[37] Barton S. S, Harrison B. H, *'Surface studies on carbon: 'Immersional energetics of spheron 6 in water'*, Carbon, **13**(1), pp 47-50, 1975

[38] Conor P. C, Owston C. N, *'Electrical resistance of single carbon fibres'*, Nature, **223**, pp 1146-1147, 1969

[39] Owston C. N, *'Electrical properties of single carbon fibres'*, British Journal of Applied Physics: 3, Physics .D, **3**, pp 1615-1626, 1970

[40] Vishay Company, handbook

[41] Cho J. W., Choi J. S., *'Relationship between electrical resistance and strain of carbon fibres upon loading'*, Journal of Applied Polymer Science, **77**, pp 2082-2087, 2000

[42] Torayca Company Web Site, http://www.torayca.com/techref/en/images/fcp02.html

[43] Curtis G. J., Milne J. M., Reynolds, *'Non-Hookean behaviour of strong carbon fibres'*, Nature, **220**, pp 1024-1025, 1968

[44] Fischbach D. B, *'Observations on the properties and structure of carbon fibres'*, In: Carbon' 80, Preprints of the 3rd international carbon conference, Baden-Baden, pp 590-597, 1980

[45] Warfield R. W, *'Characterization of polymers by electrical resistivity techniques'* In: Testing of Polymers, Vol. 1, Schmitz J. V, Interscience Publishers, New York, 1965

[46] Kroschwitz J. I, *High performance polymers and composites'*, Wiley publications, 1991

[47] Singh D. B, Kumar A, Tayal V. P, Sanyal B, *'Effect of moisture and electronic packaging exhalates on the electrical conductivity of epoxy laminate'*, Journal of Materials Science, **23**(8), pp 3015-3025, 1988

[48] Harper C. A., *'Handbook of plastics, elastomers, and composites'*, Second Edition, McGraw Hill, 1992

[49] Fuoss R. M, *'Electrical properties of solids'*, Journal of American Chemical Society, **61**(9), pp 2329-2334, 1939

[50] Barbero E. J '*Introduction to composite materials design'*, McGraw Hill, 1998.

References

[51] Angelidis N, Khemiri N, Irving PE, '*Electrical behaviour of CFRP under mechanical loading'* presented at the First European Workshop on Structural Health Monitoring, Paris-France, 2002.

[52] Todoroki A, Tanaka Y, *'Delamination identification of cross ply graphite/epoxy composites beams using electric resistance change method'*, Composite Science and Technology, **62**(5), pp: 629-639, 2001.

[53] Kupke M, Schulte K, Schüler R, *'Non-destructive testing of FRP by d.c. and a.c. electrical methods,* Composites Science and Technology, **61**(6), pp: 837-847, 2000.

[54] Chung D. D. L, '*Continuous carbon fibre polymer-matrix composites and their joints, studied by electrical measurements'*, Polymer Composites, **22**(2), pp: 250-270, 2001.

[55] Moriya K, Endo T, '*A study on flaw detection method for CFRP composite laminates (1st report) the measurement of crack extension in CFRP composites by electrical potential method'*, Trans. Japan Soc. Aero Space Science **32**(98), pp: 184-196, 1990.

[56] Irving P. E. Thiagarajan C, '*Fatigue damage characterisation in carbon fibre composite materials using an electrical potential technique'* Smart Materials & Structures **7,** pp: 456-466, 1997.

[57] Todoroki A. Tanaka M. Shimanura Y, '*Measurement of orthotropic electric conductance of CFRP laminates and analysis of the effect on delamination monitoring with an electric resistance change method*, Composite Science and Technology, **62**(5), pp: 619-628, 2001

[58] Louis M, Joshi S. P, Brockmann W, '*An experimental investigation of through thickness electrical resistivity of CFRP laminates',* Composites Science and Technology, **61**(6), pp: 911-919, 2001

[59] Lodge K. J, *'Electrical properties of joints in carbon fibre composites'*, Composites **13**(3), pp: 305-310, 1982

[60] Schueler R, Joshi S. P, Schulte K, *'Conductivity of CFRP as a tool for health and usage monitoring'*, Smart Structures and Materials, SPIE proceedings, **3041**, pp: 417-426, 1997

[61] Prabhakaran R, *'Damage assessment through electrical resistance measurement in graphite reinforced composites'*, Experimental Techniques, **14**, pp: 16-20, 1990

[62] Park J. B, Okabe T, Takeda N, Curtin W. A, *'Electromechanical modelling of unidirectional CFRP composites under tensile loading condition'*, Composites: Part A, **33**(2), pp: 267-275, 2002

[63] Park J. B, Okabe T, Song D. Y, Takeda N, Kitano A, *'In-situ health monitoring of CFRP composites using electrical characteristics'*, Smart Structures and Materials, Proceedings of SPIE, **4328**, pp: 323-331, 2001

[64] Kobayashi S, Terada K, Ogihara S, Takeda N, *'Damage-mechanics analysis of matrix cracking in cross ply CFRP laminates under thermal fatigue'*, Composites Science and Technology, **61**(12), pp: 1735-1742, 2001

References

[65] Park, J. B, Okabe T, Yoshimura A, Takeda N, Xia M, Curtin W. A, *'Determination of internal conducting network of CFRP composites using anisotropy of electrical conductivity'*, Proceedings of 7Th International SAMPE Symposium & Exhibition, Japan, pp: 13-16, 2001

[66] Xia Z, Okabe T, Park J. B, Curtin W. A, Takeda N, *'Quantitative damage detection in CFRP composites: coupled mechanical and electrical models'*, Composite Science and Technology, **63**(10), pp: 1411-1422, 2003

[67] Park J. B, Okabe T, Takeda N, Curtin W. A, *'Electromechanical study of the internal conducting network of CFRP composites'*, [in press]

[68] Curtin W. A, *'Stochastic damage evolution and failure in fibre-reinforced composites'*, Advances in Applied Mechanics, **36**, pp: 163-253, 2000

[69] Weibull W. A, *'A statistical distribution function of wide applicability'*, Journal of Applied Mechanics: ASME Journals, pp: 293-297, 1952

[70] Jones R. M, *'Mechanics of composite materials'*, McGraw-Hill, New York, 1957

[71] Knibbs R. H, Baker D. J, Rhodes G, *'The thermal and electrical properties of carbon fibre uni-directional reinforced epoxy composites'*, In: 26th Annual Technical Conference Reinforced Plastics/Composites Division, The Society of Plastics Industry, Inc., Section 8-F, pp: 1-10, 1971

[72] Bruggeman D. A. G, *'Berechnung verschiedener physikalischer konstanten von heterogenen substanzeb'*, Amm. Phys. (Leipz), **24**, pp 636-664, 1935

[73] Kováčik J, *'Electrical conductivity of two-phase composite material'*, Scripta Materialia, **39**, pp: 153-157, 1998

[74] Miller M, *'Bounds for effective electrical, thermal and magnetic properties of heterogeneous materials'*, Journal of Mathematical Physics, **14**(11), pp: 1988-2004, 1969

[75] Hashin Z, *'Assessment of the self consistent scheme approximation: conductivity of particulate composites'* Composite Materials, **2**, pp: 284-300, 1968

[76] Ueda N, Taya M, *'Prediction of the electrical conductivity of two-dimensionally misoriented short fibre composites by a percolation model'*, Journal of Applied Physics, **60**(1), pp: 459-461, 1986

[77] Uvarov N. F, *'Conductivity of composites: description in terms of general mixing rule'*, Electrochemical Society Proceeding, **24**, pp: 885-891, 1997

[78] Vilčáková J, Sáha P, Quadrat O, *'Electrical conductivity of carbon fibres/polyester resin composites in the percolation threshold region'*, European Polymer Journal **38**, pp: 2343-2347, 2002

[79] Weber M, Kamal M. R, *'Estimation of the fibre volume resistivity of conductive fibre composites by two new models'*, Polymer Composites, **18**(6), pp: 726-740, 1997

[80] Ruschau G. R, Newnham R. E, *'Critical volume fractions in conductive composites'*, Journal of Composite Materials, **26**(8), pp: 2727-2735, 1992

References

[81] Bunde A, Dieterich W, *'Percolation in composites'*, Journal of Electroceramics, **5**(2), pp: 81-92, 2000

[82] Foulger S. H, *'Electrical properties of composites in the vicinity of the percolation threshold'*, Journal of Applied Polymer Science, **72**, pp: 1573-1582, 1999

[83] Tsotra P, Friedrich K, *'Electrical and mechanical properties of functionally graded epoxy-resin/carbon fibre composites'*, Composites: Part A, **34**(1), pp: 75-82, 2003

[84] Taipalus R, Harmia T, Zhang M. Q, Friedrich K, *'The electrical conductivity of carbon-fibre-reinforced polypropylene/polyaniline complex-blends: experimental characterisation and modelling',* Composites Science and Technology, **61**(6), pp: 801-814, 2001

[85] Weber M, Kamal M. R, *'Estimation of the volume resistivity of electrically conductive composites'*, Polymer Composites, **18**(6), pp: 711-725, 1997

[86] Knibbs R. H. Morris J. B, *'The effects of fibre orientation on the physical properties of composites'*, Composites **5**(5), pp:209-216, 1974

[87] Leeds M. A, *'Electronic properties of composite materials'*, Handbook of Electronics Materials, **9**, pp: 22-24

[88] Nascimento J. F, Ezquerra T. A, Balta-Calleja F. J, *'Anisotropy of electrical conductivity and structure in polymer-carbon fibre composite materials'*, Polymer Composites, **16**(2), pp: 109-113, 1995

[89] Belani J. G, Broutman L. J, *'Moisture induced resistivity changes in graphite-reinforced plastics'*, Composites 9(4), pp: 273-277, 1978

[90] Tse K. W, Moyer C. A, Arajs S, *'Electrical conductivity of graphite fibre-epoxy resin composites'*, Materials Science and Engineering **49**(1), pp: 41-46, 1981

[91] Abry J. C, Bochard S, Chateauminois A, Salvia M, Giraud G, *'In situ detection of damage in CFRP laminates by electrical resistance measurements'*, Composites Science and Technology, **59**(6), pp: 925-935, 1999

[92] Schulte K, Baron C, *'Load and failure analyses of CFRP laminates by means of electrical resistivity measurements'*, Composites Science and Technology, **36**(1), pp: 63-76, 1989

[93] Thiagarajan C, Sturland I, Tunnicliffe D, Irving P. E, *'Electrical potential techniques for damage sensing in composite structures'*, presented at the Second European Conference on Smart Structures and Materials, Glasgow, UK, pp: 128-131, 1994

[94] Wittich H, Schulte K, Kupke M, Kliem H, Bauhofer W, *'The measurement of electrical properties of CFRP for damage detection and strain recording'*, European Conference on Composites Testing and Standardisation ECCM-CTS, Hamburg, Germany, pp: 447-457, 1994

[95] Schulte K, *'Damage development under cycling loading'*, Proceeding of the European Symposium on Damage Development and Failure Process in Composite Materials, Leuven, Belgium, pp: 39-54, 1987

References

[96] Prasse T, Michel F, Mook G, Schulte K, Bauhofer W, *'A comparative investigation of electrical resistance and acoustic emission during cycling loading of CFRP laminates'*, Composites Science and technology, **61**(6), pp: 831-835, 2001

[97] Kaddour A. S, Al-Salehi F. A. R, Al-Hassani S. T. S, *'Electrical resistance measurement technique for detecting failure in CFRP materials at high strains'*, Composite Science and Technology, **51**(3), pp:377-385, 1994

[98] Seo D. C, Lee J. J, *'Damage detection of CFRP laminates using electrical resistance measurement and neural network'*, Composite Structures, **47**(1-4), pp: 525-530, 1999

[99] Muto N, Yanagida H, *'Preventing fatal structures in carbon-fibre-glass-fibre-reinforced plastic composites by monitoring change in electrical resistance'*, Journal American Ceramic Society, **76**(4), pp: 875-879, 1993

[100] Hou L, Hayes S. A, *'A resistance-based damage location sensor for carbon-fibre composites'*, Smart Materials Structures, 11, pp: 966-969, 2002

[101] Das, N.C, Chaki T. K, Khastgir D, *'Effect of axial stretching on electrical resistivity of short carbon fibre and carbon black filled conductive rubber composites'*, Polymer International, **51**, pp: 156-163, 2002

[102] Rask O. N, Robinson D. A, '*Graphite as an embedded strain gauge'*, material technical note, SAMPE Journal, pp: 52-55, 1988

[103] Abry J. C, Chateauminois A, Dalloz B, Giraud G, Salvia M, *In-situ monitoring of damage in CFRP laminates by means of AC and DC measurements'*, Composites Science and Technology, **61**(6), pp: 855-864, 2001

[104] Wang S, Shui X, Fu X, Chung D. D. L, *'Early fatigue damage in carbon-fibre composites observed by electrical resistance measurement'*, Journal of Materials Science, 33, pp: 3875-3884, 1998

[105] Wang X, Chung D. D. L, *'Self-monitoring of fatigue damage and dynamic strain in carbon fibre polymer-matrix composite'*, Composites Part B, **29B**, pp: 63-73, 1998

[106] Cho J. W, Choi J. S, *'Relationship between electrical resistance and strain of carbon fibres upon loading'*, Journal of Applied Polymer Science, **77**, pp: 2082-2087, 2000

[107] Mei Z, Guerrero V. H, Kowalik D. P, Chung D. D. L, *'Mechanical damage and strain in carbon fibre thermoplastic-matrix composite, sensed by electrical resistivity measurement'*, Polymer Composites, **23**(3), pp: 425-432, 2002

[108] Wang X, Chung D. D. L, *'Continuous carbon fibre epoxy-matrix composite as a sensor of its own strain'*, Smart Materials Structures, **5**, pp: 796-800, 1996

[109] Wang X, Chung D. D. L, *'Inherently smart laminates of carbon fibre in a polymer matrix*', Mat. Res. Symp. Proc., **434**, pp: 299-304, 1996

References

[110] Wang X, Chung D. D. L, *'Sensing delamination in a carbon fibre polymer matrix composite during fatigue by electrical resistance measurement'*, Polymer Composites, **18**(6), pp: 692-700, 1997

[111] Song D. Y, Park J. B, Takeda N, *'Failure behavior and electrical property of CFRP and CFGFR'*, Key Engineering Materials **183-187**, pp: 1129-1134, 2000

[112] Song D. Y, Hirata Y, Takeda N, *'Correlation between damage and electrical resistance change in composites with carbon particle and carbon fibre'*, proceeding of 7th International SAMPE Symposium & Exhibition, Japan, pp: 883-886, 2001

[113] Todoroki A, Matsuura K, Kobayashi H, *'Application of electric potential method to smart composite structures for detecting delamination'*, JSME International J, Series A, **38**(4), pp: 524-530, 1995

[114] Schueler R, Joshi S. P, Schulte K, '*Damage detection in CFRP by electrical conductivity mapping'*, Composite Science and Technology, **61**(6), pp: 921-930, 2001

[115] Todoroki A, *'The effect of number of electrodes and diagnostic tool for monitoring the delamination of CFRP laminates by changes in electric resistance'*, Composites Science and Technology, **61**(13), pp: 1871-1880, 2001

[116] Todoroki A, Tanaka Y, Shimamura Y, *'Delamination monitoring of graphite/epoxy laminated composite plateo f electric resistance change method'*, Composites Science and Technology, **62**(9), pp:1151-1160, 2002

[117] Todoroki A, Tanaka Y, Shimamura Y, *'Multi-prove electric potential change method for delamination monitoring of graphite/epoxy composite plates using normalized response surface'*, Composites Science and Technology, **64**(5), pp: 749-758, 2004

[118] Todoroki A, Tanaka M, Shimamura Y, *'High performance estimations of delamination of graphite/epoxy laminates with electric resistance change method'*, Composites Science and Technology, **63**(13), pp: 1911-1920, 2003

[119] Celzard A, McRae E, Marêché J. F, Furdin G, Sundqvist B, *'Conduction mechanisms in some graphite-polymer composites: Effects of temperature and hydrostatic pressure'*, Journal of Applied Physics, **83**(3), pp: 1410, 1419, 1998

[120] Dear J.P, Brown S.A, '*Impact damage processes in reinforced polymeric materials',* Composites: Part 1, **34**, pp 411-420, 2003

[121] Greenhalgh E, Hiley M. *'The assessment of novel materials and processes for the impact tolerant design of stiffened composite aerospace structures',* Composites: Part A, **34**, pp 151-161, 2003

[122] Slöblom P.O, Hartness J.T, Cordell T. *'On low-velocity impact testing of composite materials'*, Journal Composite Materials, **22**, pp 30-52, 1988

[123] Shivakumar K.N, Elber W, Illg W, *'Prediction of low-velocity impact damage in thin circular laminates'*, AIAA Journal, **23** (3), pp 442-449, 1985

References

[124] Liu D, Malvern L E, *'Matrix cracking in impacted glass/epoxy plates'*, Journal Composite Materials, **21**, pp 594-609, 1987

[125] Joshi S. P, Sun C.T, *'Impacted-induced fracture initiation and detailed dynamics stress field in the vicinity of impact'*, Procedures American Society of Composites 2nd Tech. Conf., 23-25, pp 177-185, 1987

[126] Cantwell W.J, Morton J, *'The impact resistance of composite materials-a review'*, Appl. Mech. Rev. **44**(4), pp 155-190, 1991

[127] Rotem, A. 'Residual flexural strength of FRP composite specimens subjected to transverse impact loading', SAMPE Journal No 2, pp19-25, 1988

[128 Manders P.W, Harris W.C, *'A parametric study of composite performance in compression after impact testing'*, SAMPE Journal, **22**, pp 47-51, 1986

[129] Richardson M.O.W, Wisheart M.J, '*Review of low-velocity impact properties of composite materials',* Composites: Part A, **27A**, pp 1123-1131, 1996

[130] Abrate S '*Impact on composite structures'*, book, 1998

[131] Joshi S.P, Sun C.T, *'Impact induced fracture in laminated composite'*, Journal Composite Materials, **19**, pp 51-66, 1985

[132] Choi H.Y, Downs R.J, Chang F.K, '*A new approach toward understanding damage mechanisms and mechanics of laminated composites due to low-velocity impact: part I-experiments'*, Journal Composite Materials, **25**, pp 992-1011, 1991

[133] Liu D, *'Impact induced delamination: A view of bending stiffness mismatching'*, Journal Composite Materials, **22**, pp 674-692, 1988

[134] Matthews F. L, Rawlings R. D, *'Composite materials: Engineering and science'*, published by Woodhead Publishing Limiting, Cambridge, 1999

[135] Brooks C. R, Choudhury A, *'Failure analysis of engineering materials'*, McGraw-Hill Professional Engineering, USA, 2002

[136] Cantwell W. J, Curtis P. T, Morton J, *'Low velocity impact damage tolerance in CFRP laminates* containing *woven and non-woven layers'*, Composites, **14**, pp 301-305, 1983

[137] Chang F.K, Choi H.Y, Jeng S.T, *'Study on impact damage in laminated composites'*, Mech. Mater., **10**, pp 83-95, 1990

[138] Guild F.J, Hogg P.J, Prichard J.C, *'A model for the reduction in compression strength of continuous fibre composites after impact damage'*, Composites, **24** (4), 333-339, 1993

[139] De Moura M.F.S.F, Marques A.T, *'Prediction of low velocity impact damage in carbon-epoxy laminates'*, Composites: Part A, **33**, pp 361-368, 2002

[140] Greenhalgh E, *Characterisation of mixed-mode delamination growth in carbon fibre composites'*, PhD Thesis, Imperial College, 1998

References

[141] Choi H.Y, Chang F.K, *'A model for predicting damage in graphite/epoxy laminated composites resulting from low-velocity point impact'*, Journal Composite Materials, **26**, pp 2134-69, 1992

[142 Razi H, Kobayashi A.S, *'Delamination in cross ply laminated composite subjected to low-velocity impact'*, AIAA Journal, **31**(8), pp 1498-1502, 1993

[143] Foreman A, Curtis P, *'Optimising damage tolerance in carbon fibre composites'*, DERA/SMC/SM3/CR970187/1.0, 1997

[144] Lee S, Zahuta P, *'Instrumented impact and static indentation of composites'*, Journal Composite Materials, **25**, pp 204-222, 1991

[145] Cantwell W.J, Morton J, *'Geometrical effects in the low velocity impact response of CFRP'*, Composite Structures, **12**, pp 39-59, 1989

[146] 'Carbon and high performance fibres: Directory and databook', Edition 6, Chapman & Hall, 1995

[147] Armstrong K. B, Barret R. T, *'Care and repair of advanced composites'*, SAE International, 1997

[148] Chun-Yung Niu M, *'Composite airframe structures. Practical design information and data'*, Conmilit Press ltd, Hong Kong, 1992

[149] AGAR Scientific ltd, **www.agarscientific.com**

[150] Collings T. A. *'Moisture management and artificial ageing of fibre reinforced epoxy resins'*, Tech. Memo, Royal Aircraft Establishment, Farnborough, 1987

[151] ABAQUS Manual

[152] I-DEAS manual

[153] Felippa C. A, *'Introduction to finite element methods'*, Departments of Aerospace Engineering Sciences and Centre of Aerospace Structures, University of Colorado, USA, 2001

[154] Zienkiewicz O. C, Taylor R. L, *'The finite element method'*, fifth edition, Butterworth-Heinemann publications, Oxford, England, 2000

[155] Jin Chong Tan, *'Modelling the full-coupled-thermo-electrical interaction during resistance spot welding of porous sandwich sheets'*, PhD Thesis, University of Cambridge, England, 2003

[156] Anderson T. A, Lemoine G. I, *'An artificial neural network based damage detection scheme for electrically conductive composite structures'*, 4th International Workshop In Health Monitoring, Stanford, California, September 2003

[157] Khemiri N, Angelidis N, Irving P. E, *'Experimental and finite element study of the electrical potential technique for damage detection in CFRP laminates'*, Smart Structures & Demonstrators conference, Herriot Watt University, Edinburgh, UK, December 2001

References

[158] His-Yung T Wu and Springer G S *'Measurement of matrix cracking and delamination caused by impact on composite plates'* Journal of Composite Materials 22(6), 518-532, 1988

[159] Bakis C. E, Nanni J. A, Terosky J. A, Koehler S. W, '*Self-monitoring, pseudo-ductile, hybrid FRP reinforcement rods for concrete applications*', Composites Science and Technology, **61**(6), pp: 815-823, 2001

[160] Blackman L. C. F, *'Modern aspects of graphite technology'*, Academy Press, London and New York, 1970

[161] http://www.ladyslipper.com/waterq.htm

[162] Paniza G. A, *'Conductive polymer transducers'*, PhD Thesis, Illinois Institute-USA, 1971

[163] His-Yung T. Wu, Springer G. S, '*Measurement of matrix cracking and delamination caused by impact on composite plates'* Journal of Composite Materials, **22**(6), pp: 518-532, 1988